

# **HIGH-ENERGY PHENOMENA, SHORT-RANGE NUCLEAR STRUCTURE AND QCD**

**L.L. FRANKFURT and M.I. STRIKMAN**

*Leningrad Nuclear Physics Institute, Gatchina, Leningrad 188350, USSR*



NORTH-HOLLAND PUBLISHING COMPANY - AMSTERDAM

## HIGH-ENERGY PHENOMENA, SHORT-RANGE NUCLEAR STRUCTURE AND QCD

L.L. FRANKFURT and M.I. STRIKMAN

*Leningrad Nuclear Physics Institute, Gatchina, Leningrad 188350, USSR*

Received January 1981

*Contents:*

|   |     |   |     |
|---|-----|---|-----|
| 1. Introduction   | 217 | 6. Deep inelastic $\ell + A \rightarrow \ell' + N + X$ processes  | 291 |
| 2. Where are the relativistic effects in the deuteron essential and how to take them into account         | 220 | 6.1. The basic formulae   | 292 |
| 2.1. Some general features of relativistic bound states   | 220 | 6.2. Comparison with experiment   | 295 |
| 2.2. Relativistic impulse approximation   | 224 | 7. Production of fast backward particles in hadron (nucleus)-nucleus collisions                           | 297 |
| 2.3. The Weinberg equation. Relationship to the non-relativistic theory of the deuteron                   | 230 | 7.1. Standard picture of $hA$ scattering  | 297 |
| 2.4. Properties of the light cone nuclear wave function. Weinberg type equation                           | 235 | 7.2. Production of fast backward nucleons. The spectator mechanism  | 298 |
| 2.5. Relativistic effects in hadron scattering from deuteron  | 242 | 7.3. Production of fast backward particles. Direct mechanism  | 303 |
| 3. High-energy short-range phenomena in the deuteron. Comparison with experiment                          | 248 | 7.4. Final state interaction  | 305 |
| 3.1. Inelastic $eD$ scattering in the threshold region at high momentum transfer                          | 248 | 7.5. Production of fast backward particles in nucleus-nucleus collisions                                  | 307 |
| 3.2. Deuteron deep inelastic structure functions  | 252 | 8. Production of fast backward particles from nuclei: the basic data and their theoretical interpretation | 308 |
| 3.3. Deep inelastic $\ell + D \rightarrow \ell' + p + X$ reaction with unpolarized and polarized deuteron | 256 | 8.1. Proton production. Scaling limit   | 308 |
| 3.4. The deuteron electromagnetic form factors  | 259 | 8.2. Intermediate energies: $T_N^{imp} < 1$ GeV   | 316 |
| 3.5. Inclusive hadron production in the deuteron fragmentation region. Cumulative effect, etc.            | 266 | 8.3. Onset of scaling in $\gamma, h + A \rightarrow p + X$ reactions                                      | 321 |
| 4. QCD and the high momentum components of the nuclear wave functions                                     | 273 | 8.4. Backward production of fast light ions   | 325 |
| 4.1. QCD and the structure of the deuteron wave function  | 274 | 8.5. The fast backward pion production  | 326 |
| 4.2. Leading particle production in hadronic reactions $D \rightarrow p, \pi$ at $x_F \rightarrow 1$      | 280 | 8.6. Discussion of other models of the fast backward particle production                                  | 331 |
| 4.3. QCD and short-range nucleus structure  | 283 | 9. Summary and outlook  | 333 |
| 5. High $Q^2$ ( $ee'$ ) reactions   | 284 | Appendices:   |     |
| 5.1. The basic formulae   | 284 | A. QCD constraints for relativistic description of the nucleus  | 335 |
| 5.2. Comparison with the data   | 286 | B. Properties of $\ell + N \rightarrow \ell' + N' + X$ deep inelastic reactions                           | 336 |
| 5.3. Sum rules for the nucleus structure functions  | 287 | C. The behaviour of the QCD vertices in the limit $x \rightarrow 1$                                       | 337 |
| 5.4. Predictions for the value of the nucleus structure functions in the Bjorken limit at $x \geq 1$      | 288 | D. On the correlations between the fast backward nucleons and the forward emitted particles               | 339 |
|   |     | E. Position of the nuclear core and the non-relativistic quark model                                      | 340 |
|   |     | Note added in proof   | 341 |
|   |     | References  | 343 |

*Single orders for this issue*

PHYSICS REPORTS (Review Section of Physics Letters) 76, No. 4 (1981) 215–347.

Copies of this issue may be obtained at the price given below. All orders should be sent directly to the Publisher. Orders must be accompanied by check.

Single issue price Dfl. 61.00, postage included.

**Abstract:**

A systematic review and theoretical analysis of the experimental data on multi GeV lepton, photon, hadron, deuteron (nucleus) reactions from nuclei forbidden in the case of scattering from free nucleons is presented. It is shown that all these data can be quantitatively described as a manifestation of short-range few nucleon correlations. Calculations for elastic and (deep)inelastic electromagnetic and weak form factors of the deuteron and other nuclei, are given. The inclusive production of leading particles in the nucleus fragmentation region in high-energy lepton, hadron or nucleus-induced collisions is analyzed. The straightforward correspondence between the Weinberg equation for the light-cone wave functions of the deuteron and the non-relativistic Schrödinger equation is found. It is shown that the predictions of quantum chromodynamics for short-distance phenomena in nuclei are in agreement both with experimental data and theoretical expectations due to short range correlations in nuclei. Several feasible experiments are considered which could establish the existence of relativistic nuclear physics.

## 1. Introduction

During the last decade the investigation of deep inelastic processes, where a large energy is transferred to a target nucleon by high-energy electron and hadron probes has discovered that hadrons are built up out of quarks and gluons and that Quantum Chromodynamics (QCD) seems to be relevant for the quark-quark (gluon) interactions. Considerable progress has been achieved in the theoretical description of the short-range hadron structure, which appears to be much simpler than the long-range structure. It seems now that a similar simplification occurs also in the theoretical description of the short-range phenomena in nuclei. If so, theoretical and experimental methods of high energy physics should provide effective ways to study high momentum structure of the nuclear wave function (WF), i.e. the properties of superdense nuclear matter. On the other hand, during the last decade a number of regularities have been established [1–35] in lepton (hadron)-nucleus multi GeV reactions performed under conditions, kinematically forbidden for a free nucleon target. These data were obtained mostly in the USSR and in the USA: in the ITEP (Moscow), JINR (Dubna), SLAC, LBL, LAMPF, EPI (Erevan), FNAL and IHEP (Serpukhov) (sections 3, 5, 6 and 8). They have stimulated theoretical attempts to describe short-range phenomena in nuclei by applying the methods of non-relativistic quantum mechanics, light cone quantum mechanics, Quantum Chromodynamics, non-relativistic quark models, parton model, Reggeon calculus, etc. [36–77].

The aim of this review is to demonstrate that existing data on the high-energy processes forbidden for the scattering from free nucleons such as the elastic electromagnetic form factors of the D [4, 6], high momentum transfer ( $e, e'$ ) reactions from D [5] and  ${}^3\text{He}$  [8],  $(\bar{\nu}, \mu^+ p)$  and  $(\nu, \mu^- p)$  reactions from nuclei [9, 10], production of fast backward p,  $\pi$  in the high energy processes  $p(\pi, \gamma, \text{light nuclei}) + A \rightarrow \text{backward } p(\pi, \dots) + X$  [2, 11–35] can be quantitatively described as a manifestation of short-range few-nucleon correlations (FNC).† It was emphasized in [40] that the theoretical interpretation of these reactions is much more straightforward than in the case of low-energy reactions since high-energy processes occur instantaneously as compared to the time-scale typical for nuclear processes. For example the average momentum transfer to the target nucleon is about  $1 \text{ GeV}/c$  in an inelastic high-energy process  $h + N \rightarrow N + X$ ,‡ but much larger in deep inelastic processes. Consequently, the final state interaction, which smears out the contribution of short distances in most of the low-energy processes should be suppressed in high-energy deep-inelastic processes.

In a complete theory of high-energy processes, the intuitive picture of how a collision takes place plays an interesting, but not a crucial, role. Lacking such a theory, the intuitive picture acquires a more

†We take here the rather conservative attitude that up to nucleon momenta of about  $1 \text{ GeV}/c$  the nucleus can be described as a many-nucleon system and that the short-range NN interaction can be calculated in terms of perturbative QCD.

‡See discussion in the beginning of section 2.5.

important significance. It substitutes a theory and aids us in developing models for interpreting and correlating experimental facts. In section 2 we explain that the possibility to apply the experience of nuclear physics to high-energy processes is based on two fundamental properties of quantum field theory: (1) the space-time description of the fast particle fragmentation region has a close resemblance to the time-ordered perturbation-expansions in non-relativistic theory. Various field effects cancel [78], only the simplest contributions survive which are associated with time-ordered graphs having the same connectedness structure as in potential scattering. (2) Gribov, Ioffe and Pomeranchuk [79] were the first who realized that longitudinal distances in the strong interaction increase with initial energy. Later the phenomenon was observed in the data on the inelastic electron scattering [80]. To account for these general features of quantum field theory and to assess the role of the nucleon degrees of freedom, the infinite momentum frame (light cone) wavefunctions (WFs) should be used [40]. The necessity of using such WFs is illustrated in section 2.1 by considering a familiar example, namely  $e^+ e^-$  pair production by a virtual photon from the Coulomb nuclear field. In sections 2.3 and 2.4 the basic properties of light-cone WFs of nuclei, the Weinberg equation and the relationship with conventional nuclear-theory are discussed.

The formulae derived in sections 2 and 3, which account for the relativistic retardation, recoil and Lorentz rotation of spin and for Glauber screening (in the case of hadronic reactions) are in a good agreement with the data on elastic and inelastic high  $Q^2$  electron-deuteron scattering [4–7] obtained in SLAC. Also the data from Dubna and LBL [11–13, 20] on the backward  $p, \pi$  production in the process  $p + D \rightarrow p(\pi) + X$  showing the so called cumulative effect can be explained. These predictions are rather restrictive due to the relationship between the Weinberg equation and conventional Schrödinger equations for the deuteron WF. The derived equations predict a strong dependence of the inclusive cross sections on the deuteron polarization as a consequence of the nuclear core in the NN interaction [81].

It seems now difficult to derive all nuclear physics dynamics directly from QCD since the energy of non-perturbative vacuum is lower than the energy of perturbative vacuum. (Instanton is the simplest example of such fluctuations.) Evidently, this phenomenon leads to some suppression of colour fluctuations in a large volume, diminishing probability of quark configurations with hidden colour. Such suppression is more important for nucleus than for nucleon due to presence of white three quark subsystems. However, due to asymptotic freedom in QCD and small value of the effective coupling constant for short-range phenomena one can expect that the high momentum behaviour of the nucleus WF can be described in terms of perturbative QCD.

We demonstrate (section 4) that a rather smooth correspondence exists in a wide range of nucleon momenta ( $\leq 0.8\text{--}1 \text{ GeV}/c$ ) between the QCD perturbative quark-gluon WF of the deuteron and the two-nucleon deuteron WF with nuclear core. This ensures the duality between a description of the deuteron in terms of quark and nucleon degrees of freedom.<sup>‡</sup> The smooth correspondence disappears at large nucleon momenta which means that different quark-gluon components of the WF dominate in different processes. For example, the 6q (6 quark) component determines deep inelastic lepton-deuteron scattering at  $x_{Bj} = -q^2/2m_N v \rightarrow 2$  [37, 65] though the leading proton (pion) production is determined by 6q + 3g (6q + 5g) component [75].

Since nuclei with  $A > 2$  are more tightly bound systems than the deuteron, one should expect that in high-energy scattering from nuclei short-range phenomena play a more important role than in the case of the deuteron. Even for a loosely bound system like the deuteron realistic WFs contain a rather lar-

<sup>‡</sup> Basically, this is due to the lack of large inelasticities in the lowest NN phase-shifts and due to asymptotic freedom in QCD.

ge high momentum fraction (section 3), namely [38]:  $\int \psi_D^2(k) \theta(k - 0.3 \text{ GeV}/c) d^3k = 4\text{--}5\%$ . The estimate of the nuclear WF, using the dilute gas approximation and a calculation of a single nucleon density matrix for  ${}^4\text{He}$  [82] suggests that for heavy nuclei 15–25% of the nucleons could have momenta larger than  $0.3 \text{ GeV}/c$  (section 2.4).†

In this review we aim to demonstrate that, similarly to the deuteron case, high-energy processes can be used to find the answer to the basic questions about the short-range nuclear structure:

- (a) What is the real amount and shape of the high momentum components in the WF?
- (b) What is the relative importance of the average field configurations and two-nucleon correlations?
- (c) How to discover two-, three-nucleon correlations?
- (d) Are the colour degrees of freedom in nuclei essential, and how can one reveal them?

In section 5 we explain that deep inelastic ( $e, e'$ ) reactions at  $x_N = -q^2/2m_N q_0 > 1$  can provide an unambiguous answer to question (a). For instance in the case of the lightest nuclei  ${}^3\text{He}$ ,  ${}^4\text{He}$ , the absolute value and momentum dependence of the data on high  $Q^2$  in the  $e + {}^3\text{He} \rightarrow e + X$  reaction [8], the data on the production of fast backward protons and pions from  ${}^4\text{He}$  in high-energy hadronic reactions [13] and the data on  ${}^4\text{He}$  photo-disintegration [86] are in reasonable agreement with predictions of two body correlation approximation for the nuclear WF [45].

We want to emphasize that large cross sections for ( $e, e'$ ) reactions are expected for heavy nuclei within the two-body correlation approximation:  $(1/A)F_{2A}(x = 1.2) \approx (6\text{--}8) \frac{1}{2}F_{2D}(x = 1.2)$  for  $A > 12$  and even larger when three-body correlations are accounted for.

Deep inelastic reactions  $\ell + A \rightarrow \ell' + \text{fast backward proton} + X$  provide a real possibility to answer questions (b), (c) by measuring not only the WF but also the correlation function [45]. We explain (section 6) that the observed correlations in the recently investigated deep inelastic  $\nu(\bar{\nu}) + A \rightarrow \mu^- + p + X$  reactions [9, 10] indicate the dominance of few-nucleon correlations (mostly, two-nucleon correlation) over average field configurations at nucleon momenta  $> 0.4 \text{ GeV}/c$ . In particular, we demonstrate that the mean field models [44, 46–48, 59] underestimate the observed backward proton yield in these reactions by a factor  $\sim 300$  [87].

Significant information related to questions (a), (b), (c) can be obtained also from hadronic reactions of the type  $h + A \rightarrow (\text{fast backward } p, \pi, \dots) + X$ , where  $p(\pi, \dots)$  is registered in the region forbidden for scattering from a free nucleon (sections 7 and 8). Probably the first attempt to extract the nuclear WF from such processes have been made by Lederman and colleagues [1] who measured below threshold antiproton production:  $p + A \rightarrow \bar{p} + X$ . Later Baldin [36] emphasized the advantages of studying production of fast backward pions for the investigation of short-range phenomena in nuclei at energies where Feynman scaling is achieved. In the last few years a large amount of data on these reactions covering the range from  $E_h \sim 1 \text{ GeV}$  [23–35] up to  $E_h = 400 \text{ GeV}$  [11–22] have been accumulated. They reveal a number of simple regularities (for a review see section 8). For example, the shapes of  $p$ ,  $\pi$  inclusive spectra from the lightest ( $D$ ,  ${}^4\text{He}$ ) and heavy ( $\text{Pb}$ ) nuclei are practically the same and do not depend on the sort of projectile used ( $p, \pi, \gamma, \nu, \bar{\nu}$ , light nuclei) or on the incident energy (at  $E_h > \text{few GeV}$ ).‡ We demonstrate that these data as a whole provide a restrictive test of existing models

† There is no direct relation between the momentum distribution of nucleons, measured in the high-energy processes, where the momentum transfer to the nucleus is large ( $> 2k_F$ ), and the Fermi momentum of quasi-particles, measured in the low-energy processes. For example, the shell model “hides” the repulsive core of NN interaction in the effective potential. However, significant renormalization factors for quasi-particles [83], comparatively large cross sections of such low-energy reactions as the nuclear photo-disintegration or pion absorption are experimental indications that the high momentum component in the nuclear WF is not small [84, 85].

‡ The universality of the shape of nucleon momentum spectra was suggested in [14] on the basis of a phenomenological analysis of the data [2], where production of fast backward protons in high energy reactions was observed firstly.

of the short-range nuclear structure (section 8.6). Our analysis (sections 8.1–8.5) indicates that basic features of these reactions can be quantitatively described within the framework of the Gribov–Glauber model [89] as a manifestation of few-nucleon correlations whose WFs are consistent with the QCD analysis (section 4). We prove that the impulse approximation is valid for the inclusive production of fast backward  $\pi$ ,  $K$ ,  $\Lambda \dots$  at high energies [71]. For nucleon production the Glauber screening has a simple form. As a result the spectrum of backward nucleons-spectators is roughly proportional to the single nucleon density matrix of the nucleus [71]. Consequently the high momentum tail of the nuclear WF can be investigated with a number of cross checks. The data on fast backward  $p$ ,  $\pi$  production indicate the dominance of two-nucleon correlations in the nuclear WF (in its kinematical region) [45, 71, 74], and the presence of noticeable three and four-nucleon correlations [71, 72]. In particular, on the basis of an analysis of the Weinberg equation (section 2.4) and QCD (section 4) we calculate the absolute cross section, momentum and angular dependence of the fast backward proton, pion, deuteron, triton production in high-energy reactions, and also their dependence on the target mass number and the projectile energy. The calculated nuclear WF with the probabilities of the few-nucleon correlations extracted from the 400 GeV data [18] could describe the intermediate-energy (600–800 MeV) inclusive [23–25] and correlation [27, 28, 30, 31] data (section 8.2). Thus this theoretical analysis suggests that the effective nuclear WF extracted by Amado, Woloshin and Frankel [44, 59] from inclusive data is saturated by the few-nucleon correlations.

To answer question (d) about the role of colour degrees of freedom in the nucleus structure one must first establish definitely the two-, three-nucleon correlations by performing correlation experiments. Once they are found, they would provide a base for the search of colour effects. Some of such “second generation” experiments are discussed in this review.

## **2. Where are the relativistic effects in the deuteron essential and how to take them into account<sup>†</sup>**

In this section we shall focus our attention on two general features of high-energy scattering off a bound state:

- (a) the increase with initial energy of longitudinal distances in the strong interaction [79],
- (b) a simple form of causality in the fast particle fragmentation region – the vanishing of vacuum fluctuations [78]. These properties are common for all generally accepted models of strong interaction such as the multiperipheral model, parton model, perturbative QCD and are confirmed experimentally (for recent reviews see [80]). We show here that account of the phenomena mentioned above gives a practical possibility to describe the short-range nuclear structure in a consistent way. One should recall that the traditional methods of intermediate-energy physics like the Glauber approach do not take into account either these general features or multiparticle production. Therefore it is necessary to modify these methods to adjust them for the description of high-energy processes.

### *2.1. Some general features of relativistic bound states*

The basic purpose of this subsection is to demonstrate that the high momentum component of the WF of a relativistic bound state can be measured only in high-energy processes and that the

<sup>†</sup> A reader who is mostly interested in the discussion of the short-range phenomena can first read sections 3, 5–8 since the final formulae for any process considered in the review have an evident resemblance to the expectations of familiar Glauber theory and have a transparent interpretation within the parton model.

non-covariant light cone WF—the infinite momentum frame (IMF) WF—should be used to describe a bound state in the relativistic theory.

To elucidate the space-time evolution of a scattering process and the role of relativistic phenomena we shall consider the process of  $e^+e^-$  pair production by a fast virtual photon  $\gamma^*$  off the Coulomb field (of a heavy nucleus) in lowest order of perturbation theory. (To avoid long range forces we restrict ourselves to the case of the screened Coulomb field of the nucleus.) For a general discussion of the space-time evolution in relativistic theory see Gribov's lecture [78].

We want to express the production of a fast electron in the inclusive process  $\gamma^* + Z \rightarrow e + X$  in terms of the  $e^+e^-$  Fock component of the virtual photon ( $\gamma^*$ ) WF and to find a region where the impulse approximation is valid. In lowest order in the fine-structure constant, the  $e^+e^-$  component of the  $\gamma^*$  WF is determined by a pointlike interaction of  $e^+e^-$  with  $\gamma^*$  in coordinate space. (In some sense, this example can be considered as a relativistic generalization of the familiar Bethe-Peierls theory [154] of the deuteron, when both nucleons are out of the range of nuclear forces.) The inclusive process  $\gamma^* + Z \rightarrow e + X$  is described by four diagrams of the old fashioned noncovariant perturbation theory.

Black blobs in figs. 2.1–2.4 correspond to nuclear formfactors. The index C denotes instantaneous Coulomb photon exchange. (Here we use the Coulomb gauge.) The time axis runs from left to right. The contributions of these diagrams to the production amplitude differ mostly due to energy denominators:

$$\begin{aligned} D_1 &= -\sqrt{\mathbf{Q}^2 + q^2} + \sqrt{m_e^2 + \mathbf{p}_e^2} + \sqrt{m_e^2 + (\mathbf{p}_e + \mathbf{n})^2} \\ D_2 &= -\sqrt{\mathbf{Q}^2 + q^2} + \sqrt{m_e^2 + \mathbf{p}_e^2} + \sqrt{m_e^2 + (\mathbf{p}_e - \mathbf{Q})^2} \\ D_3 &= \sqrt{m_e^2 + \mathbf{p}_e^2} + \sqrt{m_e^2 + (\mathbf{p}_e - \mathbf{Q})^2} \\ D_4 &= \sqrt{m_e^2 + \mathbf{p}_e^2} + \sqrt{m_e^2 + (\mathbf{p}_e + \mathbf{n})^2}. \end{aligned} \quad (2.1)$$

Here  $\mathbf{Q}$ ,  $\mathbf{p}_e$ ,  $\mathbf{p}_{e^+}$ ,  $\mathbf{n}$  are the three momenta of the  $\gamma^*$ ,  $e^-$ ,  $e^+$ , and Coulomb field  $Z$  correspondingly in the nucleus rest frame and  $q^2$  is the  $\gamma^*$  mass squared.

In the particular case of the non-relativistic inner motion of the  $e^+e^-$  pair (i.e. for virtual photon with “mass”  $q^2 > 0$  and  $|q^2 - (\mathbf{p}_e + \mathbf{p}_{e^+})^2| \ll m_e^2$ ) the energy denominators for the diagrams in figs. 2.1, 2.2 are smaller than those for the diagrams in figs. 2.3, 2.4. As a result the essential diagrams for the considered process are the same as in non-relativistic quantum mechanics (no vacuum pair production). In the general case at intermediate  $\gamma^*$  energies  $q_0 \sim 2m_e$  there exists no process to which only the positive frequency high momentum component of the  $\gamma^*$  WF contributes. Indeed, in the kinematics, where the

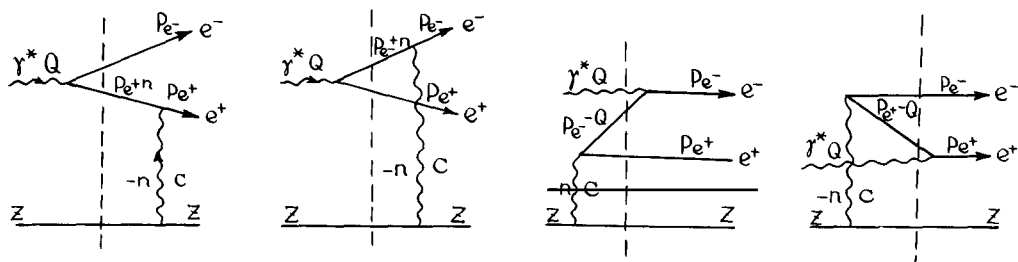


Fig. 2.1.

Fig. 2.2.

Fig. 2.3.

Fig. 2.4.

Figs. 2.1–2.4. The non-covariant diagrams for the Bethe-Heitler process:  $\gamma^* + Z \rightarrow e^+e^- + Z$ .

energy denominators  $D_1, D_2$  are large (large momentum  $n \sim m_e$  is transferred to the nucleus) the denominators  $D_3, D_4$  are also large and of the same order. As a result, all four diagrams (and in particular the diagrams in figs. 2.3, 2.4 corresponding to production of  $e^+e^-$  pair from vacuum by the Coulomb field) give comparable contributions. On the contrary, in the case of high incident energy the contribution of the vacuum polarization (diagrams 2.3, 2.4) becomes small  $\sim 1/q_0^2$  as compared to the diagrams 2.1, 2.2 ( $D_1^{-1} \sim D_2^{-1} \sim q_0, D_3^{-1} \sim D_4^{-1} \sim 1/q_0$ ) provided the photon has transverse polarization. Therefore at high energies the cross section is expressed through the positive frequency part of the  $\gamma^*$  WF (see below).

For the following analysis it is convenient to introduce the variables  $\alpha/2 = (p_{e_0} + p_{e_z})/(q_0 + q_z)$  – the light cone fraction of fast  $\gamma^*$  momentum carried by electron,<sup>†</sup>  $p_\perp$  – the electron transverse momentum (the  $z$  axis is chosen in the direction of the  $\gamma^*$  momentum). A convenient property of variable  $\alpha$  is that it is invariant under Lorentz boosts along the  $z$  direction. It is easy to demonstrate that in the essential kinematical region the fraction of the  $\gamma^*$  momentum transferred to the nucleus is negligible and therefore  $n^2 \sim -n_\perp^2$ . In the case of transverse polarization of  $\gamma^*$  the result of calculation has the form:

$$E \frac{d^3\sigma^{\gamma^*\mu_T \rightarrow e^+Z \rightarrow e^+e^-}}{d^3p} = \int d^2n_\perp \frac{d\sigma^{e^+Z \rightarrow e^+Z}}{dn_\perp^2} \frac{|\psi_{\mu_T}(\alpha, p_\perp) - \psi_{\mu_T}(\alpha, p_\perp + n_\perp)|^2}{2-\alpha}. \quad (2.2)$$

We account for the contributions of both electron and positron scattering off  $Z$  and make use of the equality of high energy cross sections

$$d\sigma^{e^- + Z \rightarrow e^- + Z}/dn_\perp^2 = d\sigma^{e^+ + Z \rightarrow e^+ + Z}/dn_\perp^2.$$

Here  $\psi_{\mu_T}(\alpha, p_\perp)$  describes the  $e^+e^-$  component of the transverse photon in lowest order in  $e^2$

$$\psi_{\mu_T} = \frac{\bar{U}(\alpha, p_\perp) \gamma_{\mu_T} V(1-\alpha, -p_\perp)}{q^2 - 4(m^2 + p_\perp^2)/(\alpha(2-\alpha))}. \quad (2.3)$$

If one introduces an auxiliary variable  $k_3$  by the equation:

$$\alpha = (1 + k_3/\sqrt{k^2 + m^2}), \quad k_\perp = p_\perp \quad (2.4)$$

eq. (2.3) takes the form of the Bethe–Peierls approximation familiar from deuteron physics

$$\psi_{\mu_T} = \frac{\bar{U}(\alpha, k_\perp) \gamma_{\mu_T} V(1-\alpha, -k_\perp)}{q^2 - 4(m^2 + k^2)}. \quad (2.5)$$

The only difference is that the deuteron mass squared is changed to  $q^2$  – the photon “mass” squared. This WF depends on the internal variables of the  $e^+e^-$  pair, i.e. the c.m. motion is separated. The spin structure of  $\psi_{\mu_T}$  and its dependence on a single variable – the invariant mass of  $e^+e^-$  system – instead of two independent variables  $\alpha, k_\perp$  follow from the condition that the system has spin 1 and consists of two particles only. We shall refer to this important constraint as to the angular condition.

The transparent form of eqs. (2.2), (2.5) is a direct consequence of the increase of longitudinal

<sup>†</sup> The definition of  $\alpha$  allows  $0 \leq \alpha \leq 2$ . This is more convenient for the purposes of nuclear physics than conventional  $\tilde{\alpha} = \alpha/2 < 1$ .

distances with initial energy. Really, at  $q_0 \rightarrow \infty$   $\gamma^*$  converts into the  $e^+e^-$  prescattering state long before  $\gamma^*$  reaches the nucleus, because the characteristic length  $c \cdot t_\gamma$  of this fluctuation is much larger than the scale  $1/|n| \sim \text{const}$ , which determines the space region, where the interaction with the nucleus occurs

$$c \cdot t_\gamma \sim \frac{c}{E_{e^+} + E_{e^-} - q_0} \sim \frac{2q_0}{4(m^2 + k_\perp^2)/\{\alpha(2-\alpha)\} - q^2} > \left| \frac{1}{n} \right|. \quad (2.6)$$

This interpretation explains the onset of the Feynman scaling. (1) At  $q_0 \rightarrow \infty$  the cross section is energy independent and is given by eq. (2.2). (2) At finite  $q_0$  eq. (2.6) gives the kinematical region, where the scaling is achieved. As a result, the scaling limit for  $E_e d^3\sigma^{\gamma^* \rightarrow e^+ e^- \dots} / d^3p_e$  is reached at different  $\alpha$  for different energies. For example the limit  $\alpha \rightarrow 2$  is reached only at  $q_0 \rightarrow \infty$ , see fig. 2.5.

The physical picture illustrated in fig. 2.5 really follows from the energy dependence of the minimal momentum transfer to the nucleus. If the energy transfer to the  $e^+e^-$  pair is sufficiently large (e.g. if  $n_\perp^2 \gg (2-\alpha)(m_e^2 + p_\perp^2)/\{\alpha(2-\alpha)\} - q^2$ ) either  $\psi(\alpha, p_\perp)$  or  $\psi(\alpha, p_\perp + n_\perp)$  is small and one could omit the interference term  $\psi(\alpha, k_\perp)\psi(\alpha, k_\perp + n_\perp)$  in eq. (2.2) and the final answer takes the form

$$E \frac{d^3\sigma^{\gamma^* \mu_T \rightarrow e^+ e^- \dots}}{d^2p} = \int d^2n_\perp \frac{d\sigma^{e^+ e^- \rightarrow e^+ e^-}}{d^2n_\perp} \{\psi_{\mu_T}^2(\alpha, p_\perp) + \psi_{\mu_T}^2(\alpha, p_\perp + n_\perp)\}(2-\alpha)^{-1}. \quad (2.7)$$

This theoretical example illustrates the origin of problems, involved in measuring the high momentum components of the bound state. In particular it follows from the above consideration that the value of the interference term, which in our case models the final state interaction is determined by the energy transferred to the bound state. If this energy is larger than the energy characterizing the bound state configuration probed, the final state interaction can be neglected and thus the measuring process is incoherent.

It is worth noting that eq. (2.7) has the form of the conventional impulse approximation: the WF of  $\gamma^*$  times the cross section of the elementary process. However the relationship between the virtual photon WF and the elementary amplitude is evidently different from the formulae of non-relativistic quantum mechanics in two ways: (a) another relation between spectator momentum and the argument of the WF. (b) There is no Möller flux factor in the numerator in eq. (2.7). On the contrary the factor  $2-\alpha$  is present in the denominator. All these differences arise due to accurate account of vacuum fluctuations in eq. (2.7) by using the IMF WF of  $\gamma^*$ . (Note that if we choose  $q^2 > 0$  and try to express the cross section in terms of the rest frame WF of  $\gamma^*$  we should include negative frequency parts of the  $\gamma^*$  WF.)

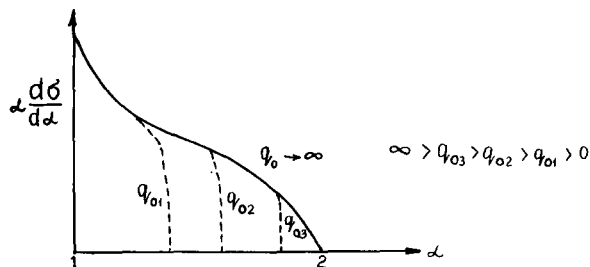


Fig. 2.5. Onset of scaling in the reaction  $\gamma^* + Z \rightarrow e^+ + X$  at large  $\alpha$  as a function of the incident photon energy.

It is easy to check by direct calculation, that the case of the longitudinal polarization is more complicated. Here the vacuum diagrams in fig. 2.3, 2.4 cannot be neglected, since the components of the longitudinal polarization vector  $\gamma^*$ :  $\epsilon^L = (q_z, q_0)/\sqrt{-q^2}$  increase with initial energy. However the amplitude for the longitudinal polarization of  $\gamma^*$  can be reconstructed through the contribution of large longitudinal distances using gauge invariance [89].

Conclusions:

1. High energies are necessary to investigate the high momentum component of the bound state experimentally. Besides, one should select processes with sufficient energy transfer to neglect the final state interaction.

2. At high energies due to the increase of longitudinal distances the prescattering state of a fast particle is formed long before the scattering occurs. As a result the cross section can be expressed through the WF of the bound state.

3.  $\psi_{\mu_T}^{\gamma^*}$  is the IMF (light cone) non-covariant WF of  $\gamma^*$ , whose spin structure and dependence on internal variables follow from the condition that the  $e^+e^-$  pair has spin 1.

4. An equivalent interpretation of eq. (2.7) is possible. If one uses eq. (2.5) for  $\psi_{\mu_T}$ , eq. (2.7) has the form of a dispersion representation of the scattering amplitude over  $q^2$  ( $\gamma^*$  mass) [89]. This physical picture and the form of eq. (2.7) are essentially more general than the considered theoretical example. They are also valid in the multiperipheral model [88], parton model [90] and for renormalizable quantum field theories like QED, QCD in the so-called leading logarithmic approximation, etc.

## 2.2. Relativistic impulse approximation

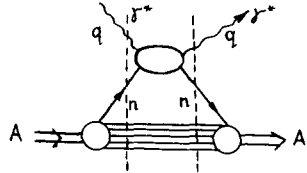
In this subsection we explain how the methods of quantum field theory can be used to account for the space-time evolution of the scattering process. To be definite, we calculate first the structure functions for deep inelastic e-nucleus scattering (i.e. the imaginary part of the forward  $\gamma^* + A \rightarrow \gamma^* + A$  scattering amplitude) at large  $q^2$ , where the impulse approximation is applicable. We restrict the consideration to the case of spinless particles (spin effects will be briefly discussed in section 2.3).

To deduce the basic formulae we start from the celebrated Lehmann, Symanzik, Zimmermann (LSZ) representation for the causal amplitude  $A_{\mu\lambda}^{\gamma^*A}$  [91], which is valid in all orders of perturbation theory

$$A_{\mu\lambda}^{\gamma^*A} = \int \exp\{iqx + ip_A(y_1 - y_2)\} \langle 0 | T j_A(y_1) j_\mu(x) j_\lambda(0) j_A(y_2) | 0 \rangle d^4y_1 d^4y_2. \quad (2.8)$$

Here the symbol T denotes, as usual, time ordering;  $j_\mu(x)$ ,  $j_\lambda(0)$  are Heisenberg operators of the electromagnetic current,  $j_A(x) = (\square + M_A^2) A(x)$  and  $A(x)$  is the Heisenberg operator, which interpolates the nucleus field.  $A(x)$  can be defined for the composite system following the Zimmermann procedure [92].  $q$  and  $p_A$  are the momenta of  $\gamma^*$  and the nucleus. All notations correspond to fig. 2.6, which describes the cross section of  $\gamma^*A$  scattering. Possible contact terms, which correspond to instantaneous interactions are omitted in eq. (2.8) since we are interested in the contribution of configurations in which the prescattering state of the nucleus is formed long before the interaction occurs (cf. section 2.1). In many important cases contact terms are absent or can be reconstructed through the contribution of large longitudinal distances by applying gauge and Lorentz invariance to the S-matrix.

In order to suppress fluctuations in the virtual photon wavefunction (production of pairs by  $\gamma^*$ ) it is convenient to choose the c.m.s. of the e and A collision and take the limit

Fig. 2.6. The cross section of  $\gamma^* A$  scattering.

$p_A = -p_e = P \rightarrow \infty$ . As a result the  $\gamma^*$  momentum is equal to  $q = ((2\nu + q^2)/4P, (-2\nu + q^2)/4P, q_\perp)$ . Here  $\nu = (p_A q)$  and  $q^2$  is the invariant mass squared of  $\gamma^*$ . In this reference frame  $\gamma^*$  is almost transverse  $q \approx q_\perp$  and cannot produce pairs. Really, if  $\gamma^*$  converts into pair of particles with momenta  $\pm \alpha P$ , the corresponding energy denominator is large  $\sim \sqrt{\alpha^2 P^2 + k_\perp^2 + m^2} + \sqrt{\alpha^2 P^2 + m^2 + k_\perp^2} - 2q_0 \approx 2|\alpha|P$ . Therefore the contribution of such diagrams vanishes at  $P \rightarrow \infty$ . For the considered process at  $\nu, -q^2 \rightarrow \infty$  and fixed  $x = -q^2/2m\nu$  the characteristic lifetime of the prescattering state  $1/(E_n - E_A) \sim 2P/(M_n^2 - M_A^2)$  (cf. eq. (2.6)) is much larger than the essential time of collision  $\sim 1/q_0 \sim 4P/(2\nu + q^2)$  [90]. As a result the impulse approximation is justified. To account for the nucleon structure of the nucleus we consider at first the dispersion approach, which appears rather successful in the description of photon scattering from nucleons and nuclei (the so called vector dominance model; for recent review see e.g. [80]).

### 2.2.1. Dispersion approach

Now, let us outline the basic steps in the derivation of the impulse approximation for the scattering from a bound state. First we claim that only the time-ordering  $y_{10} > x_0 > y_{20}$  is essential in the T-product of eq. (2.8).

In the case  $\nu > 0$  only the  $x_0 > 0$  region contributes in the imaginary part of  $A_{\mu\lambda}$ . To demonstrate this one uses the completeness of the nuclear states  $|n\rangle$ :  $1 = \sum |n\rangle\langle n|$  and chooses  $|n\rangle$  as eigenstates of the free Hamiltonian. It is easy to check (cf. section 2.1) that the essential energy denominators obtained after integration over  $d^4y_1 d^4y_2$  correspond to the time ordering chosen above. They are of order  $(M_n^2 - M_A^2)/2P$  (cf. eq. (2.6)). The energy denominators corresponding to other time orderings in eq. (2.8) are of order  $P$  or  $q^2/P$ . The diagrams with energy denominator  $\sim P$  are zero or lead to contact terms.

The essential contribution after the integration over  $d^4y_1, d^4y_2$  has the form (see fig. 2.6)

$$\text{Im } A_{\mu\lambda}^{\gamma^*+A \rightarrow \gamma^*+A} = \sum_n \int \frac{|\langle 0 | j_A | n \rangle|^2}{(M_n^2 - M_A^2)^2} dr_n \langle n | \int e^{i\tilde{q}x} j_\mu(x) j_\lambda(0) | n \rangle d^4x. \quad (2.9)$$

Here the sum goes over the nuclear states with positive energy and

$$\tilde{q} = \left( q_0 + \frac{M_A^2 - M_n^2}{2P}, \mathbf{q} \right) \quad (2.9a)$$

and  $M_n^2$  is the squared mass of the  $|n\rangle$  state. To obtain eq. (2.9) we have used the fact that in the impulse approximation the initial and final nuclear states are identical. It is convenient to define

$$\psi_A = \langle 0 | J_A | n \rangle / (M_n^2 - M_A^2), \quad (2.10)$$

which is the dispersion representation of the WF of nuclei. Evidently the cross-section can be expressed

in terms of the nucleon density matrix (for a discussion of properties of  $\rho_A^N$  see section 2.4)

$$\rho_A^N(\alpha, k_\perp) = \int |\psi_A(\alpha, k_\perp, r_{n'})|^2 dr_{n'} . \quad (2.11)$$

The integration in eq. (2.11) runs over the variables  $r_{n'}$ , characterizing residual particles in the state  $|n\rangle$ , which do not participate in the interaction with  $\gamma^*$  (see fig. 2.6). The result has the form [75]:

$$\text{Im } A_{\mu\lambda}^{\gamma^*A} = \int \rho_A^N(\alpha, k_\perp) \frac{d\alpha}{\alpha} \frac{d^2 k_\perp}{\alpha} \langle n | e^{i\vec{q}x} j_\mu(x) j_\lambda(0) | n \rangle d^4 x . \quad (2.12)$$

Here  $\alpha/A$  is the fraction of the nucleus momentum carried by the interacting nucleon. (To be specific we restrict ourselves here to the scattering from nucleons only.) The amplitude of the  $\gamma^* + n$  process is on the energy shell. The form of eq. (2.9) is rather similar to Gribov's dispersion representation on the  $\gamma^*$  mass for the amplitude of  $\gamma^*$  nucleus scattering [89].

The theoretical analysis of the ladder diagrams performed by Mandelstam [93] and the QCD analysis of short-range nucleus structure (see section 4) indicate, that the integration in the eq. (2.11) runs over states with finite mass  $M_n$  (not increasing with the initial energy). In eq. (2.12) low-energy physics, i.e. the  $A \rightarrow |n\rangle$  transition is separated from the high-energy dynamics of  $\gamma^*|n\rangle$  interaction. Thus it gives a practical possibility to find essential configurations in the process and to estimate the probabilities of different configurations.

### 2.2.2. The estimate of resonance admixtures in the nuclear WF

The approximation of only nucleon constituents for the deuteron seems to work in a rather wide region up to a nucleon momentum  $k_N$  of order 1 GeV/c. Indeed the real parameter characterizing the presence of other states in the deuteron WF is the value of inelasticities in the lowest partial waves. Existing analyses of phase shifts seemingly point out that the lowest phases  ${}^3S_1$ ,  ${}^1S_0$  are mostly elastic within experimental errors up to a kinetic energy  $T_{\text{kin}} \sim 3$  GeV in NN-scattering (see e.g. [94]). These small values of inelasticities can be foreseen theoretically, for noticeable inelasticities at low energies result from resonances production. (This seems to agree with experimental data on NN scattering at  $T_{\text{kin}} < 5$  GeV (see e.g. [95]).) As a result the lowest inelastic thresholds in the deuteron phases probably correspond to channels  $NN^*(1470)$ ,  $2\Delta(1232)$ , i.e. to a rather large invariant mass of the NN system ( $T_{\text{kin}} \sim 1.2$  GeV). Thus the two-nucleon approximation should be valid in a considerably larger energy interval than that determined by the  $\pi$ -meson mass.

This analysis is in line with the QCD analysis of section 4, which shows, that the  $\Delta\Delta$  component in the deuteron WF is suppressed. In the isospin  $T = 1$  P-wave the inelasticities are not small due to the reaction  $N + N \rightarrow N + \Delta$ . Therefore the  $\Delta$  admixture to the nuclear WF could be larger than in the deuteron.

### 2.2.3. The final formulae

To obtain the final equation from eq. (2.12), it is useful to introduce independent inelastic formfactors for any target by the formulae (see e.g. [90])

$$\text{Im } A_{\mu\lambda}^{W^*+T \rightarrow W^*+T} = \frac{W_{2T}}{M_T} \left( P_\mu - q_\mu \frac{pq}{q^2} \right) \left( P_\lambda - q_\lambda \frac{pq}{q^2} \right) - W_{1T} M_T \left( g_{\mu\lambda} - \frac{q_\mu q_\lambda}{q^2} \right) - i \epsilon_{\mu\lambda\sigma\rho} p_\sigma q_\rho \frac{W_3}{2M_T} \quad (2.13)$$

for generality we consider the amplitude of any electromagnetic or weak current scattering.

The cross section of the inclusive process  $\ell + T \rightarrow \ell' + X$  is directly expressed through these form factors (see e.g. [90]). For example in the case of electron scattering

$$\frac{d\sigma}{d\Omega dE'} = \frac{\alpha^2}{4E^2 \sin^4 \frac{1}{2}\theta} [W_2 \cos^2 \frac{1}{2}\theta + 2W_1 \sin^2 \frac{1}{2}\theta].$$

Here  $E$  is the energy of the initial electron and  $\theta$  is the scattering angle in the target rest frame.

Using eqs. (2.12), (2.13) we obtain:

$$\begin{aligned} W_{1A}(\nu, q^2) &= \frac{M_N}{M_A} \sum_N \int \rho_A^N(\alpha, k_\perp) \frac{d\alpha}{\alpha} d^2k_\perp \left\{ W_{1N}(\tilde{\nu}, q^2) + W_{2N} \frac{k_\perp^2}{2M_N^2} \right\} \frac{A}{\alpha} \\ W_{2A}(\nu, q^2) &= \frac{M_A}{M_N} \sum_N \int \rho_A^N(\alpha, k_\perp) \frac{d\alpha}{\alpha} d^2k_\perp \alpha W_{2N}(\tilde{\nu}, q^2)/A \\ W_{3A}(\nu, q^2) &= \frac{M_A}{M_N} \sum_N \int \rho_A^N(\alpha, k_\perp) \frac{d\alpha}{\alpha} d^2k_\perp W_{3N}(\tilde{\nu}, q^2). \end{aligned} \quad (2.14)$$

Here

$$\tilde{\nu} = (\nu + M_A^2 - M_n^2)\alpha/A + k_\perp q_\perp$$

(cf. eq. (2.9a)). To suppress the contribution of contact terms (vacuum fluctuations) we express  $W_{2A}$  through  $\text{Im } A_{00}^{W^*A}/P^2$  and  $W_{1A}$  through  $\text{Im } A_{\mu_1\lambda_1}^{W^*A}$ . To calculate  $W_{3A}$  we choose transverse and zero polarizations of the weak current. In the derivation we neglect possible vacuum fluctuations, which is reasonable only, if  $\nu$  is sufficiently large (cf. section 2.1). This approximation is best for  $W_{2A}$  case due to superconvergence of eq. (2.14b).

For practical applications it is important, that  $\psi_A$  given by eq. (2.10) is invariant under Lorentz transformations. Therefore independent variables are the momenta  $k_i$  of nucleons in the c.m. of the state  $|n\rangle$ . They are related to the variable  $\alpha_i$  by the Lorentz transformation:

$$\alpha_i = A(\sqrt{m^2 + k_i^2} - k_{3i}) / \sum_{j=1}^A \sqrt{m^2 + k_j^2}. \quad (2.15)$$

The dispersion method gives a possibility to calculate any high-energy process in terms of the nuclear WF. Extracting this WF from some process one can calculate any other process. It has been shown in [45] that this program works effectively for the deuteron, where a number of phenomena dominated by short internucleon distances were experimentally investigated (see also section 3).

#### 2.2.4. Light cone approach

To achieve a more transparent correspondence with conventional methods of nuclear physics we discuss below a closely related method: the light cone quantum mechanics for nuclei. As above we illustrate the technique by considering the process  $\gamma^* + A \rightarrow \gamma^* + A$  and using the LSZ representation for the scattering amplitude. We introduce the interaction representation, where the NN interaction is

switched off. As a result the scattering amplitude takes the form:

$$\begin{aligned} A_{\mu\lambda} = & \int \exp\{i(p_A y_1 - p_A y_2 + qx)\} \langle 0 | j_A(y_1) U^{-1}(x_0) | n \rangle dr_n \\ & \times \langle n | \tilde{j}_\mu(x) U(x_0) U^{-1}(0) \tilde{j}_\lambda(0) | n \rangle dr_n' \langle n' | U(0) j_A(y_2) | 0 \rangle \theta(y_{10} - x_0) \theta(-y_{20}) d^4 y_1 d^4 y_2 d^4 x. \end{aligned} \quad (2.16)$$

All the notations are the same as in eq. (2.8). Here  $U(t)$  is the operator of evolution, which accounts for the interaction between nucleons during the time intervals  $(\infty, x_0)$  and  $(0, -\infty)$ ;  $|n\rangle$  are the eigenstates of the Hamiltonian of noninteracting nucleons.  $\tilde{j}_\mu$  is the electromagnetic current in the interaction representation. Since the time of collision  $\sim 1/q_0$  is much smaller than the scale, which characterizes the strong interaction:  $1/q_0 \ll 2P/(m_n^2 - m_A^2)$ , the product of time development operator  $U^{-1}(x_0) U(0) \approx 1$  at  $q^2 \rightarrow -\infty$ , and we obtain the impulse approximation. Concerning this point we repeat conventional arguments of the parton model (see e.g. [90]), which are also true in QCD in the leading logarithmic approximation. (To simplify theoretical description we account only for nucleon degrees of freedom and neglect the off-energy-shell effects in the nucleon WF.<sup>†</sup>) The evolution operator  $U(t)$  satisfies the equation  $(1/i)(d/dt)U(t) = VU$  and  $V$  can be expressed through the operators of local fields. As a result the translation operator can be applied to perform the integration over  $d^4 y_1 d^4 y_2$  and we obtain eq. (2.11) with the amplitude of the elementary process on the energy shell. The only difference is that the IMF (light cone) WF of the nucleus is given by eq. (2.17):

$$\psi_A = \int \exp(-ip_A y) \langle n | U(0) j_A(y) | 0 \rangle \theta(-y_0) d^4 y. \quad (2.17)$$

From the viewpoint discussed here nuclear physics can be considered as the saturation of sum rules, by  $A$ -nucleon states. Experience with current algebra (see e.g. [96]) and dispersion sum rules [97] shows that the rapid saturation by one or two resonances is possible for the IMF sum rules only.

Eq. (2.12) has a transparent interpretation in terms of diagrams of the old-fashioned perturbation theory in the IMF (see fig. 2.7) since the typical energy denominator can be rewritten in the form

$$q_0 + E_A - E_r = (q_0 - E_n + E_A) + E_n - E_r = \tilde{q}_0 + E_n - E_r,$$

where  $E_r$  is the energy of the state  $|r\rangle$  after interaction with  $\gamma^*$ . Here  $\tilde{q}_0$  is the same as in eq. (2.9a). The nucleus WF  $\psi_A$  is the vertex  $A \rightarrow |n\rangle$  at fig. 2.7. The nucleon density matrix  $\rho_A^N(\alpha, k_\perp)$  can be calculated through  $\psi_A$  by applying eq. (2.11). The crucial assumption made in the analysis was use of hadrons as the  $|n\rangle$  states. QCD analysis of section 4 indicates that this is justified in a wide momentum range.

The diagrammatic interpretation indicates how to generalize the above procedure to calculate any high-energy process. For example the impulse approximation for the process  $h + A \rightarrow b + \dots$  with  $b$  in

<sup>†</sup>This is in line with observation (see e.g. [98]) that the scale of matrix elements for most of high-energy processes with a nucleon is of order 1 GeV. (The difference between this scale and the scale of quark interaction of order 0.3 GeV is due to quark combinatorics (see section 4.1).) The success of PCAC explains why the small pion mass is inessential in the dominant strong interaction processes. As a result in many short-range phenomena in nuclei pion degrees of freedom are unimportant.

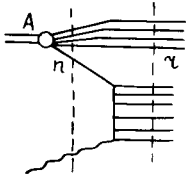


Fig. 2.7. The impulse approximation non-covariant diagram for deep inelastic scattering off nucleus,  $r$  denotes the scattering state after interaction with  $\gamma^*$ .

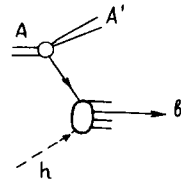


Fig. 2.8.

the nucleus fragmentation region corresponds to fig. 2.8. If a particle “ $b$ ” does not belong to the nucleus WF the cross section of this inclusive process is given at large energies by

$$E_b \frac{d^3\sigma^{h+A \rightarrow b+\dots}}{d^3p_b} = \int \rho_A^N(\alpha, k_\perp) \frac{d\alpha}{\alpha} d^2k_\perp E_b \frac{d^3\sigma^{h+N \rightarrow b+\dots}}{d^3p_b} (\tilde{\nu}, p_b), \quad (2.18)$$

where

$$\tilde{\nu} = 2(p_A p_n) \alpha / A .$$

In difference from deep inelastic processes it is impossible here to choose a ref. frame, where hadron  $h$  cannot produce particles. As a result there are energy dependent corrections as the life-time of any configuration in the hadron  $h$  depends on the ref. frame. There is not such a problem at high energies, where due to Feynman scaling inclusive cross sections become energy independent. To suppress corrections due to the structure of hadron  $h$  we choose a ref. frame, where the nucleus is fast and the hadron at rest. In this case account of finite energy effects only due to structure of energy denominators leads to the following equation:

$$E_b \frac{d^3\sigma^{h+A \rightarrow b+\dots}}{d^3p_b} = \int \rho_A^N(\alpha, k_\perp) \frac{d\alpha}{\alpha} \frac{d^2k_\perp}{\alpha} E_b \frac{d^3\sigma^{h+N \rightarrow b+\dots}}{d^3p_b} (\tilde{\nu}, p_b) \quad (2.19)$$

where

$$\tilde{\nu} = (\nu + M_A^2 - M_n^2) \cdot \alpha / A . \quad (2.19a)$$

In the sections 2.5, 7.3 we will explain that eq. (2.19) is applicable for the description of a wide range of phenomena.

In conclusion, we have demonstrated that the space-time evolution of the scattering process and vacuum fluctuations are adequately accounted for if one uses IMF (non-covariant light cone) WF of nuclei [40, 64]. On the contrary a more traditional approach to high energy nuclear reactions – so called fixed nucleon approximation – which uses the rest frame Schrödinger WF of nuclei does not take into account the increase of essential longitudinal distances with energy. The simplest way to reveal this problem is to consider the process  $h + D \rightarrow X$  and to check that the non-conservation of invariant energy in the amplitude of the elementary subprocess  $h + N \rightarrow X$  tends to infinity with increase of  $E_h$ . Really in the deuteron rest frame at

$E_h \rightarrow \infty$  the non-conservation of invariant energy in the intermediate state is as follows (all notations correspond to fig. 2.8)

$$\Delta = (p_{NN} + p_h)^2 - (p_D + p_h)^2 = M_{NN}^2 - M_D^2 + 2 \cdot E_h (2\sqrt{m_N^2 + k^2} - M_D) \rightarrow \infty.$$

Here  $M_{NN}$  is invariant mass of the two nucleon system  $M_{NN}^2 = 4(m_N^2 + k^2)$  and  $k$  is nucleon momentum in the deuteron. One should expect that due to this energy non-conservation the amplitude of elementary process tends to zero at  $E_h \rightarrow \infty$ . The origin of this puzzle is rather transparent. The characteristic time for development of the high energy process is  $P_h/m^2$  (cf. discussion in sections 2.1, 2.2). It is much larger than the characteristic life-time of the studied fluctuation in the deuteron  $\sim 1/(2\sqrt{m_N^2 + k^2} - M_D)$ . As a result the fixed nucleon approximation is inapplicable, one has to take into account fluctuations of this configuration in the deuteron!

On the contrary, if the deuteron WF is quantized at the hyperplane  $t + z = 0^*$  – so called light cone WF of the deuteron – there is no such difficulty provided the  $z$ -axis is chosen in the direction of the projectile momentum. Indeed, in this approach

$$p_+ = p_0 + p_z = (m^2 + p_\perp^2)/p_-$$

is not conserved ( $m^2 \equiv p^2$ ), though  $p_- = p_0 - p_z$  and  $p_\perp$  components of momentum  $p$  are conserved. As a result the non-conservation of invariant energy is finite at  $E_h \rightarrow \infty$ . Really in the deuteron rest frame:

$$\begin{aligned} \Delta &= (p_{NN} + p_h)^2 - (p_D + p_h)^2 = M_{NN}^2 - M_D^2 + (p_h)_+ (p_{NN} - p_D)_- + (p_h)_- (p_{NN} - p_D)_+ \\ &= M_{NN}^2 - M_D^2 + \frac{1}{2}(m_h^2/E_h) (M_{NN}^2/M_D - M_D) \approx M_{NN}^2 - M_D^2. \end{aligned}$$

Thus  $\Delta$  is finite only if the  $z$ -axis coincides with the  $p_h$  direction. We conclude that *the necessity of using the light cone WF of the bound state quantized in the direction of rapid projectile for description of high energy processes unavoidably follows from the requirement of near on shellness of the amplitudes*.

It is easy to demonstrate that light cone WFs are equivalent to the IMF WFs (see e.g. [101]). This equivalence will be of much use for the understanding of relationship between IMF (light cone) WFs of nuclei and conventional non-relativistic theory of nuclei. It helps also to generalize the fixed nucleon approximation to the relativistic case and to understand the cause of the difference between the spectator momentum and the internal momentum of nucleon produced in the  $p + D \rightarrow p + X$  reaction discussed in section 2.5.

### 2.3. The Weinberg equation. Relationship to the non-relativistic theory of the deuteron

Recently a number of phenomena have been measured, where the high momentum components of the deuteron (nucleus) WF give the dominant contribution (see sections 3, 5). Thus a consistent relativistic description of the nuclear bound state becomes a practical necessity. However without a complete theory of strong interactions such a description can only be approximate. Not surprisingly a

\* The light cone quantization was introduced by P. Dirac in 1949 [207].

number of rather different and nonequivalent approaches has been proposed (see [99] and refs. therein). All of them practically coincide in the description of phenomena, determined by the low momentum components of the nucleus WF. However they give different description of effects due to the high momentum components of the nuclear WF. In this review we shall use the IMF non-covariant light cone WF of nuclei to account for the space-time evolution of the strong interaction (cf. sections 2.1 and 2.2).

Weinberg has been first [100] to elucidate the advantages of the IMF-WF for the description of bound states. He writes: "The Feynman rules provide a perturbation theory in which the Lorentz invariance of the  $S$  matrix is kept visible at every step. However this is accomplished only at the cost of manifest unitarity, by lumping together intermediate states with different numbers of particles and antiparticles. Thus when we try to sum Feynman diagrams to obtain integral equations like the Bethe-Salpeter equation it proves very difficult to justify the omission of any particular diagrams since there is no one-to-one relation between internal lines and intermediate states.

At the same time in the old-fashioned perturbation theory vacuum fluctuations and other topological complexities of relativistic theories make it difficult to derive useful integral equations by summing series of old-fashioned perturbation theory [100]. Weinberg [100] has proved that diagrams of the old-fashioned perturbation theory for the WF of a fast particle do not contain vacuum fluctuations† (problems related to the existence of wee partons [90] are out of the scope of this paper). In consequence, the connectedness structure of IMF perturbation theory is the same as found when old-fashioned perturbation theory is applied to non-relativistic problems [100]. Thus there is some rationale for performing calculations of the Tamm-Dancoff type for the IMF WF. In subsections 2.3 and 2.4 we shall treat the nucleus as a system of nucleons neglecting possible admixtures of baryon resonances, mesons etc. Experimental reasons for the validity of this approximation were discussed in the previous subsection.

### 2.3.1. The Weinberg equation for the deuteron WF

The exact integral equations for the light cone WF of a bound state have been obtained by S. Weinberg long ago [100]. Therefore we consider here problems specific for relativistic nuclear physics. In order to minimize the algebra we shall consider nucleons as spinless particles of equal mass (for the discussion of spin effects see below). As usual, to obtain a Lippman-Schwinger type equation one should include all diagrams without two-nucleon intermediate state into the definition of the irreducible kernel, the potential  $V$ . Moreover, following the ideas of renormalizable quantum field theory (the notion of bare and dressed particles), all fluctuations whose life-time is considerably smaller than the scale of fluctuations studied, should be included into the definition of the potential, renormalized coupling constants and vertices. As a result, within the two-nucleon approximation the graphical Weinberg equation (fig. 2.9) is valid for the off-energy-shell amplitude  $T$  of the NN interaction.  $T$  and  $V$  depend on light cone variables  $\alpha_i$ ,  $k_{i\perp}$ , which characterize the momenta of the initial and final particles. Due to momentum conservation law they satisfy equations

$$\begin{aligned} 2 &= \alpha_1 + \alpha_2 = \alpha_3 + \alpha_4 = \alpha_5 + \alpha_6 \\ k_{1\perp} + k_{2\perp} &= k_{3\perp} + k_{4\perp} = k_{5\perp} + k_{6\perp}. \end{aligned}$$

† The IMF diagram technique is nicely described in the review by Kogut and Susskind [101].

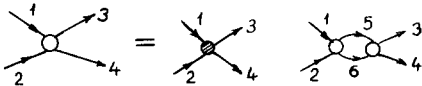


Fig. 2.9. The graphical representation of the two-body Weinberg equation.

The energy denominator for the propagation of a two-nucleon system at  $p_1 + p_2 = P \rightarrow \infty$  has the form

$$\frac{1}{2P} \frac{1}{E_1 + E_2 - E_5 - E_6} = \frac{1}{M_{1,2}^2 - M_{5,6}^2}.$$

Here

$$M_{1,2}^2 = 4 \frac{(m^2 + k_{1\perp}^2)}{\alpha_1(2 - \alpha_1)} \quad \text{and} \quad M_{5,6}^2 = 4 \frac{m^2 + k_{5\perp}^2}{\alpha_5(2 - \alpha_5)}$$

are the invariant masses of initial and intermediate states of NN systems. Consequently the Weinberg eq. (2.20) for  $T$  has the form:

$$T(\alpha_1, k_{1\perp}, \alpha_3, k_{3\perp}) = V(\alpha_1, k_{1\perp}, \alpha_3, k_{3\perp}) + \int \frac{V(\alpha_1, k_{1\perp}, \alpha_5, k_{5\perp})}{M_{5,6}^2 - M_{1,2}^2} \frac{d\alpha_5}{\alpha_5(2 - \alpha_5)} \frac{d^2 k_{5\perp}}{(2\pi)^3} T(\alpha_5, k_{5\perp}, \alpha_3, k_{3\perp}). \quad (2.20)$$

Here  $\{d\alpha/\alpha(2 - \alpha)\} d^2 k_\perp$  is the phase volume for a two-nucleon system. This equation has been discussed recently in many papers (see e.g. [101–103] and refs. therein). In the vicinity of a bound state pole ( $M_{1,2}^2 \rightarrow M_D^2$ )  $T$  has the form:  $T = \chi(\alpha_1, k_{1\perp})\chi(\alpha_3, k_{3\perp})/(M_{1,2}^2 - M_D^2)$ . As a result a Schrödinger-like equation for the WF of the bound state:  $\psi_D = \chi(\alpha, k_\perp)/(M_{1,2}^2 - M_D^2)$  is valid:

$$\frac{1}{4}(M_{1,2}^2 - M_D^2) \psi_D(\alpha_1, k_{1\perp}) = \int V(\alpha_1, k_{1\perp}, \alpha_3, k_{3\perp}) \psi_D(\alpha_3, k_{3\perp}) \frac{d\alpha_3}{\alpha_3(2 - \alpha_3)} \frac{d^2 k_{3\perp}}{4(2\pi)^3}. \quad (2.20a)$$

Angular momentum conservation leads to a considerable simplification of this equation. Generally in quantum field theory the generators of angular momentum depend on the interaction between particles, number of particles, etc. However, when it is possible to neglect all but nucleon degrees of freedom, the generators of angular momentum have the same form as for free nucleons. Therefore  $\psi_D(\alpha, k_\perp)$  depends on one argument – the invariant mass of the two-nucleon system  $4(m^2 + k_\perp^2)/\alpha(2 - \alpha)$  instead of two independent variables  $\alpha, k_\perp^2$  (cf. theoretical example section 2.1 and dispersion approach section 2.2). Following Foldy's approach [104] Terent'ev suggested this result [105] in connection with the quark model (see also sections 2.1 and 2.2). We shall demonstrate in section 3.1 that the form of the angular momentum condition discussed here seems now to be confirmed experimentally in a wide range of nucleon momenta.

The angular condition takes a quite transparent form if one introduces as in section 2.1 the variable  $k$ , corresponding to the nucleon momentum in the c.m. system:

$$k = \sqrt{\frac{m^2 + k_\perp^2}{\alpha(2 - \alpha)} - m^2} \quad \alpha = 1 + k_3/\sqrt{m^2 + k^2}. \quad (2.21)$$

The convenience of the  $k$ -variable was emphasized in refs. [105, 40, 51c]. Evidently the account of the angular momentum condition leads to a simplification:  $V(\alpha_1, k_{1\perp}, \alpha_3, k_{3\perp}) = V(k, \tilde{k}) = V(k^2, \tilde{k}^2, (k - \tilde{k})^2)$  [106]. Here  $k(\alpha_1, k_{1\perp})$ ,  $\tilde{k}(\alpha_3, k_{3\perp})$  are nucleon momenta in the initial and final states. As a result eq. (2.20a) takes the form, which is rather similar to the Schrödinger equation in conventional non-relativistic theory of the deuteron:<sup>†</sup>

$$(k^2 + k_D^2) \psi_D(k) = \int V(k, k') \frac{d^3 k'}{\sqrt{k'^2 + m^2}} \psi_D(k'). \quad (2.22)$$

Here  $k_D^2 \approx m\epsilon_D$  and  $\epsilon_D$  is the binding energy of the deuteron. Spin and isospin effects can be accounted for in eq. (2.22) in the same way as in non-relativistic quantum mechanics.

In conclusion, we have demonstrated that the Schrödinger equation has practically the same form in the relativistic and non-relativistic theory of a two-nucleon system due to the small value of inelasticities. Since the parameters of the effective phenomenological NN potential are determined from the phase-shift analysis using really eq. (2.20) with  $V = V(k, \tilde{k})$  (supplemented by the hypothesis of a nuclear core) the conventional non-relativistic WF should be a reasonable approximation for the relativistic WF of the deuteron in a wide  $k$ -range. This correspondence seems to explain the otherwise puzzling success of the non-relativistic deuteron WFs of Hamada–Johnston [107], Reid [108] in the quantitative description of all phenomena related to the high momentum component of the deuteron WF (see section 3).

Eq. (2.22) coincides with the so-called minimal relativity equation discussed in [99], and with one of the versions of the Schrödinger equation for light cone WFs suggested in [67] in an attempt to construct relativistic quantum mechanics for a fixed number of particles within Foldy's approach. In contrast to [67] we consider eq. (2.20) as an approximate equation, valid for the deuteron WF due to the small value of inelasticities only, and, observe, that the form of eq. (2.22) for the deuteron WF is unambiguously determined by the physical approximations discussed above. Eq. (2.20) coincides with the light cone form of the quasipotential equation [103]. However in this approach the angular condition restrictions have not been imposed. Thus, in ref. [103] eq. (2.22) has not been obtained.

### 2.3.2. Properties of the light cone WF of the deuteron

1. Due to the rotational invariance in the transverse plane  $\psi_D(\alpha, k_\perp) = \psi_D(\alpha, k_\perp^2)$ .
2. In the two-nucleon approximation for the deuteron WF due to antisymmetry  $\psi_D(\alpha, k_\perp) = -\psi_D(2 - \alpha, k_\perp)$ .
3. Within the two-nucleon approximation due to the angular condition  $\psi_D(\alpha, k_\perp) = \psi_D(k^2)$ , see the discussion above.
4. Account of the deuteron and nucleon spins. The form of the IMF deuteron WF follows from the space parity conservation and from the condition that the two nucleon system has the total angular momentum equal to 1:

$$\psi_\mu^D \epsilon_\mu^D = \bar{U}(p_1) \{ \gamma_\mu \Gamma_1(M_{NN}^2) + (p_1 - p_2)_\mu \Gamma_2(M_{NN}^2) \} U(-p_2) \epsilon_\mu^D. \quad (2.23)$$

Here  $p_1$  and  $p_2$  are the momenta of the proton and of the neutron.  $M_{NN}^2 = 4(m^2 + k_\perp^2)/\{\alpha(2 - \alpha)\}$  is the invariant mass of two nucleon system.  $\epsilon_\mu^D$  is the deuteron polarization vector. Evidently, eq. (2.23) is a direct generalization of the  $\gamma^*$  WF considered in section 2.1.

<sup>†</sup> In Foldy's approach for light-cone WFs this equation was considered in [105].

In the case of the longitudinal deuteron polarization, due to the increase of the components of the vector  $\varepsilon_\mu^D$  with the deuteron momentum, energy non-conservation in the vertex  $D \rightarrow NN$  requires special treatment. As a result it is necessary to account for the terms of the order  $1/P$  in the spin structure of the vertex  $D \rightarrow NN$  (really the vacuum pairs in the deuteron WF). If the contact terms in the high energy scattering amplitude are absent the contribution of the longitudinal deuteron polarization can be calculated from the physical requirement that the deuteron is mostly formed long before the moment of the interaction. Consequently, the conservation of the angular momentum leads to a constraint on the light cone WF of deuteron that the two nucleon system has angular momentum equal to 1. Therefore

$$\varepsilon_L^D = \{(p_1 + p_2)_z, (p_1 + p_2)_0\}/M_{NN}. \quad (2.24)$$

Eq. (2.24) enables to separate effects of the nucleon inner motion in the deuteron. In the deuteron rest frame the constraint due to angular momentum conservation is simplified and the vector  $\varepsilon_L^D$  coincides with  $e_z$ . Eq. (2.24) naturally arises in the dispersion approach since in this case the “mass” of the deuteron is equal to the mass of the two nucleon system.

In the case of  $\gamma^*$  eqs. (2.23, 2.24) are not valid for the longitudinal polarization of  $\gamma^*$  as the point-like nature of  $\gamma$  allows small longitudinal distances. The method to reconstruct this amplitude was suggested by Gribov [89].

For applications it is convenient to express  $\psi_D$  through the two-component spinors  $\varphi$  in the two-nucleon rest frame, and the S- and D-wave functions of deuteron,  $U(k^2)$ ,  $W(k^2)$ , which are solutions of eq. (2.22)

$$\psi_D = \varphi^* \left\{ \sigma_\mu U(k^2) - \frac{W(k^2)}{\sqrt{2}} \left( \sigma_\mu - \frac{k_\mu(\sigma k)}{k^2} \right) \right\} \varphi. \quad (2.25)$$

Here  $M_{NN}^2 = 4(m^2 + k^2)$ ,  $\frac{1}{3} \sum |\psi_D|^2 = U^2 + W^2$ , the sum goes over nucleon, deuteron spin states. It is convenient to normalize these WF as

$$\int \frac{1}{3} \sum |\psi_D|^2 d^3k = \int [U^2(k) + W^2(k)] d^3k = 1. \quad (2.26)$$

Comparing eqs. (2.23) and (2.25) and using the standard formulae

$$U(k) = \sqrt{\varepsilon + m} \begin{pmatrix} 1 \\ \sigma k / (\varepsilon + m) \end{pmatrix} \varphi, \quad U(-k) = \sqrt{\varepsilon + m} \begin{pmatrix} \sigma k / (\varepsilon + m) \\ 1 \end{pmatrix} \varphi$$

which express Dirac-spinors through two-component spinors  $\varphi$ , we obtain:

$$\Gamma_1(M^2) = \frac{1}{\sqrt{\varepsilon}} \left[ U(k) - \frac{W(k)}{\sqrt{2}} \right] \quad (2.27)$$

$$\Gamma_2(M^2) = -\frac{\sqrt{\varepsilon}}{2k^2} \left\{ \frac{\varepsilon - m}{\varepsilon} U(k) + \frac{2\varepsilon + m}{\varepsilon} \frac{W(k)}{\sqrt{2}} \right\}. \quad (2.28)$$

Here  $\varepsilon = \sqrt{m^2 + k^2}$ .

## 2.4. Properties of the light cone nucleus WF. Weinberg type equation

### 2.4.1. The many-body equation

For simplicity we shall consider here a nucleus as a many-nucleon system neglecting possible admixtures of other components. In this case one can easily obtain a Weinberg type equation for the light-cone nuclear WF, if one allows only two-nucleon forces. It has the habitual graphical form. The black blob in fig. 2.10 is for the NN potential, which is the same as in eq. (2.20). The sum goes over nucleon pairs  $i, j$ . As in section 2.3  $V_{ij}$  depends on the internal variables of the pair  $(ij)$ .

$\gamma_i = \alpha_i/(\alpha_i + \alpha_j)^\dagger$  and  $\tilde{k}_{i\perp} = k_{i\perp} - \gamma_i(k_i + k_j)_\perp$ . Thus we obtain the Weinberg type eq. (2.29) for  $\psi_A(\alpha_1 \dots \alpha_A, k_{1\perp} \dots k_{A\perp})$

$$\left[ \sum_{j=1}^A \frac{m_j^2 + k_{j\perp}^2}{\alpha_j} - \frac{M_A^2}{A} \right] \psi = \sum_{ij} \int V_{ij} \frac{d\gamma_i}{\gamma_i} \frac{d\gamma_j}{\gamma_j} d^2 \tilde{k}_{i\perp} d^2 \tilde{k}_{j\perp} \times \delta(1 - \gamma_i - \gamma_j) \delta(\tilde{k}_{i\perp} + \tilde{k}_{j\perp}) \psi(\gamma_i, (\alpha_i + \alpha_j), k_{i\perp}, \alpha_r, k_{r\perp}). \quad (2.29)$$

The form of eq. (2.29) follows from the space-time evolution of the strong interaction (the form of the energy denominators) and from the restriction to two-body forces. Note that the equations for a relativistic bound state suggested in ref. [67] do not satisfy the last condition and effectively contain non-local many-body forces. It is easy to demonstrate that eq. (2.29) is in close correspondence with the non-relativistic Schrödinger equation at small nucleon momenta (see discussion below). As the importance of many-body forces is unknown, we shall not discuss here the role of relativistic effects for the calculation of traditional nuclear physics phenomena such as the energy binding etc. Our approach to the short-range effects in nuclei is based on the observation that many characteristic for relativistic theory properties of nucleus WF follows from the very existence of equation (2.29) but not from detailed form of the potential  $V$  or even from restriction by two-body forces.

### 2.4.2. Sum rules for the nucleon density matrix

It was shown in section 2.2 (see also sections 3, 5 and 7) that to calculate a number of phenomena it is sufficient to know the nucleon density matrix,  $\rho_A^N(\alpha, k_\perp)$ , and the density matrix of protons,  $\rho_A^P(\alpha, k_\perp)$ , and neutrons,  $\rho_A^N(\alpha, k_\perp)$ ,  $\rho_A^N = \rho_A^P(\alpha, k_\perp) + \rho_A^N(\alpha, k_\perp)$ , i.e.

$$\begin{aligned} \rho_A^N(\alpha, k_\perp) &= \int \psi^2(\alpha_1 \dots \alpha_A, k_{1\perp} \dots k_{A\perp}) \prod_{i=1}^A \frac{d\alpha_i}{\alpha_i} d^2 k_{i\perp} \delta\left(1 - \frac{\sum \alpha_i}{A}\right) \delta\left(\sum_{i=1}^A k_{i\perp}\right) \\ &\times \sum_{i=1}^A \alpha_i \delta(\alpha - \alpha_i) \delta(k_{i\perp} - k_\perp) \end{aligned} \quad (2.30)$$

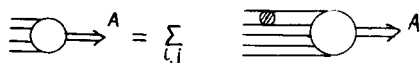


Fig. 2.10. The graphical Weinberg-type equation for the light cone many-body wave function with two-body interactions.

<sup>†</sup> As before  $\alpha_i/A$  is light cone fraction of nucleus momentum carried by nucleon  $i$ :  $\alpha_i = A(\sqrt{m^2 + p_i^2} + p_{iz})/(\sqrt{m_A^2 + p_A^2} + p_{Az})$ . Thus  $0 < \alpha_i < A$ .

$$\begin{aligned} \rho_A^N(\alpha, k_\perp) = & \int \psi^2(\alpha_1 \dots \alpha_A, k_{1\perp} \dots k_{A\perp}) \prod_{i=1}^A \frac{d\alpha_i}{\alpha_i} d^2 k_{i\perp} \delta\left(1 - \frac{\sum \alpha_i}{A}\right) \\ & \times \delta\left(\sum_{i=1}^A k_{i\perp}\right) \sum_{i=1}^A \alpha_i \delta(\alpha - \alpha_i) \delta(k_{i\perp} - k_\perp). \end{aligned} \quad (2.31)$$

Here  $\psi$  is the light cone nucleus WF, the solution of Weinberg equation (2.29), which is normalized as usually for bound state:

$$\int \psi^2(\alpha_1 \dots \alpha_A, k_{1\perp} \dots k_{A\perp}) \prod_{i=1}^A \frac{d\alpha_i}{\alpha_i} d^2 k_{i\perp} \delta\left(1 - \frac{\sum \alpha_i}{A}\right) \delta(\sum k_{i\perp}) = 1. \quad (2.32)$$

It is easy to check that  $\rho_A^N(\alpha, k_\perp)$  as defined in eq. (2.31) satisfies two important sum rules:

$$\int_0^A \rho_A^N(\alpha, k_\perp) \frac{d\alpha}{\alpha} d^2 k_\perp = A \quad (2.33)$$

$$\int_0^A \alpha \rho_A^N(\alpha, k_\perp) \frac{d\alpha}{\alpha} d^2 k_\perp = \int_0^A \rho_A^N(\alpha, k_\perp) \frac{d\alpha}{\alpha} d^2 k_\perp \frac{\sum \alpha_i}{A} = A. \quad (2.34)$$

These sum rules can be derived in a somewhat independent way. Eq. (2.33) represents the sum rule for the baryon charge conservation. It follows directly from the condition that the matrix element of the baryon current at zero momentum transfer is equal  $\langle A | j_0^B | A \rangle / p_A|_{p_A \rightarrow \infty} = A$ . Eq. (2.34) represents the sum rule for the momentum conservation. To obtain this sum rule we can use the fact that the matrix element of the energy-momentum tensor  $T_{\mu\lambda} (\langle A | T_{\mu\lambda} | A \rangle / p_A^2|_{p_A \rightarrow \infty})$  at zero momentum transfer does not depend on the target. This property of  $T_{\mu\lambda}$  is a consequence of the universality of gravitation.

*Comment.* To check the consistency of the developed approach one can use the celebrated Adler, Dashen, Gell-Mann, Fubini sum rules [109] and momentum conservation sum rule [110] valid for an arbitrary target in any renormalizable quantum field theory (QCD) [111]. The application of these sum rules together with eqs. (2.14) for the nucleus structure functions leads to eqs. (2.33), (2.34) correspondingly. Note however that both of these sum rules are not fulfilled in the approaches based on the Bethe-Salpeter WF with the off-mass-shell interacting nucleon (see the discussion in Appendix A).

#### 2.4.3. Connection with non-relativistic theory of the nucleus

To obtain the usual Schrödinger equation from the Weinberg type eq. (2.29) the approximation

$$\alpha_i = 1 - k_{3i}/m, \quad (2.35)$$

should be used (cf. eq. (2.16)). In this approximation  $\rho_A^N(\alpha, k_\perp)$  is simply related to the single nucleon density matrix  $n(k)$ :

$$n(k) = \int \tilde{\psi}_A^2(k_1 \dots k_A) \prod_{j=1}^A d^3 k_j \delta\left(\sum_{j=1}^A k_j\right) \sum_{i=1}^A \frac{\delta(k - k_i)}{A}. \quad (2.36)$$

Here  $\tilde{\psi}_A^2 = \psi_A^2/m^{A-2}$  and therefore  $\int n(k) d^3k = A$ . From the comparison of eqs. (2.35), (2.36) and eq. (2.30) we have

$$\rho_A^N(\alpha, k_\perp) = m n(k), \quad k = \sqrt{m^2(1-\alpha)^2 + k_\perp^2}. \quad (2.37)$$

An equivalent though more complicated procedure is to consider IMF diagrams for the nuclear WF and to verify that the angular condition for an  $A$ -nucleon system has the same form as for free nucleon system in the approximation  $k/m \ll 1$  (i.e. the Schrödinger equation can be directly derived from IMF diagrams). Eq. (2.29) combined with eq. (2.35) gives a practical possibility to apply existing experience in nuclear physics to estimate short-range phenomena.

For a long time two qualitatively different hypotheses on the high momentum components of nuclear WF have been discussed. It was suggested that  $n(k)$  is determined either by short-range two-nucleon correlations or by the average field configurations.

The pair correlation hypothesis was proposed in early 1950's to explain nuclear photodisintegration [112–113], absorption of slow pions [114] and it is still successfully applied for description of these and other experiments, sensitive to the quasideuteron pn configuration with nucleon momenta  $k_p \approx -k_n \approx 400 \text{ MeV}/c$  [84]. The up to date analysis of photonuclear reactions indicates that contribution of the triplet pn pairs (quasideuterons) to  $n(k)$  is given by  $n(k) = L \cdot N(Z/A) \psi_D^2(k)$  where  $L$  is the Levinger factor 8–10 (see e.g. [84]). After consideration of the singlet pn and pp pairs in the Wigner-model, this analysis suggests that 25–40% (?) of the nucleons in the nucleus have momenta larger than  $300 \text{ MeV}/c$ .

At the same time one can estimate the high momentum components in the deuteron using the Hamada–Johnstone or the Reid soft core WF's which describe well the short-range part of the deuteron WF. We obtain  $\int \psi_D^2(k) d^3k \theta(k - 0.3 \text{ GeV}/c) \approx (4-5)\%$ . For  ${}^4\text{He}$  the calculations performed in [82] with the Reid potential lead to  $\frac{1}{4} \int n(k) d^3k \theta(k - 0.3 \text{ GeV}/c) \approx 10\%$ . For heavier nuclei the estimations using gas approximation indicate that the probability of a two nucleon correlation increases with atomic number  $A$  by a factor  $\sim 1.5$  in the range  $A = 12-207$  (see eq. (2.40))†. Thus the existing experience in the non-relativistic nuclear physics hints that 15–25% of nucleons (not quasiparticles) have momenta above the Fermi surface of the non-interacting system.

It seems instructive to estimate the value of two-nucleon correlations using the nuclear WF in coordinate space. Really due to the large value of the D-state for realistic deuteron WFs  $\psi_D(k) = \int e^{ikr} \psi_D(r) d^3r$  for  $k = 0.4 \text{ GeV}/c$  is determined by integration in coordinate space over a large region near the nuclear core  $r_0 \sim 1.2-1.4 \text{ fm} \geq r > r_c$  ( $r_c \sim 0.4 \text{ fm}$  is the position of nuclear core). Therefore for heavy nuclei the probability  $a_2$  of pair correlation is proportional to the probability for two nucleons to be in a volume of the radius  $r_0$ ;  $a_2 \approx (r_0/r_{NN})^3$ . Here  $r_{NN}$  is mean distance between nucleons in nuclei. Taking a realistic value for  $r_{NN} \sim 2 \text{ fm}$  we obtain  $a_2 \sim (10-20)\%$ . This purely geometric estimate indicates that:

(1) In most of the phenomena related to the high momentum component in the nucleus WF essential relative distances between nucleons are considerably larger than  $r_c$ . Therefore overlapping between quarks which belong to different nucleons is not large.

(2) Since  $a_2$  is large, three, four-body correlations could not be small.

In difference from the pair correlation model in the average field models it is assumed that  $n(k)$  is

† Calculations made in [82] for  ${}^{16}\text{O}$  do not show the increase with  $A$  of the value of high momentum tail of the nuclear WF as compared to  ${}^4\text{He}$ . Possibly this is due to the restriction [82] to S-waves in the input WF. (One of us (L.F.) is indebted to Dr. W. Glöckle for a discussion of this point.)

dominated by the configurations, where the momentum of a fast nucleon- $k$  is balanced by the rest of the nucleus (i.e. the nucleon configuration  $p_1 = k$ ;  $p_2 \sim p_3 \cdots \sim p_A \sim -k/A - 1$ ). This hypothesis has recently been revived by Amado and Woloshyn [44] in their analysis of the backward nucleon production at initial energies  $T_p = 600\text{--}800$  MeV. Practically the same hypothesis was discussed by Blankenbecler and Schmidt in connection to the backward  $p, \pi$  production at large energies in the framework of the Bethe-Salpeter light cone formalism [46–48].

At the same time for a realistic NN potential with a core, the contribution of two-nucleon correlations dominates at  $k \rightarrow \infty$ . This follows from the large difference between the scales of the long-range potential characterizing the depth of the potential well ( $\sim 40$  MeV), and of the short-range repulsive potential (the value of the barrier is  $\geq 0.6$  GeV for the realistic NN potentials). Numerical calculations with realistic potentials [82] indicate that two-nucleon correlations dominate in  $n(k)$  at  $k \geq 0.4\text{--}0.5$  GeV/c.

In relativistic theory the answer is more complicated. It seems fruitful for the theoretical analysis of hard phenomena to define formally the notion of  $j$ -nucleon correlation. Look at a subsystem of  $j$  nucleons in the ground state having invariant mass  $\approx jm_N$ , where nucleons obtain large relative momenta due to hard short-range interactions between all  $j$  nucleons. Typical example of the three-nucleon correlation is shown in fig. 2.11. Before a hard interaction the  $j$  nucleons are in the average configuration ( $\alpha_i \sim \alpha_j \sim 1$ ),  $j$ -nucleon correlation contribute to  $\rho_A^N(\alpha, k_\perp)$  in the region  $\alpha < j$  only due to momentum conservation. In the non-relativistic Schrödinger equation this kinematic decomposition of  $j$ -nucleon correlations is not evident. Therefore one cannot relate simply  $n(k)$  to  $\rho_A^N(\alpha, k_\perp)$  for  $\alpha \geq 2$ .

Though at  $\alpha \rightarrow A$   $A$ -nucleon correlation should dominate  $\rho_A^N(\alpha, k_\perp)$ , in the region  $1 < \alpha \ll A$  relative contributions of different configurations are determined by the competition of two factors: the small probability  $a_j$  to find a correlation with large  $j$  and the enhancement of higher correlations due to a slower decrease of their contribution to  $\rho_A^N(\alpha, k_\perp)$  at large  $\alpha$  (see eq. (2.43)). Therefore it seems natural to expect that at least in the region of not too large  $\alpha \lesssim 3$  (which is probed until now) few-nucleon correlations (FNC) dominate. Thus, the nucleon density matrix  $\rho_A^N(\alpha, k_\perp)$  can be effectively expanded over the contribution of  $j$ -nucleon correlations  $\rho_j(\alpha, k_\perp)$ :

$$\frac{1}{A} \rho_A^N(\alpha, k_\perp) = \sum_{j=2}^A a_j \rho_j(\alpha, k_\perp). \quad (2.38)$$

More accurate treatment is required to account for the c.m. motion of the  $j$ -nucleon configuration in the mean field of the nucleus. It is expected that this effect should lead to small corrections except near the edge of the  $j$ -nucleon correlation. This is because the scale of the repulsive potential is considerably larger than that for the long-range potential.

The  $a_j$ 's in eq. (2.38) can be estimated on the basis of the non-relativistic Schrödinger equation for nuclear WF since they are determined by the mean internucleon distances. The well known fact that the

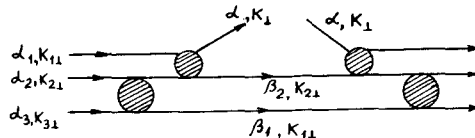


Fig. 2.11. A typical diagram for the three-nucleon correlation.

nucleon density in the center of the nucleus is larger than near the surface leads to a certain dependence of  $a_j$  on the atomic number. This dependence can be estimated in the gas approximation where<sup>†</sup> for  $j \ll A$

$$a_j \sim (1/A) \int [\rho_A(r)]^j d^3r. \quad (2.39)$$

Here  $\rho_A(r)$  is the nucleon density in the coordinate space normalized according to  $\int \rho_A(r) d^3r = A$ . The calculation using the conventional fits of  $\rho_A(r)$ , obtained in electron and proton scattering data [115–116] leads to a rather similar  $A$  dependence of  $a_j$ , which can be roughly approximated as

$$a_2 \sim A^{0.15}; \quad a_3 \sim A^{0.22}; \quad a_4 \sim A^{0.27} \quad (2.40)$$

in the range  $A = 12\text{--}207$ . Thus  $\rho_A^N(\alpha, k_\perp)$  should be a practically universal function of  $\alpha, k_\perp$  in a wide  $\alpha, k_\perp$  range. In momentum space  $\rho_j(\alpha, k_\perp)$  corresponds to the contribution of  $j$ -nucleon configuration, where the large momentum of the fast nucleon is balanced by the other  $(j-1)$  nucleons of this configuration (see fig. 2.12). The momentum dependence of  $\rho_2$  is expected to be similar to that of the deuteron, since the short distance behaviour is independent of the nucleus structure. (In principle some difference could arise from the presence of pp, pn pairs in spin singlet states and different orbital momenta of nucleons.) The calculation of  $n_{^4\text{He}}$ , using the Reid potential is in agreement with  $n(k) \sim \psi_D^2(k)$  [82].

To estimate  $\rho_{j=3}(\alpha, k_\perp = 0)$  at large  $\alpha$  we assume that a fast nucleon with  $\alpha \rightarrow j$  collects the large momentum as a result of  $j-1$  hard two-body collisions with other nucleons. A typical diagram for the three-nucleon correlation is shown in fig. 2.11. The black blob in fig. 2.11 corresponds to the off-energy-shell two-nucleon amplitude (solution of the Weinberg type eq. (2.22)). Following the QCD analysis of section 4 we shall approximate it below by the WF of the two-nucleon correlation. In the calculation we neglect the Fermi motion of the nucleons in the initial configuration, i.e. we take  $\alpha_i = 1, k_{i\perp} \approx 0$ . Within the approximations the expression for  $\rho_3(\alpha, k_\perp = 0)$  is given by

$$\begin{aligned} \rho_3(\alpha, k_\perp = 0) &= \int \frac{d\beta_1}{\beta_1} d^2k_{1\perp} \frac{d\beta_2}{\beta_2} d^2k_{2\perp} \delta(\beta_1 + \beta_2 + \alpha - 3) \\ &\times \delta(k_{1\perp} + k_{2\perp} + k_\perp) \psi^2(2 - \beta_1, k_{1\perp}) \psi^2\left(2 - \frac{2\beta_2}{\alpha}, k_{2\perp}\right). \end{aligned} \quad (2.41)$$

Here  $\psi$  is the WF of a two-nucleon correlation. The additional dependence of the upper blob in fig. 2.11 on  $\beta_1, \beta_2$  can be neglected, since in the essential region of integration  $\beta_1, \beta_2 \rightarrow 0$ , when  $\alpha \rightarrow 3$ . Here we

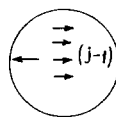


Fig. 2.12. A typical configuration for the  $j$ -nucleon correlation.

<sup>†</sup> We thank Prof. V.A. Khodel for the explanation, how these formulae can be obtained within the Fermi liquid theory. Similar expression for  $a_2$  was discussed by Erikssons [117]. This estimate is rather rough, since gas approximation is not good if large hard core effects are present.

use the evident consequence of eq. (2.19) that the short-range behaviour of the WF is determined by the singularities of the potential and is independent of the binding energy.

Assuming that  $\psi^2(2 - \beta_1, k_\perp)_{\beta_1 \rightarrow 0} \sim (2 - \beta_1)^{n+1} f(k_\perp^2)$  we obtain

$$\rho_3(\alpha, k_\perp = 0) \sim (3 - \alpha)^{2n+1}. \quad (2.42)$$

To generalize this result to the case of any  $j$ -nucleon correlation at  $\alpha \rightarrow j$  we assume that its WF can be approximated by the convolution of two-nucleon correlations. Simple calculations lead to:

$$\rho_j(\alpha, k_\perp = 0) \sim (j - \alpha)^{n(j-1)+j-2}. \quad (2.43)$$

The factor  $(j - \alpha)^{(1+n)(j-1)}$  is due to  $j - 1$  two-body amplitudes. The factor  $(j - \alpha)^{-1}$  is due to phase volume of fast nucleon. A similar expression was obtained by Schmidt and Blankenbecler in the case  $j = A$  [46]. Now it seems difficult to calculate absolute value of  $\rho_j(\alpha, k_\perp)$ . To account for inclusive origin of  $\rho_j(\alpha, k_\perp)$  we assume that

$$\frac{1}{j} \int_1^j \rho_j(\alpha, k_\perp) \frac{d\alpha}{\alpha} d^2 k_\perp$$

is independent of  $j$ . A violation of the last condition would lead to redefinition of  $a_j$  in eq. (2.38). The final formula for  $\rho_A^N(\alpha, k_\perp = 0)$  is as follows

$$\rho_A^N(\alpha, k_\perp = 0) = \sum_{j=2}^A a_j C_j \left(1 - \frac{\alpha - 1}{j - 1}\right)^{n(j-1)+j-2} \quad (2.44)$$

where  $\rho_j = C_j (1 - (\alpha - 1)/(j - 1))^{n(j-1)+j-2}$ .  $C$  is practically independent of  $j$  and fixed by the condition  $\rho_2 = \rho_D^N$ .

In summary:

(1) The estimate of  $\rho_j(\alpha, k_\perp = 0)$  is in accordance with the Brodsky-Farrar attempt to calculate high momentum component of hadron WF in terms of quark models [118]. Eq. (2.41) can be obtained more formally by transforming the many-body equation into a Faddeev type equation [119] and by finding its asymptotic solution. It follows from this analysis that in eq. (2.41) the region  $\beta_1 > \beta_2 > \dots > \beta_{j-1}$  mostly contributes. As a result the invariant mass of the recoiling system is different from the mass of a nucleus with the atomic number  $j$ .

(2) It seems now that a rather complicated behaviour of  $\rho_2(\alpha, k_\perp)$  expected for  $\alpha > 1.8$  (see section 4.2) does not influence strongly the form of  $\rho_A^N(\alpha, k_\perp = 0)$  because in this kinematic region  $\rho_2(\alpha, k_\perp = 0)$  is small and therefore the three-nucleon correlation dominates (see analysis of experimental data in the section 8.1).

(3) If  $\alpha$  is not large eq. (2.43) can be approximated as

$$\rho_j(\alpha) \approx \exp \left[ -\alpha(n+1) \left\{ 1 - \frac{1}{j} \left( \frac{n+2}{n+1} - \frac{\alpha}{2} \right) \right\} \right].$$

In other words at  $\alpha < 1.8$  the contributions of two and three-nucleon correlations into  $\rho_A^N(\alpha, k_\perp = 0)$  have similar functional form.

(4) It is well known that the high momentum behaviour of deuteron WF is dominated by D wave in a large kinematical region. Therefore the above calculation of  $\rho_j(\alpha, k_\perp)$  really indicates that contribution of partial waves with  $L \neq 0$  is large in the nuclear WF.

It is difficult now to calculate  $k_\perp$  dependence of  $\rho_j$  for  $j \geq 3$ : (1) At small  $k_\perp$  one should know the distribution of nucleons in the ground state. (2) At large  $k_\perp$  and  $\alpha < 2$  the method suggested is inapplicable for  $j \geq 3$  since the contribution of two-nucleon correlation dominates in this limit. However a rough estimate can be made by imposing the angular condition discussed in section 2.2. It follows from the angular condition that the WF depends on the internal variables of the  $j$ -nucleon system. This condition is trivially fulfilled in the dispersion approach (see section 2.2), though at present is not clear whether a restriction to 2-body forces in Weinberg equation is compatible with the angular condition. In [102] it was shown how to satisfy the angular condition by introducing effectively non-local many-body forces.

To calculate the  $k_\perp$  dependence of  $\rho_j^N(\alpha, k_\perp)$  it is convenient to perform an integration in the eq. (2.30) over all variables which characterize the  $(j-1)$  system, except its invariant mass  $\mu^2 \equiv M_{j-1}^2$ . Due to the angular condition  $\psi_j(\alpha_1 \dots \alpha_j, k_{i_1} \dots k_{i_j})$  depends on the internal variables of the  $j$ -nucleon system (see the discussion in section 2.2). As a result we obtain:

$$\rho_j(\alpha, k_\perp) = \frac{1}{(j-\alpha)} \int f_j \left( \mu^2, \frac{\mu^2 + k_\perp^2}{1 - \alpha/j} + \frac{m^2 + k_\perp^2}{\alpha/j} \right) d\mu^2. \quad (2.45)$$

Here

$$M_j^2 = \frac{\mu^2 + k_\perp^2}{1 - \alpha/j} + \frac{m^2 + k_\perp^2}{\alpha/j}$$

is the mass of  $j$  nucleon system and

$$f_j \equiv \int \psi_j^2 \prod \frac{d\alpha_i}{\alpha_i} d^2 k_{i_1} \delta \left( \frac{\sum \alpha_i}{A} - 1 \right) \delta \left( \sum k_{i_1} \right) \cdot (j-\alpha) \sum_{n=1}^j \alpha_n \delta(\alpha - \alpha_n) \delta(k_\perp - k_{\perp n}) \delta[M_{j-1}^2 - \mu^2].$$

It is convenient to introduce the variables

$$\mu^2 = (j-1)^2 m^2 + \Delta^2, \quad \frac{M^2}{j^2} = m^2 + \frac{\Delta^2}{\alpha j} + \frac{k_\perp^2 + m^2(1-\alpha)^2}{\alpha(j-\alpha)}. \quad (2.46)$$

The variable  $\Delta^2$  characterizes the energy transferred to the recoiling system during  $j-1$  hard interactions. At large  $\alpha$  (especially for  $\alpha \rightarrow j$ ) it seems natural to neglect  $\Delta^2$  as compared to the last term in eq. (2.46) due to the power law decrease of  $\psi$  with increase of  $M^2$ . In this case we obtain:

$$\rho_j(\alpha, k_\perp) \simeq \frac{1}{(j-\alpha)} F_j \left[ \frac{k_\perp^2 + m^2(1-\alpha)^2}{\alpha(j-\alpha)} \right]. \quad (2.47)$$

In the case of the two-nucleon system,  $j = 2$  and  $\Delta^2 = 0$ , since the mass of the recoiling system is  $m^2$ . Thus  $\rho_D^N(\alpha, k_\perp)$  is expressed through the WF of deuteron (see eq. (2.30)) as follows

$$\rho_D^{pn}(\alpha, k_\perp) = \frac{\psi_D^2(\alpha, k_\perp)}{2-\alpha}. \quad (2.48)$$

Due to the angular condition  $\psi_D(\alpha, k_\perp) = \psi_D(k)$  (see discussion in section 2.3 and eq. (2.22)). For practical calculations it is useful to express the  $\rho_D^N(\alpha, k_\perp)$  through the S and D state of the deuteron WF using eqs. (2.23), (2.25)

$$\rho_D^N(\alpha, k_\perp) = [U^2(k^2) + W(k^2)] \frac{\sqrt{m^2 + k^2}}{2 - \alpha}. \quad (2.49)$$

Here the factor  $2 - \alpha$  is due to the two-nucleon phase volume. The factor  $\sqrt{m^2 + k^2}$  arises from the Jacobian in the transformation of the phase volume

$$\frac{d\alpha}{\alpha} \frac{d^2 k_\perp}{(2 - \alpha)} = \frac{d^3 k}{\sqrt{m^2 + k^2}}.$$

## 2.5. Relativistic effects in the hadron scattering from deuteron

A theoretical description of high-energy hadron–deuteron interactions is considerably more complicated than that for lepton–deuteron scattering processes. Realistic models of these reactions however can be constructed by applying traditional physical approximations like the impulse approximation or Glauber theory generalized by Gribov [120] to the high energy processes with multiparticle production (see also [121]). There exist two important reasons for the validity of these approximations for high-energy hadronic processes: (a) In the high-energy process the fast deuteron prescattering state is formed long before the target at distances of order

$$\sim \frac{1}{E_{N_2} + E_{N_2} - E_D} \sim \frac{2P}{4(m^2 + k_\perp^2)/\alpha(2 - \alpha) - M_D^2}. \quad (2.50)$$

Moreover, due to Lorentz dilatation the characteristic time between different fluctuations within the fast deuteron becomes larger at high energy than the characteristic time for the interaction with the target  $\sim 1/m$ . Therefore the deuteron in some sense can be considered as a collection of free nucleons. In typical high energy hadronic reactions the energy transfer is not sufficient to resolve quarks and gluons. Thus, soft hadronic processes could not be considered as incoherent in terms of pointlike quarks and gluons. That is why they are usually described in terms of hadron exchanges. (b) Experimentally average Feynman  $x, p_\perp$  for nucleon in inelastic  $h + N \rightarrow N + X$  reaction are about 0.5 and 0.4 GeV/c respectively. Thus in inelastic hD reaction large momentum  $\sim 1$  GeV/c is transferred to the target nucleon in the deuteron rest frame.

Let us now consider inclusive high-energy reactions



where the produced hadron  $b$  is kinematically forbidden for the scattering from a free nucleon. Let particle “ $b$ ” be in the deuteron fragmentation region. At infinite energies this kinematic region corresponds to the condition that the light cone fraction of the deuteron momentum carried by particle “ $b$ ”  $\alpha_b/2 = (E_b + p_{bZ})/(E_D + p_{DZ})$  is within the limits  $2 > \alpha_b > 1$ . The condition  $\alpha_b = 1$  is the kinematic boundary for the elementary processes  $h + N \rightarrow b + X$ . In the deuteron rest frame and  $E_h \rightarrow \infty$  this condition has the form:<sup>†</sup>

<sup>†</sup> Evidently at intermediate energies kinematic restrictions are more stringent and part of the region  $\alpha_b < 1$  is forbidden for the scattering from free nucleon.

$$2 > \alpha_b \equiv 2(\sqrt{m_b^2 + p_b^2} - p_{bz})/M_D > 1 \quad (2.51)$$

where the  $Z$  axis is chosen along the projectile direction. For light particles  $b$  like  $N, \pi, k$  this region covers backward angles only. For  $m_b > m_N$  it covers also forward angles. In this review we restrict ourselves to the discussion of fast backward (FB) particles production, since only this kinematic region has been investigated experimentally. These particles are referred to in the literature as cumulative particles [3], backward particles [9], backward emitted particles [26] etc.

Since these reactions are typical fragmentation processes their inclusive cross section should be independent of initial energy at  $E_h \rightarrow \infty$ :

$$E_b \frac{d^3\sigma^{D+h \rightarrow b+\dots}}{dp_b^3} \equiv G_h^{D/b}(E_D, p_b) = G_h^{D/b}(\alpha_b, p_{b_\perp}). \quad (2.52)$$

This property is known as Feynman scaling [90] and it is observed for all high energy hadron reactions if  $\alpha_b$  is not small (see e.g. [88]). The experience in quantum field theory (cf. section 2.1) hints that  $G_h^{D/b}$  contains information on the deuteron WF.

### 2.5.1. Direct mechanism of fast backward (FB) particles production

Let us first consider the case of FB particles “ $b$ ” absent in the deuteron WF ( $\pi, k, \Lambda$ ). A natural mechanism for this reaction is the production of particle “ $b$ ” in the scattering of an initial hadron  $h$  from a nucleon with  $\alpha > 1$  (a backward nucleon in the deuteron rest frame) [11, 38, 40, 51]. In impulse approximation the direct mechanism corresponds to diagram 2.13 for the inclusive cross section. The dotted line in fig. 2.13 indicates the final state for the considered process. We shall now demonstrate that Glauber screening is absent for the FB particle [42, 81]. Really this result is a consequence of unitarity of the theory and can be formally proved by application of Abramovsky, Gribov, Kancheli (AGK) rules for the calculation of inclusive spectrum within reggeon field theory†. The condition  $\alpha_b > 1$  necessarily selects subprocesses with large energy transfer. Therefore the final state interaction of the particle “ $b$ ” with a second nucleon should be rather small. Consequently it will be neglected in the following analysis. Additional arguments in favour of this approximation are provided by QCD (section 4.2).

Typical reggeon diagrams for the total cross section are described in figs. 2.14–2.15. The wiggly lines in figs. 2.14–2.15 represent the exchange of the Pomeron, the vacuum reggeon. We omit here enhanced reggeon diagrams as a theoretical analysis (see e.g. [121]) shows that conventional Gribov–Glauber model of hadron–nucleus scattering without enhanced reggeon diagrams works up to energies of the order of 200–400 GeV‡. To calculate inclusive spectrum from reggeon diagrams one should substitute

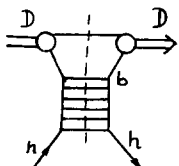


Fig. 2.13.

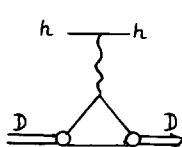


Fig. 2.14.

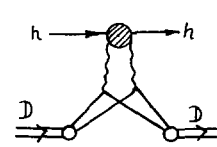


Fig. 2.15.

† The AGK rules are nicely described in a number of reviews, see e.g. [98]. A more intuitive derivation will be given in section 7.

‡ Actually it follows from the AGK rules that the contribution of the triple-Pomeron diagrams into the inclusive yield of particles with  $\alpha \geq 1$  is cancelled.

the wiggly lines by the ladders (to cut the reggeon). To perform this procedure it is important that we use the IMF light cone WF of the deuteron with on mass shell nucleons. Since the energy of the fast deuteron is partitioned between nucleons long before the interaction there is no problem of energy non-conservation in the reggeon vertex. Thus AGK rules can be applied for the calculation of the inclusive yield of FB particles. Cutting the reggeon in fig. 2.14 leads to diagram 2.13 for the inclusive cross section. On the contrary reggeon diagram 2.15 gives zero contribution to the inclusive spectrum. In fact for fig. 2.15 we obtain two diagrams where one reggeon is cut. Each diagram has sign  $(-1)$ . At the same time if both reggeons are cut we obtain a twice as big positive contribution  $(+2)$ . (Particle "b" could be produced from either of two ladders.) The sum is zero. In general one can show that due to the topological structure of AGK combinatorics (unitarity of the theory) all reggeon diagrams, where reggeons are attached to both nucleons give zero contribution into the inclusive spectrum. The sum of reggeon diagrams, where  $h$  interacts with one nucleon should be included in the amplitude of the elementary process  $h + N \rightarrow b + \dots$ . Therefore the inclusive production of FB particles via direct mechanism is described by impulse approximation (cf. eq. (2.19)) both for lepton and hadron projectiles. We want to emphasize that there is no such cancellation for exclusive and semiinclusive reactions – impulse approximation does not hold in this case (see also the discussion in sections 7.2 and 7.3).

For practical calculations it is necessary to express the inclusive cross section through the deuteron WF. It can be done by applying the general equation (2.19) for the impulse approximation and eq. (2.49) for  $\rho_D^N(\alpha, k_\perp)$ . The final formula has the form

$$E_b \frac{d^3\sigma^{D+h \rightarrow b+\dots}}{d^3p_b} = \int [U^2(k) + W^2(k)] d^3k E_b \frac{d^3\sigma^{h+N \rightarrow b+\dots}}{d^3p_b} (\tilde{\nu}, p_b). \quad (2.53)$$

Here  $\tilde{\nu}$  is given by eq. (2.19a) and the relationship between  $\alpha$  and  $k$  is given by eq. (2.21).

### 2.5.2. Spectator mechanism of fast backward nucleon production

The so called spectator mechanism dominates FB nucleon production (see fig. 2.16a). One of nucleons of the deuteron scatters from hadron  $h$ , loses its energy and therefore releases its neighbour-spectator. In the impulse approximation the cross section of this process is determined by the imaginary part of the zero-angle amplitude (see fig. 2.16b)

$$\frac{d\sigma^{D+h \rightarrow N+\dots}}{(d\alpha/d\alpha) d^2k_\perp} = \frac{1}{\nu} \text{Im } f[\tilde{\nu}] \frac{\psi_D^2(\alpha, k_\perp)}{(2-\alpha)^2}. \quad (2.54)$$

Here  $\psi_D(\alpha, k_\perp)$  is the light cone deuteron WF. All notations correspond to eq. (2.19). In section 2.4 it has been found that  $\psi_D^2$  is directly expressed through the S, D deuteron WF:  $\psi_D^2(k) =$

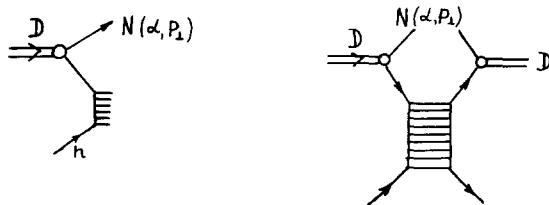


Fig. 2.16. The spectator mechanism of the nucleon production.

$[U^2(k) + W^2(k)]\sqrt{m^2 + k^2}$  (cf. eq. (2.49)). The factor  $(2 - \alpha)^{-2}$  in the eq. (2.54) is due to the initial and final state phase volume of the interacting nucleon.  $\tilde{\nu}$  is given by eq. (2.19a). Because of the optical theorem  $\text{Im } f(\nu) = \nu \sigma_{\text{tot}}(\nu)$ . We neglect here elastic and diffractive processes because energy transferred to the interacting nucleon is not large in this case and therefore final state interaction will suppress yield of spectators (cf. section 7.4). Finally we obtain [40]:

$$\frac{d\sigma^{D+h \rightarrow N+\dots}}{(d\alpha/\alpha) d^2 p_\perp} = \sigma_{\text{inel}}^{hN} [\tilde{\nu}] \cdot \frac{[U^2(k) + W^2(k)]}{(2 - \alpha)} \sqrt{k^2 + m^2}. \quad (2.55)$$

The relationship between  $\alpha$  and  $k_\perp$  is given by eq. (2.21).

### 2.5.3. Glauber screening of spectator mechanism

Eq. (2.55) overestimates the spectator yield since the projectile  $h$  can transfer positive longitudinal momentum to the FB nucleon provided both nucleons are at close impact parameters, see fig. 2.17.

This is the Glauber correction familiar from the analysis of total and elastic cross sections. Recall that AGK cancellation is not complete in this case since the spectator itself participates in the reggeon-deuteron interaction. To explain basic features of this phenomenon we assume that similar to quantum mechanics Glauber screening corresponds to the eikonal diagram 2.18. Within the eikonal approach this procedure overestimates the Glauber screening as rescattering diagrams of next order fig. 2.19 will somewhat reduce the contribution of diagram fig. 2.18.

The wiggly line in fig. 2.18 represents the amplitude of the elastic  $hN$  scattering. In the calculation we neglect: (1) processes with small multiplicity, where initial nucleon loses a small part of its energy. This contribution is suppressed by final state interaction if we select FB nucleons with  $\alpha > 1.2-1.3$  (cf. section 7.4); (2) excitations of hadron  $h$  in the intermediate state. In line with experimental data we assume that  $S$ -channel helicity is conserved. The result of the calculation [71a] of the time-ordered diagram 2.18 following standard prescriptions of reggeon field theory (see [98]) can be represented in the form of a screening factor  $\kappa_h$  in eq. (2.56)

$$E_N \frac{d^3 \sigma^{h+D \rightarrow N+\dots}}{d^3 p_N} = \kappa_h \sigma_{\text{inel}}^{hN} \rho_D^N(\alpha, p_\perp) \quad (2.56)$$

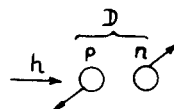


Fig. 2.17. Illustration of the Glauber screening for the spectator mechanism.

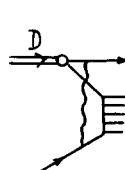


Fig. 2.18. The first order diagram for the Glauber screening.

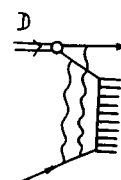


Fig. 2.19. The second order diagram for the Glauber screening.

$$\begin{aligned}
1 - \kappa_h = & \frac{1}{\sigma_{in}^{hN}} \left\{ \int \frac{U(k) U(k') + W(k) W(k') [\frac{3}{2}(kk')^2/k^2 \cdot k'^2 - \frac{1}{2}]}{U^2(k) + W^2(k)} \right. \\
& \times f^2(q_1) \left[ \frac{\sqrt{m^2 + k^2}}{\sqrt{m^2 + k'^2}} \right]^{1/2} \frac{d^2 q_\perp}{(2\pi)^2} - \frac{1}{4} \int \frac{U(k_1) U(k_2) + W(k_1) W(k_2) [\frac{3}{2}(k_1 k_2)^2/k_1^2 k_2^2 - \frac{1}{2}]}{U^2(k) + W^2(k)} \\
& \times \left. \frac{\sqrt{m^2 + k^2}}{\sqrt{(m^2 + k_1^2)(m^2 + k_2^2)}} f(q_{1\perp}) f(q_{2\perp}) f(q_{1\perp} + q_{2\perp}) \frac{d^2 q_{1\perp}}{(2\pi)^2} \frac{d^2 q_{2\perp}}{(2\pi)^2} \right\}. \quad (2.57)
\end{aligned}$$

Here  $f(q_\perp)$  is the amplitude of elastic  $hN$  scattering normalized according to condition  $\text{Im } f(0) = \sigma_{tot}^{hN}$ .  $U(k)$ ,  $W(k)$  are deuteron WF (cf. eq. (2.25)).  $k = k(\alpha, p_\perp)$ ,  $k' = k(\alpha, p_\perp + q_\perp)$ ,  $k_1 = k(\alpha, p_\perp + q_{1\perp})$ ,  $k_2 = k(\alpha, p_\perp + q_{2\perp})$ . We account for the spin of deuteron and nucleons following prescription of section 2.3. The analysis [71] shows that spin effects somewhat diminish the Glauber correction. It is easy to check by numerical evaluation of eq. (2.57) that  $\kappa_h$  is practically constant at  $\alpha > 1.4$ . This is because the large  $\alpha$  behaviour of  $\kappa_h$  is determined by slow  $k$ -dependence  $U(k)$ ,  $W(k)$ .

The calculations in quantum field theory models show that reggeization of the particles is related to inelasticities. Therefore it is reasonable to expect that at  $\alpha \rightarrow 2$ , where inelasticities in the deuteron WF dominate, the triple-reggeon contribution (fig. 2.20) will determine the cross section. In this region:

$$\alpha \frac{d\sigma}{d\alpha d^2 p_\perp} \sim (1 - \alpha/2)^{\beta_p(0) - 2\beta_N(p_\perp^2)} G(p_\perp^2) \quad (2.58)$$

where  $\beta_p(p_\perp^2)$ ,  $\beta_N(p_\perp^2)$  are the vacuum and the nucleon trajectories. Note that for arbitrary  $\psi_D(k)$  eqs. (2.56) and (2.58) predict different dependence of the cross section on  $\alpha$ ,  $p_\perp$ .

We have discussed above the contribution of small-distances effects in the deuteron. In relativistic theory the backward protons could be also produced due to large longitudinal distances effects. For example  $N^*$  can be diffractionally produced in the first scattering of  $h$  from one of the nucleons and then  $N^*$  can produce backward nucleon in the second interaction (see fig. 2.21). It is easy to check that the final nucleon can obtain  $\alpha \geq 1$  due to the large mass of  $N^*$  even if the initial nucleons of the deuteron have  $\alpha_{1,2} = 1$ . Indeed  $m_N^2/0.5 + m_{N^*}^2/0.5 = 4(m^2 + k^2)/\alpha(2 - \alpha)$ . For example in the case of  $N^*(1688)$   $\alpha$  can be as large as 1.72. As no detailed information on  $NN^* \rightarrow NN$  amplitudes exists now, we shall not make real estimation here. Note however that the process like fig. 2.21 contains some small factors; small value of diffraction processes, the small factor  $|\psi_D(r = 0)|^2$ . In any case, since the mechanism like fig. 2.21 leads to events with small multiplicity this background can be suppressed by selecting events with multiplicity  $\langle n \rangle = \langle n \rangle_{S'=(2-\alpha)S} + 1$  (here  $\langle n \rangle$  is the average hadron multiplicity for the process  $h + N \rightarrow X$ ).

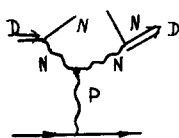


Fig. 2.20. The triple-reggeon diagram for the  $D + h \rightarrow p + X$  reaction in the limit  $\alpha \rightarrow 2$ .

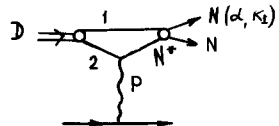


Fig. 2.21. Production of fast nucleon via rescattering of heavy baryon resonance.

### 2.5.4. Relativistic generalization of the Glauber approximation [64]

To illustrate the general ideas we shall consider here only the elastic rescattering effects, omitting the important question of inelastic screening, where similar formulae can be derived. The basic formula (2.59), (2.61) can be obtained in the framework of non-covariant diagram technique in the IMF. However, we shall give here only semiquantitative derivation.

In the non-relativistic theory the amplitude of high-energy scattering of hadron  $h$  from a nucleus in the Glauber approximation has the form [89, 123]:

$$F_{\text{Gl.}}(q_\perp) = \sum_{l=1}^A F_l(q_\perp).$$

Here  $F_l(q)$  is the amplitude of  $l$ -fold rescattering:

$$F_k(q_\perp) = (i/8\pi^2)^{k-1} C_N^k \int \prod_{l=1}^k d^2 q_l f(q_{l\perp}) \phi_k(q_1, q_k) \delta\left(\sum q_{l\perp} - q_\perp\right). \quad (2.59)$$

$q$  is the momentum transferred ( $q \approx q_\perp$ ),  $f(q)$  is the amplitude of  $hN$  elastic scattering, normalized according to optical theorem:  $\text{Im } f(q=0) = \sigma_{\text{tot}}(hN)$ . For simplicity we neglect here spin effects.  $C_N^k$  is the binominal coefficient.  $\phi(q_1, q_k)$  is the multiple form factor of the nucleus:

$$\begin{aligned} \phi_k(q_1, \dots, q_k) &= \int \prod_{j=1}^k d^3 p_j \psi^*\left(p_1 + q_1 - \frac{q}{N}, \dots, p_k + q_k - \frac{q}{N}, p_{k+1} - \frac{q}{N}, \dots, p_N - \frac{q}{N}\right) \\ &\times \psi(p_1, \dots, p_N) \delta\left(\sum_{j=1}^N p_j\right). \end{aligned} \quad (2.60)$$

Here  $\psi$  is the nucleus wave function, normalized according to

$$\int |\psi(p_1, \dots, p_N)|^2 \delta\left(\sum_{j=1}^N p_j\right) d^3 p_i = 1.$$

$|\phi(q_1, \dots, q_k)|^2$  has clear physical interpretation. It is the probability for nucleus not to be destroyed when momenta  $q_1, q_k$  are transferred to nucleons  $1, 2, \dots, k$ .

In relativistic theory the formula for elastic Glauber rescattering is quite similar. The only important difference is the recoil effect. To take it into account one should change  $\phi_l$  in the same fashion as for the deuteron form factor (see section 3.4):†

$$\begin{aligned} \phi_l(q_1, \dots, q_l) &= \int \prod_{i=1}^A \frac{d\alpha_i}{\alpha_i} d^2 p_{i\perp} \psi\left(\alpha_1, \dots, \alpha_N, \right. \\ &\quad \left. p_{1\perp} + q_{1\perp} - \frac{\alpha_1}{A} q_\perp, \dots, p_l + q_{l\perp} - \frac{\alpha_l}{A} q_\perp, \dots, p_{N\perp} - \frac{\alpha_N}{A} q_\perp\right) \\ &\times \psi(\alpha_1, \dots, \alpha_N, p_{1\perp}, \dots, p_{N\perp}) \delta\left(\sum p_{i\perp}\right) \delta\left(\sum \frac{\alpha_i}{A} - 1\right) \end{aligned} \quad (2.61)$$

† More formally this expression can be obtained using the non-covariant light cone diagram technique, similar to the Gribov's derivation of the Glauber series for high-energy hadron-nucleus scattering [120].

where

$$\mathbf{q}_\perp = \sum_{i=1}^l \mathbf{q}_{i\perp}.$$

What qualitative effects follow from eq. (2.61)? For rescatterings of the order less than  $A$  the recoil effect leads to a slower fall of the amplitude with  $q^2$  increase as in the case of the deuteron form factor (see section 3). For  $A$ -fold rescattering there is compared with the non-relativistic case the additional decrease with  $q^2$  because in relativistic theory the integrations over longitudinal and transverse momenta are not separated. Let us illustrate the last point by the example of the scattering from the deuteron. We shall use the Gaussian type WF;

$$\varphi(M^2) = N \exp(-A(M^2 - 4m^2)/4). \quad (2.62)$$

The amplitude of hN scattering is taken in the form:

$$f_{hN}(q) = i \sigma_{tot}(hN) \exp(-Bq^2). \quad (2.63)$$

It is easy to check that the different dependence on  $q^2$  compared with non-relativistic case is due to corrections to the WF of the order  $k^2/m^2$ . After substituting (2.62), (2.63) into eqs. (2.59), (2.61) and performing the integration we obtain at  $Am^2 \gg 1$

$$F \sim \exp(-Bq^2/2) / \sqrt{1 + (q^2/4m^2)B/(A + 4B)}. \quad (2.64)$$

This should be compared with  $F \sim \exp(-Bq^2/2)$  in non-relativistic case.

This example shows that the real parameter which characterizes the importance of relativistic effects in rescattering is  $\kappa = q^2/4m^2$  as in the case of the deuteron form factor (section 3.4). Evidently this parameter is small for the processes studied in conventional nuclear physics. This notion explains why Glauber formulae based on non-relativistic quantum mechanics work in a wide kinematical region.

### 3. High-energy short-range phenomena in the deuteron. Comparison with experiment

The deuteron is the simplest two-body nuclear system. Its light-cone WF is known in a wide range of nucleon momenta due to simple relationship between Weinberg and Schrödinger equations (section 2.3) and the possibility of using QCD for estimating the high momentum component of WF (section 4.2). Consequently high energy processes dominated by the high momentum component of the deuteron WF can be calculated. They provide a good testing ground for a relativistic theory of the bound state. To be definite, in the numerical calculations we shall use realistic light-cone WFs like the Hamada–Johnston [107] and the Reid soft core [108] WFs, since these WFs have momentum dependence rather close to the QCD estimate of section 4.2. We shall demonstrate below that such a choice of WF describes quantitatively all existing data on the high-energy short-range phenomena in the deuteron.

#### 3.1. Inelastic eD scattering in the threshold region at high momentum transfer [75]

We shall consider here the process  $e + D \rightarrow e + X$  at large  $q^2$  ( $0.8 < -q^2 < 6 \text{ GeV}^2$ ) below and near the

pion threshold, which was measured by American University group in SLAC [5]. Experimentally pion production is small below  $\Delta$ -isobar threshold [124]. Thus we neglect this contribution. In the kinematic region of [5]  $\Delta$ -excitation could contribute only at  $-q^2 \geq 4 \text{ GeV}^2$ , where it gives but small correction due to threshold factor and small transition form factor at large  $-q^2$  (as compared to elastic nucleon scattering). Therefore in the kinematics of [5] the two-nucleon final state gives dominant contribution into the inclusive cross section.

Within the two-nucleon approximation for the deuteron WF this process is described by two diagrams of old-fashioned perturbation theory in the IMF. Black blobs in figs. 3.1, 3.2 denote electromagnetic nucleon form factors. Open blobs denote the deuteron WF. As in the previous section we choose a c.m. system of  $e$  and  $D$ , where  $q = ((2\nu + q^2)/4P, (-2\nu + q^2)/4P, q_\perp)$ ,  $q_\perp^2 = -q^2$ ,  $p_D = -p_e \equiv P \rightarrow \infty$  to suppress the vacuum pair production by  $\gamma^*$ .

Energy conservation implies

$$\frac{W^2 - 4m^2}{4} = \frac{m^2(1-\alpha)^2 + (k_\perp - \frac{1}{2}\alpha q_\perp)^2}{\alpha(2-\alpha)}. \quad (3.1)$$

Here  $W^2 = (p_D + q)^2$  is the invariant energy square and  $(\alpha, p_\perp)$  is the light-cone momentum of the spectator nucleon (see fig. 3.1). It follows from eq. (3.1) that at large  $q_\perp^2$  and fixed  $W^2$  essential  $k_\perp$  are of order  $q_\perp/2$ . Therefore at large  $q^2$  this process probes the short range structure of the deuteron WF.

We restrict our analysis to the kinematical region  $(W^2 - 4m^2)/4m \gg \varepsilon_D$  to avoid large final state interaction, which considerably enhances the cross section at small  $W^2 - 4m^2$  due to presence of deuteron pole and singlet virtual state. (For discussion of final state interaction effects see e.g., ref. [125].)

In the impulse approximation (fig. 3.1) the deuteron structure functions for the considered process are given by

$$W_1(q^2, W^2) = \sum_{N=p,n} \left( (F_{1N}(q^2) + F_{2N}(q^2))^2 \cdot \frac{-q^2}{4m^2} \cdot j_1(q^2, W^2) + \left( F_{1N}^2(q^2) + \frac{-q^2}{4m^2} F_{2N}^2(q^2) \right)^2 \cdot j_3(q^2, W^2) \right) \quad (3.2)$$

$$W_2(q^2, W^2) = \sum_{N=p,n} \left( F_{1N}^2(q^2) + \frac{-q^2}{4m^2} F_{2N}^2(q^2) \right) \cdot j_2(q^2, W^2). \quad (3.3)$$

Here  $F_{1,2N}(q^2)$  are Dirac form factors of nucleon ( $F_{1N}(0) = 1$ ,  $F_{2N}(0) = \mu_N$ ), and  $j_1, j_2, j_3$  are overlapping integrals

$$j_1(q^2, W^2) = \frac{4m^2}{M_D} \int \rho_D^N(\alpha, k_\perp) \frac{1}{\alpha} \delta(\tilde{\nu} + q^2) \cdot \frac{d\alpha dk_\perp}{\alpha} \quad (3.4)$$

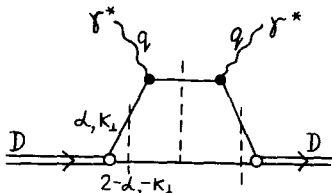


Fig. 3.1.

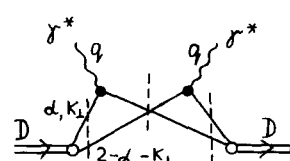


Fig. 3.2.

Figs. 3.1, 3.2. Impulse approximation and interference diagrams for the  $e + D \rightarrow e' + N + N$  reaction.

$$j_2(q^2, W^2) = M_D \int \rho_D^N(\alpha, k_\perp) \delta(\tilde{\nu} + q^2) \frac{d\alpha dk_\perp}{\alpha} \quad (3.5)$$

$$j_3(q^2, W^2) = \frac{2}{M_D} \int \frac{k_y^2}{\alpha} \cdot \rho_D^N(\alpha, k_\perp) \delta(\tilde{\nu} + q^2) \frac{d\alpha dk_\perp}{\alpha}. \quad (3.6)$$

Here  $\tilde{\nu} = \frac{1}{2}\alpha(2(p_D q) + M_D^2 - M_{NN}^2) + 2k_\perp q_\perp$ ,  $M_{NN}^2 = 4\{(m^2 + k_\perp^2)/\alpha\}/(2 - \alpha)$ .  $q_\perp$  is along  $x$  axis.  $\rho_D^N(\alpha, k_\perp)$  is expressed through the deuteron WF according to eq. (2.49). The overlapping integrals can be rewritten in a more simple form if one introduces variables  $k_i(\alpha, k_\perp)$ , the momentum of a nucleon in the initial state (eq. (2.21)) and  $k_f$ , the momentum of the spectator nucleon in the c.m.s. of produced nucleons ( $W^2 \equiv M_f^2 = 4(m^2 + k_f^2)$ ):

$$\begin{aligned} j_1(q^2, W^2) &= \frac{2m^2}{M_D} \int \frac{(u^2(k_i) + w^2(k_i))}{\alpha} \sqrt{\frac{m^2 + k_i^2}{m^2 + k_f^2}} \delta(M_f^2/4 - m^2 - k_f^2) d^3 k_f \\ j_2(q^2, W^2) &= \frac{M_D}{2} \int \alpha (u^2(k_i) + w^2(k_i)) \sqrt{\frac{m^2 + k_i^2}{m^2 + k_f^2}} \delta(M_f^2/4 - m^2 - k_f^2) d^3 k_f \\ j_3(q^2, W^2) &= \frac{2}{M_D} \int \frac{k_y^2}{\alpha} (u^2(k_i) + w^2(k_i)) \sqrt{\frac{m^2 + k_i^2}{m^2 + k_f^2}} \delta(M_f^2/4 - m^2 - k_f^2) d^3 k_f. \end{aligned} \quad (3.7)$$

In the non-relativistic limit, where

$$\alpha = 1 + k_{3i}/\sqrt{m^2 + k_i^2} \approx 1 + k_{3i}/m \approx 1 + k_{3f}/m,$$

and where corrections of order  $k_i/m$ ,  $\epsilon_D/m$  should be neglected;  $j_1, j_2$  take the form familiar from the non-relativistic quantum mechanics and  $j_3 = 0$ :

$$j_1(q^2, W^2) = j_2(q^2, W^2) = \int (u^2(k) + w^2(k)) \delta(\omega - (k^2 + (k + q)^2)/2m) d^3 k. \quad (3.8)$$

Here  $\omega, q$  is the photon momentum in the deuteron rest frame.

Because the interference diagram 3.2 leads to rather lengthly formulae we present here expressions for  $W_2$  only, since in the kinematic region of experiment ( $\theta = 8^\circ$ ) the  $W_1$  contribution is negligible. In the calculation of spin effects we use eq. (2.24) for  $\psi_D$  and sum over the deuteron polarizations. The interference term is equal:

$$\begin{aligned} \frac{1}{M_D} W_{2D}(W^2, q^2) &= \int d^3 k \ 2\delta((q + p_D)^2 - W^2) \cdot \left\{ 2U(k) U(k') \left[ F_1^p(q^2) F_1^n(q^2) + \frac{q^2}{12m^2} F_2^p(q^2) F_2^n(q^2) \right] \right. \\ &\quad \left. + F_1^p(q^2) F_1^n(q^2) W(k) W(k') \left[ \frac{3(kk')^2}{k^2 k'^2} - 1 \right] + \frac{q^2}{m^2} F_2^p(q^2) F_2^n(q^2) \left[ \frac{U(k) W(k')}{\sqrt{2}} \left( \frac{1}{3} - \frac{k_y^2}{k'^2} \right) \right. \right. \\ &\quad \left. \left. + \frac{U(k') W(k)}{\sqrt{2}} \left( \frac{1}{3} - \frac{k_y^2}{k^2} \right) \right] + \frac{3q}{4m} [F_2^p(q^2) F_1^n(q^2) + F_1^p(q^2) F_2^n(q^2)] \frac{W(k) W(k') k_y^2}{k^2 k'^2} [k, k']_y \right\} \end{aligned}$$

$$+ \frac{1}{4} F_2^p(q^2) F_2^n(q^2) W(k) W(k') \left[ \frac{3(kk')^2}{k^2 k'^2} - \frac{6k_y^2(kk')}{k^2 k'^2} + \frac{2k_y^2}{k^2} + \frac{2k_y^2}{k^2} - \frac{5}{3} \right] \quad (3.9)$$

where  $k = k(\alpha, k_\perp)$ ,  $k' = k(\alpha, k_\perp + q_\perp)$ .

For the given kinematics the contribution of eq. (3.9) constitutes a rather small correction ( $\leq 20\%$ ) to the impulse approximation (eq. (3.2)). This is because large momenta  $k$  are essential in eq. (3.9) and because an additional factor  $1/3$  is present in eq. (3.9) for magnetic transition since only the zero deuteron helicity contributes in this case.

In the numerical calculation we use, in line with analysis of Weinberg equation in section 2.3 and QCD analysis of section 4.2, the realistic WFs of the deuteron. For  $F_{IN}(q^2)$  we use the conventional dipole fits for Sachs form factors  $G_{Ep}$ ,  $G_{Mp}$ ,  $G_{Mn}$  and neglect the small  $G_{En}$  contribution. We want to emphasize that the cross section of the considered process is not sensitive to the value of  $G_{En}(q^2)$  at  $-q^2 \geq 1 \text{ GeV}^2$ , which is poorly known experimentally. Thus, it can be calculated more reliably than the elastic form factor of the deuteron (see section 3.4).

The agreement is reasonable (see fig. 3.3) though high  $Q^2$  data agree better with Reid soft core WF. (It is worth noting that the high momentum behaviour of this WF is closer to the QCD prediction, cf. eq. (4.10).) The data points below the kinematical limit  $W = M_D$  are due to finite resolution of the incident electron beam. ( $\Delta E_i/E_i$  was approximately  $\pm 0.3\%$  to  $\pm 0.5\%$ .)†

Note that at different  $W$ ,  $q^2$  different combinations of  $\alpha$ ,  $k_\perp$  corresponding to equal  $k$  are essential. Thus this comparison with the experiment checks that  $\rho_D^N(\alpha, k_\perp)(2-\alpha)$  does indeed depend on one variable in accordance with discussion of section 2.

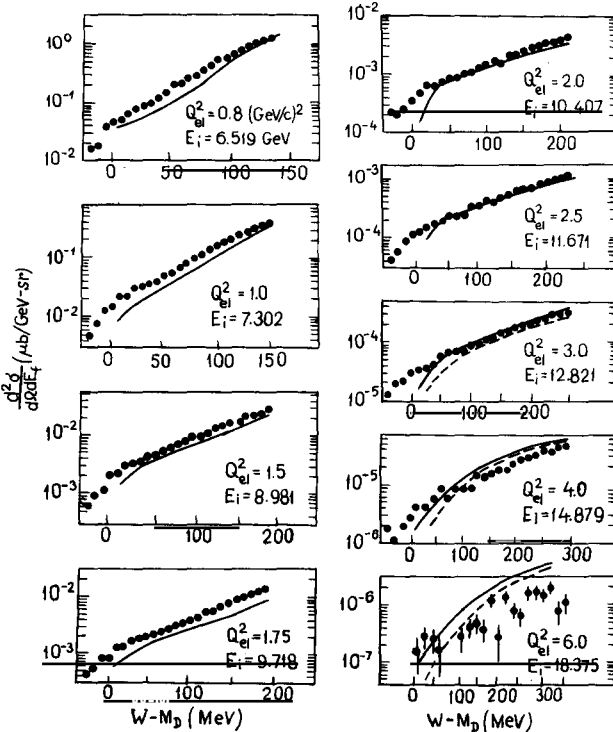


Fig. 3.3. Comparison of the  $e + D \rightarrow e + X$  data [5] with the calculation based on eqs. (3.3) and (3.9).

† We are indebted to Prof. R. Arnold for illuminating correspondence on this point.

We do not discuss here the data [126] obtained at smaller momentum transfer. In this case relativistic effects are small – eq. (3.8) can be used. So our approach would lead to the same predictions as non-relativistic approach of ref. [125], which reasonably explains these data.

In refs. [46, 48, 49] the data [5] were analysed within Bethe-Salpeter light cone formalism<sup>†</sup> using the deuteron WF suggested by Blankenbecler and Schmidt on the basis of quark counting rules and their analysis of  $p + D \rightarrow p + X$  reaction. It was demonstrated by Blankenbecler and Schmidt [47] and by Chemtob [69] that this WF underestimate cross section by the factor 5–30 at large  $q^2$ . In ref. [69] this discrepancy was interpreted as an indication that a slower decrease of  $\rho_D^N$  with  $\alpha$  (more close to the QCD estimate of section 4.2) is necessary to fit the data. On the contrary Schmidt have suggested [48] that this discrepancy with the model [46] is due to final state two-nucleon resonance (presumably wide resonance (resonances!) with  $M_R = M_D + 0.1\text{--}0.2\text{ GeV}$ , since kinematical region covered in [5] corresponds to  $M_D < W < 0.35\text{ GeV} + M_D$ , see fig. 3.3).

### 3.2. Deuteron deep inelastic structure functions

We consider here deep inelastic  $\gamma^*$  scattering from the unpolarized deuteron, i.e. the process  $e + D \rightarrow e + X$  at large  $q^2$  and large invariant mass  $W^2$  of the hadron state  $X$ . The basic equations describing this process were derived in section 2.2. It is convenient to introduce conventional notations:

$$\begin{aligned} F_{1N}(x, q^2) &= M_N W_{1N}(\nu, q^2), & F_{1D}(x, q^2) &= M_D W_{1D}(\nu, q^2), \\ F_{2N}(x, q^2) &= \frac{\nu W_{2N}(\nu, q^2)}{M_N}, & F_{2D}(x, q^2) &= \frac{\nu W_{2D}(\nu, q^2)}{M_D}, \\ F_{3N}(x, q^2) &= \frac{\nu W_{3N}(\nu, q^2)}{M_N}, & F_{3D}(x, q^2) &= \frac{\nu W_{3D}(\nu, q^2)}{M_D}. \end{aligned} \quad (3.10)$$

As a result eq. (2.14) obtains at  $q^2 \rightarrow -\infty$  the form convenient for a comparison with the parton model and the QCD predictions

$$\begin{aligned} F_{1D}(x, q^2) &= \int \sum_{N=p,n} F_{1N}\left(\frac{x}{\alpha}, q^2\right) \rho_D^N(\alpha, k_\perp) \frac{2}{\alpha} \frac{d\alpha d^2k_\perp}{\alpha - \alpha} \\ F_{2D}(x, q^2) &= \int \sum_{N=p,n} F_{2N}\left(\frac{x}{\alpha}, q^2\right) \rho_D^N(\alpha, k_\perp) \frac{d\alpha d^2k_\perp}{\alpha} \\ F_{3D}(x, q^2) &= \int \sum_{N=p,n} F_{3N}\left(\frac{x}{\alpha}, q^2\right) \rho_D^N(\alpha, k_\perp) \frac{2}{\alpha} \frac{d\alpha d^2k_\perp}{\alpha} \end{aligned} \quad (3.11)$$

where

$$\begin{aligned} \rho_D^N(\alpha, k_\perp) &= \frac{\sqrt{m^2 + k^2}}{2 - \alpha} [U^2(k) + W^2(k)], & x &= -q^2/(qP_D) \\ \alpha &= 1 + k_3/\sqrt{m^2 + k^2} \end{aligned} \quad (3.11a)$$

<sup>†</sup> Here and after we shall refer to the Bethe-Salpeter approach which use the light cone normalization condition [43, 46–48, 58, 61, 69] as the light cone Bethe-Salpeter approach.

(see eqs. (2.49), (2.21)). We want to remind the reader that the impulse approximation is well founded at large  $q^2$ . The impulse approximation, eq. (3.10), can be applied also at small  $q^2$  if  $\nu$  is sufficiently large (otherwise the cross section cannot be accurately expressed through the deuteron WF, cf. section 2.1).

Eqs. (3.11) have a simple parton interpretation: the probability of finding a parton in the deuteron, carrying a fraction of the deuteron momentum  $x/2$ , is equal to the product of the probability of finding a nucleon with a fraction of the deuteron momentum  $\alpha/2$  and the probability of finding a parton in the nucleon with a fraction of the nucleon momentum  $x/\alpha$ .

One of the important tests of the applicability of the relativistic quantum mechanics developed in section 2 to the deuteron would be the measurement of the deuteron structure function in the region  $x = -q^2/p_{Dq} > 1$  but not specially close to 2. Due to the restriction  $\alpha > x$ , the cross section at  $x > 1$  is determined by the high momentum component of the deuteron WF. The results of the calculation of  $F_{2D}(x, q^2)$  in the Bjorken limit  $-q^2 \rightarrow \infty$  but fixed  $x$  [40] are presented in fig. 3.4. In line with discussion of sections 2.3, 4.2 we choose for  $U^2(k) + W^2(k)$  the Hamada–Johnston WF with hard core and the Reid WF with soft core (solid and dashed curves in fig. 3.4). To account for a small scaling violation we use the conventional parametrization [127] for  $F_{2p}(\omega')$  (where  $\omega'$  is the Bloom–Gilman scaling variable  $\omega' = (\nu + m^2)/-q^2$ ), and the interpolation formulae  $F_{2n}(\omega', q^2) = (1 - \frac{3}{4}/\omega') F_{2p}(\omega', q^2)$ , which describes the SLAC data well at  $\omega' > 1$ .

Until now there exist no measurements of  $F_i^D(x, Q^2)$  in the region  $x > 1$  in the Bjorken limit, where both  $W^2$  and  $Q^2$  are large. However it was observed in [5] that the spectra for  $e + D \rightarrow e + X$  reaction

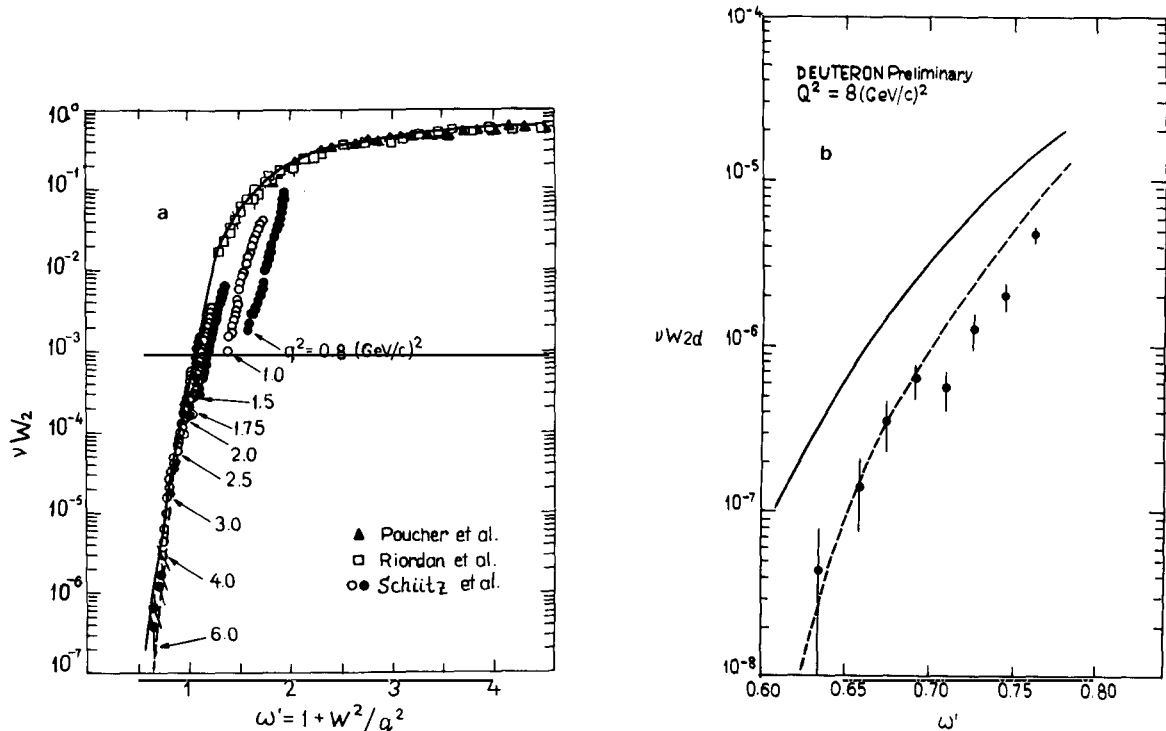


Fig. 3.4. The solid (dashed) curve is the result of the calculation in the scaling limit based on eq. (3.10) with Hamada–Johnston hard core (Reid soft core) wave functions. The data are from [5].

discussed in section 3.1 merge with increasing  $q^2$  (for  $-q^2 \geq 2 \text{ GeV}^2$ ) into an universal  $\nu W_{2D}(\omega')$  curve (see fig. 3.4), though  $M_x$  is still small. (In line with the Bloom–Gilman duality [127] this precocious scaling in  $\omega'$  could be interpreted as a consequence of lack of two-nucleon resonances.) Assuming as in [5] that this limiting curve does indeed represent  $F_{2D}(\omega')$  in the scaling limit it is possible to compare the data [5] with  $F_{2D}(x)$  calculated above [40]. It can be seen from the comparison in fig. 3.4 that the data at  $-q^2 > 2 \text{ GeV}^2$  and the limiting theoretical curve are in a reasonable agreement. In particular  $F_{2D}(\omega)$  calculated for the Hamada–Johnston WF can be roughly fitted in the region  $0.65 < \omega < 0.9$  as  $F_{2D}(\omega) = 0.02(\omega - 0.5)^n$ , where  $n = 5.67$  though the experimental fit gives  $n = 6 \pm 0.5$  [5a]. The latest data [5b] at smallest  $\omega'$  prefer the Reid soft core WF (fig. 3.4b) where

$$F_{2D}^{\text{Reid}}(x) = 0.44(1 - \frac{1}{2}x)^{10} - 0.03(1 - \frac{1}{2}x)^9 x \quad \text{at } 0.6 < \omega' < 0.9 \quad (\omega' = 1/x).$$

It is worth noting that the observed behaviour of  $F_{2D}(x)$  can be roughly fitted (within a factor 2) as  $(2 - x)^{10}$ , which is really the QCD prediction [65].

*Comparison with other approaches.* Another attempt [128] to take into account the deuteron structure assumes that the scattering amplitude is given by the Feynman diagram with an off-mass-shell interacting nucleon and an on-mass-shell spectator. The vertex function (i.e. the Bethe–Salpeter WF) is identified with the deuteron WF. In the Bjorken limit expression e.g. for  $F_{2D}(x, q^2)$  is as follows:

$$F_{2D}(x, q^2) = \sum_{N=p,n} \int F_{2N}\left(\frac{x}{\alpha}, q^2\right) \rho_D^N(\alpha, k_\perp) \frac{\alpha d\alpha d^2k_\perp}{(2 - \alpha)} \quad (3.12)$$

where  $(\alpha, k_\perp)$  is the light cone momentum of interacting nucleon.  $\rho_D^N(\alpha, k_\perp)$  depends only on the off-shellness of the interacting nucleon

$$m^2 - t = 2\alpha \left[ \frac{m^2 + k_\perp^2}{\alpha(2 - \alpha)} - \frac{M_D^2}{4} \right].$$

$\rho_D^N(\alpha, k_\perp)$  is identified with the non-relativistic deuteron WF [128] as

$$\rho_D^N(\alpha, k_\perp) = (U^2(k) + W^2(k))\sqrt{m^2 + k^2}, \quad (3.13)$$

where  $\alpha$  and  $k$  are related as

$$\begin{aligned} \alpha &= (m_D - \sqrt{m^2 + k^2} + k_3)/m \\ k_3 &= \sqrt{k^2 - k_\perp^2}. \end{aligned} \quad (3.14)$$

Eqs. (3.12)–(3.14) considerably underestimate  $F_{2D}(x)$  at  $x > 1$ . To demonstrate the magnitude of the effect we present in fig. 3.5 the ratio of  $F_{2p}(x)$  smeared with the Hamada–Johnston WF according to eqs. (3.10)–(3.11) and according to eqs. (3.12)–(3.14) at  $-q^2 \rightarrow \infty$ . This strong difference in the predicted value of  $F_{2D}(x)$  for  $x > 1$  is mainly due to the different relationship between  $\alpha$  and  $k$  in the eq. (3.11) and in eq. (3.14) (to obtain the same large  $\alpha > 1$  much larger  $k$  are necessary according to eq. (3.14) than according to eq. (3.11)). It was demonstrated in [43] that eq. (3.12) violates baryon charge conservation and universality of graviton interaction (see discussion in Appendix A). As a result the

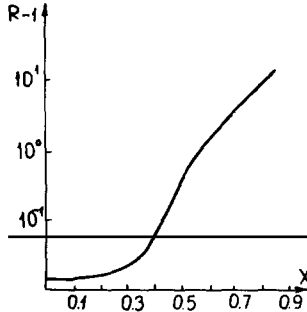


Fig. 3.5.  $R = F_{2D}^{(1)}(x)/F_{2D}^{(2)}(x)$  is the ratio of  $F_{2p}(x)$  smeared according to eq. (3.10) and according to eq. (3.12).

procedure to extract the neutron structure function from eD scattering based on the theoretical work of ref. [128] used by SLAC and BNL groups contains the so called West correction [128] which is absent if Feynman diagrams are calculated exactly [43, 58]. For example  $\sigma_{\gamma n}$  and the neutron structure function  $F_{2n}(x)$  extracted from  $\gamma^* D$  scattering are systematically overestimated by not less than 3%. As a result some important sum rules like the Gottfried sum rule

$$I = \int_0^1 [F_{2p}(x, q^2) - F_{2n}(x, q^2)] \frac{dx}{x}$$

become logarithmically divergent, as procedure used in [124] to extract  $F_{2n}(x)$  leads to  $F_{2p}(0) \neq F_{2n}(0)$ . The Gottfried sum rule can be rewritten in a more convenient form, which precisely takes into account the smearing correction:

$$I = \int [F_{2D}(x, q^2) - 2F_{2p}(x, q^2)] dx/x = \frac{1}{3}. \quad (3.15)$$

To obtain this equation we use the sum rule

$$\int_0^1 [F_{2D}(x, q^2) - F_{2p}(x, q^2) - F_{2n}(x, q^2)] dx/x = 0, \quad (3.16)$$

which follows directly from eq. (3.10) and from the normalization of the deuteron WF (eqs. (2.32), (2.33)). In this analysis a possible effect of Glauber screening (at small  $x$  and large  $q^2$ ) is neglected. It is not clear now whether this assumption (generally accepted in the analysis of the data) is consistent with QCD.

In the application of the light-cone Bethe-Salpeter formalism it was assumed [46–48, 61, 69] that  $\rho_D^N$  depends not on the interacting nucleon off-shellness but separately on  $\alpha$  and on  $k_\perp$ . Thus in [46–48, 61, 69] actually a non-covariant light-cone approach was used. In difference from [40] (eq. (2.49)) the angular condition was not taken into account. Consequently one could not exploit the relationship between Weinberg and Schrödinger equations and had to make some model assumptions about WF even in the region of small nucleon momenta, where this relationship can be directly checked by calculation of the IMF diagrams.

### 3.3. Deep inelastic $\ell + D \rightarrow \ell' + p + X$ reaction with unpolarized and polarized deuteron

#### 3.3.1. Unpolarized case

Reaction  $\ell + D \rightarrow \ell' + p + X$ , where a slow proton in the deuteron rest frame is selected can provide an independent information about the deuteron WF and about the ratio  $F_{2n}(x)/F_{2p}(x)$  at  $x \rightarrow 1$ . In this subsection we present the necessary equations for this reaction and give an estimate of background contribution arising from misidentification of the spectator.

As the data on  $\nu(\bar{\nu})D$  scattering will be available soon, we shall mainly consider this case. There are two essential contributions for this process (a) the spectator mechanism (fig. 3.6), where  $W^*$  scatters off the neutron and releases the proton, (b) the direct mechanism (fig. 3.7), where the proton is produced in the elementary interaction.

The spectator contribution has the form

$$I_{\text{spec}} = \frac{d\sigma^{\nu(\bar{\nu})+D \rightarrow \mu^{\pm} + p + X}}{dx dy (d\alpha/\alpha) d^2 p_\perp} = \frac{G_F^2}{\pi} M_N E_\nu (2 - \alpha) \rho_D^N(\alpha, p_\perp) \\ \times \left[ F_2^{\nu(\bar{\nu})n} \left( \frac{x}{2 - \alpha}, q^2 \right) (1 - y) + \frac{y^2}{2} \frac{2x}{2 - \alpha} F_1^{\nu(\bar{\nu})n} \left( \frac{x}{2 - \alpha}, q^2 \right) \mp y \left( 1 - \frac{y}{2} \right) \frac{x}{2 - \alpha} F_3^{\nu(\bar{\nu})n} \left( \frac{x}{2 - \alpha}, q^2 \right) \right]. \quad (3.17)$$

Here  $\alpha/2$  is the light cone fraction of deuteron momentum carried by the spectator proton. In the deuteron rest frame  $\alpha = 2[\sqrt{m_N^2 + p^2} - (\mathbf{p}\mathbf{q})/|\mathbf{q}|]/m_D$  and  $\rho_D^N(\alpha, k_\perp)$  is given by eq. (2.49).

To obtain expression for the case of  $e, \mu D$  reaction one should omit the  $F_3$  term and substitute  $(4\pi\alpha)^2/(4m_N E_e x^2 y^2)$  instead of  $(G_F/\sqrt{2})^2 m_N E_\nu$ . The contribution of the direct mechanism is a particular case of eq. (2.7)

$$I_{\text{dir}} = \frac{d\sigma^{\nu(\bar{\nu})+D \rightarrow \mu^{\pm} + p + X}}{dx dy (d\alpha/\alpha) d^2 p_\perp} = \sum_{N=p,n} \int_{x+\alpha}^2 \frac{d\beta}{\beta} \int d^2 k_\perp \rho_D^N(\beta, k_\perp) \\ \times \frac{d\sigma^{\nu(\bar{\nu})+N \rightarrow \mu^{\pm} + p + X}}{dx dy (dz/z) d^2 t_\perp} \left( \beta E_\nu, \frac{x}{\beta}, y, \frac{\alpha/\beta}{1 - x/\beta}, p_\perp - \frac{\alpha}{\beta} k_\perp \right). \quad (3.18)$$

Here  $\{d\sigma^{\nu(\bar{\nu})+N \rightarrow \mu^{\pm} + p + X}/dx dy (dz/z) d^2 t_\perp\}$  ( $E_\nu, x, y, z, t_\perp$ ) is the inclusive cross section of the elementary process, which is estimated in Appendix B,  $z \equiv (E_p + p_{pz})/((E_N + p_{Nz})(1 - x))$ , and  $k_\perp$  is the transverse momentum of the proton.

The results of calculation of  $I_{\text{dir}}/I_{\text{spec}}$  are presented in fig. 3.8 for  $eD$  scattering as a function of  $x, \alpha$ . At  $x < 0.5$  this ratio for  $\nu D(\bar{\nu} D)$  scattering differs by the factor  $\sim 0.6(1.2)$ . It is evident from fig. 3.8 that the contribution of the direct mechanism is negligible over a large range of  $\alpha$ . With increase of  $x$  the

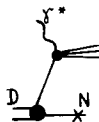


Fig. 3.6. The spectator mechanism for the  $\ell + D \rightarrow \ell' + p + X$  reaction.

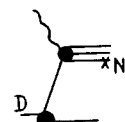


Fig. 3.7. The direct mechanism for the  $\ell + D \rightarrow \ell' + p + X$ .

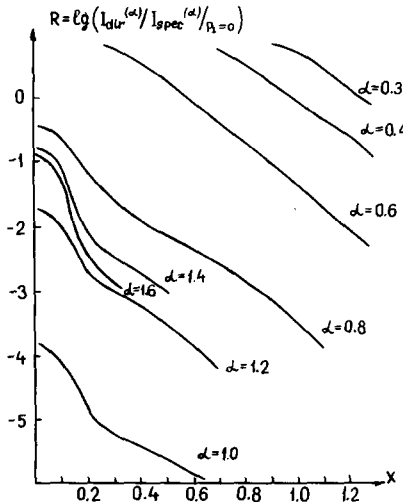


Fig. 3.8. The ratio of the direct and spectator contributions in reaction  $e + D \rightarrow e + p + X$ .

region, where the spectator contribution dominates extends to  $\alpha \sim 0.5$ , where in hadronic reactions the direct mechanism dominate.<sup>†</sup> Since the energy transfer to the target is large in deep inelastic processes and increases with  $x$ , one should not expect a significant final state interaction in this case. Therefore we conclude that both the deuteron WF and the neutron structure function can be unambiguously extracted from the analysis of the discussed reaction.

### 3.3.2. Inclusive scattering from the polarized deuteron and the nuclear short range interaction [81]

The success of the description of the deuteron using realistic WFs seems to confirm the existence of a short range nucleon-nucleon repulsive interaction. However this evidence is rather indirect. To verify this hypothesis one should check that the deuteron WF has a sharp edge at  $r_c \sim 0.4$  fm and consequently it oscillates in momentum space. In particular S-wave should have a node at  $k \sim 300$  MeV/c and S-, D-waves should be comparable at large nucleon momenta (for example, for the Hamada-Johnston WF D-wave is larger than S-wave at  $250$  MeV/c  $< k < 750$  MeV/c).

Generally it was proposed (see e.g. [130]) to study elastic eD scattering off a polarized deuteron. This experiment is technically very difficult. Moreover one cannot measure here the D-wave functions themselves but only their convolutions. Thus such an experiment is not very sensitive to the shape of WF [131].

At the same time the spectator distribution in  $\ell(h)D$  scattering is proportional to the square of the deuteron WF. Therefore this reaction can be used to separate S- and D-waves providing a straightforward check of the “nuclear core” hypothesis. Qualitatively it predicts that, for spectator momenta  $\geq 300$ – $400$  MeV/c, where the S-wave has a node, the cross section is determined by the D-wave and therefore strongly depends on the deuteron polarization. The expected effect is large ( $> 30\%$ ) for a spectator with momentum  $p > 200$  MeV/c.

<sup>†</sup> Really the SLAC data on the reaction  $e + p \rightarrow e + p' + X$  [132] indicate that the proton spectrum has maximum at  $z \sim 0.2$ . If true, this would lead to some additional decrease of direct mechanism as compared to the calculation using the model of Appendix B.

In the impulse approximation the cross section depends on the deuteron polarization vector in the same way as in quantum mechanics. The ratio of cross sections for the scattering from polarized and unpolarized deuteron is as follows (here we neglect the dependence of the  $\ell N$  amplitude on the nucleon polarization, which can be easily taken into account)

$$\eta^\xi(\alpha, p_\perp) \equiv E \frac{d^3\sigma^\xi}{dp^3} / E \frac{d^3\sigma}{dp^3} = r(\xi, k) \quad (3.19)$$

$$r(\xi, k) = 1 + \left( \frac{3(k\xi)^2}{k^2} - 1 \right) \frac{\sqrt{2}u(k)w(k) + w^2(k)/2}{u^2(k) + w^2(k)}. \quad (3.20)$$

$\xi$  is the D-polarization in the D-rest frame (the D-spin is quantized along the scattering axis, which will be labelled as 3-axis;  $\xi = (1, \pm i, 0)/\sqrt{2}$  for  $\lambda_D = \pm 1$ ,  $\xi = (0, 0, 1)$  for  $\lambda_D = 0$ ). The relation of  $k$  and  $\alpha, p_\perp$  is given by eq. (2.21).

Eq. (3.30) should be compared with the similar quantum mechanical expression

$$\eta^\xi(p) = r(\xi, p). \quad (3.21)$$

It follows from eqs. (3.20), (3.21) that for  $|U(k)| \leq |W(k)|$  the ratio  $\eta^\xi$  strongly depends on the D-polarization. According to eq. (3.20)  $\eta^\xi$  is the function of  $(\xi k)/k$  at fixed  $M_{NN}$ , but according to eq. (3.21) it is function of  $(\xi p)/p$  at fixed  $p$ . To illustrate difference of predictions we present in fig. 3.9a  $\eta^\xi$  for the scattering from the deuteron with longitudinal polarization  $\lambda = 0$ . (Dashed and dotted curves are the results of the calculation on the basis of eqs. (3.20) and (3.21) respectively for the Hamada–Johnston WF.) Evidently the expected effect is large for  $p_N \geq 0.3$  GeV/c. It is important that the value and form of momentum and angular dependence of  $\eta^\xi$  predicted by eqs. (3.20), (3.21) are rather different at large momenta.

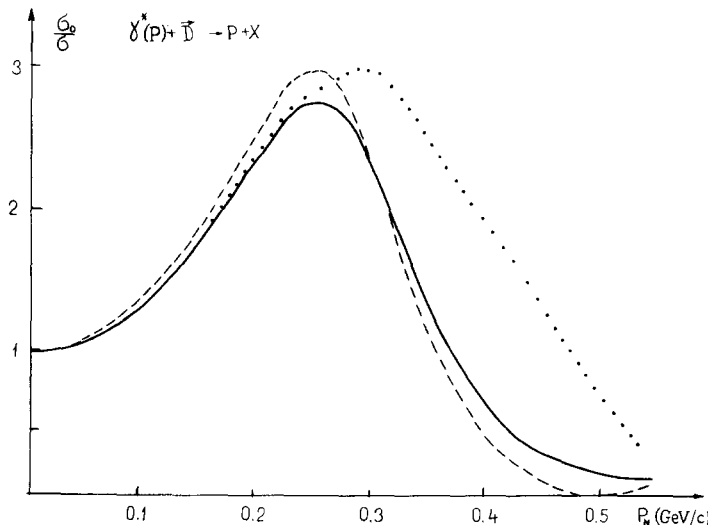
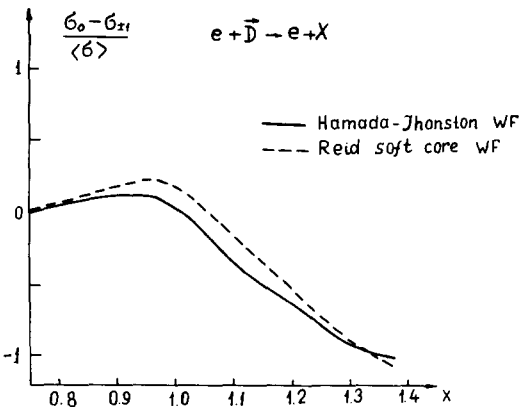


Fig. 3.9a. Polarization effects in the scattering from deuteron with  $\lambda = 0$  at  $p_\perp = 0$ . The dashed (dotted) curve is the result of the calculation within the relativistic (non-relativistic) impulse approximation. The solid curve is the result of the calculation of the Glauber effects for the  $p + D \rightarrow p + X$  reaction.

Fig. 3.9b. The dependence of  $F_{2D}(x)$  on the deuteron polarization.

In the case of hadronic reaction it is necessary to account for Glauber screening effects. Calculation using the procedure of section 2.5 shows that this effect does not significantly change the expected effect (see solid line in fig. 3.9a).

A similar dependence on  $\xi$  is expected in the deep inelastic scattering from the deuteron, which is described by the same eq. (3.11) for  $F_{iD}(x, q^2)$  with the additional factor  $r(\xi, k)$  in the integrant (see fig. 3.9b).

### 3.3.3. Search for resonance admixtures in the deuteron

It can be seen from the mathematical structure of eqs. (3.17), (3.18) that the contribution of the direct mechanism is suppressed for  $\alpha \geq 1$  not only in the two-nucleon approximation but also in the case of resonance admixtures. So the details of the deuteron WF can be studied in the reactions  $\gamma^*(W^*) + D \rightarrow \Delta(N^*) + X$  by investigation of baryon resonances with  $\alpha > 1$ . Lack of diffraction, and the condition  $z < 1 - x$  represent the evident advantages of these reactions over the similar hadronic reaction in investigation of the deuteron structure. These advantages are especially revealed in the reactions  $\nu(\bar{\nu}) + D \rightarrow \mu^\mp + \Delta^{++}(\Delta^-) + X$  at  $x \geq 0.2$ . Really in the valence quark approximation  $\nu$  scatters on “d” quarks but  $\bar{\nu}$  on “u” quarks. Therefore in  $\nu(\bar{\nu})$  scattering  $\Delta^{++}(\Delta^-)$  but not  $\Delta^-(\Delta^{++})$  can be the spectators.

The reaction  $\nu(\bar{\nu}) + D \rightarrow \mu^\mp + p + X$  can give the unique possibility to study meson admixtures in the deuteron WF. Indeed, by increasing the momentum of the spectator one can suppress the contribution of the normal NN configuration. As a result we should see a visible increase of the seaquark contribution, which would be revealed for example in the change of the  $y$  distribution<sup>†</sup> (for a more detail discussion see [64]). The process  $\nu(\bar{\nu}) + D \rightarrow \mu^\mp + p + p + X$  seems to be best for investigation of the meson field in the deuteron. Events with both protons in the forward direction should be selected. Such a selection suppresses NN configuration and increase the fraction of the deuteron momentum carried out by  $\pi$  meson in NN configuration ( $\alpha_\pi = 1 - \alpha_{p1} - \alpha_{p2}$ ).

## 3.4. The deuteron electromagnetic form factors [64]

### 3.4.1. How and where relativistic effects manifest themselves

In the relativistic theory the calculation of form factors through the deuteron WF requires accurate

<sup>†</sup> Remind that  $y = (E_\nu - E_\mu)/E_\nu$ .

account of the space-time evolution of the strong interaction. To clarify this point we consider the form factor of the system of two point-like scalar particles. (It has been proven to be a good method to demonstrate advantages of IMF by this theoretical example, see e.g. [101, 133, 64].) In this model the form factor is described by the triangle Feynman diagram, which is equal to the sum of six non-covariant diagrams (see typical diagrams 3.10–3.12). Only the first diagram 3.10 resembles the usual quantum mechanical expression for the form factor. Though e.g. diagram 3.11 corresponds to production of an  $N\bar{N}$  pair from the vacuum by the incident photon and subsequent absorption of  $\bar{N}$  by the deuteron. (The dotted lines in figs. 3.10–3.12 correspond to the time development of the process. The time axis is directed from left to right.)

Since at large  $q^2$  the contributions of these diagrams are of the same order, the form factor cannot be expressed through the usual Schrödinger wave functions.

Though the initial triangle diagram is Lorentz invariant, its separation into the diagrams of the non-covariant perturbation theory depends on the reference frame. As above, it is convenient to use the c.m.s. of the electron and the deuteron. Here  $q = (0, -q^2/2P, q_\perp)$ . The diagrams 3.11, 3.12 vanish in this reference frame since the photon cannot either produce or absorb vacuum pairs. Indeed, the energy denominators for these diagrams are of the order  $P \rightarrow \infty$  but for fig. 3.10 it is equal to

$$E_D - E_1 - E_2 = \frac{M_D^2/2}{P} - \frac{m^2 + k_\perp^2}{\alpha P} - \frac{m^2 + k_\perp^2}{(2-\alpha)P}. \quad (3.22)$$

Here  $\alpha$  has the same meaning as in the section 2.

The exact calculation of fig. 3.10 leads to eq. (3.23) for the electromagnetic form factor  $F_D(q^2) = \langle D | j_z | D \rangle / 2P$  (we take into account that the nucleon electromagnetic current is proportional to  $P_{Nz} = \alpha P/2$ )

$$F_D(q_\perp^2) = \int \frac{d\alpha d^2 k_\perp}{\alpha(2-\alpha)} \frac{\kappa}{(m^2 + k_\perp^2)/\{\alpha(2-\alpha)\} - m_D^2/4} \cdot \frac{\kappa}{(m^2 + (k_\perp + ((2-\alpha)/2)q_\perp)^2)/\{\alpha(2-\alpha)\} - m_D^2/4}. \quad (3.23)$$

This equation can be rewritten in the form convenient for generalization on the realistic case of the two-body system:

$$F_D(q_\perp^2) = \int_0^2 \frac{d\alpha}{\alpha(2-\alpha)} \int d^2 k_\perp \varphi(M_i^2) \varphi(M_t^2). \quad (3.24)$$

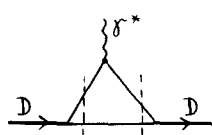


Fig. 3.10.

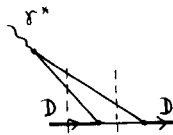


Fig. 3.11.

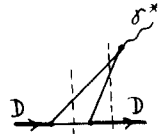


Fig. 3.12.

Figs. 3.10–3.12. The typical non-covariant diagrams for the deuteron form factor.

Here  $\varphi(M^2) = 4\kappa/(M_{NN}^2 - M_D^2)$  is the relativistic Bethe–Peierls WF of the deuteron (cf. subsection 2.1)

$$M_i^2 = \frac{4(m^2 + k_\perp^2)}{\alpha(2-\alpha)}, \quad M_f^2 = \frac{4m^2 + 4(k_\perp + \{(2-\alpha)/2\}q_\perp)^2}{\alpha(2-\alpha)}$$

are the squares of invariant mass of the initial and final two-nucleon systems. Eq. (3.24) has been discussed by Terent'ev within the frame of the constituent quark model [105].

The essential difference of eq. (3.24) from the conventional quantum mechanical expression is that the momentum transfer  $q$  is multiplied by the factor  $(2-\alpha)/2$  instead of  $1/2$ . This result follows from the Lorentz kinematics and takes into account recoil. Indeed, if the boost in transverse plane of a fast moving system is made the transverse momentum is divided in proportion of longitudinal momenta of constituents (see, e.g. [101]).

It is easy to see that for a monotonically decreasing wave function, eq. (3.24) leads to a more slow decrease of form factor with  $q$  as compared with non-relativistic quantum mechanics. Let us illustrate this by a simple example of the Gaussian type wave function:

$$\varphi(M^2) = N \exp(-A(M^2 - 4m^2)/4). \quad (3.25)$$

Applying, at  $Am^2 \gg 1$  the steepest descent method, we obtain:

$$F(q^2) \sim 4\sqrt{\tau} \exp(-Am^2(\tau - 1))(1 + \tau)^{-2}, \quad (3.26)$$

where  $\tau = \sqrt{1 + q_\perp^2/4m^2}$ ,

$$\begin{aligned} \text{for } q_\perp^2/4m^2 \ll 1, \quad F &\sim \exp(-Aq^2/8); \\ \text{for } q^2/4m^2 \gg 1, \quad F &\sim \exp(-Amq_\perp/2)(2m/q_\perp)^{3/2}. \end{aligned} \quad (3.27)$$

In the non-relativistic case where  $k^2/m^2$  terms are neglected

$$F(q_\perp^2) = \int \varphi(k) \varphi(k + q/2) d^3k \sim \exp(-Aq^2/8). \quad (3.28)$$

It follows from comparison of eqs. (3.27) and (3.28) that in the region  $q^2/4m^2 \ll 1$  both approaches give the same result; however, at  $q^2/4m^2 \gg 1$  relativistic effects change the form factor behaviour significantly.

### 3.4.2. Deuteron form factor: general discussion, the approximation

Above we have considered the example of point-like constituents. To describe the deuteron form factor one should take into account the nucleon structure. We shall use the IMF approach and will choose again  $q = (0, -q_\perp^2/2P, q_\perp)$ . At small  $q^2$  this process can be described by conventional quantum mechanics. Small corrections can result from the simultaneous interaction of the photon with both nucleons (see fig. 3.13). However, at large  $q^2$  the photon interacts with point-like partons. Experimentally the approximate scaling is fulfilled as early as  $q^2 \geq q_0^2 = 0.5 (\text{GeV}/c)^2$ . Therefore we expect that at  $q^2 \geq q_0^2$  the matrix element of the current will be reduced to the scattering from a free nucleon.



Fig. 3.13.

Contributions like that of fig. 3.13 (they are often discussed in the literature as exchange currents) should rapidly decrease with  $q^2$  since they do not correspond to the interaction of  $\gamma^*$  with one parton.

The additional arguments for applicability of this approach at  $q^2 < q_0^2$  follows from the well-known success of the constituent quark model in the description of baryon magnetic moments and the scaling of nucleon form factors. According to this model, the photon interacts with separate quarks even at  $q^2 = 0$ . Since in our approach the deuteron WF describes effectively the quark distribution in the deuteron we expect that corrections from simultaneous interaction of  $\gamma^*$  with both nucleons should be small. For example, correction to the deuteron magnetic moment arising from the diagrams like fig. 3.13 could be as large as (0.5–1)%. Factor  $\sim(5\text{--}10)\%$  is due to a small probability for two nucleons to be at small relative distances and factor  $\sim 10\%$  is the accuracy of the constituent quark model for the magnetic moments of baryons. Estimates of exchange currents for  $\mu_D$  lead to similar numbers [99].

What is the range of applicability of the two-nucleon approximation for the form factor? The analysis of section 2 reveals that it should work up to nucleon momenta of the order  $1 \text{ GeV}/c$ . On the other hand, the form factor is determined by nucleon momenta in the  $WF \leq q_\perp/2$ . (This is a non-relativistic estimate. In the relativistic case the essential momenta are a little bit smaller.) Therefore, one could expect that the two-nucleon approximation should be reasonable up to  $-q^2 = 4(\text{GeV}/c)^2$ .

The approximation discussed is more rough for the deuteron form factor than in the deep inelastic case since the overlap of WFs of the initial and the final states could be more sensitive to the value of the admixtures in the deuteron WF.

### 3.4.3. Deuteron form factor: calculational procedure

Here we present the calculation of the deuteron electromagnetic form factor, which takes into account not only the recoil but also the nucleon structure and the rotation of deuteron and nucleon spins. Since the final expression is rather lengthy, we will only explain the procedure and present the results of numerical calculations.

It is convenient to write down the deuteron electromagnetic vertex in the form (see e.g., [134]):

$$F_{\alpha\beta}^\mu(q) = \left( F_1(q^2) g_{\alpha\beta} - F_2(q^2) \frac{q_\alpha q_\beta}{2M_D^2} \right) P^\mu - G_1(q^2) (q_\alpha g_\beta^\mu - q_\beta g_\alpha^\mu). \quad (3.29)$$

Here  $\alpha, \beta, \mu$  are the indices corresponding to polarizations of initial and final deuteron and photon.  $P^\mu$  is equal to the sum of initial and final momenta of the deuteron. It is useful also to introduce three linear combinations of these form factors, which are similar to the Sachs form factors of the nucleon

$$\begin{aligned} F_{\text{CH}}(q^2) &= F_1(q^2) - G_1(q^2) + F_2(q^2)(1 + \eta), \\ F_Q(q^2) &= F_1(q^2) - G_1(q^2) + F_2(q^2)(1 + \eta), \quad F_{\text{mag}}(q^2) = (1 + \eta)^{-1/2} G_1(q^2), \end{aligned} \quad (3.30)$$

where  $\eta = -q^2/4M_D^2$ .

The differential cross section of electron scattering on unpolarized deuteron is as follows:

$$\frac{d\sigma}{d\Omega_{\text{Lab}}} = \frac{d\sigma_{\text{Mott}}}{d\Omega_{\text{Lab}}} \left( A(q^2) + B(q^2) \tan^2 \left( \frac{\theta}{2} \right) \right) \quad (3.31)$$

where

$$A(q^2) = F_{\text{CH}}^2(q^2) + \frac{8}{9} F_{\text{O}}^2(q^2) + \frac{2}{3}(1+\eta) F_{\text{mag}}^2(q^2)$$

$$B(q^2) = \frac{4}{3}\eta(1+\eta)^2 F_{\text{mag}}^2(q^2).$$

$A(q^2)$  is now measured up to  $-q^2 = 6(\text{GeV}/c)^2$  [4] and  $B(q^2)$  is measured up to  $-q^2 = 1(\text{GeV}/c)^2$ . To separate all three form factors it is necessary to perform polarization experiments. (For a discussion of polarization experiments and cross sections of scattering on a polarized deuteron see e.g., [130, 134].) It was explained above that the angular momentum is conserved in our approach but the mass of the two-nucleon system is not equal to  $M_D$ . As a result, the calculation of the deuteron form factor is similar to the dispersion (over the deuteron “mass”) calculation of the Feynman diagram fig. 3.14.

As in the previous sections (see especially section 2.2) we take into account only space-time configurations where the deuteron is formed as the two-nucleon state before the interaction with  $\gamma^*$ . We shall calculate the form factor for fixed polarizations of the deuteron (initial and final state)  $e_i^\alpha, e_f^\beta$ , and the photon,  $n_\mu$  respectively. The deuteron vertex function  $\Gamma_\mu(M^2)$  can be described by two invariant vertex functions (see eq. (2.23)). We shall use as integration variables  $\alpha/2$ , the fraction of longitudinal momentum carried by the interacting nucleon and  $k_\perp$  its transverse momentum:  $p_\mu^a = (\alpha P/2 + (m^2 + k_\perp^2)/\alpha P, \alpha P/2, k_\perp)$ . The form factor is as follows:

$$e_i^\alpha e_f^\beta n_\mu \Gamma_{\alpha\beta}^\mu(q_\perp) = \int \frac{d\alpha d^2 k_\perp}{\alpha^2 (2-\alpha)} \text{Sp}((\Gamma_1(M_i^2) \hat{e}_i + \Gamma_2(M_i^2)(a - c, e_i))$$

$$\times (m + \hat{a}) n_\mu G^\mu(q_\perp^2) (m + \hat{b}) (\Gamma_1(M_f^2) \hat{e}_f + \Gamma_2(M_f^2)(b - c, e_f)) (m - \hat{c}) \quad (3.32)$$

where  $G^\mu(q_\perp^2)/2$  is the nucleon isoscalar electromagnetic form factor

$$G^\mu(q^2) = G_E(q^2)\gamma_\mu + (G_E(q^2) - G_M(q^2))(b + c)\gamma^\mu/(2m - q^2/2m),$$

$$G_E(q^2) = G_{Ep}(q^2) + G_{En}(q^2), \quad G_M(q^2) = G_{Mp}(q^2) + G_{Mn}(q^2), \quad (3.33)$$

and where the scalar products are equal

$$(ac) = M_i^2/2 - m^2; \quad (bc) = M_f^2/2 - m^2, \quad ab = m^2 - q^2/2.$$

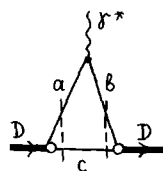


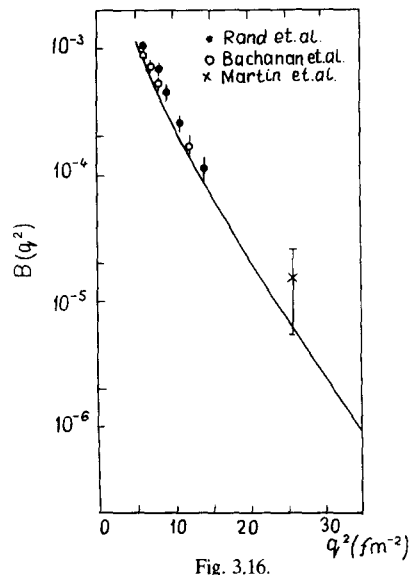
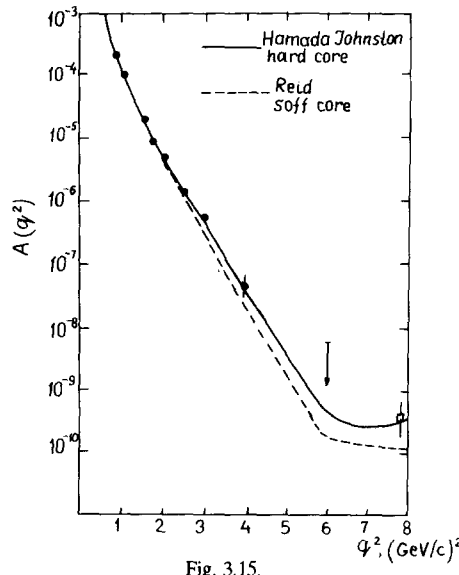
Fig. 3.14.

In the calculation of charge and quadrupole form factors of the deuteron we choose the  $j_0$  component of the electromagnetic current and transverse polarizations of the deuteron to suppress the production of the vacuum pairs by the photon. To calculate the magnetic form factor of the deuteron we choose also the  $j_0$  component of the electromagnetic current to suppress vacuum pair production by the photon. Due to antisymmetry of the tensor  $q_\alpha g_\beta^\mu - q_\beta g_\alpha^\mu$  the longitudinal polarization for the deuteron in the initial state (given by eq. (2.24)) and transverse polarization for the deuteron in the final state should be chosen. To elucidate this point it seems fruitful to use here instead of IMF technique an equivalent approach – light cone quantum mechanics for the deuteron and to calculate the matrix element of “good”  $-j_0 + j_z$  component of the electromagnetic current. (Remind that the light cone WF is quantized at hyperplane  $t+z=0$  instead of  $t=0$  [207]. The direction of the  $z$  axis is arbitrary. For fruitful classification of the currents into “good” and “bad” ones and analysis of their properties see e.g. [96].) We choose also  $q_+ = 0$  otherwise the deuteron form factor could not be expressed through the light cone WF, because production of the vacuum pairs by the photon will be essential (cf. example of section 3.4.1). One can check the necessity of  $q_+ = 0$  condition and the choice of “good” components of the electromagnetic current by direct calculation of noncovariant light cone diagrams from covariant Feynman diagrams by taking residue over variable  $k_0 - k_z$  and rewriting propagators into energy denominators. Evidently this can be done in any reference frame. However the conservation of angular momentum has a transparent form in the deuteron rest frame where it leads to the longitudinal polarization vector (2.24) for the deuteron.

In comparison with the experiment we use the following fits [135] to the magnetic nucleon form factors and the proton electric form factor:

$$G_{Ep}(q^2) = G_{Mp}(q^2)/\mu_p = G_{Mn}(q^2)/\mu_n = (1 - q^2/0.46)^{-1} (1 - q^2/1.46)^{-1}. \quad (3.34)$$

The neutron electric form factor was taken in the standard form (see e.g. [6]):



Figs. 3.15, 3.16. The comparison of the theory with the data [4, 6] for the deuteron form factors  $A(q^2)$ ,  $B(q^2)$ . The data point at  $Q^2 = 8 \text{ GeV}^2/c^2$  is the result of an indirect experimental determination of  $A(Q^2)$  [5b].

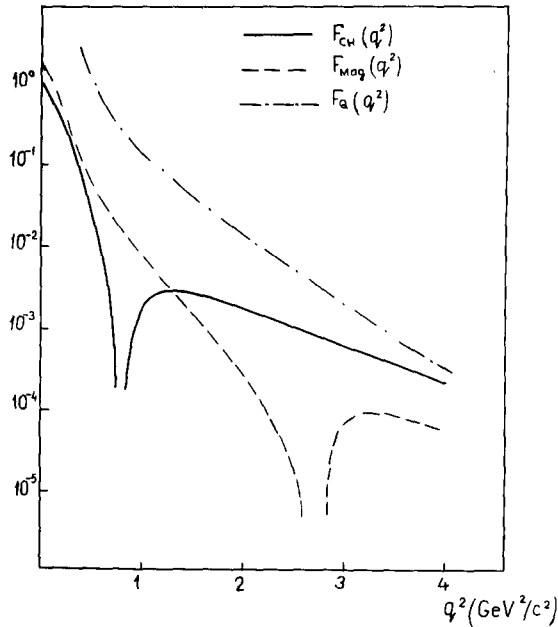


Fig. 3.17.

$$G_{En}(q^2) = \frac{\tilde{\eta} G_{Mn}(q^2)}{1 - 5.4\eta}, \quad \tilde{\eta} = \frac{q^2}{4m_N^2}. \quad (3.35)$$

In figs. 3.15, 3.16 we present the comparison of the theory with the experiment for  $A(q^2)$ ,  $B(q^2)$ . The theoretical curves reasonably describe the data. However  $G_{Ep}(q^2)$ ,  $G_{En}(q^2)$  are poorly known at large  $q^2$ . Thus this comparison with experiment has considerable uncertainty (for extensive discussion of this problem see [77]). A detailed comparison with quantum mechanical calculation reveals that relativistic effects do not significantly change the form factor behaviour at  $-q^2 \lesssim 4 M_N^2$ . In particular the oscillations of the form factors (see fig. 3.17) are still present. Due to relativistic effects both the zeroes and maxima of the form factors are moved to larger  $q^2$ . It is just due to this simultaneous shift of the zeroes and maxima of  $F_{CH}$ ,  $F_Q$  the difference of  $A(q^2)$  from its quantum mechanical value is small.

#### 3.4.4. Comparison of the light-cone (dispersion) approach and of the formalism with virtual nucleon

There exist now several attempts to take into account relativistic effects in the deuteron form factor (see e.g., [77, 48, 69] and references therein). Here we shall make a comparison with the approach developed by F. Gross, which seems to be the most popular in nuclear physics. In this approach the deuteron form factor is identified with the triangle Feynman diagram with on-mass-shell spectator and the off-mass-shell interacting nucleon. The vertex functions  $D \rightarrow NN$  are identified with the quantum mechanical WFs.

In the detailed analysis performed by Arnold, Carlson and Gross [77] it was shown that the relativistic procedure of [77] considerably reduces the size of  $A(q^2)$  over what it would be in the non-relativistic approximation. For example for the Reid soft core WF the decrease is by a factor of 2.5 (4) at  $Q^2$  of 2 (4)  $\text{GeV}^2$ . As a result this approach considerably underestimates  $A(q^2)$ , e.g., by a factor of 10 at  $Q^2$  of 4  $\text{GeV}^2$  for the Reid soft core WF [77]. On the contrary in our approach the relativistic effects slightly increase  $A(q^2)$  at large  $q^2$ . The different pattern of the relativistic effects in the two

approaches is of the same nature as in the case of deep inelastic scattering described in section 3.2. It is mostly due to the different relationship between non-relativistic and relativistic WF in these approaches and in particular due to lack of symmetry between the interacting nucleon and the spectator nucleon in the formalism [77].

Another principal advantage of the approach [40] used in this review is that one can impose the condition that the deuteron consists of two nucleons only, using the light-cone noncovariant technique but not the Feynman diagrams<sup>†</sup> (see discussion in section 2.3 and in particular quotation from S. Weinberg). As a result in the approach [77] the deuteron is described by 4 invariant vertex functions, though in our approach there are only two functions as in quantum mechanics.

### 3.4.5. Comparison with predictions of the quark counting rules

It was pointed out in the previous section that both quantum mechanical and light-cone descriptions of deuteron predict presence of zeroes for  $F_{\text{CH}}(q^2)$  at  $q^2 \sim 0.8 (\text{GeV}/c)^2$  and for  $F_{\text{mag}}(q^2)$  at  $q^2 \sim 2.5 (\text{GeV}/c)^2$  due to the nuclear core. On the contrary the quark counting rules predict a smooth behaviour of  $F_D(q^2) \sim q^{-10}$  [37, 118, 136]. In the comparison with the experiment the authors use  $q^2$  as small as  $0.5 (\text{GeV}/c)^2$ . If the quark counting rules can be applied to description of  $F_{\text{CH}}$ ,  $F_Q$  then these rules (i.e. the absence of oscillations) are in conflict with the standard theory of the deuteron at  $q^2 \lesssim 1 (\text{GeV}/c)^2$ , where relativistic effects are just a small correction.

Therefore we come to the conclusion that quark counting rules for  $-q^2 \lesssim 1 (\text{GeV}/c)^2$  contradict the conventional quantum mechanical theory of the deuteron where the presence of nuclear core is assumed. Since there exist both theoretical and experimental indications in nuclear physics supporting the hypothesis of the nuclear core we conclude that quark counting rules could not be applied at  $q^2 \lesssim 1 (\text{GeV}/c)^2$ . Really the analysis of essential QCD diagrams (see [37, 38, 75] and section 4.1) indicates that the transition from the two-nucleon description to six-quark description could take place at  $q^2 \gtrsim 4 \text{ GeV}^2$ .

## 3.5. Inclusive hadron production in the deuteron fragmentation region. Cumulative effect, etc.

During many years high-energy hadron processes have been one of important instruments for the study of the deuteron structure. The basic aim of this subsection is to demonstrate that investigation of fast backward proton (pion...) production in the reaction (3.36) provides an effective method of probing the short-range deuteron structure

$$h + D \rightarrow p(\pi) + \dots \quad (3.36)$$

(Remind that current experience in the analysis of high-energy hadron collisions indicates that due to multiparticle production inclusive processes give much more direct information about hadronic structure than exclusive reactions [90].) The interest in this problem was greatly stimulated by development of the relativistic deuteron beams in Dubna [3], Berkeley [11] and also at the Intersecting Storage Rings at CERN [137].

Quantitative description of reactions (3.36) can be constructed by accounting for space-time evolution characteristic for high-energy processes: impulse approximation, Glauber screening. The basic formulae were obtained in section 2.5. In this review we consider only those processes, which contribute to  $\sigma_{\text{tot}}^{\text{HD}}$  also at high energy. For an attempt of application of methods developed in section 2.5 to describe

<sup>†</sup> For an attempt of accounting for the angular condition in the frame of the light cone Bethe-Salpeter approach see [69].

quantitatively high momentum transfer exclusive processes like backward pD scattering, which cross section decreases with initial energy, see e.g. [68].

### 3.5.1. Fast backward proton production in the high energy hadron scattering from the deuteron

The dominant contribution into cross section of this reaction is given by the so called spectator mechanism (see fig. 2.16). It has the form (cf. eq. (2.56))

$$G_h^{D/p}(p) = E_p \frac{d^3\sigma^{h+D \rightarrow p+X}}{d^3p} = \kappa_h \sigma_{inel}^{hN} \frac{U^2(k) + W^2(k)}{2 - \alpha} \sqrt{m^2 + k^2}. \quad (3.37)$$

Here

$$k_\perp = p_\perp \quad \text{and} \quad \alpha = 1 + k_3/\sqrt{k^2 + m^2}. \quad (3.38)$$

In the deuteron rest frame the proton momentum  $-p$  and  $\alpha$  are related as (note the difference of  $p$  and  $k$ ):

$$\alpha = \frac{\sqrt{m^2 + p^2} - p_3}{M_D/2}; \quad (3.39)$$

$U(k)$ ,  $W(k)$  are S-, D-WFs of the deuteron (see section 2.3),  $\kappa_h$  is the Glauber screening factor, which is given by eq. (2.57).

Here we neglect the contribution of elastic hN scattering since small energy is transferred in such process. As a result it is suppressed by the final state interaction (section 7.4). For small nucleon momenta, say  $< 0.3 \text{ GeV}/c$ , one should use  $\sigma_{tot}^{hN}$  instead of  $\sigma_{in}^{hN}$ .

A second contribution to the yield is the scattering of the initial hadron from the backward nucleon with emission of a backward nucleon, the so called direct mechanism (see fig. 2.13; in refs. [46, 47, 61] only this mechanism was considered). Its contribution into  $G_h^{D/p}(p)$  is given by eq. (2.18)

$$G_{h(\text{direct})}^{D/p}(p) = \sum_{N=p,n} \int d^3k (U^2(k) + W^2(k)) G_h^{N/p} \left( \frac{\beta\nu}{2}, \beta, p_\perp + \frac{\alpha}{\beta} k_\perp \right). \quad (3.40)$$

For the backward nucleon production contribution of the direct mechanism is rather small since initial particle pushes the backward nucleon forward. Thus, dominant contribution in eq. (3.40) is given by elastic and diffractive hN interactions, which constitute small part of  $\sigma_{tot}^{hN}$ :  $(\sigma_{el} + \frac{1}{2}\sigma_{diff})/\sigma_{tot} \sim \frac{1}{4}$ . This mechanism is further suppressed by the final state interaction (cf. section 7.4). The characteristic property of the direct mechanism is small multiplicity of particles, which accompany the backward proton since (quasi)elastic processes give dominant contribution in eq. (2.40). Thus selection of events with sufficiently large multiplicity will suppress the contribution of this mechanism.<sup>†</sup> At the same time the direct mechanism leads to practically the same  $\alpha$  dependence as the spectator mechanism since in the quasielastic processes  $\alpha$  is slightly changed. (This is well known consequence of the rapid fall off of the elastic amplitude with momentum transfer.) Effectively the direct mechanism can be taken into account by renormalization of the factor  $\kappa_h$  in eq. (2.57) by the factor  $\sim 1.2$ .

There are several physical uncertainties, which make it difficult now to calculate precisely  $\kappa_h$ . (1) The calculation of the contribution of processes with small multiplicity such as elastic scattering of h from forward and backward nucleons, neglected in eq. (2.57), requires account of the final state interaction.

<sup>†</sup> Such selection would suppress also possible contribution of the final state rescatterings (see section 2.5).

(2) QCD predicts some suppression of Glauber screening due to compression of leading nucleon (see section 4.3). It is important that account of both these effects increases the absolute value of  $\kappa_h$  as compared to eq. (2.57) by a factor, which weakly depends on  $\alpha$ . Due to these uncertainties one could expect that at high energies

$$\kappa_h^{\text{eff}} = (1.4 \pm 0.2) \kappa_h^0, \quad (3.41)$$

where  $\kappa_h^0$  is given by eq. (2.57). Thus at high energy  $\kappa_h^{\text{eff}}$  could be much closer to 1 than according to eq. (2.57), where  $\kappa_h$  is rather small e.g.  $\kappa_p(p_N = 0.5 \text{ GeV}/c, p_\perp = 0) \approx 0.55$ ,  $\kappa_\pi(p_N = 0.5 \text{ GeV}/c, p_\perp = 0) \approx 0.65$  for the Hamada–Johnston WF. Estimates using realistic deuteron WFs show that relative contribution of the direct mechanism increases with  $p_\perp$  (at fixed  $\alpha$ ). However the spectator mechanism dominates in a wide  $p_\perp$  range, e.g. at least up to  $p_\perp \sim 0.7 \text{ GeV}/c$  for  $\alpha$  in the range 1.4–1.6.

### 3.5.2. Onset of Feynman scaling

Available data on the discussed reaction were obtained at the preasymptotic incident energies. Thus before comparison of eq. (3.37) with the data we have to discuss first the range of applicability of derived equations and the onset of Feynman scaling in the fragmentation processes.

The necessary condition for the applicability of eqs. (3.37), (3.40) is that the life-time of the studied short range configuration  $\sim 1/(E_{NN} - E_D)$  should be considerably larger than the characteristic time-scale of the strong interaction ( $\sim 1/m_\rho$ )

$$\frac{1}{E_{NN} - E_D} \approx \frac{2P_D}{4(m^2 - k_\perp^2)/\{\alpha(2 - \alpha)\} - M_D^2} \gg \frac{1}{m_\rho}. \quad (3.42)$$

In subsection 2.1 we have demonstrated that this condition is necessary to suppress the contribution of vacuum fluctuations.

It follows from inequality (3.42) that the kinematical region, where eqs. (3.37), (3.40) are applicable, increases with initial energy. (This fact is well known in the hadron physics as decrease of  $t_{\min}$  at  $E_h \rightarrow \infty$ .) This discussion shows that the form of Feynman scaling onset is expected to correspond to fig. 2.5 since it follows from the general structure of the theory. In particular it is easy to demonstrate that the scaling onset like in fig. 2.5 is expected practically in any realistic model of the strong interaction: parton model, multiperipheral model, leading logarithmic approximation in QCD, etc.

Thus to account for the violation of Feynman scaling due to the increase of the available phase-space we use light-cone variable  $\alpha$  as scaling variable for intermediate energies also [71]

$$\frac{\alpha}{2} = \frac{E_N + p_{Nz}}{E_D + p_{Dz}} = \frac{\sqrt{m^2 + p^2} - p_z}{M_D}. \quad (3.43)$$

This variable is convenient since it is invariant under Lorentz boosts along the  $z$  direction. At finite energy the region of accessible proton momenta in the deuteron rest frame is smaller due to energy conservation law. Consequently the kinematic boundary  $\alpha \rightarrow 2$  can be reached at infinite energy only. (E.g. in  $pD \rightarrow p + X$  reaction at  $E_N = 5 \text{ GeV/nucleon}$   $\alpha_{\max} = 1.8$ .) Really the region of applicability of eqs. (3.37), (3.40) is more narrow than given by restrictions due to phase space because near the kinematic boundary inequality (3.42) is not fulfilled. The above discussion provides the explanation of the relationship between precocious Yang limiting fragmentation [138] and Feynman scaling [90] (i.e. if Yang limiting fragmentation is fulfilled, only the  $\alpha$  variable leads to exact Feynman scaling).

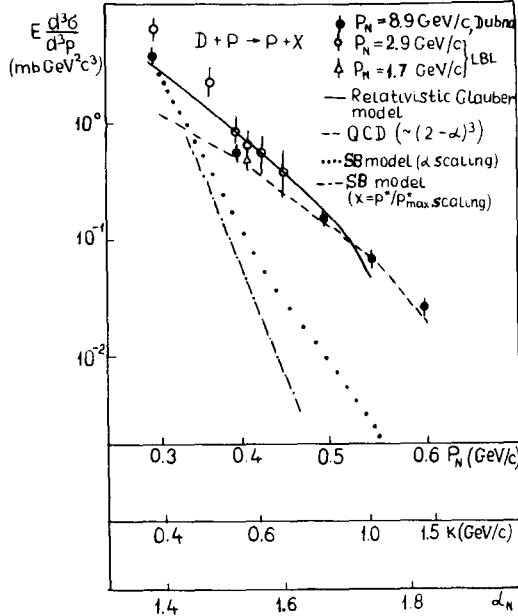


Fig. 3.18. The fast backward proton production in the pD scattering at  $p_\perp = 0$  [13, 20b]. The solid curve is the result of calculation in the relativistic Glauber approximation. Dashed curve is the QCD prediction of section 4 normalized at  $p_N = 0.5 \text{ GeV}/c$ . The broken (dashed) curves is the prediction of the Schmidt–Blankenbecler model [46] assuming  $\alpha(x = p_{cm}/p_{cm\ max})$  scaling normalized at  $p_N = 0.3 \text{ GeV}/c$ .

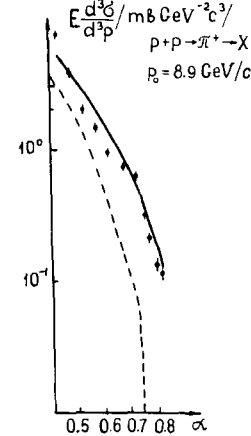


Fig. 3.19. Test of the  $\alpha$  scaling hypothesis in  $p + p \rightarrow \pi^+ + X$  reaction at  $p_N = 8.9 \text{ GeV}/c$  [13] ( $p_\perp = 0$ ). The solid and dashed curves are the predictions based on the high energy data [140] assuming  $\alpha$  scaling and radial scaling ( $x = E_{cm}/E_{cm\ max} \approx p_{cm}/p_{cm\ max}$ ) correspondingly.

Comparison [71] of the data on reaction  $p + D \rightarrow p + X$  at  $p_N^{inc} = 2.9 \text{ GeV}/c$  [20] and  $p_N^{inc} = 8.9 \text{ GeV}/c$  [13] (fig. 3.18) indicates that the backward proton yield is practically energy independent at  $p_N < 0.4 \text{ GeV}/c$ , but at larger proton momenta inclusive spectrum increases with the initial energy increase (at  $\theta = 180^\circ$ ,  $p_N^{max} = 0.48 \text{ GeV}/c$  for  $p_{inc} = 2.9 \text{ GeV}/c$ ). Similar trend is observed in the data [139] on  $D + A \rightarrow n + X$  reaction, where the region of spectator momenta  $\leq 0.2 \text{ GeV}/c$  was investigated.

The same pattern of scaling onset is observed for the process  $p + p \rightarrow \pi^+ + X$  (fig. 3.19). We want to emphasize that condition (3.42) is not fulfilled if standard variables such as  $x = p_L^*/p_{max}^*$  or  $E^*/E_{max}^*$  are used (see e.g., [11, 19, 46]) to compare asymptotic formulae with experiment. In particular these variables vary up to  $x = 1$  at any incident energy. As a result an artificial violation of the Yang scaling is introduced, see e.g. fig. 3.19 and the dotted curve in fig. 3.18. This is especially clear for the region of small spectator momenta  $p_N$ , where the validity of the impulse approximation can be strictly proved. For example the use of variable  $x = p^*/p_{max}^*$  leads to a change of the cross-section of the  $p + D \rightarrow p + X$  reaction by a factor of 300 at  $x = \frac{1}{2}$ ,  $p_\perp = 0$  in the range  $E_N^{inc} = 2\text{--}100 \text{ GeV}$  (at large energy  $x = \frac{1}{2}$ ,  $p_\perp = 0$  corresponds to  $p_N = 0$ ).

In fig. 3.18 a calculation of  $p + D \rightarrow p + X$  [40, 71] using eq. (3.37) is compared with experimental data [13, 20]. We use the Hamada–Johnston WF of the deuteron-solution of Weinberg eq. (2.22) and scaling variable  $\alpha/2 = (\sqrt{m^2 + p^2} - p_3)/m_D$ . The result of the calculation overestimates experimental data by (30–50)% †. It is worth noting that in the studied range of spectator momenta the dominant contribution

† We consider this as one of the evidences that the absolute normalization of the data [13] should be increased by a factor 1.5–2 (cf. footnote ¶ on p. 313). Note also that it is necessary to check the accuracy of scaling in variable  $\alpha$  at  $\alpha \geq 1.5$  at higher energies.

is given by D-wave. To check this important feature of the realistic WFs experiments with polarized deuteron beams are necessary (see [81] and section 3.3).

### 3.5.3. Comparison with other approaches

First we compare predictions of eq. (3.37) with the quantum mechanical approach and the Bethe-Salpeter approach [42], which is similar to approaches [128, 77] for the deuteron structure functions and the deuteron form factor, which were discussed in the previous subsections. These approaches lead to eqs. (3.44) and (3.45) respectively†

$$G_h^{D/N}(p) = \sigma_{\text{tot}}^{\text{hN}} \psi_D^2(p) (1 + p_3/M) \theta(2 - \alpha). \quad (3.44)$$

$$G_h^{D/N}(p) = \sigma_{\text{tot}}^{\text{hN}} \psi_D^2(p) (2 - \alpha) \theta(2 - \alpha). \quad (3.45)$$

Here  $p$  is the spectator momentum in the deuteron rest frame.  $1 + p_3/M$ ,  $(2 - \alpha)$  is the Möller flux factor, which reflects the Doppler shift for the frequency of the interacting nucleon.  $\alpha$  is given by eq. (3.43) and  $\psi^2(p) = (U^2(p) + W^2(p)) / (\sqrt{m^2 + p^2})$ .  $\theta(2 - \alpha)$  accounts for the phase space restrictions due to energy conservation.

Eq. (3.37) and eqs. (3.44), (3.45) correspond to a qualitatively different space-time picture of the strong interaction. Thus it seems instructive to compare predictions of these models for the nucleon yield. To be definite we use the deuteron rest frame.

(1) In the Bethe-Peierls approximation when  $p/m \ll 1$  ( $p^2 \leq m\varepsilon_D$ ) all formulae coincide. Really this case corresponds to the pointlike vertex  $D \rightarrow NN$ , where expression (3.37) follows from the exact calculation of the Feynman diagrams [40, 64].

(2) For the realistic deuteron WFs eqs. (3.37), (3.44), (3.45) predict rather similar inclusive cross sections in a wide kinematic region. For the illustration we present in fig. 3.20 inclusive cross section for the process (3.36) at spectator momentum  $p_N = 0.5 \text{ GeV}/c$  as a function of  $\theta$ , the angle between the directions of the initial particle and the spectator. The solid line in fig. 3.20 is calculated on the basis of eq. (3.37), the dotted line corresponds to the non-relativistic approach, eq. (3.44). In the non-relativistic and Bethe-Salpeter approaches  $\theta$ -dependence of the cross section arises due to the flux factor only, though in the light-cone approach (eq. (3.37)) additional angular dependence arises due to special relationship between the inner momentum  $k$  and the spectator momentum  $p$  (see eqs. (3.38), (3.39)).

(3) In fig. 3.21 we compare the predictions of three approaches for the proton yield at  $p_{N\perp} = 0$  (solid (dashed) curve is the ratio of calculations using eqs. (3.45), (3.44) and eq. (3.37) and the Hamada-Johnston WF). It can be seen from this figure that up to nucleon momenta  $p_N \sim 0.5 \text{ GeV}/c$  predictions of all these approaches are rather similar. Thus all these approaches (with account of Glauber screening [71]) should reasonably fit Dubna data [13] at  $p_N = 8.9 \text{ GeV}/c$ . In [42] it was demonstrated that the Bethe-Salpeter approach (and consequently light-cone approach) explain also LBL data at  $p_N^{\text{inc}} = 1.7-2.9 \text{ GeV}/c$ , where the region of the spectator momenta  $0 < p_N < 0.4 \text{ GeV}/c$  was investigated. Note that the similarity of predictions of all three prescriptions in the region  $p_N > 0.2 \text{ GeV}/c$  (where the Bethe-Peierls contribution is small) is rather accidental. In particular this would not be the case for the scattering from a polarized deuteron (see fig. 3.9a).

(4) Eqs. (3.44), (3.45) with the conventional normalization  $\psi(p)$ :  $\int \psi_D^2(p) d^3p / \sqrt{m^2 + p^2} = 1$  violate additivity of cross section even in the impulse approximation (so called West correction [128]) (see also Appendix A).

† To simplify the comparison we consider here the predictions of the models in the impulse approximation.

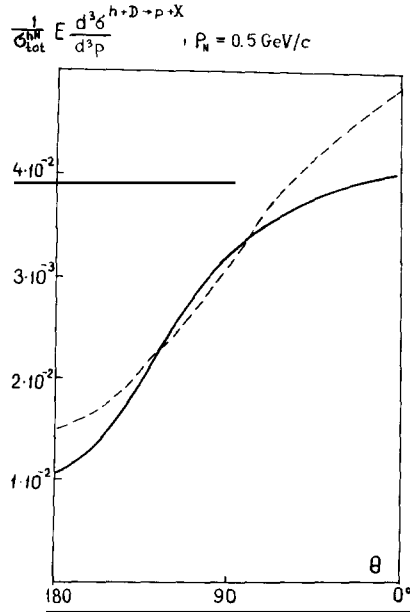


Fig. 3.20.

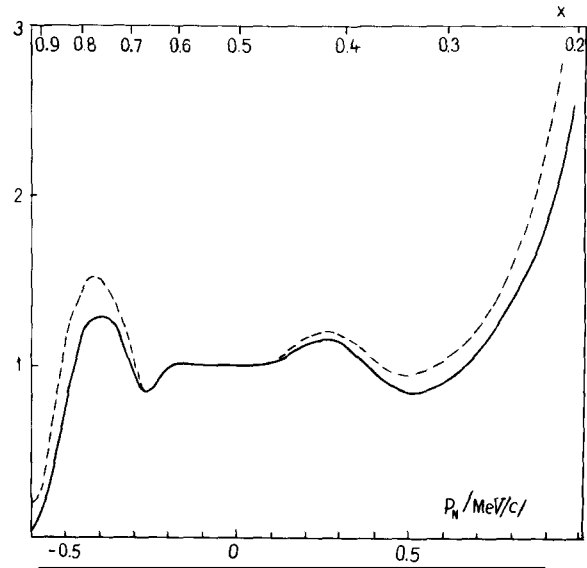


Fig. 3.21.

In ref. [46] Schmidt and Blankenbecler have applied the Bethe-Salpeter light cone approach [43, 46, 58] for the description of the  $p + D \rightarrow p + X$  reaction. They took into account the direct mechanism only and assumed that only diffractive processes contribute into the nucleon yield. It was demonstrated in [46] that the WF chosen on the basis of the quark counting rules reasonably describes the shape of the LBL data [11] assuming  $x = p^*/p_{\max}^*$  scaling. However the comparison with the Dubna data (fig. 3.19) obtained at a higher projectile energy reveals that the WF [46] poorly describe the data. It seems difficult also to explain in this approach the absolute value of the cross section since the direct mechanism constitutes small correction only to the well established spectator mechanism. At the same time the WF [46] enables to describe the data [4, 6] on the deuteron form factors [76]. Thus lack of agreement in the case of  $p + D \rightarrow p + X$  reaction indicates importance of the angular condition discussed in section 2, which is not fulfilled for the WF [46].

### 3.5.4. Cumulative effect

The reaction  $D + p \rightarrow \pi + X$  has attracted recently much attention. This reaction was studied both experimentally [3, 11–13] and theoretically. A considerable cross section of producing a fast pion, carrying a large fraction the deuteron momentum was called the cumulative effect in [3]. The existing theoretical works, which pretend to explain this phenomenon can be classified into the following groups: (a) light cone quantum mechanics for the deuteron [40, 71] with cancellation of Glauber screening; (b) impulse approximation using BS-WF of the deuteron [42, 46, 51]; (c) impulse approximation based on non-relativistic quantum mechanics [11, 12]; (d) account of the quark structure of the deuteron by applying quark counting rules [38, 41]; (e) account of the deuteron quark-gluon structure by applying QCD [75]; (f) introduction of special configurations, which correspond to space fluctuations in the deuteron density (see [52] and refs. therein).

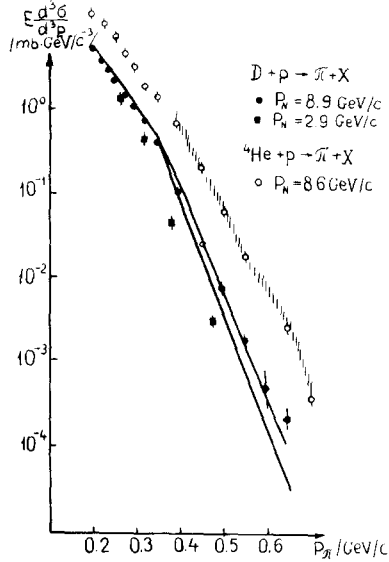


Fig. 3.22. Cumulative pion production in the pD, pHe scattering [11–13]. The curves (described in the text) are the result of the calculation for the deuteron in the relativistic impulse approximation. The shaded region is the calculation of the pion yield from  ${}^4\text{He}$  described in section 8.5.

In the frame of quark counting rules it is easy to obtain the dimensional estimate [38, 41]  $G_h^{D/\pi}(\alpha, p_\perp)/G_h^{N/\pi}(\alpha/2, p_\perp) \sim (2 - \alpha)^6$ , which is roughly consistent with the Dubna experimental data at  $\alpha \leq 1.4$ . (Note that QCD predicts much slower decrease of this ratio,  $(2 - \alpha)^3$  at larger  $\alpha$  (see section 4.3).) Evidently such an estimate is not sufficient for a quantitative description of the process. To calculate the cross section of the process in the framework of relativistic impulse approximation we will use eq. (2.19). (Recall that the Glauber correction is absent for this process.) To understand the magnitude of the observed cross section we have performed the following estimate. The inclusive cross section was calculated at high energy using cross section of the elementary process in the form:  $G_p^{p/\pi^+} = 30.2(1 - x)^{3.2} \cdot (1 + k_\perp^2/0.66)^{-4}$  [140] with Hamada–Johnston WF and the approximate relation  $G_p^{p/\pi^+} = G_p^{p/\pi^-}$  the lower curve in fig. 3.22. (We have checked that the chosen form of  $G_p^{p/\pi^+}$  fits well  $p + p \rightarrow \pi^+ + X$  data at  $p_N = 8.9 \text{ GeV}/c$ ,  $\theta = 180^\circ$  if  $\alpha$  scaling is assumed up to  $\alpha = 0.8$  (see fig. 3.19). Note that reactions  $p + p \rightarrow \pi^\pm + X$ ,  $p + D \rightarrow \pi^\pm + X$  [13] were measured in the same experiment. Thus uncertainties in the data normalization do not affect the following comparison. To account for the fact that the data on the reaction  $N + N \rightarrow \pi + X$  are known at large  $x$  for large  $k_\perp$  only (for example for  $x \sim 0.8$ ,  $k_\perp \geq 1 \text{ GeV}/c$ ) we use triple reggeon limit for  $x > 0.8$  for elementary reaction:  $G_N^{p/\pi}(x, k_\perp = 0) \sim (1 - x)^{1-\beta_{4(0)}} \sim (1 - x)^{1.6}$ . This form of  $G_N^{p/\pi}(x, k_\perp)$  and the deuteron WF (smoothed according to QCD estimate and in accordance with the data on the reaction  $p + D \rightarrow p + X$ , fig. 3.18) leads to the upper curve in fig. 3.22. This asymptotic calculation was compared with the data [13] assuming that  $\alpha$ -scaling is valid. Unfortunately hypothesis of  $\alpha$ -scaling for  $p + D \rightarrow \pi + X$  reaction is not checked experimentally well enough since data only at  $p_N = 8.9 \text{ GeV}/c$  and  $p_N = 2.9 \text{ GeV}/c$  exist now. (See however fig. 3.22, which indicates that these data are roughly consistent with the idea of  $\alpha$  scaling.)

Much larger incident energies are necessary for the unambiguous comparison of eq. (2.19) with the data and for determination of the  $\alpha$  region, where contribution of the QCD mechanism of hard gluon emission  $(2 - \alpha)^5$  would become dominant.

Deuteron fragmentation into the pion has been studied also at a smaller incident energy in LBL using the deuteron beam with  $E_D = 1.05$ ; 2.1 GeV/nucleon and nuclear targets. These data were reasonable explained by Bertocci and Treliani [42] in the frame of Bethe-Salpeter formalism (see also [51]). Due to a rather low  $E_D$  only rather small nucleon momenta in the deuteron WF were essential in this case. Thus in this region predictions of our approach and that of ref. [42] are rather similar. However at larger  $\alpha$  similar to the case of  $F_{2D}(x)$  the light-cone approach [40] leads to considerably larger cumulative pion yield (cf. fig. 3.5).

In conclusion, we have demonstrated in this section that light-cone quantum mechanics is in reasonable agreement with the available data of the short range phenomena in the deuteron. At the same time we explained above that it smoothly goes over to the conventional theory of the deuteron in the non-relativistic limit. Therefore it inherits all its achievements.

#### 4. QCD and the high momentum components of the nuclear wavefunctions

Evident success of QCD in the description of deep inelastic processes has strongly stimulated attempts to describe short-range phenomena in nuclei in terms of perturbative QCD<sup>†</sup>. It was suggested in a number of works [31, 38, 41, 55, 56] that the deuteron could be in a quark bag state, where quarks interact via colour forces. However it appears difficult to formulate this hypothesis in a consistent way since one should take into account that the physical system can lower its energy by expanding into the unconfinement channels (e.g. NN channel). In particular Jaffe and Low [141] argued that states with hidden colour which exists in the bag models [142, 56] are really due to specific boundary condition in the bag model and do not correspond to the poles of the  $S$ -matrix [141].

The theoretical analysis of short range phenomena in the deuteron presented in sections 2, 3 is naturally compatible with the little bag model [51] where the radius of the nucleon bag is of the order of the radius of the nuclear core  $r_c \sim 0.4$  fm and effective running coupling constant is small. Really calculations with the realistic deuteron WFs show that most of the phenomena investigated in this review are determined by the distances when both nucleons are mostly outside of the region of nuclear core (cf. section 2.4). If the nucleon bag radius is considerably larger than  $r_c/2$  it seems difficult now to establish direct correspondence between quark-gluon and hadron degrees of freedom in nuclei<sup>‡</sup>. The physical answer depends strongly on the radius of colour forces confinement. The region where all quarks are collectivized can be effectively searched in the high energy processes from the polarized deuteron (section 3.3). In difference to the two-nucleon approximation, there seems to be no reason for a strong dependence of the cross section on the deuteron polarization in the MIT type bag model.

To reveal when and where description of the deuteron in terms of quarks and gluons becomes adequate we consider in this section short-range phenomena which could be calculated in terms of perturbative QCD.

<sup>†</sup> In the kinematical region where conventional theory of the deuteron (nuclei) is usually applied (nucleon momenta  $\leq 0.5$  GeV/c) non-perturbative effects such as confinement of colour forces, quark interchange diagrams etc. could be essential since the running coupling constant is large here. However in spite of these complexities the position of the nuclear core in the coordinate space  $r_c \approx 0.35$  fm can be semiquantitatively estimated within the quark model, see Appendix E.

<sup>‡</sup> cf. discussion at the end of Appendix C and the first note added in proof.

## 4.1. QCD and the structure of the deuteron wave function

### 4.1.1. Asymptotic estimates

Experience in the calculation of the asymptotics of WF in quantum mechanics shows that high momentum component of WF is determined by the behaviour of the potential at high momenta. Brodsky and Farrar have generalized this analysis to the case of a quantum field theory of hadrons, as a system of few pointlike quarks [118]. In particular, they have demonstrated that in the case of the deuteron electromagnetic form factor  $F_D(q^2)$  the essential diagrams correspond to the so called democratic chain approximation (fig. 4.1). The high momentum WF is calculated in terms of hard gluon exchanges which determine the evolution of D from the configuration where momenta are equally partitioned between 6 quarks of the (pre)postscattering configuration. Calculation of these diagrams leads to the so called quark counting rule predictions [118, 136]

$$F_D(q^2) \sim 1/q^{10}. \quad (4.1)$$

Here the factor  $(q^{-2})^{10}$  is due to 10 quark and gluon propagators with large virtuality and factor  $q^{10}$  is due to 10  $gq\bar{q}$  vertices (traces over the fermion lines).

This asymptotical estimate can be used only if *all* quark and gluon propagators are far off-mass-shell. Therefore the minimal momentum in the gluon line in the diagram (4.1) (the gluon exchange between quarks 1, 2)  $\sim q/6$  should be larger than the typical momenta of a quark in the nucleon (deuteron),  $\langle k \rangle \sim (0.3-0.4) \text{ GeV}/c$ . Consequently [118, 37, 38], the asymptotic region could be reached only at

$$-q^2 \geq 36 \langle k^2 \rangle \sim (4-5) \text{ GeV}^2. \quad (4.2)$$

Similarly for the case of the nucleus consisting of  $A > 2$  nucleons asymptotical formulae† [37]:

$$F_A(q^2) = 1/q^{2(3A-1)} \quad (4.3)$$

should be applied only at very large  $q^2$ :

$$-q_{\text{critical}}^2 \geq 9 \langle k^2 \rangle \cdot A^2 \sim A^2 (\text{GeV})^2. \quad (4.4)$$

As there are no data on the nuclear form factors in the region  $-q^2 > -q_{\text{critical}}^2$ , Brodsky and Chertok [37] have suggested a phenomenological procedure for taking into account the mass corrections to eqs.

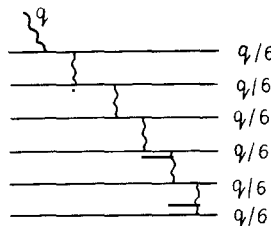


Fig. 4.1. A typical QCD diagram for the deuteron form factor.

† Hereafter we neglect logarithmic corrections in the strong coupling constant.

(4.2), (4.4). They have been able to fit experimental behaviour of  $F_D(q^2)$  at  $-q^2 \geq 1 \text{ GeV}^2$ . However, the comparison of the predictions for  $F_{\text{He}}(q^2)$ ,  $F_{\text{He}}(q^2)$  with the recent SLAC experiment [4] made by Chertok [143] have demonstrated that additional refinements of the model seem to be necessary in this case.

Similar approach was used also to calculate the deep inelastic structure functions at  $x \rightarrow A$  ( $x = -q^2/2m_N v$ ) [65]

$$\begin{aligned} F_{2A}(x) &= (A - x)^{6A-3} && \text{for odd } A \\ F_{2A}(x) &= (A - x)^{6A-2} && \text{for even } A. \end{aligned} \quad (4.5)$$

The difference between two cases is due to vector coupling selection rules [118] (see Appendix C).

Though the described approach enables one to estimate the functional dependence of form factor of deuteron (but not nuclei) it does not fix the normalization of  $F_D(q^2)$  since there is no simple correspondence between this description and conventional theory of the deuteron. Moreover, applications [46, 66] of this approach to hadronic reactions  $h + D \rightarrow p + X$  contradict experimental data [13] (dotted and dotted-dashed curves in fig. 3.18 and discussion below). On the other hand experience with current algebra [96] and QCD [97] in the saturation of sum rules by few hadron resonances, the success of the vector dominance model in the description of high energy photo-production [80] shows that correspondence between quark-gluon and hadron degrees of freedom should be rather simple in a wide kinematical region if IMF-WFs (dispersion relations) are used. This was one of the important reasons for a construction of relativistic quantum mechanics of the deuteron (nuclei) (section 2). The analysis of sections 2, 3 suggests that two-nucleon approximation is reasonable up to nucleon momenta  $k \sim (0.8-1.0) \text{ GeV}/c$ . For the deuteron form factor this corresponds to

$$-q^2 \leq (2k)^2 \sim (2.5-4) \text{ GeV}^2,$$

which is rather close to the  $q^2$  critical (eq. (4.2)). Thus one should expect that there exists a rather smooth transition between the two-nucleon and the six-quark descriptions of the deuteron.

#### 4.1.2. Transitional region

To estimate the deuteron WF in the transitional region

$$0.5 < k < 1.0 \text{ GeV}/c,$$

where two-nucleon system is far off-energy shell, one has to consider a process which is hard at finite  $x$  and which can be simultaneously described in terms of QCD diagrams and in terms of NN wave function of the deuteron. Recall that  $\alpha/2$  is the fraction of the deuteron momentum carried by the nucleon in the infinite momentum frame (IMF) of the deuteron, the so-called light cone fraction.

One of the simplest processes is the deep inelastic reaction:

$$\ell + D \rightarrow \ell' + N(\alpha) + X$$

at average  $x \sim \frac{1}{4}-\frac{1}{3}$  and  $\alpha \rightarrow 2-x$  ( $\alpha = 2-x$  is the phase space boundary for this reaction). In the calculation we assume that the fast nucleon (colourless 3q system) is formed before the  $\gamma^*$  interaction.

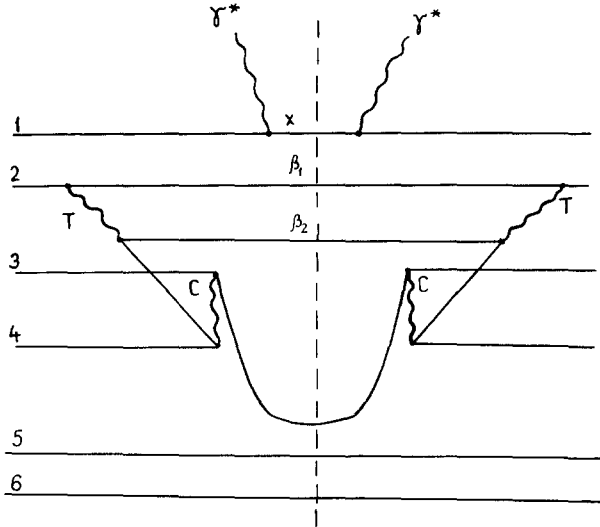


Fig. 4.2. The dominant QCD diagram for the process  $\ell + D \rightarrow \ell' + N + X$  at fixed  $x \sim \frac{1}{3}$  and  $\alpha \rightarrow 2 - X$  in the 6q model of the deuteron.

As a result the scattering from configurations in the deuteron with finite number of partons (6q configuration) gives dominant contribution due to finite phase space restrictions.

Under these assumptions the space-time evolution of the process is described by noncovariant diagrams of old-fashioned perturbation theory in the infinite momentum frame of the deuteron (fig. 4.2)<sup>†</sup>. In the initial state the quarks (1,2,3) and (4,5,6) form two nucleons in the average configuration ( $x_{qi} \sim 0.2 - 0.3$ ). Only hard gluon exchanges are shown in fig. 4.2. The Coulomb and transverse gluons are labelled as C and T, respectively. For dominant diagrams C, T gluon exchanges are alternated. Due to the vector coupling selection rule [145] a rather peculiar diagram 4.2 with q̄q pair emission in the intermediate state gives dominant contribution – other diagrams are suppressed at least by factor  $(2 - \alpha - x)$ , (cf. the analysis of the nucleon structure function in Appendix C).

Neglecting weak  $\alpha$  dependence of the overlapping integral of the 3q system (4,5,6) with the nucleon (see below) we obtain for the QCD diagram (fig. 4.2)

$$F_2^{D/N}(x, Q^2, \alpha) \sim \int_0^{2-\alpha-x} \frac{d\beta_1 d\beta_2}{\beta_1 \beta_2} \delta(\alpha_4 + \alpha_5 + \alpha_6 + \beta_1 + \beta_2 - 2 + x) \times (\sqrt{\beta_1} \sqrt{\beta_2})^{-2} (\beta_1 (1/\beta_1 + 1/\beta_2)^{-2})^2 \sim (2 - \alpha - x)^3. \quad (4.6)$$

The factor  $\sim (2 - \alpha - x)^6$  originates from 6 hard energy denominators, factor  $\sim (2 - \alpha - x)^{-2}$  is due to four g<sub>T</sub>q̄q vertices; factor  $(2 - \alpha - x)^{-1}$  is due to phase-space integration. Since the quark 1 which interacts with  $\gamma^*$  is in the average configuration, the weak  $x$  dependence due to quark soft interactions is not explicitly written here. In the derivation we neglect the final state interaction between the colourless (4',5,6) system and the quarks (2,3') as in deep inelastic scattering energy  $\geq 1$  GeV is

<sup>†</sup> The rules of calculation are the same as in QED [144] because three, four gluon vertices are inessential in the lowest order in strong coupling constant  $\alpha_s$ . The rules necessary for the calculation of the asymptotics of QCD diagrams in the limit under consideration are given in Appendix C.

transferred to the struck nucleon (see [64] and discussion in section 3.3). The condition that 3q state (quarks 4',5,6) is colourless is necessary also to avoid large gluon bremsstrahlung which would otherwise suppress the yield of leading particles due to the Sudakov type form factor.

The derived expression is justified for  $x \sim 0.2\text{--}0.4$  and  $1.5 \leq \alpha \leq 2 - x \sim 1.8$ . The low boundary is determined from the condition for the energy denominators to be far off the energy shell. The upper boundary is due to the condition that no additional hard gluon exchanges are necessary.

The overlapping integrals of 3q systems (1,2,3'), (4',5,6) with nucleon can be roughly estimated as  $F_{2N}(x/(2-\alpha))$  and  $F_{2N}((\alpha - \frac{2}{3})/\alpha)$ , correspondingly, since the leading quark carries a large fraction of nucleon momentum  $x/(2-\alpha)$ ,  $(\alpha - \frac{2}{3})/\alpha$ . (Note that the same type estimate is valid for admixture of baryon resonances since quark distribution at large  $x$  has a universal form [90].) It is easy to check that in the discussed  $\alpha$  range the overlapping integral for nucleon with light-cone fraction  $\alpha$  rather weakly depends on  $\alpha$ . Actually the dependence of this overlapping integral is even weaker since  $F_{2N}(x)$  includes contributions of configurations like 3qg, which decrease faster with  $x$  than the 3q contribution.

Neglecting the admixture of baryon resonances in the deuteron WF we can compare eq. (4.6) with the two-nucleon approximation (section 3) according to which

$$F_{2D}(x, \alpha) = F_{2N}(x/(2-\alpha)) \rho_D^N(\alpha, k_\perp = 0). \quad (4.7)$$

Here  $\rho_D^N(\alpha, k_\perp)$  is the single nucleon density matrix of the deuteron (for formal definition of  $\rho_D^N$  see eq. (2.31)). The comparison of eqs. (4.6) and (4.7) at  $x/(2-\alpha) \sim 1$ , where eq. (4.6) is applicable, gives [75]

$$\rho_D^N(\alpha, k_\perp = 0) \sim (2-\alpha)^3 \quad \text{at } 1.5 < \alpha < 1.8. \quad (4.8)$$

The presence of NN\* component in the deuteron WF would not affect eq. (4.8) – in this case  $\rho_D^N$  would correspond to inclusive distribution of nucleons in the deuteron. At small transverse momenta of the nucleon the  $k_\perp$  dependence of  $\rho_D^N$  cannot be calculated within perturbative QCD as is determined by the primordial quark distribution in the initial state. However in the two-nucleon approximation the  $k_\perp$  dependence can be reconstructed using the angular condition (eq. (2.22)).

Eq. (4.8) should be compared with quark counting rules expectations [46, 66]  $\rho_D^N(\alpha) \sim (2-\alpha)^6$ . (Here and below we give predictions of quark counting rules accounting for QCD selection rules [145].)

Since inclusive cross section of FB nucleon production in  $h + D \rightarrow p + X$  reaction,  $\alpha d\sigma/d\alpha d^2k_\perp$ , is proportional to  $\rho_D^N(\alpha, k_\perp)$  [40], eq. (4.8) predicts  $\alpha$  dependence of this reaction at  $k_\perp \approx 0$ . Recent high energy data [13] on the  $p + D \rightarrow p + X$  reaction are consistent with eq. (4.8) and contradict the quark counting rule predictions [46, 66] (see fig. 3.18).

We would like to emphasize that the derived momentum dependence of deuteron WF and the realistic deuteron WFs like the Reid, Hamada–Johnston WF practically coincide in a range of nucleon momenta  $0.5 < k < 0.8 \text{ GeV}/c$ . Consequently, there exists a smooth transition between non-relativistic and QCD description of the deuteron. At the same time this means that we predict not only the momentum dependence but also the absolute value of cross section of this process since Hamada–Johnston WF describes the data up to  $\alpha < 1.7$  (see fig. 3.18).

Note, however, that for rare components like  $\bar{q}$  the NN approximation (with  $\rho_D^N$  from (4.8)) and QCD perturbation approach lead to different predictions for the semi-inclusive reactions [75]

$$\begin{aligned} [F_2^{DN}(\alpha, x) - x F_3^{DN}(\alpha, x)] &\sim (2-\alpha-x)^7 \text{ in QCD} \\ &\sim (1-x/(2-\alpha))^7 (2-\alpha)^3 \text{ in NN approximation.} \end{aligned}$$

Therefore smooth correspondence exists for dominant configuration only. At the same time antiquark distribution in the deuteron is the same in both approaches.

#### 4.1.3. Estimate of $\Delta$ admixture in the deuteron

Diagram 4.2 describes not only nucleon but also  $\Delta$  production at large  $\alpha$ . However  $\Delta$  production is suppressed due to flavour combinatorics of “u” and “d” quark interchange and due to zero deuteron isospin. As a result [146]  $\rho_D^{\Delta++}(\alpha)/\rho_D^N(\alpha) \sim 1/7$ . One should also take into account the difference in the energy denominators due to the difference of  $\Delta$ , N masses:

$$(m_D^2 - 4(m_\Delta^2 + k_\perp^2)/\alpha)/(2 - \alpha) \quad \text{and} \quad (m_D^2 - 4(m_N^2 + k_\perp^2)/\alpha)/(2 - \alpha).$$

Evidently, a comparison of two components should be made for the case of equal energy denominators. Thus we obtain [146]

$$P_{\Delta\Delta} \sim \frac{2}{7} \int \psi_D^2 \theta(\sqrt{m_\Delta^2 - m_N^2} - k) d^3k \sim (1-2) \times 10^{-3}.$$

This is somewhat smaller than the recent estimates of  $\Delta\Delta$  component based on the One Boson Exchange Potential (OBEP) giving 0.5% [147]. However, our estimate (4.9) is consistent with the recent experimental limit ( $0.1 \pm 0.2$ )% [148].

Analysis of diagram 4.2 demonstrates also that since light cone fractions  $\alpha_4, \alpha_5, \alpha_6$  are rather different ( $\alpha_5/\alpha \sim \alpha_6/\alpha \sim \frac{1}{3}/\alpha \sim 0.2$ ;  $\alpha_4 \sim (\alpha - \frac{2}{3})/\alpha \sim 0.6$ ), the overlapping integral for this system with excited baryon states like  $N^*$  could be large.

#### 4.1.4. QCD and OBEP

It is worth noting that there is no apparent correspondence between perturbative QCD and OBEP approach [149]. Indeed in QCD short-range NN interaction is described by diagram 4.2, which is similar to diagram 4.3 considered by Kisslinger [150a] and Pirner [150b]. This diagram is evidently absent in  $N\bar{N}$  channel. However quark annihilation diagram 4.4 is present in this case. Therefore in QCD different intermediate states are responsible for short-range NN and  $N\bar{N}$  interaction, though in OBEP prescription it is determined by the same vector meson exchanges ( $\omega, \rho$ ).

#### 4.1.5. On the role of $q\bar{q}$ admixture in the deuteron WF

In the above analysis we considered the 6q term in the deuteron WF. However the contribution of the 7q +  $\bar{q}$  component of the deuteron WF into fast nucleon yield is enhanced at large  $\alpha$ . It corresponds to the same diagram fig. 4.2 as above mechanism but  $q\bar{q}$  annihilation due to Coulomb gluon exchange

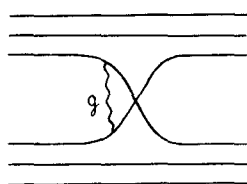


Fig. 4.3.

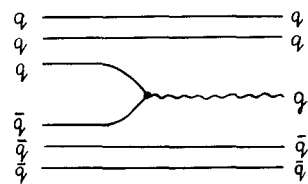


Fig. 4.4.

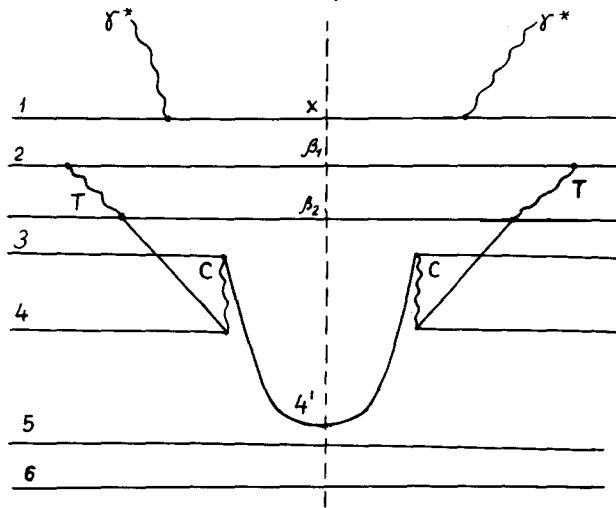


Fig. 4.5. QCD diagram for the contribution of the  $7q + \bar{q}$  component of the deuteron WF into fast nucleon yield.

occurs after  $\gamma^*$  interaction (see fig. 4.5). As a result the energy denominators which correspond to the time evolution of quark-gluon system after  $\gamma^*$  interaction do not contain factors  $(2 - x - \alpha)$ . The simple calculation shows that

$$F_2^{D/N}(\alpha, k_\perp = 0) \sim (2 - x - \alpha). \quad (4.9)$$

The difference between eqs. (4.6), (4.9) is that energy denominators which correspond to  $q\bar{q}$  annihilation is  $(\beta_1^{-1} + \beta_2^{-1})$  for diagram 4.2 and  $\sim 1$  for diagram 4.5. However the contribution of diagram 4.5 into nucleon yield is suppressed numerically due to the overlapping integral between  $4q\bar{q}$  system and nucleon.

*Baryon production in the 6q model at  $\alpha \rightarrow 2$ .* To calculate baryon production in the process  $e + D \rightarrow e + N(\alpha) + X$  at  $\alpha \rightarrow 2$  in the 6q model we have to include additional hard gluon exchanges since quark (1) should transfer its light cone fraction to other quarks. As a result, calculation in the limit  $\alpha \rightarrow 2$  but  $x/(2 - \alpha) \sim 1$  fixed, leads to

$$F_2^{D/N}(x, \alpha) \sim (2 - x - \alpha)^3 x^3 \sim (2 - x - \alpha)^3 (2 - \alpha)^3$$

i.e.

$$\rho_D^N(\alpha) \sim (2 - \alpha)^6. \quad (4.10)$$

Note that eq. (4.10) corresponds to a much faster decrease of the WF at  $\alpha \rightarrow 2$  than a WF with a hard core and is more close to the soft core WF. Eq. (4.10) accounts for the QCD vector coupling selection rules [145] and leads to well-known QCD prediction [65] for  $F_{2D}(x)|_{x \rightarrow 2} \sim (2 - x)^{10}$ . Note that the model [46] for two-nucleon deuteron WF based on quark counting rules leads to  $F_{2D}(x)|_{x \rightarrow 2} \rightarrow (2 - x)^9$ .

As in the derivation of eq. (4.9) it is easy to demonstrate that  $7q + \bar{q}$  component of the deuteron WF leads to a considerably slower dependence of  $F_2(x, \alpha, k_\perp = 0)$

$$F_2^{D/N}(x, \alpha, k_\perp = 0)|_{x \rightarrow 0} \sim (2 - \alpha)^4. \quad (4.11)$$

The difference between eqs. (4.10) and (4.11) has a transparent origin. In the latter case  $q\bar{q}$  annihilates after  $\gamma^*$  interaction. This mechanism is suppressed numerically (see discussion after eq. (4.9)).

To summarize, we have found a set of essential QCD diagrams which determine the deuteron WF and the spectrum of the leading nucleons for  $\alpha > 1.5$  in the high energy processes. The found diagrams lead to a considerably larger high momentum nucleon component of the deuteron WF and to a more slow  $\alpha$  dependence of the leading nucleon spectrum (eqs. (4.8), (4.9), (4.11)) than expected according to quark counting rules eq. (4.10). The discovered enhancement is a manifestation of a general property of multiquark systems where asymptotic estimates [37, 46] could be valid in a narrow region and for special processes only. In other words, the collectivization of all quarks (which corresponds to democratic chain diagrams with all propagators in the asymptotic conditions) is strongly suppressed by asymptotic freedom. We want to emphasize that description of all high-energy processes from the deuteron in terms of the universal two nucleon WF is reasonable in the valence quark approximation only (cf. eqs. (4.6), (4.10) and eqs. (4.9), (4.11)).

#### 4.1.6. $\rho_D^N(\alpha, k_\perp)$ at large $k_\perp$

It seems instructive to estimate  $\rho_D^N(\alpha, k_\perp)$  for  $\alpha \sim 1$  but large  $k_\perp$ . The dominant diagram (fig. 4.6) corresponds to quark interchange due to hard gluon exchange between nucleons and nucleon formation after  $\gamma^*$  interaction. (Interchange is necessary since nucleons are colourless.) Simple calculation leads to

$$\rho_D^N(\alpha, k_\perp) \sim 1/k_\perp^8.$$

The factor  $(1/k_\perp^2)^2$  is due to quark interchange via hard gluon exchange. The additional factor  $(1/k_\perp^2)^2$  is due to overlapping integral of 3q system with the nucleon. This estimate is reasonable if

$$k_\perp > 3\langle k_q \rangle \sim 0.9 \text{ GeV}/c.$$

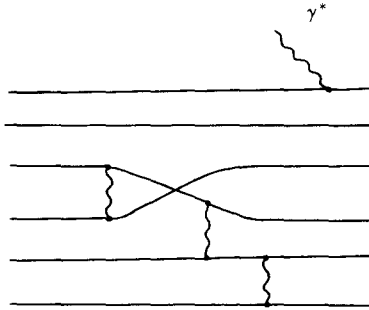


Fig. 4.6. The QCD diagram for production of the nucleon with  $\alpha \sim 1$  and large  $k_\perp$ .

#### 4.2. Leading particle production in hadronic reactions $D \rightarrow p, \pi$ at $x_F \rightarrow 1$

Above we have calculated the WF of the 6q component of the deuteron at  $\alpha \rightarrow 2$ . However in inclusive hadronic reactions the component of WF containing hard gluons gives much larger contribution into the spectrum of leading particles.

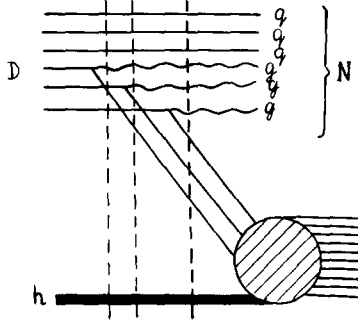


Fig. 4.7.

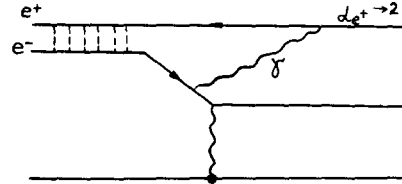


Fig. 4.8.

Let us first consider the  $D \rightarrow p$  fragmentation. It is easy to check that the dominant contribution (in lowest order in  $\alpha_s$ ) is given by diagram 4.7 which corresponds to formation of a nucleon in the final state from 3q 3g component of quark-gluon WF of D. Since the formation of nucleon takes place long after the interaction with hadron h, the overlap integral is suppressed only numerically. Integrating over transverse momenta we obtain [75]

$$\begin{aligned}
 G_h^{D/p}(\alpha) \equiv \alpha \frac{d\sigma^{h+D \rightarrow p+X}}{d\alpha} &\sim \int_0^{2-\alpha} \int_0^{2-\alpha} \int_0^{2-\alpha} \frac{d\beta_1}{\beta_1} \frac{d\beta_2}{\beta_2} \frac{d\beta_3}{\beta_3} \delta(2-\alpha-\beta_1-\beta_2-\beta_3) \\
 &\times \sigma^{h\bar{q}q\bar{q}}(s' = (2-\alpha)s)(\sqrt{\beta_1\beta_2\beta_3})^2 \left[ \frac{1}{\beta_1^{-1}} \right]^2 \left[ \frac{1}{\beta_1^{-1} + \beta_2^{-1}} \right]^2 \\
 &\times \left[ \frac{1}{\beta_1^{-1} + \beta_2^{-1} + \beta_3^{-1}} \right]^2 \sim (2-\alpha)^2. \tag{4.12}
 \end{aligned}$$

Here the factors  $(2-\alpha)^6$ ,  $(2-\alpha)^{-3}$ ,  $(2-\alpha)^{-1}$  arise from 6 energy denominators, 6 vertex functions  $g_{\bar{q}q\bar{q}}$ , and from the phase volume and the amplitude of h scattering from slow  $\bar{q}q\bar{q}$  system, respectively. Since the invariant mass of 3q 3g system is finite ( $\sim 1$  GeV) and does not increase with  $\alpha$ , the overlap integral is practically  $\alpha$  independent. In the calculation of fig. 4.7 we make a usual assumption that interaction of a recoiling 3q system with h (which is denoted by black blob) corresponds to an energy independent cross section. Eq. (4.12) is in a smooth correspondence with the expectations of the triple reggeon approach:

$$G^{D/P}(\alpha) \sim (2-\alpha)^{1-2\alpha_N(0)}. \tag{4.13}$$

This is not accidental, since fig. 4.5 is actually the lowest order diagram for nucleon reggeization in QCD. In this order  $\alpha_N(0) = -\frac{1}{2}$ , corresponding to 3 elementary quark exchanges. (One can check by considering the process: positronium + Coulomb center  $\rightarrow e^- (x_F \rightarrow 1) + X$  that in QED similar diagrams (fig. 4.8) do indeed lead to triple-reggeon limit.<sup>†</sup>) Consequently we have demonstrated that similar to

<sup>†</sup> We thank L.N. Lipatov for drawing our attention to this process.

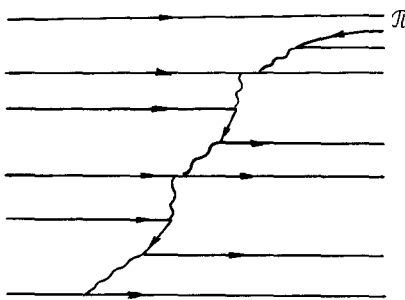


Fig. 4.9.

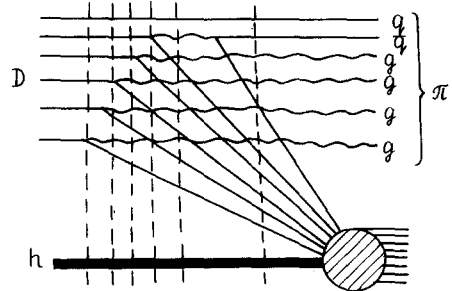


Fig. 4.10.

the case of Pomeron exchange, where single gluon exchange leads to  $\alpha_p(0) = 1$  the lowest order QCD diagram for nucleon exchange seems to be a reasonable first approximation for the nucleon reggeization.

Let us now consider the reaction  $h + D \rightarrow \pi + X$ . The contribution of 6q configuration (diagram 4.9) leads to‡

$$G_h^{D/\pi}(\alpha) \sim (2 - \alpha)^9, \quad (4.14)$$

though the contribution of diagram 4.10 with hard gluon emission [75] is proportional to

$$G_h^{D/\pi}(\alpha) \sim (2 - \alpha)^5. \quad (4.15)$$

Therefore the contribution of diagrams 4.7, 4.10 into  $G^{D/p, \pi}(\alpha)$  decreases more slowly with  $\alpha$  than that of 6q configuration. However, the overlap integral of 3q 3g ( $q\bar{q}4g$ ) state with nucleon (pion) seems to be much smaller numerically than for 3q( $q\bar{q}$ ) state. Thus it is not clear whether mechanism of fig. 4.5 for  $p(\pi)$  production dominates in all region  $\alpha > 1.8$  ( $\alpha > 1.5$ §) changing smoothly effective power  $(2 - \alpha)^n$  from  $n = 3$  ( $n \sim 7$ ) to  $n = 2$  ( $n = 5$ ), or the contribution of 6q state would lead to a break in the  $\alpha$  dependence of the cross section in the transitional region. (Similar approach can be used for hadronic reactions  $p \rightarrow \pi$ ,  $\pi \rightarrow p$  at  $x \rightarrow 1$ , leading to¶ [75]):

$$G_h^{p/\pi}(x) \sim (1 - x)^2 \quad (4.16a)$$

$$G_h^{\pi/p}(x) \sim (1 - x)^2. \quad (4.16b)$$

This behaviour of  $G_h^{p/\pi}$ ,  $G_h^{\pi/p}$  is in agreement with the data [151, 152] in the range  $x > 0.7$ ,  $k_\perp \sim 0$ ;  $0.8 > x > 0.4$ ,  $k_\perp \sim 0$  respectively.) It follows from the above calculation of the diagrams 4.7, 4.10 that the transverse momenta of produced quarks (gluons) are determined by the energy scale of hard interaction, which appears to be larger than the scale of confinement determining the hadron WF in the average configuration. Therefore, the leading hadrons in the nucleus fragmentation region are

‡ This behaviour of  $G^{D/\pi}(\alpha)$  was suggested in [38, 41].

§ This number is not more than an educated guess.

¶ Eq. (4.16b) was recently derived in [153] within a somewhat different approach.

produced in the compressed state (in the case of diagram 4.2 for nucleon production some compression arises also due to asymmetry of light cone fractions of quarks in nucleon). Because of this their interaction with the residual nucleus could be smaller than according to naive free path estimates of cascade models.

### 4.3. QCD and short-range nucleus structure

We have demonstrated in section 2.4 that the density matrix of the  $j$ -nucleon correlation can be expressed through WF of two nucleon correlation as

$$\rho_j(\alpha) \sim [(j - \alpha)/(j - 1)]^{(j-1)n+j-2} \quad \text{if } \rho_2(\alpha) \sim (2 - \alpha)^n.$$

It follows from analysis of section 4.1 that in the valence quark approximation  $n_{\text{eff}}$  for  $\rho_2(\alpha)$  changes from  $n_{\text{eff}} \sim 3$  at  $\alpha < 1.7$ –1.8 to  $n_{\text{eff}} \sim 6$  at larger  $\alpha$ . This change of  $n_{\text{eff}}$  should lead to the change of  $n_{\text{eff}}^{(3)}$  from  $n_{\text{eff}}^{(3)} = 7$  at  $\alpha \leq 2.4$  to  $n_{\text{eff}}^{(3)} = 13$ .

However QCD diagrams like those shown in fig. 4.9, which cannot be described as a convolution of two-nucleon interactions lead to the slower decrease of  $\rho_3(\alpha)$ :  $n_{\text{eff}} = 11$ . This effect is a consequence of the QCD selection rule which is present for the 6q but not the 9q system.<sup>†</sup> Therefore, QCD predict certain short-range three body-forces. It is worth noting also that the recoiling 6q system has a rather complicated color symmetry. As a result, contribution of configurations with hidden colour is enhanced in this case. Therefore deep inelastic scattering, say off  ${}^3\text{He}$ , at  $x \geq 2$  seems to be a good place for investigation of hidden colour. For example, one could try to study the mass distribution of two-nucleon ( $\Delta\Delta, \Delta N?$ ) system.

A rather interesting situation could exist also in a reaction like  ${}^3\text{He} \rightarrow p$  at  $\alpha > 2.4$ , where 9q contribution could be more essential in a certain  $\alpha$  range than the contribution of diagrams similar to those of fig. 4.7 corresponding to the formation of nucleon in the final state from 3q 6g system. Indeed, although a 3q 6g contribution decreases with  $((3 - \alpha)^5)$  much slower than 9q contribution  $((3 - \alpha)^{11})$ , it is suppressed due to a considerably smaller overlap integral of the 3q 6g configuration with the nucleon. Similar interplay of two mechanisms should take place for higher nucleon correlations. To investigate these important phenomena the experiments with light ( $A = 3, 4$ ) nuclei are necessary.

In summary, we have demonstrated in this section that perturbative QCD provides an effective

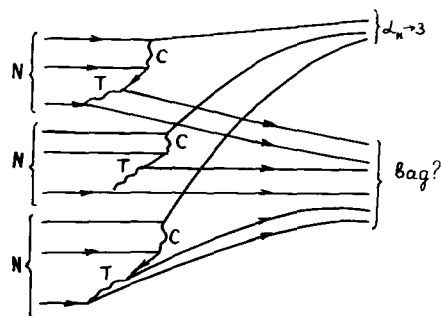


Fig. 4.11.

<sup>†</sup>For a discussion of the QCD vector coupling selection rules [145] see Appendix C.

method of estimating the short-range nuclear correlations and cross section of fragmentation processes. It enables also to determine the region of applicability of relativistic description of the nucleus in terms of nucleon degrees of freedom.

## 5. High $Q^2(e e')$ reactions

In this section we start a discussion of high energy reactions appropriate for investigation of few nucleon (short-range) correlations (FNC) in nuclei. Presence of FNC is often referred to as an elusive property of the nuclei [155]. Indeed, in the past apparently convincing proposals to measure FNC have failed to obtain unambiguous results. It was found that large distance multistep processes seem to overshadow FNC contributions. Basically this difficulty arises from the impossibility of studying this region by intermediate – energy probes where the short-range final state interaction is important. This point was recently reemphasized by Amado [156]. However, this difficulty is not of fundamental nature. It merely reflects a lack of difference between the energy scale of FNC and the average energy transfer in the probe-nucleon interaction at intermediate energy (see e.g. theoretical example of section 2.1). On the contrary at multi GeV energies these scales become quite different and therefore FNC's can be unambiguously measured.

We start from an investigation of deep inelastic lepton-nucleus scattering since in the Bjorken limit  $x = -q^2 A/(2(p_A q))$  fixed,  $Q^2 \rightarrow \infty$  the deep inelastic cross section is directly expressed through the ground-state WF of the target. The final state interaction is precisely accounted for by the closure approximation. This result is strictly valid both in quantum field theory [90] and in quantum mechanics [157]. Consequently the absolute value and the shape of the high momentum component of the nucleus WF can be determined by measuring deep inelastic cross section at  $x > 1$  where the low momentum component does not contribute due to the kinematics (experiments of this type would be a natural extension of the celebrated deep-inelastic lepton-nucleon experiments, which have provided the detailed information about the quark-parton WF of nucleon).

We discuss also the transitional region  $x > 1$ ,  $Q^2$  large but the invariant mass of the produced system –  $W_A$  is not large yet. Importance of studying this kinematical domain was emphasized recently in a number of works (see [39, 158, 159] and references therein).

### 5.1. The basic formulae

#### 5.1.1. The Bjorken limit

Similar to the deuteron case (section 2.3) the structure functions of deep inelastic  $\ell A$  scattering –  $F_{1,2,3}^A(x, q^2)$  can be expressed, in the Bjorken limit  $x = -Aq^2/2(qP_A)$  fixed,  $-q^2 \rightarrow \infty$  through the convolution of the single-nucleon light cone density matrix of nuclei –  $\rho_A^N(\alpha, k_\perp)$ , summed over nucleon spins and averaged over nucleus polarization and nucleon structure functions  $F_{1,2,3}^N(x, q^2)$  as follows (for definitions of  $\rho_A^N(\alpha, k_\perp)$  and  $F_{1,2,3}(x, q^2)$  see eqs. (2.31), (3.10) correspondingly) [64, 160]

$$F_{1,3}^A(x, q^2) = \sum_{N=p,n} \int \frac{A}{\alpha} F_{1,3}^N\left(\frac{x}{\alpha}, q^2\right) \rho_A^N(\alpha, k_\perp) \frac{d\alpha d^2 k_\perp}{\alpha} \quad (5.1)$$

$$F_2^A(x, q^2) = \sum_{N=p,n} \int F_2^N\left(\frac{x}{\alpha}, q^2\right) \rho_A^N(\alpha, k_\perp) \frac{d\alpha d^2 k_\perp}{\alpha}.$$

The eqs. (5.1) have a simple interpretation in the parton language: probability to find a parton in nuclei carrying the fraction of nucleus momentum  $x/A$  is equal to the product of the probability to find a nucleon carrying a fraction  $\alpha/A$  of the nucleus momentum and the probability to find a parton within the nucleon carrying a fraction  $x/\alpha$  of the nucleon momentum.

### 5.1.2. High $Q^2$ threshold region

To estimate the structure functions in the intermediate region of large  $Q^2$ ,  $x > 1$ , but comparatively small  $W - m_A$ , where the restrictions on the mass of the recoiling  $A - 1$  nucleon system are important, it is appropriate to introduce  $\tilde{\rho}_A^N(\alpha, k_\perp, M_{\text{Rec}}^2)$ , the light cone spectral function.  $\tilde{\rho}_A^N$  is a direct generalization of the spectral function  $S(k, E)$  well known in quantum mechanics (see e.g. [161]). By definition,  $(1/A)\tilde{\rho}_A^N$  represents the probability that if a nucleon with light cone momentum  $(\alpha, k_\perp)$  were removed instantaneously from the target, the excited state with the invariant mass  $M_{\text{Rec}}$ , remains in the rest of the nucleus. Evidently, summing over the mass of recoiling system we obtain:

$$\rho_A^N(\alpha, k_\perp) = \int \tilde{\rho}_A^N(\alpha, k_\perp, M_{\text{Rec}}^2) dM_{\text{Rec}}^2. \quad (5.2)$$

The final-state interaction between the struck nucleon and the residual nucleon is thought to be small if  $Q^2 > (2p_F)^2$  and  $W - M_A \geq 100$  MeV. (See e.g. disc. in [161].) Our calculation of  $eD \rightarrow e' + X$  reaction (section 3.1) is in line with this idea.

We use general expression (2.12) and calculate  $A_{tt}$ ,  $A_{ty}$ ,  $A_{yy}$  components of current-nucleus amplitude and reconstruct structure functions using gauge invariance (the  $x$  axis is chosen in the  $q_\perp$  direction). After integrating over the internal variables of WF of residual nucleus we obtain [75]:

$$\begin{aligned} M_A W_1^A(\nu, q^2) &= \sum_{N=p,n} \int \left[ M_N W_1^N(\tilde{\nu}, q^2) + k_y^2 \frac{W_2^N(\tilde{\nu}, q^2)}{M_N} \right] \frac{A}{\alpha} \tilde{\rho}_A^N(\alpha, k_\perp, M_{\text{Rec}}^2) d\tau \\ \frac{1}{M_A} W_2^A(\nu, q^2) &= \sum_{N=p,n} \int \frac{\alpha W_2^N(\tilde{\nu}, q^2)}{M_N A} \tilde{\rho}_A^N(\alpha, k_\perp, M_{\text{Rec}}^2) d\tau \\ \frac{1}{M_A} W_3^A(\nu, q^2) &= \sum_{N=p,n} \int \frac{W_3^N(\tilde{\nu}, q^2)}{M_N} \tilde{\rho}_A^N(\alpha, k_\perp, M_{\text{Rec}}^2) d\tau \\ \tilde{\nu} &= \frac{\alpha}{A} (\nu + M_A^2 - M_X^2) + k_\perp q_\perp, \quad d\tau = \frac{d\alpha}{\alpha} \frac{d^2 k_\perp}{\alpha} dM_{\text{Rec}}^2. \end{aligned} \quad (5.2')$$

$M_{\text{rec}}$  is the mass of the rest of nucleus,  $M_X^2 = A((M_{\text{rec}}^2 + k_\perp^2)/(A - \alpha) + (m^2 + k_\perp^2)/\alpha)$ . By substituting  $M_X^2$  instead of  $M_n^2$  we effectively take into account the final state interaction. This prescription is similar to [161].

It is worth noting that in the limit of high  $Q^2$  and fixed  $W^2 - M_A^2$  the only contribution in eq. (5.2) comes from the kinematical region of large  $k_\perp^2$  and  $\alpha \sim 1$ . On the contrary in the Bjorken limit and  $x > 1$  (eq. (5.1)) dominant contribution is given by the region of small  $k_\perp^2$  and large  $\alpha$ .

To estimate  $\tilde{\rho}_A^N$  at large  $\alpha$  we can use the decomposition of WF over the few nucleon correlations (section 4). As a result  $\tilde{\rho}_A^N$  can be approximated as

$$\tilde{\rho}_A^N(\alpha, k_\perp, M_{\text{Rec}}^2) = A \sum_{j=2}^A a_j \tilde{\rho}_j(\alpha, k_\perp, M_j^2) \delta(M_{\text{Rec}}^2 - M_j^2). \quad (5.3)$$

$M_j$  can be expressed through the invariant mass of  $j-1$  recoiling nucleons of the correlation  $-M_{j-1}^{\text{Rec}}$ , and the mass of the spectator nucleus consisting of  $A-r$  nucleus  $M_{A-j}$ :

$$M_j^2 = (A-\alpha)(M_{A-j}^2/(A-j) + ((M_{j-1}^{\text{Rec}})^2 + k_\perp^2)/(j-\alpha)) - k_\perp^2. \quad (5.4)$$

For the two-nucleon correlation eq. (5.4) takes more simple form

$$M_2^2 = (A-\alpha) \left( \frac{M_{A-2}^2}{A-2} + \frac{m_N^2 + k_\perp^2}{2-\alpha} \right) - k_\perp^2. \quad (5.4')$$

It was explained in section 2.4 that the dominant  $j$ -nucleon correlation configuration corresponds to the system of  $j-1$  nucleons with mass  $M_{j-1}^{\text{Rec}}$ , which balance one fast nucleon  $(\alpha, k_\perp)$ . The relative momenta in the recoiling  $j-1$  nucleon system should be rather large as the contribution of any particular diagram corresponds to a rather asymmetric configuration. Consequently the average  $M_{j-1}^{\text{Rec}}$  could be considerably larger than the mass of the nucleus consisting of  $j-1$  nucleons. Note however that the final state interaction between  $j-1$  nucleons tends to reduce  $M_{j-1}^{\text{Rec}}$ .

## 5.2. Comparison with the data

Here we shall discuss the expected magnitude of effects of short-range nuclear correlations.

As  $F_2^N(x, q^2) \approx 0$  for  $x > 1$ , the value of  $F_2^A(x, q^2)$  at  $x > 1$  is determined entirely by the high momentum component of the nuclear WF with  $\alpha > x$ . Therefore changing  $x$  one can suppress in succession the contributions of average field  $k \leq k_F$ ,  $\alpha \geq 1 + k_F/m_N \approx 1.25$ , pair correlations  $\alpha \geq 2$ , etc.

First we consider the scattering from the few-nucleon systems. The measurements of  $(\nu W_2)^{3,4}\text{He}$  in high  $Q^2$ , near the threshold region were performed recently in SLAC and the data on the scattering from  ${}^3\text{He}$  are now published [8] (see fig. 5.1). So the comparison is possible in this case.

For a rough estimate of  ${}^3\text{He}$ ,  ${}^4\text{He}$  structure functions in the kinematical region where the pair correlation contribution dominates in  $\rho_A^N$  we can use the analysis [71] of FB proton and pion production

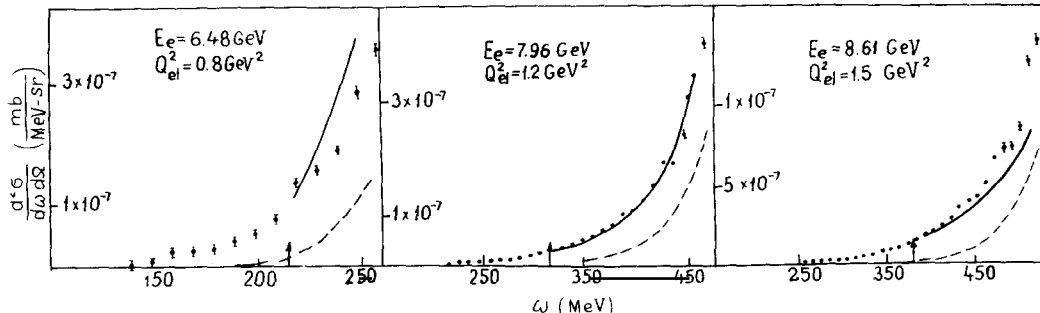


Fig. 5.1.  ${}^3\text{He}$  structure function versus energy transfer  $E_i - E_f$ . The solid curve is the result of the calculation in the two-nucleon correlation approximation described in the text. The dashed curve is the result of non-relativistic calculation [8]. The arrows indicate the kinematical boundaries for the scattering off the deuteron.

[13, 11, 20] from D,  ${}^4\text{He}$  (see section 8). It indicates that

$$\rho_{{}^4\text{He}}^p(\alpha, k_\perp) \sim 8\rho_D^p(\alpha, k_\perp) \quad \text{for } 1.3 < \alpha < 1.7. \quad (5.5)$$

This estimate is consistent with the  ${}^4\text{He}$  photodisintegration data (see e.g. [84, 86]) if one uses the Wigner model [162] to estimate the contribution of the singlet NN pairs, and with quantum mechanical estimate of  $\rho_{{}^4\text{He}}^N(k)$  made by Zabolotsky and Ey [82]. Consequently

$$W_2^{{}^4\text{He}}(x, Q^2) \approx 8W_2^D(x, Q^2) \quad \text{for } 1.5 \geq x > 1.$$

We can also use this information on  $\rho_{{}^4\text{He}}^N$  to estimate  $\rho_{{}^3\text{He}}^N$ . We assume in line with the Wigner model [162] that for lightest nuclei relative probabilities of pp, nn, pn pairs summed over spin of the pair are 1:1:4. To account for the different number of neighbours in  ${}^3\text{He}$ ,  ${}^4\text{He}$  we use the fact that the electromagnetic radii of  ${}^3\text{He}$  and  ${}^4\text{He}$  are practically equal. Thus we take the probabilities of given pair per bond to be equal.

In  ${}^4\text{He}$  there are 4 pn, 1 pp, 1 nn bonds and in  ${}^3\text{He}$  there are 2 pn, 1 pp bonds. Therefore

$$\frac{\rho_{{}^3\text{He}}^p}{\rho_{{}^4\text{He}}^{p,n}} = \frac{4 \cdot 2 + 2 \cdot 1}{4 \cdot 4 + 2 \cdot 1} = \frac{5}{9}, \quad \frac{\rho_{{}^3\text{He}}^n}{\rho_{{}^4\text{He}}^{p,n}} = \frac{4 \cdot 2}{4 \cdot 4 + 2 \cdot 1} = \frac{4}{9}. \quad (5.6)$$

As a result

$$\frac{\nu W_2^{{}^3\text{He}}}{\nu W_2^D} \approx 8 \frac{\nu W_2^{{}^3\text{He}}}{\nu W_2^{{}^4\text{He}}} = 8 \frac{\frac{5}{9}\sigma_{ep} + \frac{4}{9}\sigma_{en}}{\sigma_{ep} + \sigma_{en}} \approx 4.4 \quad (5.7)$$

as  $\sigma_{en} \ll \sigma_{ep}$ . This estimate is in a reasonable agreement with the data [8] in the pair correlation region (see fig. 5.1). For comparison we use  $F_{2D}(\nu, q^2)$  calculated in section 3.1 on the basis of eq. (3.3) which reasonably fits  $eD \rightarrow e + X$  data [5] (see fig. 3.3) which are in the same  $q^2$  range. Note that the models considered in [8] underestimate the cross section of the process  $e + {}^3\text{He} \rightarrow e + X$  in this region by the factor 3–5. Therefore these models seem to underestimate high momentum tail of  ${}^3\text{He}$  WF†. An estimate of  $\nu W_2^{{}^3,4\text{He}}$  in the frame of light-cone average field approach is given in [69].

In the region of large  $x$  the ratio  $F_2^{{}^3\text{He}}(x, Q^2)/F_2^D(x, Q^2)$  should increase due to the presence of 3-nucleon correlations. This is also qualitatively consistent with the data.

It is worth noting that due to large difference of ep, en cross section for large  $x$ :  $F_{2n}(x)/F_{2p}(x) \sim 0.3 - 0.4$  at  $x \sim 0.8$  it is possible in principle to separate  $\rho_{{}^4\text{He}}^p(\alpha)$  and  $\rho_{{}^3\text{He}}^n(\alpha)$  at large  $\alpha$  using  ${}^3\text{H}$  target and isotopic invariance ( $\rho_{{}^3\text{He}}^{p(n)}(\alpha) = \rho_{{}^3\text{H}}^{n(p)}(\alpha)$ ).

### 5.3. Sum rules for the nucleus structure functions

By measuring  $F_i^A(x, q^2)$  in sufficiently wide  $x$  range it is possible to determine the average characteristics of density matrix in a model independent way. Indeed the moments of  $\rho_A^N(\alpha)$  (here for the sake of simplicity we take  $Z = N$  and assume  $\rho_A^p = \rho_A^n = \frac{1}{2}\rho_A^N$ )

† It is tempting to suggest that the well-known difficulties in the description of the  ${}^3\text{He}$  elastic formfactor (calculated with the same WF's) are due to underestimation of the value of the short-range correlations.

$$I_k^N = \int \alpha^{k-1} \rho_A^N(\alpha, k_\perp) \frac{d\alpha}{\alpha} d^2 k_\perp \quad (5.8)$$

are simply expressed [75] through the moments of deep inelastic structure functions of nucleon and nuclei

$$M_{k(i)}^{A(N)}(q^2) = \frac{1}{A} \int x^{k-1} F_i(x, q^2) dx. \quad (5.9)$$

We have

$$\begin{aligned} I_{k+1}^N &= M_{k(2)}^A(q^2) \cdot 2/(M_{k(2)}^p(q^2) + M_{k(2)}^n(q^2)) \\ I_k^N &= M_{k(1,3)}^A(q^2) \cdot 2/(M_{k(1,3)}^p(q^2) + M_{k(1,3)}^n(q^2)). \end{aligned} \quad (5.10)$$

$I_{1,2} \equiv 1$  due to normalization of  $\rho_A^N(\alpha, k_\perp)$  and due to the symmetry properties of WF correspondingly (see eqs. (2.33), (2.34)). In the limit  $k/m \ll 1$ ,  $\alpha = 1 + k_3/m$  (see eq. (2.35)) therefore  $\frac{3}{2}(I_3 - 1)m_N$  is equal to the average kinetic energy of nucleon in the nucleus. Note also that, if  $j > 2$  correlations could be neglected, the even momenta  $I_k$  are expressed through the lower momenta. For example  $I_4 = 3I_3 - 2$ .

#### 5.4. Predictions for the value of the nucleus structure functions in the Bjorken limit at $x \geq 1$

To estimate the influence of the FNC on the behaviour of  $F_{2A}(x)$  at  $x > 1$  we choose the model WF in accordance with conventional nuclear physics and QCD analysis (see section 4).

*Choice of nuclear WF for large A.* The shape of high momentum component of WF was estimated in section 2.4.  $\rho_A^N(\alpha, k_\perp)$  corresponding to eq. (2.44) with the coefficients  $a_j$  determined from the comparison with  $p + A \rightarrow p + X$  data† (fig. 8.5) can be roughly fitted as

$$\begin{aligned} \rho_A^N \sim \rho(\alpha, k_\perp) &= \exp(-7\alpha - Bk_\perp^2) \\ B &= (8.9 - 2.66) \theta(2.4 - \alpha) + 2.5 \theta(\alpha - 2.4)(\text{GeV}/c)^{-2} \quad \text{for } \alpha > 1.65. \end{aligned}$$

In the region of small momenta  $k < k_F \sim 0.26 \text{ GeV}/c$  the nucleon distribution can be approximated by a constant. In the intermediate region we assume that  $\rho_A^N(\alpha, k_\perp) \sim \rho_B^N(\alpha, k_\perp)$ .

Therefore we choose following WF for  $A \geq 12$ :

$$\frac{1}{A} \rho_A^N(\alpha, k_\perp) = \begin{cases} C_0 & \text{for } k < k_F = 0.26 \text{ GeV}/c \\ \lambda_A \psi_B^2(k) \frac{\sqrt{m^2 + k^2}}{2 - \alpha} & \text{for } \alpha < 1.65 \text{ and } k > k_F \\ C_1 \rho(\alpha, k_\perp) & \text{for } \alpha > 1.65. \end{cases} \quad (5.11)$$

† This procedure could overestimate the ratio  $a_j/a_2$  by factor 1.5–3 depending on  $j$ .

$C_1$  and  $C_0$  are determined from continuity of  $\rho_A^N$  at  $\alpha = 1.65$  and normalization condition for  $\rho_A^N$  correspondingly. On the basis of data on  $\ell + A \rightarrow \ell' + N + X$  reaction, cumulative pion production and nuclear photodisintegration reactions we take  $\lambda_A = 6$  neglecting  $A$  dependence of  $\lambda_A$ . Variables  $k$  and  $\alpha, k_\perp$  are related according to eq. (2.21):

$$\alpha = 1 + k_3/\sqrt{m^2 + k^2}. \quad (5.12)$$

Let us enumerate the basic consequences of eqs. (5.1) for  $F_{2A}(x)$ :

(a) For rough estimate it is fruitful to apply in the region  $1 < x < 2$  the pair correlation approximation which reasonably describes many phenomena [87, 86, 71]. For nuclei with  $Z \sim N$  eq. (5.1) predicts

$$\eta_A(x) = \frac{F_{2A}(x, Q^2)/A}{F_{2D}(x, Q^2)/2} \Big|_{2 \gg x \geq 1} \approx \lambda_A \sim (6-8). \quad (5.13)$$

Due to fast decrease of  $F_{2D}(x, q^2)$  with  $x$  the contribution of three(four) nucleon correlations in  $\eta_A(x)$  could be larger even at  $x \sim 1$ . To estimate the role of 3-nucleon correlation we use the nucleus WF introduced above. (Really we expect universal shape of  $F_{2A}(x)$  at  $x > 1$  for  $A > 12$  as contributions of two and three-nucleon correlation have similar  $A$ -dependence, eq. (2.40).)  $F_{2A}(x)$  calculated on the basis of eq. (5.1) with  $F_{2p}(x)$  from [127] and  $F_{2n}(x)/F_{2p}(x) = 1 - \frac{3}{4}x$  can be fitted as† [75]

$$F_{2A}(x) = 1.9 \times 10^{-3} \exp((-6.45(x-1))/x^3) \cdot A \text{ at } 2 > x > 0.8. \quad (5.14)$$

This result shows that  $\eta_A(x)$  rapidly increases with  $x$  (see fig. 5.2). It is explained in section 7.1 that eq. (5.11) could overestimate  $a_{3,4}/a_2$ . If so eq. (5.14) can overestimate  $F_{2A}(x)$  by factor 2–3 for  $x \geq 1.5$ . Another possible cause of the overestimation of  $F_{2A}(x)$  at large  $x$  (but not of the ratio  $\eta_A(x)$ ) is the gluon mechanism of fig. 4.7, which contributes into the fast backward nucleon yield but not to the deep inelastic structure functions.

To understand what region of  $\alpha$  is probed by the measurement of  $F_{2A}(x)$  at given  $x$  it is instructive to estimate  $F_{2A}(x)$  by the steepest descent method. For illustration we take  $F_{2N}(x) = (1-x)^n$  ( $n \sim 3$ ),  $\rho(\alpha) = A \exp(-B\alpha)$ . The saddle point is

$$\begin{aligned} \alpha_{sp} &= \frac{1}{2} \left[ x - \frac{1}{B} + \sqrt{\left( x + \frac{1}{B} \right)^2 + \frac{4xn}{B}} \right] \approx x + \frac{n}{B} - \frac{n(n+1)}{B(Bx + 2n + 1)}; \\ F_{2A}(x) &\approx \frac{A \exp(-B\alpha_{sp})}{\{B\alpha_{sp}/n\}^{n+1}} \sqrt{\frac{2\pi}{n}} \left[ 1 - \frac{n+1}{Bx + 2n + 1} \right]^{-n-1}. \end{aligned} \quad (5.15)$$

It follows from the equation that for realistic  $B \approx 7$ ,  $n \approx 3$  the region  $\alpha \approx x + \frac{3}{7} - \frac{1}{4}/(1+x)$  is probed.

(b) For light nuclei a rather peculiar  $A$  dependence of  $F_{2A}(x)/A$  is expected due to cluster effects. For example within the cluster model  ${}^6\text{Li}$  consists of  ${}^4\text{He} + \text{D}$ . As a result

$$F_2^{{}^6\text{Li}}(x) = F_2^{{}^4\text{He}}(x) + 1.5F_2^{\text{D}}(x).$$

† For different estimate of  $F_{2A}(x)$  at  $x \geq 1$  within the cumulative model of the nuclei (see [206]), for estimate based on the quark counting rules (see [54]). Note that QCD predicts [103] large scaling violation for  $F_{2N}(x, Q^2)$  at  $x \sim 1$ . In this case one should use directly eq. (5.1).

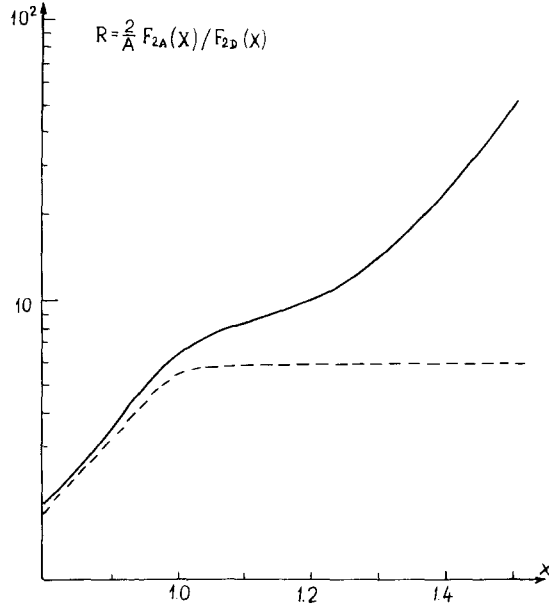


Fig. 5.2. The estimate of the  $(F_{2A}(x)/A)/(F_{2D}(x)/2)$  ratio using realistic nuclear WF with few-nucleon correlations (eq. (5.11)) (solid curve) and using the two-nucleon correlation approximation.

The factor 1.5 arises due to compression of the deuteron cluster [164]. Therefore the ratio  $F_{2A}(x)/A$  should decrease in transition from  $A = 4$  to  $n = 6$ .

Similarly in the frame of cluster model one can obtain:

$$F_2^{7\text{Li}}(x) = F_2^{4\text{He}}(x) + F_2^{3\text{H}}(x), \quad F_2^{9\text{Be}}(x) = 2F_2^{4\text{He}}(x) \quad \text{for } x > 1, \quad F_2^{12\text{C}}(x) = 3F_2^{4\text{He}}(x).$$

The check of these relationships would help to understand the range of applicability of these models, which are usually applied to description of the average distance effects.

In the range of  $12 < A < 200$  the  $A$  dependence of  $F_{2A}(x)/A$  can be estimated using analysis of [72] (eq. (2.40)) where  $A$  dependence of few-nucleon correlations was estimated in the framework of dilute gas approximation.  $F_{2A}(x)/A \sim A^{n(x)} F(x)$  where  $n(x) \sim 0.2$  and rather weakly increases with  $x$  since different few-nucleon correlations have rather similar  $A$  dependence for  $A > 12$  (see section 2.4). To conclude, we have demonstrated in this section that investigation of high energy deep inelastic reactions enables to investigate absolute magnitude of the short range nucleon WF and probably its cluster decomposition.

*A comment.* One can use the measurements of  $F_{iA}(x, Q^2)$  in the near-threshold region to determine the values of  $a_i$ . Indeed, applying the FNC the composition of  $\rho_A^N(\alpha, k_\perp)$  we obtain:

$$F_{iA}(x, Q^2) = A \sum_{j=2}^A a_j(A) \sigma_i^j(x, Q^2) \tag{5.16}$$

where  $\sigma_i^j(x, Q^2) = 0$  for  $x > j$ . Evidently by choosing the appropriate kinematical region one can suppress here contributions of 2,3-nucleon correlations, thus enhancing high correlations.  $\sigma_i^2$  can be calculated using eq. (3.3) (as in the  ${}^3\text{He}$  case); though e.g.  $\sigma_i^3$  can be determined from  ${}^3\text{He}$  data, etc.

## 6. Deep inelastic $\ell + A \rightarrow \ell' + N + X$ processes

Though inclusive measurements could provide an unambiguous information on  $\rho_A^N$ , they could give little information about  $p_\perp$  dependence of  $\rho_A^N(\alpha, p_\perp)$  and on the structure of recoiling system. To obtain such information semi-inclusive measurements are necessary.

In this section we shall consider semi-inclusive reactions like

$$\ell + A \rightarrow \ell' + p + X . \quad (6.1)$$

Due to simplicity of theoretical interpretation and rather large counting rates such reactions are more effective to study short-range nuclear structure, than more traditional investigation of elastic nuclear form factors at large  $q^2$ .

In deep inelastic processes the lepton strikes a single nucleon removing it from the nucleus. This process can be considered as instantaneous since the energy transfer to the struck nucleon is much larger than the energy scale of FNC. For example the average energy transfer in an elementary high-energy deep-inelastic collision is about one GeV. As a result the final state interaction of the knocked out nucleon and the residual nucleons of the correlation can be neglected at least in the case of lightest nuclei. (Really by selecting large  $x$  processes one can additionally increase the average energy transfer.)

To enhance the FNC contribution it is necessary to select the kinematical region forbidden for scattering from a free nucleon. One way is to investigate reaction (6.1) in the  $x \geq 1$  region. It is possible to study here the spectral function  $\tilde{\rho}_A^N(\alpha, k_\perp, M_{\text{Rec}}^2)$ . One can in particular investigate the increase with  $x$  of the average number of fast forward nucleons which balance the momentum of struck nucleon. However the cross section of this reaction is rather low and the final state interaction between forward going nucleons could be essential.

Therefore it seems much more feasible to use as a trigger the presence of a fast nucleon ( $p_N > 0.3 \text{ GeV}/c$ ) in the backward (relative to  $\gamma^*, W^*$ ) hemisphere. This selection enhances the contribution of short range correlations, because such protons cannot be produced in a collision of a free nucleon or in the nucleus evaporation. (In fact the data on such reaction were accumulated as byproduct on the DST of all big neutrino bubble chambers for a long time. First analysis of such data was undertaken recently by Fermilab-ITEP-IHEP-Michigan collaboration in FNAL [9] and SCAT collaboration in Serpukhov [10].) An evident advantage of using a leptonic probe (instead of hadronic one) is that the lepton provides a rather direct information about the struck nucleon momentum. At the same time the study of the final state gives information about the structure of correlation. (Therefore in a certain sense reaction (6.1) is more close to low energy  $eA \rightarrow e' + p + p + X$  reactions discussed e.g. in [165, 158] than to  $eA \rightarrow e' + p + X$  reactions.)

A natural mechanism for reaction (6.1) is the following:  $\gamma^*, W^*$  strikes one of the nucleons of the correlated system, which has a forward momentum in the nucleus rest frame releasing the backward going nucleon from the correlation (see fig. 6.1). Before starting a formal derivation let us consider what one should expect if reaction (6.1) is dominated by the scattering off the pair correlation. In this case large  $\alpha$  of the backward nucleon<sup>†</sup> is balanced by  $\alpha' \approx 2 - \alpha$  of the struck nucleon. Consequently the average light cone momentum carried by the quarks of the balancing nucleon is  $2 - \alpha$  times smaller than

<sup>†</sup> In the nucleus lab. frame  $\alpha = (\sqrt{m^2 + p^2} - (pq)/|q|)/m_N$ , where  $p$  is the lab. frame nucleon momentum. Large  $\alpha > 1$  corresponds to backward going nucleon in the nucleus rest frame.



Fig. 6.1. Production of a fast backward nucleon in the  $W^*$  scattering from the two-nucleon correlation spectator mechanism.

for the average nucleon with  $\alpha \sim 1$ . Therefore the mean  $x$  for events with backward nucleon should be smaller than in the average case:

$$\langle x \rangle_\alpha = (2 - \alpha)\langle x \rangle. \quad (6.2)$$

The decrease of  $\langle x \rangle_\alpha$  was first predicted in [15] and it is observed now in two experiments [9, 10].

### 6.1. The basic formulae

To describe the reaction (6.1) quantitatively it is necessary to introduce the production function  $\rho_A^{N_1 N_2}(\alpha_1, k_{1\perp}, \alpha_2, k_{2\perp})$ . By definition  $\rho_A^{N_1 N_2}(\alpha_1, k_{1\perp}, \alpha_2, k_{2\perp})/\rho_A^{N_2}(\alpha_2, k_{2\perp})$  is the probability for a nucleon  $N_1$  to be produced if a nucleon  $N_2$  is instantaneously removed from the nucleus. In principle  $\rho_A^{N_1 N_2}$  can be calculated by solving the many-body Weinberg type equation for the nuclear WF and decomposing the WF of the recoiling system over the free particle states (nucleons, nucleus fragments). This procedure is analogous to that used for the calculation of the nuclear spectral function.

It is important that the removal of a nucleon from the nucleus in the reaction (6.1) can well be considered as instantaneous because the energy transfer to the target nucleon in  $\nu N$  scattering is large at any  $x$ . Thus, the spectator contribution to the cross section of the reaction (6.1) is given by eq. (6.3) (cf. equations for the  $\ell + D \rightarrow \ell' + p + X$  reaction in section 3.3) which is really a particular case of the sudden approximation:

$$\begin{aligned} \frac{d\sigma^{\nu(\bar{\nu})+A \rightarrow \mu^\pm + p + X}}{dx dy (d\alpha/d\alpha) d^2 k_\perp} &= \frac{G_F^2}{\pi} E_\nu \frac{M_A}{A} \int \frac{d\alpha_1 d^2 k_{1\perp}}{\alpha_1} \sum_{N=p,n} \rho_A^{pN}(\alpha, k_\perp, \alpha_1, k_{1\perp}) \\ &\times \left[ F_{2N}\left(\frac{x}{\alpha_1}, Q^2\right)(1-y) + \frac{1}{2}y^2 \frac{x}{\alpha_1} 2F_1\left(\frac{x}{\alpha_1}, Q^2\right) \pm y(1-\frac{1}{2}y) \frac{x}{\alpha_1} F_3\left(\frac{x}{\alpha_1}, Q^2\right) \right]. \end{aligned} \quad (6.3)$$

Integrating eq. (6.3) over  $x, y$  we obtain

$$\alpha \frac{d\sigma^{\nu(\bar{\nu})+A \rightarrow \mu^\pm + p + X}}{d\alpha d^2 k_\perp} = \sum \sigma_{\nu(\bar{\nu})N}(E_\nu) \frac{M_A}{AM_N} \int \rho_A^{pN}(\alpha, k_\perp, \alpha_1, k_{1\perp}) \alpha_1 \frac{d\alpha_1 dk_{1\perp}}{\alpha_1}. \quad (6.4)$$

The contribution to the cross section arising from  $\gamma^*(W^*)$  scattering from a fast backward nucleon



Fig. 6.2. Direct mechanism of fast backward nucleon production.

(fig. 6.2) (so called direct mechanism) is described by eq. (6.5)

$$\begin{aligned} \frac{d\sigma^{\nu(\bar{\nu})+A \rightarrow \mu^\pm + p + X}}{dx dy (d\alpha/\alpha) d^2 p_\perp} &= \sum_{N=p,n} \int_{x+\alpha}^A \frac{d\beta}{\beta} \int d^2 k_\perp \rho_A^N(\beta, k_\perp) \\ &\times \frac{d\sigma^{\nu(\bar{\nu})+N \rightarrow \mu^\pm + p + X}}{dx dy (dz/z) d^2 k_\perp} \left( \beta E_\nu, \frac{x}{\beta}, y, \frac{\alpha/\beta}{1-x/\beta}, p_\perp - \frac{\alpha}{\beta} k_\perp \right) \end{aligned} \quad (6.5)$$

where

$$\frac{d\sigma^{\nu(\bar{\nu})N \rightarrow \mu^\pm + p + X}}{dx dy (dz/z) d^2 k_\perp} (E_\nu, x, y, z, k_\perp)$$

is inclusive cross section of elementary process  $z \equiv (E_p + p_p^z)/\{(E_N + p_N^z)(1-x)\}$  and  $k_\perp$  is transverse momentum of the proton. Numerical estimates [87] indicate that direct contribution is smaller than spectator contribution by a factor  $\sim 100$  and can be neglected.

Probably the simplest measurement would be determination of the average light cone fraction of interacting nucleon  $\alpha_1$ . Indeed,

$$\begin{aligned} \langle x \rangle_\alpha / \langle x \rangle &= \int dx dy d^2 k_\perp x \frac{d\sigma^{\nu+A \rightarrow \mu+p+X}}{dx dy (d\alpha/\alpha) d^2 k_\perp} / \int dx dy d^2 k_\perp \frac{d\sigma^{\nu+A \rightarrow \mu+p+X}}{dx dy (d\alpha/\alpha) d^2 k_\perp} \\ &\equiv \int \rho_A^{pN}(\alpha, \alpha_1) \alpha_1 \frac{d\alpha_1}{\alpha_1} / \int \rho_A^{pN}(\alpha, \alpha_1) \frac{d\alpha_1}{\alpha_1} = \langle \alpha_1 \rangle_\alpha. \end{aligned} \quad (6.6)$$

In the derivation of eq. (6.6) we have assumed that

$$\frac{\int_0^1 \frac{x (2F_{2p}(x) \pm F_{3p}(x) x) dx}{\int_0^1 (2F_{2p}(x) \pm F_{3p}(x) x) dx}}{\int_0^1 \frac{(2F_{2n}(x) \pm F_{3n}(x) x) dx}{\int_0^1 (2F_{2n}(x) \pm F_{3n}(x) x) dx}} = \frac{\int_0^1 x (2F_{2n}(x) \pm F_{3n}(x) x) dx}{\int_0^1 (2F_{2n}(x) \pm F_{3n}(x) x) dx}$$

which roughly satisfied experimentally. Similarly dispersion of  $\alpha_1$  can be measured studying

$$\langle \alpha_1^n \rangle_\alpha = \langle x^n \rangle_\alpha / \langle x^n \rangle. \quad (6.7)$$

*Comment 1.* It is easy to check that the  $y$  distribution is not changed for events with backward nucleon (we neglect here small change due to logarithmic increase of the sea contribution with the energy). Consequently the same eqs. as eqs. (6.6) are valid for  $v = xy$  distribution, which could be measured experimentally with smaller systematical uncertainties.<sup>†</sup>

<sup>†</sup>We thank M.M. Savitsky for drawing our attention to the experimental advantages of studying correlations in terms of  $v$ .

*Comment 2.* Large differences of cross sections for  $\nu$ ,  $\bar{\nu}$ , e scattering off protons and neutrons (for example  $\sigma_{\nu n}/\sigma_{\nu p} \sim 2$ ,  $\sigma_{\bar{\nu} n}/\sigma_{\bar{\nu} p} \sim 0.5$ ) could be used to determine relative importance of  $\rho_A^{pp}$ ,  $\rho_A^{pn}$ .

To evaluate eq. (6.3) we can use the decomposition over the contributions of  $j$ -nucleon correlations:

$$\frac{1}{A} \rho_A^{pn}(\alpha, k_\perp, \alpha_1, k_{1\perp}) = \sum_{j=2}^A a_j \rho_j^{pn}(\alpha, k_\perp, \alpha_1, k_{1\perp}). \quad (6.8)$$

For  $j = 2$   $\rho_2^{pn}$  is simply expressed through  $\rho_2$  as

$$\rho_2^{pn}(\alpha_1, k_{1\perp}, \alpha, k_{2\perp}) = \alpha_2 \rho_2(\alpha_1, k_{1\perp}) \delta(2 - \alpha_1 - \alpha_2) \delta(k_{1\perp} + k_{2\perp}) \quad (6.9)$$

where the factor  $\alpha_2$  is due to the phase-space of the nucleon  $N_2$  since by definition

$$\int \rho_2^{pn}(\alpha_1, k_{1\perp}, \alpha_2, k_{2\perp}) \frac{d\alpha_2}{\alpha_2} d^2 k_{12} = \rho_2(\alpha_1, k_{1\perp}).$$

For higher correlations ( $j > 3$ )  $\rho_j^{N_1 N_2}$  cannot be expressed through  $\rho_j$  since the removal of only one nucleon cannot completely destroy the correlation. To calculate e.g.  $\rho_3^{N_1 N_2}$  it is necessary to solve the Weinberg type three-body equation, introduced in section 2.4.

However several features of the reaction (6.2) can be understood now. In the pair correlation approximation it follows from eq. (6.9) that  $\langle x_\alpha \rangle$  should decrease with  $\alpha$  increase according to eq. (6.2). Note that the spectrum multiplied by the factor  $\langle x \rangle / \langle x_\alpha \rangle$  is the same as for similar hadronic reactions:

$$\frac{\langle x \rangle}{\langle x_\alpha \rangle} \frac{d\sigma^{\nu+A \rightarrow \mu+p+X}}{(d\alpha/\alpha) d^2 k_\perp} = \sigma_{\nu N}(E_\nu) \frac{M_A}{AM_N} \rho_A^N(\alpha, k_\perp). \quad (6.10)$$

Due to the similar  $A$ -dependence of  $a_j$  (eq. (2.40)) we expect that the shapes of the nucleon yields from different targets would practically coincide. At the same time for large  $\alpha \geq 2$  where  $j \geq 3$  correlations dominate  $(\langle x \rangle / \langle x_\alpha \rangle) \alpha d\sigma^{\nu+A \rightarrow \mu+p+X} / d\alpha d^2 k_\perp$  decreases faster with  $\alpha$  than the inclusive cross section of the similar hadronic processes, because hadrons but not leptons can effectively destroy the  $j \geq 3$  correlation. The  $x-\alpha$  correlation should also persist for  $\alpha > 2$ . In this case

$$\langle x_\alpha \rangle / \langle x \rangle = \left( \frac{3 - \alpha}{2} \right) \beta(\alpha)$$

where  $\beta(\alpha) < 1$  and  $\beta(1) = 1$ . This is because the maximal energy is transferred to the correlation if  $W^*$  knocks out the nucleon with minimal  $\alpha$ . Thus  $\langle x_1 \rangle$  decreases with  $\alpha$  increase. This leads to an additional decrease of the differential cross section due to  $F_i(x/\alpha)$ 's decrease. Moreover for large  $x$  ( $x > 0.3$  and  $\alpha > 2 - x$ ) the pair correlation simply cannot contribute to the cross section due to kinematics, though in the case of a hadronic projectile it gives the dominant contribution for  $\alpha < 1.7$ . Consequently the normalized cross section of reaction (6.1) should be considerably smaller than in the case of hadronic projectiles for  $\alpha > 1.75$  and  $x > 0.25$ .

Let us now discuss the structure of events with backward nucleon within the FNC approximation:

- (a) The associated hadron multiplicity (without produced nucleons) is expected to be approximately

the same as for normal events and should slightly decrease with an increase in  $\alpha$ :

$$n_A(E, \alpha) = n(E, \alpha_1) \approx n(E, (2 - \alpha)). \quad (6.11)$$

For example for  $\alpha \sim 1.4$ ,  $n_{ch}$  decreases by about 0.7. For FNC the decrease of  $n_{ch}$  is smaller, besides that additional fast nucleons are produced due to destruction of correlation.

(b) The total charge of hadrons produced in association with backward proton (without evaporation protons which have  $p < 0.3 \text{ GeV}/c$ ) is approximately the same as for average events. Some deviations can arise due to different number of pp and pn pairs. An increase of the number of evaporation nucleons is expected as in such processes larger energy is transferred to the nucleus as compared to the average process.

(c) Since the struck nucleon has small  $\alpha_1 > 1$  a fast forward nucleon (with  $\langle \alpha' \rangle \sim 0.5\alpha_1$ ) is expected to be present in the event. Its average momentum is larger than  $1 \text{ GeV}/c$  so it cannot be identified in the bubble chamber.

(d) At large  $\alpha$  where  $j = 3$  correlation becomes essential, number of protons associated with backward proton should increase, leading to a visible increase of the total charge. An additional fast nucleon in the forward hemisphere is expected with the average momentum  $\sim (3 - \alpha)/2, -k_\perp/2$ . Let us now discuss the problem of cascades.

We have neglected the effects of secondary interactions of the quark struck by  $\gamma^*$ ,  $W^*$  with the rest of the nucleus. However recent experiments [166, 167] appear to observe such effect. For light nucleus the average number of secondary interaction per  $\gamma^*(W^*)$  interaction  $-\kappa_A$  seems to be rather small. E.g. for  $^{12}\text{C}$  attenuation of leading hadrons is about 10% [166]. For  $A \sim 100$  it is about  $\sim 0.5$  [166]. Therefore  $\kappa_{100} \geq 0.5$ .

Some qualitative properties of cascades are the following ones:

The  $\langle x \rangle_{\alpha} - \alpha$  correlation decreases

$$\frac{\langle x \rangle_{\alpha}}{\langle x \rangle} = \left( \lambda_1(2 - \alpha) + \lambda_2 \left( \frac{3 - \alpha}{2} \right) + \lambda_3 + \kappa_A \lambda_4 \right) / (1 + \kappa_A). \quad (6.12)$$

Here  $\lambda_1(\lambda_2)$  is the probability of producing proton in  $\gamma^*$  scattering off 2-, 3-nucleon correlation,  $\lambda_3$  is the contribution of nuclear evaporation, which can give a noticeable contribution for large  $A$  at  $0.3 < p_N < 0.4 \text{ GeV}/c$ ,  $\lambda_4$  is the probability of producing a nucleon in the secondary interaction.

The  $A$  dependence of the cross section is larger than according to the  $A$  dependence of the few nucleon correlation by the factor  $(1 + \kappa_A)$ .

A selection of events with backward protons enhanced contribution of central interactions and therefore the probability of secondary interactions leading to some increase of associated multiplicity.

## 6.2. Comparison with experiment

First let us review the  $\bar{\nu} + \text{Ne} \rightarrow \mu^+ + p + X$  data [9]. They seem to be in reasonable agreement with predictions of the two-nucleon correlation approximation [45]: Their momentum dependence is approximately the same as expected for the scattering from the deuteron [45]. The  $\langle x \rangle_{\alpha}$ ,  $\langle y \rangle_{\alpha} - \alpha$  correlation observed in the experiment is consistent with eq. (6.2). (See fig. 6.3.) To estimate the absolute value of cross section we can use the photodisintegration data, which indicate that number of quasideuterons is equal  $= (8-10) NZ/A$ . Using SU(4) symmetry [162] to calculate the number of spin

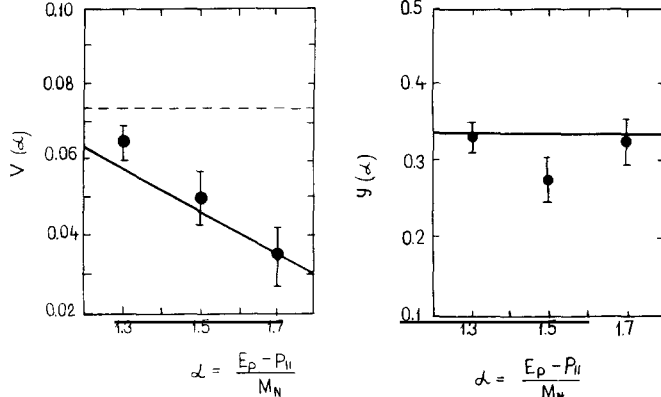


Fig. 6.3.  $v(\alpha)$ ,  $y(\alpha)$ -dependence for events with backward protons. Experimental points are from [96]. Solid lines – the FNC model prediction [45] within the two-nucleon correlation approximation. Dashed line – the average  $v$  for the total sample.

singlet pairs we obtain the following estimate for the multiplicity of backward nucleons with  $p_N > 0.3 \text{ GeV}/c$ :  $\langle n_p \rangle_{\bar{\nu}Ne} \approx (5-6)\%$  and  $\langle n_p \rangle_{\nu Ne} \sim 1.5 \langle n_p \rangle_{\bar{\nu}Ne}$  (the factor 1.5 is due to the difference of  $\nu(\bar{\nu})p$ ,  $\nu(\bar{\nu})n$  cross sections and due to different number of pp and pn pairs). Experimentally  $\langle n_p \rangle_{\bar{\nu}Ne} = (8 \pm 0.5)\%$ .

Triple correlations could contribute in this case  $\sim 30\%$ , and lead to some small decrease of  $\langle x \rangle_\alpha - \alpha$  correlation and to increase of associated nucleon multiplicity. They also lead to decrease of the difference between  $\langle n_p \rangle_\nu$  and  $\langle n_p \rangle_{\bar{\nu}}$ .

However a warning should be made here. The visible charge observed both in the total sample [9] and in the events with backward proton seems to be considerably larger than expected on the basis of the destruction of pair correlations. This fact indicates the importance of nucleon evaporation and/or cascades. To distinguish between these possibilities an investigation of the momentum and the angular distribution of forward protons should be made.

Next we want to consider data [10] on the  $\nu(\bar{\nu}) + \text{CF}_3\text{Br} \rightarrow +p + X$  reaction. Assuming that  $\langle n_p \rangle$  weakly depends of  $E_\nu$  (this is consistent with [9, 10]) and taking  $\langle n_p \rangle_{\nu Ne} \approx \langle n_p \rangle_{\nu C,F}$  we obtain

$$\langle n_p \rangle_{\nu Br} / \langle n_p \rangle_{\nu Ne} \sim 2.5.$$

This ratio is much larger than according to the estimate of  $A$ -dependence of 2, 3-nucleon correlations, eq. (2.40), based on the standard theory of the nuclei.

As the data [165] indicate for Br, the contribution of secondary interactions inside the nucleus is large  $\kappa_{Br} \geq 0.5$ . Therefore the following interpretation of these data is possible. Indeed taking  $\kappa_{Br} \sim 1$  and neglecting for simplicity the contribution of triple correlations we obtain from eq. (6.12)

$$\langle x \rangle_\alpha = \frac{1}{2}(2 - \alpha + 1) \sim \frac{1}{2}(3 - \alpha)$$

which is in agreement with [10]. At the same time the  $A$  dependence becomes

$$\langle n_p \rangle_{\nu Br} / \langle n_p \rangle_{\nu Ne} \sim (1 + \kappa) A^{0.15} \sim 2.5,$$

and the associated proton multiplicities are explained. Recall a factor  $A^{0.15}$  accounts for  $A$ -dependence of pair correlations, cf. section 2.4.

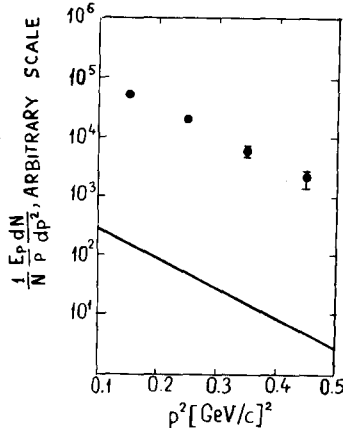


Fig. 6.4. Inclusive invariant backward protons' spectra. Experimental points are from [9]. Solid line – Monte Carlo calculation [87] based on the Amado–Woloshyn–Frankel model [44, 59] adjusted to fit the high energy data on the  $p + A \rightarrow p + X$  reaction [18]. (The use of parameters of WF from [44, 59] further decreases the predicted yield.) The result of calculation for the Schmidt–Blankenbecler model lead practically to the same curve.

Though the existing data seem to be consistent with the few-nucleon-correlation model, they can hardly be explained if the average field configuration dominates [44, 46]. In this case diagram 6.2 would dominate. An estimate of the magnitude of cross section, e.g. in the Amado–Woloshyn–Frankel model, using existing data on the  $\ell + N \rightarrow \ell' + N' + X$  reaction give that even for a momentum distribution with large momenta i.e.

$$\int n(k) \theta(k - 0.3 \text{ GeV}/c) d^3k \sim 0.5,$$

where  $n(k)$  is the single nucleon distribution in momentum space, the number of backward protons is small:  $\langle n_p \rangle < 10^{-4}$ , i.e. the models [44, 46] cannot explain even the order of magnitude of observed cross section (fig. 6.4). On the contrary if one would assume that fast backward nucleon originates from the secondary hadron interactions the existence of  $\langle x \rangle_\alpha - \alpha$  correlations could hardly be explained.

In conclusion, we have demonstrated in this section that inclusive and semi-inclusive high energy deep-inelastic reactions provide a new effective tool of investigating the existence of few nucleon correlations (FNC) in nuclei.

## 7. Production of fast backward particles in hadron(nucleus)–nucleus collisions

### 7.1. Standard picture of hA scattering

The interaction of high-energy hadrons with nuclei is not well understood so far. However it is widely realized that the basic observed features of particle production in high-energy hA scattering can be quantitatively described within the framework of a geometrical picture which is often referred to as “standard picture” [168] by experimentalists. This space-time picture of hA interaction is incorporated in a wide class of theoretical models such as the conventional Glauber-type models, generalized by

Gribov [120] to account for multiparticle production (see, e.g. ref. [121]) or the Gottfried energy flux model [169], etc.

According to the standard picture, the incident hadron interacts *incoherently* with  $\nu$  nucleons of the target, which are aligned at the projectile impact parameter and knocks them out. The number  $\nu$  can be treated as the average number of nucleons in the tube of cross section  $\sim \sigma_{\text{in}}^{\text{hN}}$ . Therefore the average  $\bar{\nu}$  value can be estimated as

$$\bar{\nu} = A\sigma_{\text{in}}^{\text{hN}}/\sigma_{\text{in}}^{\text{hA}}. \quad (7.1)$$

In this picture it is assumed that fast secondary hadrons produced in the interaction are formed outside of the nucleus and do not increase significantly the number of “wounded” nucleons.

Firstly we shall examine the basic consequences of this geometrical picture for the production of fast backward nucleons using the conventional Glauber model of high energy scattering. Then, we shall apply the reggeon calculus to derive more general expressions for inclusive hadron (nucleus)–nucleus collisions. The total inelastic cross section in the Glauber model is given by [170]:

$$\sigma_{\text{in}}^{\text{hA}} = \int d^2 b [1 - (1 - \sigma_{\text{in}}^{\text{hN}} T(\mathbf{b}))^A] = \sum_{n=1}^A \frac{(-1)^{n+1} A!}{(A-n)! n!} \int d^2 b [\sigma_{\text{in}}^{\text{hN}} T(\mathbf{b})]^n \quad (7.2)$$

where  $T(\mathbf{b})$  is the usual thickness function, which is equal in the optical limit to  $\int_{-\infty}^{\infty} dz \rho_A(\mathbf{b}, z)$ . (Note that in eq. (7.2) correlations in the nuclear WF are neglected.) Eq. (7.2) can be rewritten as a sum of positive cross sections [171]

$$\sigma_{\text{in}}^{\text{hA}} = \sum_{n=1}^A \sigma_n, \quad \sigma_n = \frac{A!}{(A-n)! n!} \int d^2 b [\sigma_{\text{in}}^{\text{hN}} T(\mathbf{b})]^n [1 - \sigma_{\text{in}}^{\text{hN}} T(\mathbf{b})]^{A-n} \quad (7.2a)$$

where  $\sigma_n$  denotes the cross section of the physical process in which  $n$  nucleons have been involved in inelastic interactions with the projectile. Then the average number of interactions  $\bar{\nu}$  may be expressed as

$$\begin{aligned} \bar{\nu} &= \sum_{n=1}^A n \sigma_n / \sum_{n=1}^A \sigma_n = \frac{\sigma_{\text{in}}^{\text{hN}}}{\sigma_{\text{in}}^{\text{hA}}} \int d^2 b \sum_{n=1}^A \frac{A!}{(A-n)! (n-1)!} (T(\mathbf{b}) \sigma_{\text{in}}^{\text{hN}})^n (1 - T(\mathbf{b}) \sigma_{\text{in}}^{\text{hN}})^{A-n} \\ &= \frac{\sigma_{\text{in}}^{\text{hN}}}{\sigma_{\text{in}}^{\text{hA}}} \int d^2 b A T(\mathbf{b}) = \frac{A \sigma_{\text{in}}^{\text{hN}}}{\sigma_{\text{in}}^{\text{hA}}}, \end{aligned} \quad (7.3)$$

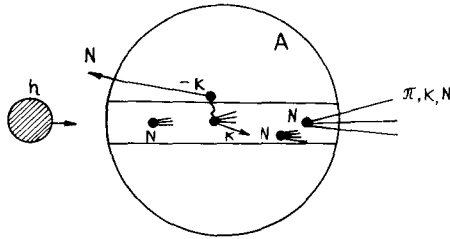
which coincides with the naive estimate (7.1).

## 7.2. Production of fast backward nucleons. The spectator mechanism

Now we can use eq. (7.3) to calculate the cross section of the reaction



As above, we denote a particle as FB (fast backward) if it is produced in the nucleus fragmentation

Fig. 7.1. Production of fast backward spectators in  $hA$  collision.

region forbidden for scattering from a free nucleon. This kinematic region has a simple form in terms of  $\alpha_b/A$  the light-cone fraction of nucleus momentum carried by particle “b” (cf. sections 2.1, 2.2):  $\alpha_b > 1$ .  $\alpha_b$  can be simply expressed through the momentum of particle “b” in the nucleus rest frame as

$$\alpha_b = (\sqrt{m_b^2 + \mathbf{p}_b^2} - |\mathbf{p}_b \cdot \mathbf{p}_h|)/|\mathbf{p}_h| > 1.$$

In the case of nucleon production, we impose also the condition  $p_N > 0.3 \text{ GeV}/c$ , to avoid any significant contribution of nucleon evaporation. To simplify the presentation, we shall use, for a while the two-nucleon (pair) correlation approximation for the nuclear WF (see section 2.4).

At large incident energy, the average energy transfer to each of the  $\nu$  inelastically interacting nucleons is of the order 0.5 GeV (the same as in the elementary  $hN$  inelastic interaction). Similar to the deuteron case this energy is sufficient to destroy all pair correlations associated with any of  $\nu$  nucleons, i.e. the incident hadron  $h$  going through the nucleus knocks out nucleons moving forward (in the nucleus rest frame) releasing backward moving nucleons of the pair correlations (see fig. 7.1). Similarly to the case of deuteron stripping it is natural to call this process a spectator mechanism [45]. In the approximation of the pair correlation matrix the probability to find a nucleon with momentum  $p_N(\alpha, p_\perp)$ , correlated with a given nucleon is equal to  $(1/A)\rho_A^N(\alpha, p_\perp)$ . (Cf. eq. (2.38). Recall that  $\rho_A^N(\alpha, p_\perp)$  is the single nucleon density of the nucleus in the momentum space.) Therefore using eq. (7.3) we obtain [71, 72]<sup>†</sup>

$$G_{hA}^{A/N}(\alpha, p_\perp) = \sum_{n=1}^A \frac{1}{A} \rho_A^N(\alpha, p_\perp) n \sigma_n = \sigma_{in}^{hN} \rho_A^N(\alpha, p_\perp) \quad (7.5)$$

since the nucleon can be emitted in each of the  $n$  collisions.

Eq. (7.5) is quite similar to the impulse approximation. This is so because we neglected in the derivation that the spectator could have had the same impact parameter as the projectile and, thus, would lose its  $\alpha$  due to inelastic interactions with the incoming hadron. Taking into account this possibility, we are lead, similarly, to the deuteron case (section 2.5), to the Glauber screening factor  $\kappa_h$  in eq. (7.5)

$$G_{hA}^{A/N}(\alpha, p_\perp) = \kappa_h A \sigma_{in}^{hN} \rho_A^N(\alpha, p_\perp). \quad (7.6)$$

The inclusion of  $j$ -nucleon correlations with  $j > 2$  may modify eq. (7.6). In this case,  $\kappa_h$  will depend on  $\alpha$ , as the efficiencies of breaking 2- and 3-nucleon correlations are somewhat different (cf. eq. (7.10)).

<sup>†</sup>  $G_{a+b}^{b+c}(x, p_\perp) \equiv x d\sigma^{a+b \rightarrow c+X}/dx d^2p_\perp$  is the inclusive cross section of the reaction  $a + b \rightarrow c + X$ .

Consequently, in a wide region,  $G_h^{A/N}(\alpha, p_\perp)$  is proportional to  $\rho_A^N(\alpha, p_\perp)$  and therefore measurement of  $G_h^{A/N}$  provides a direct information about the nuclear WF.

We explained in section 2.5 that  $\alpha, p_\perp$  dependence of  $\rho_A^N$  varies slowly with  $A$ . Thus, it follows from eq. (7.6) that  $G_h^{A/N}(\alpha, p_\perp)$  should universally depend on  $A, \alpha, p_\perp$  for different projectiles. In particular the following universal relationship is valid

$$G_{h_1}^{A_1/N}(\alpha, p_\perp)/G_{h_2}^{A_1/N}(\alpha, p_\perp) = G_{h_1}^{A_2/N}(\alpha, p_\perp)/G_{h_2}^{A_2/N}(\alpha, p_\perp). \quad (7.7)$$

One should not be confused by the resemblance of the form (7.5) with the impulse approximation. It reflects merely the inclusive nature of the reaction (7.4): not one but several target nucleons participate in the collision and are knocked forward in each hA collision. To illustrate this point, we calculate  $G_h^{A/(N_1+N_2)}$  – inclusive cross section for production of two FB nucleons which is equal zero in the impulse approximation, provided only scattering from pair correlations is taken into account. Using eq. (7.2a) we have

$$\begin{aligned} G_h^{A/(N_1+N_2)}(\alpha_i, p_{i\perp}) &= \frac{1}{A^2} \sum_{n=1}^A n(n-1) \rho_A^N(\alpha_1, p_{1\perp}) \rho_A^N(\alpha_2, p_{2\perp}) \\ &\times \int \frac{A!}{(A-n)! n!} (\sigma_{in}^{hN} T(b))^n (1 - \sigma_{in}^{hN} T(b))^{A-n} d^2 b \\ &= (1 - A^{-1}) \rho_A^N(\alpha_1, p_{1\perp}) \rho_A^N(\alpha_2, p_{2\perp}) (\sigma_{in}^{hN})^2 \int (T^2(b)) d^2 b. \end{aligned} \quad (7.8)$$

From eq. (7.5) and eq. (7.8)

$$G_h^{A/(N_1+N_2)}(\alpha_i, p_{i\perp}) = (1 - A^{-1}) G_h^{A/N_1}(\alpha_1, p_{1\perp}) G_h^{A/N_2}(\alpha_2, p_{2\perp}) \int T^2(b) d^2 b \quad (7.9)$$

which is valid as well if Glauber screening is taken into account in the destruction of the pair correlation.

A similar expression can be obtained easily for the reaction  $h + A \rightarrow kN + X$ . However with increasing  $k$  the contribution of the terms with  $n \gg \nu$  becomes essential. Evidently, in this case the assumption of an uncorrelated nuclear WF used to calculate the number of “active” nucleons with the same impact parameter becomes doubtful.

To derive eq. (7.5) in a more general approach and to calculate  $\kappa_h$ , we apply the conventional Gribov–Glauber model of hadron–nucleus scattering without enhanced reggeon diagrams. This theory is known to be reliable in a wide energy range up to 200–400 GeV (see e.g. ref. [121]). If the interaction of secondary particles with the nucleus is neglected, the set of reggeon diagrams can be rearranged in terms of hN amplitudes [121]. The resulting expansion is equivalent to the Glauber series for the total cross section. Supplemented by the Abramovsky, Gribov and Kancheli (AGK) cutting rules [122] these reggeon diagrams (fig. 7.2) can be used for calculation of the inclusive cross sections. In the pair correlation approximation, similar to the case of deuteron fragmentation, only the reggeon diagrams in figs. 7.4, 7.5 are responsible for screening and antiscreening of the impulse approximation diagram 7.3. The contribution of all other diagrams where  $h$  interacts with nucleons  $3, \dots, A$ , which do not belong to the pair correlation is cancelled. The simplest example of the AGK cancellation is the absorptive

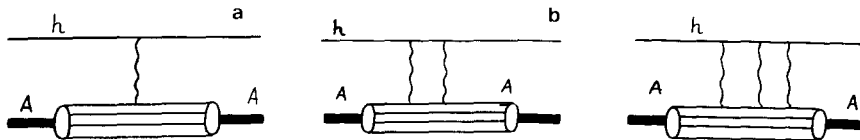


Fig. 7.2.

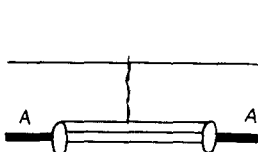


Fig. 7.3.

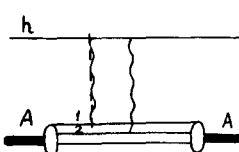


Fig. 7.4.

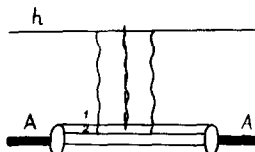


Fig. 7.5.

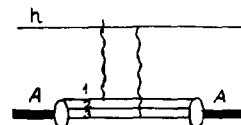


Fig. 7.6.

correction (fig. 7.6) to the impulse approximation due to elastic scattering of  $h$  from nucleon "3" which is compensated by the contribution of the diagram 7.7, where  $h$  inelastically interacts with nucleon "3".

As a result in the pair correlation approximation  $\kappa_h^A \approx \kappa_h^D$ , because the WFs of the deuteron and of the pair correlation are roughly proportional.

Since the hadron  $h$  can knock out several nucleons of the correlation (cf. eq. (7.3)) which are at the same impact parameter it effectively destroys  $j$ -nucleon correlation for not too large  $j$ . Therefore one could expect that  $\kappa_h^j \sim \kappa_h^2$ . In any case  $\kappa_h^j$  does not increase faster than the inelastic cross section of the scattering on  $j - 1$  balancing nucleons

$$\kappa_h^{(j)} \sim \sigma_{in}^{h+(j-1)N} / \sigma_{in}^{hN} \simeq (j-1)^{2/3} \kappa_h^{(2)}. \quad (7.10)$$

Using the expansion of  $\rho_A^N(\alpha, p_\perp)$  over few nucleon correlations (FNC) (see eq. (2.38)) the cross section  $G_h^{A/p}$  can be rewritten in the form

$$G_h^{A/p}(\alpha, p_\perp) = \sum_{j=2}^A A a_j \kappa_h^{(j)} \rho_j(\alpha, p_\perp). \quad (7.11)$$

Since the factor  $\kappa_h^{(j)}$  does not depend on  $A$ , the Glauber screening leads mainly to a multiplicative renormalization of  $a_j$ .

*The incident energy dependence of  $G_h^{A/h}$ :* In section 3.5 we explained that the energy dependence of reaction  $D + h \rightarrow p + X$  can be treated in the first approximation (cf. fig. 2.5) as:

$$G_h^{D/N}(\alpha, p_\perp) = \kappa_h \rho_D^N(\alpha, p_\perp) \sigma_{in}^{hN} \theta(\alpha_{max}(E_h, p_\perp) - \alpha), \quad (7.12)$$

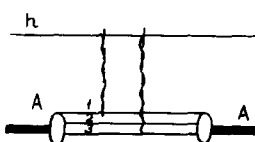


Fig. 7.7.

i.e. the momentum distribution in the deuteron rest frame depends weakly on  $E_h$  except near the phase-space boundary.

In the case of nuclei with large  $A$  the scaling onset is more complicated due to increase of essential longitudinal distances with  $E_h$ . Indeed, we assumed above that the longitudinal size of  $h$ , which is proportional to  $E_h$  [79], is larger than the nuclei diameter  $D_A$ :

$$E_h/m_{\text{strong}}^2 > D_A. \quad (7.13)$$

We also assumed that  $E_h$  is high enough that the energy transfer to each of  $\nu$  nucleons is sufficient to destroy correlations associated with these nucleons:

$$E_h/\nu > E_0(\alpha). \quad (7.14)$$

$E_0(\alpha)$  increases with  $\alpha$ . In the two-nucleon correlation approximation  $E_0(\alpha)$  can be estimated using eq. (7.12) from the condition  $\alpha_{\max}^{(2)}(E_0, p_\perp) = \alpha$ . Since at low incident energies the projectile dissipates a large fraction of its energy in the first inelastic collision, practically no FB particles can be produced in subsequent collisions. Thus at low energies one probes in reaction (7.4) the nuclear surface only, not the whole nuclear volume [71, 72, 172]. As a result the factor  $\sum_{n=1}^A n\sigma_n = A\sigma_{\text{in}}^{\text{hN}}$  in eq. (7.5) has to be substituted in the low-energy limit by the factor  $\sum_{n=1}^A \sigma_n = \sigma_{\text{in}}^{\text{hA}}$ , leading to a change of  $A$ -dependence of  $G_h^{\text{AN}}$  by a factor  $\nu_{\text{eff}} \sim A^{1/3}$ .†

To estimate roughly  $G_h^{\text{AN}}$  at low energies ( $\sim 1$  GeV) it is reasonable to assume that the scaling onset for the scattering from  $j$ -nucleon correlation is similar to eq. (7.13). Then in first approximation:

$$G_h^{\text{AN}}(E_n, \alpha, p_\perp) = \sigma_{\text{in}}^{\text{hA}} \sum_{j=2}^A \kappa_j a_j^{\text{A}} \rho_j^{\text{N}}(\alpha, p_\perp) \theta(\alpha_{\max}^{(j)}(E_n, p_\perp) - \alpha). \quad (7.15)$$

Formally eq. (7.15) leads to some breaks at  $\alpha = \alpha_{\max}^j$  (see solid line in fig. 8.6 below). However near  $\alpha \sim \alpha_{\max}^j$  contribution of  $j$ -nucleon correlation should decrease faster due to suppression from final state phase-space.‡ At the same time due to the Fermi motion of the  $j$ -nucleon correlation it should give some contribution for  $\alpha > \alpha_{\max}^j$ . These effects would smooth down the theoretical curve (see dotted line in fig. 8.10). Note also that  $\kappa_j$  for large  $j$  is considerably smaller at low energies, where the projectile cannot effectively destroy the many-body correlations.

Due to phase-space restrictions the contribution of two-, three-nucleon correlations into FB nucleon production is strongly suppressed at low energies (see e.g. fig. 7.8). Thus the correlations of a larger number of nucleons determine the magnitude of  $G_h^{\text{AN}}$  in a kinematical region, where at higher energies two-nucleon correlation gives predominant contribution.

In conclusion, the energy dependence of  $G_h^{\text{AN}}$  is determined by two factors: (1) growing role of two, three-nucleon contributions due to increase of available phase-space, (2) increase of  $\nu_{\text{eff}}$  with  $E_h$  from  $\nu_{\text{eff}} = 1$  to  $\nu_{\text{eff}} \sim A^{1/3}$ .

The possible role of the nuclear cascade and final state interaction will be considered below in sections 7.4 and 7.5.

† Actually due to the secondary hadron interaction  $\nu_{\text{eff}}$  is larger than according to the Glauber model (section 7.4).

‡ Remind that in the average  $j$ -nucleon correlation the mass of  $j-1$  balancing nucleons is rather large. Thus, it is difficult to push such configuration on the energy shell at small energies where the final state phase space is restricted. This could lead to a modification of  $j$ -nucleon correlation contribution over the entire  $\alpha$ -range.

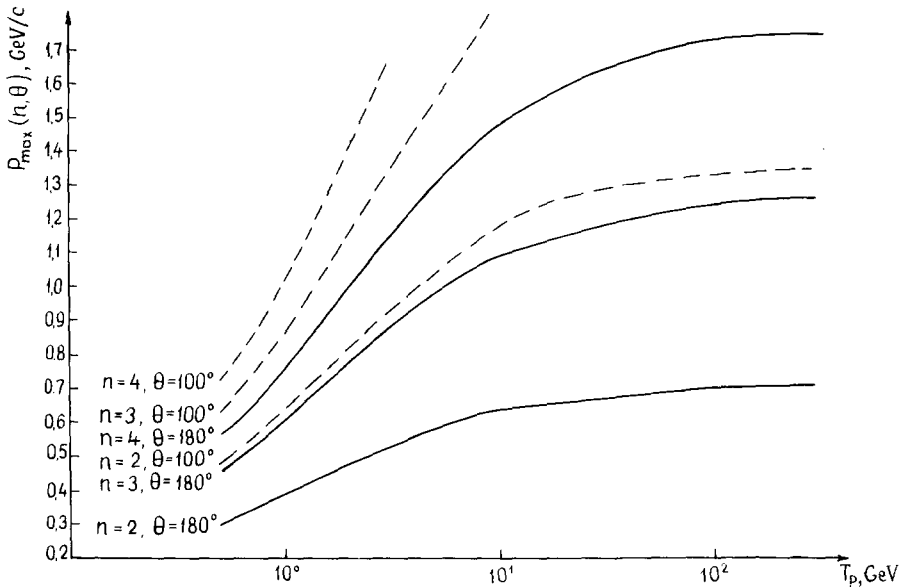


Fig. 7.8. The kinematical boundaries of 2-, 3-, 4-nucleon correlations in the  $p + A \rightarrow p + X$  reaction versus the incident energy.

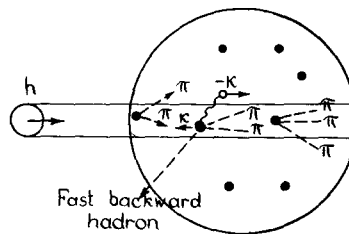


Fig. 7.9. Production of fast backward pions in the  $hA$  collision.

### 7.3. Production of fast backward particles. Direct mechanism

A natural mechanism for production of FB particles, which are absent in the nuclear WF ( $\pi, K, \Lambda, \dots$ ), in the reaction



is the scattering of the incident hadron  $h$  from a fast backward nucleon (see fig. 7.9). We shall refer to this mechanism, which was suggested in many works [1, 11, 12, 45, 46] as the direct mechanism.

Within the framework of the Gribov-Glauber model at sufficiently high energy the impulse approximation is valid for inclusive production of particles in nucleus fragmentation region (see e.g. ref. [121]). This can be understood semiquantitatively using argumentation of previous subsection (eq. (7.5)). Namely, if the incident energy is high enough, the probability of emission of the particle “ $b$ ” in each of  $\nu$  collisions is independent of  $E_h$  due to the Feynman scaling and equals  $G_h^{N/b}(x_b, p_\perp)$ . Therefore in the fixed nucleon approximation (which is reasonable only at  $0 < x_b < 1$ ) we obtain

$$G_h^{A/b}(x_b, p_\perp) = (\text{probability of inelastic hA interaction}) \times (\text{number of hN interactions}) \times (\text{probability of emission of b in one elementary interaction}) = \sigma_{\text{inel}}^{\text{hA}} \cdot \nu \cdot G_h^{\text{N}/b}(x, p_\perp) / \sigma_{\text{inel}}^{\text{hN}} = A G_h^{\text{N}/b}(x_b, p_\perp). \quad (7.17)$$

Using a more consistent reggeon field theory technique, which fully accounts for unitarity [98] it is easy to prove that the observed cancellation of Glauber screening correction follows just from AGK combinatorics and does not depend on momenta of the interacting nucleons. As a result  $G_h^{A/b}$  is equal to the convolution of the single nucleon density  $\rho_A^{\text{p,n}}(\alpha, k_\perp)$  and  $G_h^{\text{N}/b}(x, p)$  (see eq. (2.18) and section 2.5, where reaction  $\text{h} + \text{D} \rightarrow \text{b} + \text{X}$  is considered) [71]<sup>†</sup>:

$$G_h^{A/b}(\alpha, p_\perp) = \sum_{N=p,n} \int \rho_A^N(x, k_\perp) G_h^{\text{N}/b}\left(\alpha/x, p_\perp - \frac{\alpha}{x} k_\perp\right) \frac{dx}{x} d^2 k_\perp. \quad (7.18)$$

As in the case of nucleon production, expressions for more complicated processes such as double inclusive reaction  $\text{h} + \text{A} \rightarrow \text{b}_1 + \text{b}_2 + \text{X}$  ( $\text{b}_{1,2} = \pi, \text{p}, \text{K}; \alpha_{\text{b}_i} > 1$ ) have no resemblance with the impulse approximation. They are described by eq. (7.9) after the substitution  $N_i \rightarrow b_i$ .

*Energy dependence of  $G_h^{A/b}$ :* Just as in the case of the spectator mechanism sufficiently high energies are necessary for the validity of eq. (7.18)

$$E_h/\nu > E_0(\alpha). \quad (7.19)$$

Here  $E_0(\alpha)$  is the minimal incident energy at which an approximate Feynman scaling in the elementary reaction can be used to estimate  $G_h^{\text{N}/b}(\alpha, k_\perp)$ . Evidently in this case  $E(\alpha)$  is considerably larger than in the case of nucleon production because higher energies are necessary to produce particle “b” with large  $\alpha$  (e.g. in reaction  $\text{p} + \text{p} \rightarrow \pi^+ + \text{X}$ ,  $\alpha_{\text{max}}(E_p) = 0.73$ ). Thus at  $E_h$  less than several GeV the scattering from back of the nuclear surface will be predominant. As a result  $\nu_{\text{eff}} \approx 1$  in this region.

Another complication which has to be taken into account at the intermediate energies is the recoil of residual nucleons involved in the correlation. Similar to the case of deep inelastic scattering (eq. (5.2)) the cross section can be estimated using the light cone spectral function  $\tilde{\rho}_A^N(\alpha, k_\perp, M_{\text{Rec}}^2)$  defined in section 5.2 and/or using its decomposition over FNC:

$$G_h^{A/b}(\nu_h, \alpha, k_\perp) = \frac{\sigma_{\text{in}}^{\text{hA}}}{\sigma_{\text{in}}^{\text{hN}} A} \sum_{N=p,n} \int \tilde{\rho}_A^N(x, p_\perp, M_{\text{Rec}}^2) G_h^{\text{N}/b}\left(\tilde{\nu}, \frac{\alpha}{x}, k_\perp - \frac{\alpha}{x} p_\perp\right) \frac{dx}{x} d^2 p_\perp, \\ \nu_h = (p_h p_A), \quad \tilde{\nu} = (\nu_h + M_A^2 - M_X^2)\alpha/A. \quad (7.20)$$

*Contribution of direct mechanism to  $G_h^{A/N}$ :* Direct mechanism can give some contribution to  $G_h^{A/N}$  via diffractive processes (eq. (7.18)) and/or the elastic hN scattering:

$$G_{h(\text{el})}^{A/N}(\alpha, p_\perp) = \int \rho_A^N(\alpha, k_\perp - p_\perp) \frac{1}{\pi} \frac{d\sigma_{\text{el}}^{\text{hN}}}{dt}(k_\perp^2) d^2 k_\perp. \quad (7.21)$$

<sup>†</sup> Equations similar to eq. (7.18) were applied by Blankenbecler and Schmidt [46] for description of the proton yield at  $T_N \sim (1-2)$  GeV while Amado, Woloshyn and Frankel [44, 59] used an equation similar to eq. (7.21) to describe the data at  $T_N = 0.6-0.8$  GeV. Both these groups assumed that impulse approximation is applicable at these low energies.

In the case of N production in the essential integration region of eq. (7.19) and especially of eq. (2.21) main contribution is given by subprocesses with small energy transfer. Such a contribution is suppressed due to the final state interaction [53, 71b] (see section 7.4.1). Similar to the deuteron case (section 3.5) the contribution of the direct mechanism into  $G_h^{A/N}$  is roughly proportional to  $\rho_A^N(\alpha, p_\perp)$ . Thus, (cf. eq. (3.41)) all uncertainties can be included into renormalization of the factor  $\kappa_h$ :

$$\kappa_h \rightarrow (1.4 \pm 0.2)\kappa_h . \quad (7.22)$$

## 7.4. Final state interaction

### 7.4.1. Destruction of the average field configuration

In this review we have argued that in the FNC approximation the spectrum of FB particles is determined by  $\rho_A^N$  provided a sufficient energy is transferred locally to the correlated nucleons.

If this condition is not fulfilled, the spectrum is strongly reduced due to final state interaction. To be definite we consider destruction of the average field configuration  $p_1 = k$ ,  $p_{2,\dots,A} \sim -k/(A-1)$  (see fig. 7.10) in the photoabsorption reaction, where photon knocks out one of the nucleons with momentum  $|p_2| \sim |k/(A-1)| \ll k$ . Following ref. [71b], we demonstrate that the FB proton yield decreases with  $k$  faster than  $n(k)$ -single nucleon density matrix. (Analysis of the similar suppression in a reaction, where projectile knocks out fast nucleon via elastic photon scattering off this nucleon can be found in refs. [53, 156].)

Due to photon interaction with nucleon 2 the residual nucleus obtains small additional energy

$$\Delta E \approx -U(r_2) \approx p_2^2/2m + \varepsilon ,$$

where  $\varepsilon$  is the nucleon binding energy. Thus the WF of the  $A-1$  nucleon system  $-\psi_{A-1}$  is described by the Schrödinger equation

$$H_{A-1}\psi \approx (M_A - m_N - U(r_2))\psi_{A-1} \approx \left( M_A - m_N + \varepsilon + \frac{k^2/(A-1)^2}{2m} \right) \psi_{A-1} . \quad (7.23)$$

It follows from eq. (7.23) that due to the energy conservation law the nucleon 1 with large momentum  $k$  cannot be produced in nuclear break up. Thus the final state interaction would reduce the momentum of nucleon 1, suppressing the contribution arising from the discussed reaction mechanism. Meanwhile if the photon inelastically scatters from the forward going nucleon in the pair correlation then  $U(r_2)$  is large. Consequently the energy transfer to the nucleus will be large and therefore final state interaction will be inessential in a wide momentum range.

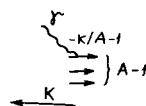


Fig. 7.10.

#### 7.4.2. Production of fast backward light nuclei

The next example of the role of the final state interaction is the production of FB light nuclei D, ... In a typical collision a fast projectile practically instantaneously destroys several FNCs arranged at the projectile impact parameter. Then FB nucleons from different FNCs may form light nuclei in the nuclear field near the surface. The estimate of the overlapping integral can be made in the following way due to Butler and Pearson [173]. The cross section for production of FB light nucleus B (D, T ...) has a simple form for  $p_B > B p_F$ ,  $p_\perp \approx 0$ , if the angular anisotropy of the nucleon spectrum can be neglected [72]:

$$G_h^{A/B}(p) = \xi_B [G^{A/p}(p/B)]^{Z_B} [G^{A/n}(p/B)]^{N_B} (\sigma_{in}^{hN} A p^2 / (B^2 p_F^2))^{-B+1} \quad (7.24)$$

where  $Z_B$ ,  $N_B$  are number of protons and neutrons in B. The factor  $\xi_B (p/(B p_F))^{-2B+2}$  is due to the overlap integral of  $B$  fast backward nucleons with the WF of the nucleus B. Eq. (7.24) leads to much faster  $A$ -increase of  $G_h^{A/B}$  than that suggested by Butler and Pearson since in Glauber approach produced nucleons have close impact parameters, although in [173] it was assumed that nucleons are produced in the whole volume of the nucleus.

#### 7.4.3. Problem of fast backward nucleon absorption

We explained above that suppression due to the final state interaction within the FNC is not large provided sufficiently large energy is transferred to FNC. However for large  $A$  the FB nucleons can interact with the nucleons which do not belong to the destroyed correlation. At present, no consistent treatment of this problem exists. The standard estimates based on the mean free path overestimate attenuation (1) because of the inclusive nature of the reaction rescattered nucleons can contribute to the yield, i.e. the transport NN cross section but not  $\sigma_{tot}^{NN}$  is essential here, (2) destruction of the nucleus by the incident hadron was not taken into account, (3) the Fermi motion of the target nucleons leads to some suppression of the effective cross section for the interaction of secondary particles due to their wave origin [174], (4) QCD analysis of section 4 indicates that FB nucleons are produced in the compressed state which would lead to some suppression of their secondary interactions. Similar trend was observed in the phenomenological analyses of a number of intermediate-energy phenomena (for recent discussion see [175]).

Thus in the following analysis we shall neglect absorption of FB protons though this approximation may be bad for medium and heavy nuclei.

#### 7.4.4. Effects of cascades in particle production

In recent years large amount of data has been accumulated on the multiparticle production from nuclei (for recent review see [176, 177]).

They are consistent with the expectations of the parton and multiperipheral models [178] according to which fast secondary particles don't participate in the secondary interactions. The recent analyses of the data seem to indicate that most of cascade interactions correspond to the energies of the order 1–5 GeV [176, 177].

Thus in the case of FB nucleon production secondary interactions (mostly of  $\pi$ -,  $\rho$ -mesons) will mainly change  $A$ -dependence of  $G_h^{A/N}$  but not the momentum dependence, since experimentally the shape of  $G_h^{A/N}$  is practically energy independent at  $E_\pi \geq 1$  GeV. Therefore these secondary interactions can be roughly taken into account by introducing the additional factor  $\lambda_A$  in eq. (7.6). The final expression for  $G_h^{A/N}$  is then

$$G_h^{A/N}(\alpha, k_\perp) = \lambda_A \kappa_h \rho_A^N(\alpha, k_\perp) \sigma_{in}^{hN}. \quad (7.25)$$

Since the destruction of FNC by secondary particles occurs mostly on the impact parameters close to the projectile impact parameter, the secondary interactions could increase the effective number of wounded nucleons by the factor  $\lambda_A \sim A^{1/3}$ . For example, an estimate within the framework of the two-component parton cascade model leads to  $\lambda_A \sim A^{0.2}$  [188].

For FB  $\pi, K$  production the effects of secondary cascades should be smaller because the contribution from the scattering of low energy particles ( $E \lesssim 2$  GeV) is suppressed due to the kinematical boundaries. Thus,  $1 \leq \lambda^K \leq \lambda'' < \lambda^P$ . Actual value of  $\lambda'', \lambda^K$  and their  $\alpha, p_\perp$  dependence are rather sensitive to the rate of cascading for secondary particles at intermediate energies ( $\sim 5$  GeV) which is practically unknown now.

For heavy nuclei slow secondary pion absorption by quasi-deuteron pairs due to the reaction  $\pi^+ + (pn) \rightarrow p + p$  could be an essential source of FB nucleons [28]. Some suppression of this mechanism as compared to cascade approach [28], occurs due to the wave nature of slow secondary particles. It reduces the interaction of produced light (heavy) particle with momentum  $k \leq k_F$  by a factor  $\sim k^2/p_F^2 (\sim k/p_F)$  [174]. Here  $p_F$  is the average momentum of the nucleon in the nucleus. On the whole, the comparison of the yields of the different BF particles from heavy nuclei could become an effective method of studying the space-time evolution of strong interaction and the time of secondary hadron formation (see also the discussion in the end of section 8.3).

### 7.5. Production of fast backward particles in nucleus–nucleus collisions [180]

The AGK technique used above for the hA reactions can be applied also to calculate the cross section of FB particle production in nucleus–nucleus collisions. As in the above discussion of the direct mechanism, where properties of hadron h were inessential, we can apply eq. (7.18) for the description of  $G_B^{A/\pi, K}$  having done the substitution  $h \rightarrow B$ . For the process  $A + D \rightarrow \pi + X$ , the absence of Glauber screening was first derived by Bertocchi and Treliani within the eikonal model [42].

Since the region  $x/\alpha \geq 0.8$  gives a predominant contribution in eq. (7.18), the  $B$  dependence of  $G_B^{A/b}$  and  $G_B^{N/b}$  at  $x_b > 0.8$  should be approximately the same.

It is straightforward to demonstrate for the spectator mechanism that only those diagrams are essential, which describe the interaction between the nucleons belonging to the FNC and the nucleus B. Thus,  $\kappa_B$  does not depend on  $A$ , therefore eq. (7.6) and the universality relationship (7.7) are valid for nucleus–nucleus collisions also. To estimate  $\kappa_B$  one can note that if the two-(three) nucleon configuration occurs at a small impact parameter of the nucleus B no spectators would be produced. Thus  $\kappa_B$  is proportional, in first approximation to the probability of peripheral interaction of FNC with B, where a spectator nucleon of the correlation does not participate in inelastic collisions. The probability of such a collision can be estimated within the Glauber model as (this is a more accurate estimate than that of [180]):

$$\kappa_B \sigma_{in}^{NB} = \kappa_N \int [1 - \sigma_{in}^{NN} T(b)]^{A-1} [1 - (1 - \sigma_{in}^{NN} T(b))^A] d^2 b. \quad (7.26)$$

Eq. (7.26) for  $\kappa_B$  is meaningful only for large  $\alpha$  and small  $p_\perp$  when elastic rescattering of the FB nucleon from the nucleus B can be neglected (the case of large  $p_\perp$  is discussed in ref. [70]) since for large nuclei B the thickness of the edge is approximately constant, then  $\kappa_B \sigma_{in}^{NB} \sim B^{1/3}$  (see fig. 8.9b).

At sufficiently high energies and large  $\alpha$  eq. (7.26) could underestimate the  $B$  dependence of  $G_B^{A/N}(\alpha)$  because of the QCD compression of FB nucleons (section 4.2).

Owing to time dilatation the FB nucleon would fly through the nucleus B in the compressed state interacting weakly with B. As a result, not the edge of nucleus but the entire volume will contribute to FB nucleon yield resulting in the faster  $B$  dependence of  $G_B^{A/N}$ .

At energies  $E_B/B \geq 10$  GeV when  $G_B^{N/N} \sim B^\gamma$  for  $\gamma \sim 0.5$  (while  $\gamma \sim 0.3$  at lower energies) contribution of the direct mechanism to the proton yield would be proportional to  $B^\gamma$ , resulting in the similar effect. However this contribution can be subtracted using eq. (7.18). Moreover relative contribution of direct mechanism does not increase with  $\alpha$ . So, unlike the effect of the QCD compression discussed above, the direct mechanism does not lead to increase of  $\gamma_{\text{eff}}$  with  $\alpha$ .

## 8. Production of fast backward particles from nuclei: the basic data and their theoretical interpretation

In this section we review the basic experimental results on the production of the fast backward (FB) particles in the high energy inclusive reactions of the type

$$a + A \rightarrow b + X \quad (a = \gamma, \pi, p, \text{nucleus}; b = p, d, t, \pi), \quad (8.1)$$

and compare them with the predictions of the few nucleon correlation (FNC) model [45, 71, 72, 74] described in section 7. In section 8.6 a brief comparison with the predictions of several alternative approaches is also given.

The most extensive data exist now for the FB nucleon production which we shall discuss first.

### 8.1. Proton production. Scaling limit

From the viewpoint of kinematics the reaction (8.1) and in particular nucleon production is a typical fragmentation process since particle “b” carries large  $\alpha = x$  and low transverse momentum  $p_{\perp}$ .<sup>†</sup> Therefore similar to the case of hadronic collisions the cross section of these reactions should satisfy Feynman scaling – Yang limiting fragmentation, i.e. the inclusive cross section of  $h + A \rightarrow N + X$  reaction  $G_h^{A/N}(p_N)$  should weakly depend on  $E_h$  at sufficiently high projective energies. Experimentally it was found [14–16, 18] that scaling is satisfied at  $E_h \geq \text{few GeV}$ . To simplify the presentation we discuss first the data obtained in the scaling region where all nuclear volume effectively works. Secondly, we discuss the data on proton-nuclear collisions at  $E_p \leq 1$  GeV where only nuclear surface can contribute (section 8.2). In section 8.3 the transitional region between the two limiting cases is considered.

#### 8.1.1. High energies. The momentum dependence of $G_h^{A/P}(p_N)$

Apparently the most important experimental finding is the universality of the FB nucleon spectra i.e. the momentum dependence of  $G_h^{A/P}$  is practically projectile and  $A$ -independent starting from  $A = 4$  in a wide momentum range [13–18]<sup>‡</sup>. As an illustration we present in fig. 8.1 the data [17] on the FB nucleon production at lab angle  $\theta = 180^\circ$ , together with the ratio  $G_N^{\text{Pb}/P}(p_N)/G_N^{\text{He}/P}(p_N)$  divided by the mean value of this ratio. Moreover the shapes of the spectra from  ${}^4\text{He}$  and D are rather similar (fig. 8.2). The detailed data [18] obtained recently at  $E_p = 400$  GeV demonstrate that universality is valid practically in

<sup>†</sup> Here  $\alpha = x$  is conventional Feynman variable (for definition see eq. (7.4)). For nucleons which fly backward in the nucleus lab. frame  $\alpha > 1$ . To suppress contribution of evaporation processes we impose the supplementary condition  $p_N > 0.3$  GeV/c.

<sup>‡</sup> Such universality and early onset of limiting fragmentation for the FB nucleon production were first suggested by Leksin and collaborators [14] in the phenomenological analysis of the pioneer data [2] on the FB proton production from carbon and copper. They called this phenomenon nuclear scaling.

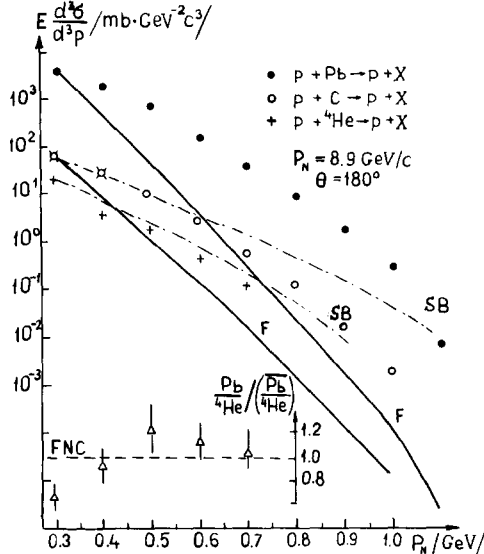


Fig. 8.1. The invariant spectra of the FB nucleons in the  $p + A \rightarrow p + X$  reaction at  $p_\perp = 0$  [17]. To calculate  $\Sigma$  points the data [15] were used. Solid curves are prediction of the Amado-Woloshyn-Frankel model [44, 59] with parameters of WF taken from the recent analysis [24] of the low energy data. The dot-dashed curves are prediction of the Schmidt-Blankenbecler model [46] assuming  $\alpha$ -scaling (if the scaling variable  $x = P_{cm}/P_{cm\max}$  is used the curves would be much steeper (cf. fig. 3.18)). Predictions of both models are normalized at  $P_N = 0.3$  GeV/c. The dashed curve is the prediction of the FNC model.

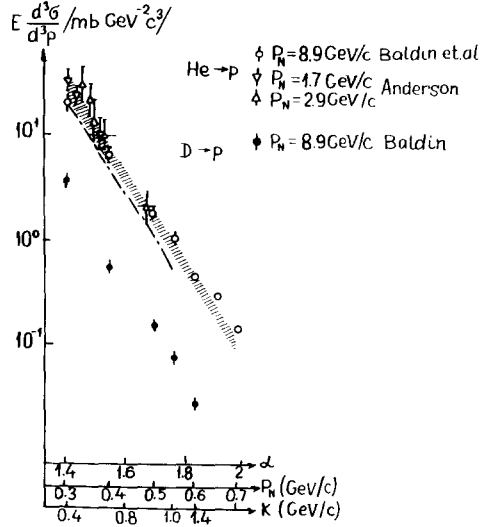


Fig. 8.2. Comparison of the FB nucleon yields from  ${}^4\text{He}$  and D. The experimental points from [13, 20] illustrate preocious limiting fragmentation for  $p + {}^4\text{He} \rightarrow p + X$  reaction. Dot-dashed curve for  ${}^4\text{He}$  is the calculation in the two-nucleon correlation approximation which uses as input  $n(k)$  from [82]. The shaded region is the calculation with inclusion of three-nucleon correlations described in the text.

all backward hemisphere at  $\alpha \geq 1.2$ . For example the ratio

$$R(p_N, T_a, C) = \frac{1}{A_{T_a}} G_p^{T_a/P}(p_N) / \frac{1}{A_c} G_p^{C/P}(p_N)$$

does not change more than by a factor  $\sim 2$  (fig. 8.3) while the cross sections decrease by a factor  $2 \times 10^4$ !

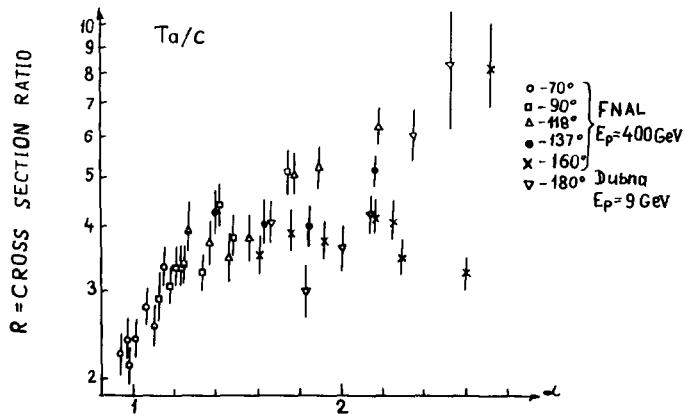


Fig. 8.3. The ratio of the differential cross sections per nucleon for the  $p + A \rightarrow p + X$  reaction ( $A_1 = \text{Ta}$ ,  $A_2 = \text{C}$ ) for different emission angles. The experimental data are from 400 GeV measurement for  $70 \leq \theta \leq 160^\circ$  [18] and 9 GeV measurement for  $\theta = 180^\circ$  [17].

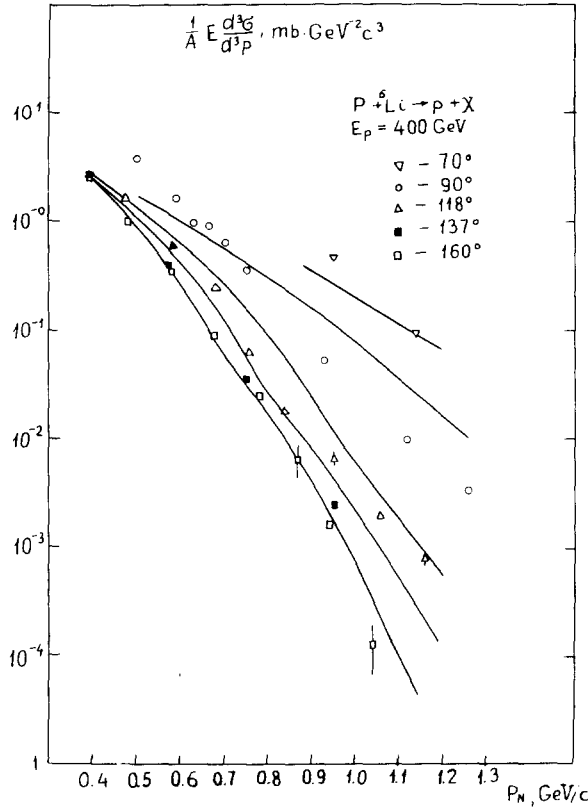


Fig. 8.4.

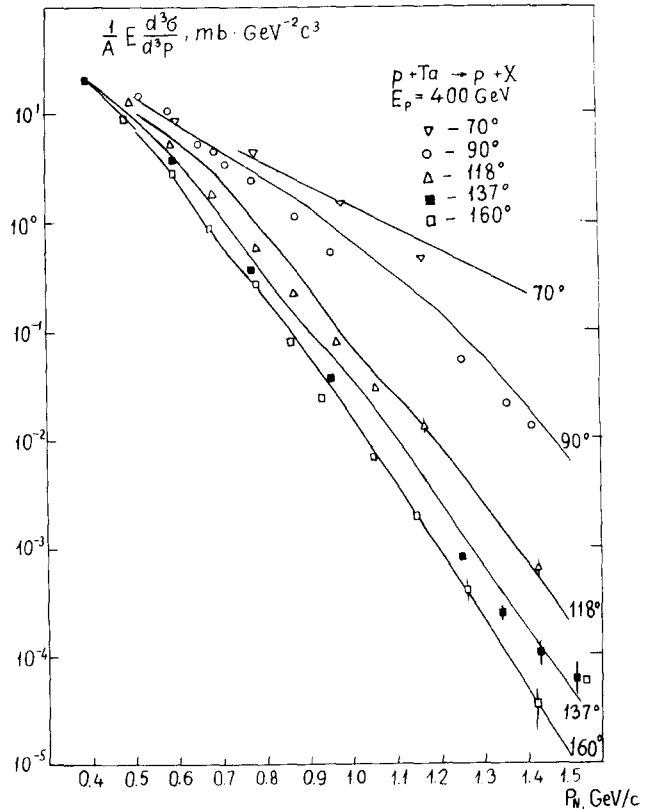


Fig. 8.5.

Figs. 8.4, 8.5. Comparison of the FNC model with the 400 GeV data [18].

(see figs. 8.4, 8.5). (The data [17, 18] indicate some small increase of the ratio  $R(p_N, Ta, C)$  and also  $R(p_N, Ta, {}^6\text{Li})$  in the region  $\alpha \geq 2.2$  though in the region  $1.2 < \alpha < 2.2$  the ratio is constant within experimental accuracy.)

At small nucleon momenta ( $p_N \sim 0.4$  GeV/c)  $G_a^{AN}$  rather weakly depends on the emission angle  $\theta$ , though with increase of  $p_N$  the spectrum becomes strongly anisotropic (figs. 8.4, 8.5).

To compare the data obtained using different targets and projectile it is convenient to fit  $G_a^{AN}(p_N)$  in the form

$$G_a^{AN}(p_N) = C_a \exp\{-T/T_0(\theta)\} \approx C_a \exp\{-B(\theta)p_N^2\}$$

which reasonably describes the data (especially  $\exp(-T/T_0)$  fit) up to  $p_N \sim 1$  GeV/c (as usually  $T$  is kinetic energy of the FB nucleon).

Comparison of the data [21, 15, 16] indicates that the slope parameter  $B(\theta)$  does not depend on  $A$ , on the projectile ( $\gamma$ ,  $\pi$ ,  $p$  and even  $\nu$ ,  $\bar{\nu}$ ) and its energy with accuracy  $< 10\%$  (see, e.g. fig. 8.6).  $B(\theta)$  does not change also if events with fixed number of FB nucleons (2, 3, 4) are selected [181, 182].

There are some indications of irregularities in the momentum shape of  $G_h^{AN}$ : a bump was observed in  $n, \pi^- + C \rightarrow p + X$  reactions at  $p_N = 0.4$  GeV/c ( $p_n = 7$  GeV/c,  $p_{\pi^-} = 4$  GeV/c) and in  $p + D \rightarrow p + X$  reaction at  $p_N = 0.35$  GeV [184] ( $E_N = 1$  GeV); in  $D(p) + Pb \rightarrow p + X$  collisions a minimum was observed at  $150^\circ$  ( $170^\circ$ ) [185] in the angular dependence of  $G_{D(p)}^{Pb/P}(p_N)$  at  $p_N = 0.5$  GeV/c.

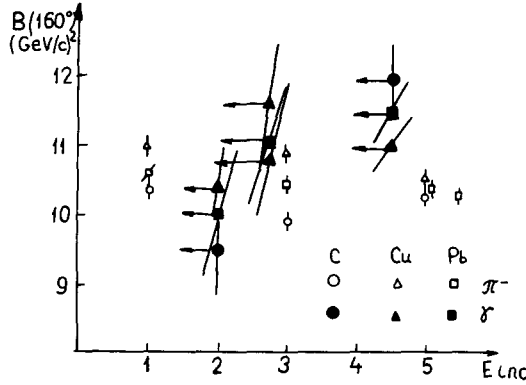


Fig. 8.6. The dependence of the slope parameter  $B$  on the incident energy for different targets [15, 21].

**Theoretical discussion.** According to the few nucleon correlation (FNC) model an incident particle knocks out the forward moving nucleons of the correlations releasing the backward spectators. Therefore similarity of the nucleon spectra from the deuteron and other nuclei (which was actually predicted in [45]) follows from the dominance of the short-range two-nucleon correlations which evidently does not depend on  $A$ . Since FB nucleons mostly originate from the destruction of different FNCs, a selection of events with a fixed number of FB nucleons should not change significantly the shape of nucleon spectra. Universality of the spectra for large  $A$  follows from the similar  $A$ -dependence of two- and three-nucleon correlations (see section 2.4). Since contribution of higher correlations ( $j = 3, 4$ ) is larger in heavy nuclei than in light ones the ratio  $R(p_N, A_1, A_2)$  should slightly increase at  $\alpha \geq 2$  (e.g. eq. (2.40) leads to the factor  $\sim 1.3$  increase in the case  $A_1 = \text{Pb}$ ,  $A_2 = \text{C}$ , which is not inconsistent with the data).

To describe the spectra quantitatively we can use eq. (7.5) according to which  $G_n^{A/P}$  is proportional to the single nucleon density  $\rho_A^N(\alpha, k_\perp)$  and FNC decomposition of  $\rho_A^N(\alpha, k_\perp)$  (section 2.4) combined with the QCD analysis of section 4.

Due to the simple relationship between Weinberg equation for light cone WF of nuclei and conventional Schrödinger equation (section 2.4) one can estimate  $\rho_A^N$  at not too large  $\alpha$  using conventional non-relativistic theory of nuclei. Applying eq. (7.6) we obtain dashed curve in fig. 8.2 where  $n^{^4\text{He}}(k)$  is taken from the calculation of Zabolitsky and Ey [82].

To explain small difference of  $\alpha$  dependence of  $G_p^{^4\text{He}/P}$  and  $G_p^{D/P}$ , and to describe the data points in the region  $p_N > 0.6 \text{ GeV}/c$ , forbidden for the scattering from the deuteron [13], it is necessary to take into account the three-nucleon correlations. To avoid the problem of absolute normalization of the data we shall use the data on the reaction  $p + D \rightarrow p + X$ , analysed in section 3.5, which were obtained in the same experiment and use eq. (2.42) to calculate the  $\alpha$  dependence of the three-nucleon correlation:

$$\begin{aligned} \frac{1}{4} G_p^{^4\text{He}/P}(\alpha, p_\perp) &= \frac{1}{2} (a_2 G_p^{D/P}(\alpha, p_\perp) + a_3 \rho_3(\alpha, p_\perp)) \\ &\approx \frac{1}{2} \kappa (a_2 \rho_2(\alpha, p_\perp) + a_3 \rho_3(\alpha, p_\perp)). \end{aligned} \quad (8.2)$$

Remind that  $\rho_j(\alpha, k_\perp)$  are the contributions of  $j$ -nucleon correlations into  $\rho_A^N(\alpha, k_\perp)$  ( $\rho_A^N(\alpha, k_\perp) = A \sum a_j \rho_j$ ) and  $a_j$  is proportional to the probability of  $j$ -nucleon correlation (cf. eq. (2.38)). We take  $a_2 = 4$  which is consistent with the data on  $e + {}^3\text{He} \rightarrow e' + X$  reaction (see section 5) and with the

data on the  ${}^4\text{He}$  photo-disintegration (see e.g. [84]), choose  $n = 2.8$  in eq. (2.44) for  $\rho_3(\alpha, k_\perp)$ . Therefore  $\rho_3(\alpha, 0) \sim (3 - \alpha)^{6.6}$  ( $n = 2.8$ , which is close to the QCD prediction  $n = 3$ , gives the best fit to the  $p + D \rightarrow p + X$  data [13]). The result of calculation with  $a_3/a_2 = 1.0/4.5$  is shown in fig. 8.2 by the shaded region. The errors are due to the errors of the  $G_p^{\text{DP}}$  data points. The agreement is reasonable, though the shape of  $\rho_3(\alpha, k_\perp)$  at  $\alpha > 2$  is not probed in the comparison. This can be done using the 400 GeV data [18] for the scattering from  ${}^6\text{Li}$ . The  ${}^6\text{Li}$  nucleus is reasonably described by the cluster model as a  $D + {}^4\text{He}$  system (see, e.g. [164]).

Thus

$$\rho_2^{{}^6\text{Li}}(\alpha, k_\perp) \approx \rho_2^{{}^4\text{He}}(\alpha, k_\perp) + 1.5\rho_2^D(\alpha, k_\perp) \quad (8.3a)$$

$$\rho_3^{{}^6\text{Li}}(\alpha, k_\perp) \approx \rho_3^{{}^4\text{He}}(\alpha, k_\perp). \quad (8.3b)$$

The factor 1.5 in eq. (8.3a) follows [171] from the variational calculation of the  ${}^6\text{Li}$  WF [146]. It accounts for compression of the deuteron cluster. As a result using eq. (8.3) and the above estimate of  $a_3/a_2|_{{}^4\text{He}}$  we obtain  $a_3/a_2|_{{}^6\text{Li}} = 0.2$ . We include also the  $a_4$  term:  $a_4/a_3 = 0.02$ , which is however poorly determined from the experimental data and neglect contribution of the 5-nucleon correlation which is evidently small in the kinematical region investigated in [18].

Using eq. (2.44) with  $n = 2.8$  to describe the  $\alpha$ -dependence of  $\rho_j(\alpha, k_\perp)$  and the approximate angular condition (2.47) to estimate the  $k_\perp$  dependence of  $\rho_j(\alpha, k_\perp)$  we obtain a reasonable description of the data (see fig. 8.4) (the absolute normalization is described below)†. Similar fits reasonably describe the FB proton production from other light nuclei.

For nuclei of average range and for heavy nuclei a number of additional effects (which are not well understood yet) like the final state interaction of secondary particles could be essential (section 7.4). However the FNC model allows to describe even the spectra of heavy nuclei. The results of the fit with  $a_3/a_2 = 1/4.5$  (the same as for  ${}^4\text{He}$ ),  $a_4/a_2 = 1/20$ ,  $a_5/a_2 = 1/75$ ,  $a_6/a_2 = 1/300$  are presented in fig. 8.5. Note that in this case the experiment covers the region up to  $\alpha = 3.4$  where 5-, 6-nucleon correlations dominate. It is worth noting that the ratio  $a_j/a_2$  extracted from the experimental data for Ta [18] fastly decreases with  $j$ , roughly as  $(a_3/a_2)^{j-2}$ . However the fast decrease of  $a_j$  is compensated by the slower decrease of  $\rho_j$ . As a result relative contribution of high correlations rather rapidly increases with  $\alpha$ .

To summarize, the FNC model enables to describe the momentum and angular dependence of the nucleon spectra with few free parameters. However for unambiguous conclusion a study of the FB nucleon production from  ${}^{3,4}\text{He}$  at  $\alpha > 2$  is necessary.

### 8.1.2. High energies. A-dependence of $G_a^{\text{AN}}(p_N)$

(a) The second fact of principal importance is the large absolute magnitude of the FB nucleon cross section. For example, the average multiplicity of the backward nucleons  $\langle n_p \rangle$  with  $p_N > 0.3 \text{ GeV}/c$  in the reaction  $p + \text{Ta} \rightarrow p + X$  for  $E_p = 400 \text{ GeV}$  [18] is about 0.8! Thus, emission of the FB nucleons occurs in an average hadron-heavy nucleus collision with probability of the order unity.

We explained above that  $G_h^{\text{AN}}(p_N)$  have a rather similar momentum dependence in a wide  $p_N$  range.

† Note that in the case of  $90^\circ$  spectra in the region  $p_N \geq 0.9 \text{ GeV}/c$  the angular condition for the two-nucleon correlation contribution (which dominates in the studied kinematical region) could be strongly violated since the invariant mass of the two-nucleon system  $M_{NN} \geq 4 \text{ GeV}$  in this case (cf. section 2.3).

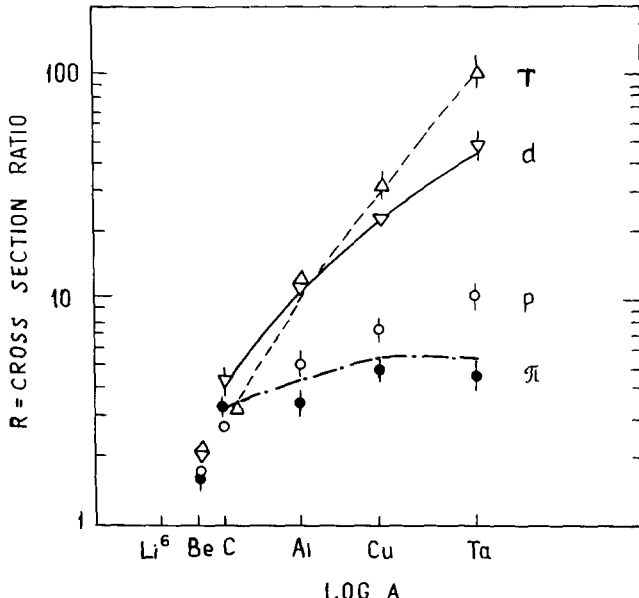


Fig. 8.7. The ratio ( $R$ ) of invariant cross sections per nucleon for the various targets relative to that of carbon for  $\theta = 160^\circ$  and  $\alpha > 1$  [18]. Refer to the text (sections 8.4, 8.5) for the calculation of  $A$ -dependences of D, T,  $\pi$  yields.

Thus  $(1/A) G_a^{A/N}(p_N)$  can be approximately written in a factorized form

$$\frac{1}{A} G_a^{A/N}(p_N) = C_a^{A/N} f_a(p_N); \quad (8.4)$$

at  $A \geq 7$   $C_h^{A/N}$  fastly increases with  $A$  (see fig. 8.7). In the case of  ${}^6\text{Li}$  and  ${}^7\text{Li}$  the data [13, 17] indicate that  $C_h^{A/N}$  decreases from  $A = 4$  to  $A = 6(7)$  by the factor  $\sim 0.72$  (0.76).‡

(b) Comparison of the data [15–18, 21] obtained using different projectiles reveals [71] that  $A$ -dependence of  $C_a^{A/N}$  is rather similar for  $\gamma$ ,  $\pi$ , p projectiles within the accuracy of existing data. For example the ratio  $C_a^{Pb/N}/C_a^{C/N}$  is equal to  $3.5 \pm 0.3$  at  $E_p = 400$  GeV [18]§,  $2.5 \pm 0.1$  at  $E_p = 8.5$  GeV [16],  $4.1 \pm 0.2$  at  $E_p = 8.9$  GeV/c [17]¶,  $2.9 \pm 0.3$  at  $E_\pi = 6.3$  GeV [15],  $2.3 \pm 0.2$  at  $E_\gamma^{\max} = (3-4.5)$  GeV [21]. Thus at sufficiently high energy inclusive cross section  $G_a^{A/N}(p_N)$  for quite different projectiles (like  $\gamma$  and  $\pi$ , p) depends on  $A$  in a practically universal fashion. This approximate universality of  $A$ -dependence demonstrates an important difference of the discussed process from hadron-hadron fragmentation reactions  $a + b \rightarrow c + X$  where  $G_a^{b/c}(p_c)/\sigma_{in}^{ab}$  is usually projectile independent due to factorization. Such factorization suggested in [14] in the frame of the nuclear scaling hypothesis would lead to a rather fast decrease of the ratio  $C_{\pi,p}^{A/N}/C_\gamma^{A/N} \sim \sigma_{in}^{hA}/\sigma_{in}^{\gamma A} \sim A^{-0.3}$  at large  $A$  though experimentally it slightly increases with  $A$  (see above example).

‡ This effect was investigated and observed in one experiment only and it clearly needs confirmation.

§ Actually in [18] the Ta/C ratio was measured, which is rather close to Pb/C ratio.

¶ There is some discrepancy between the Dubna data [17] at  $E_p = 8.9$  GeV and the data of two ITEP experiments [15, 16] at  $E_p = 8.6$  GeV in  $A$ -dependence of  $G_p^{A/N}$  for  $A > 12$ . In addition the absolute value of Dubna cross section is smaller by a factor of 2. Our analysis of the reaction  $p + D \rightarrow p + X$  in section 3, the comparison with Batavia 400 GeV data [18], with LBL data [20, 22] on the FB p,  $\pi$  production, and also with the  $\bar{\nu} + \text{Ne} \rightarrow \mu^+ + X$  data [9] analysed in section 6 suggest that the absolute normalization of all Dubna data [13, 17] should be increased by a factor 1.5–2.

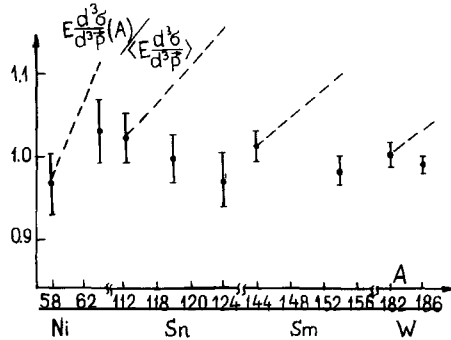


Fig. 8.8. The proton yields from different isotopes [186]. The dashed lines indicate expectations of the overall fit of the form  $A$ .

(c) The proton yield from the isotopes like  $^{112}\text{Sn}$ ,  $^{124}\text{Sn}$  with quite different number of neutrons is practically the same (see fig. 8.8) i.e.  $G_p^{A/P}(p_N)$  mainly depends on  $Z$ , the number of protons in the nucleus [186, 17]. This is in line with the experimental observation made in [187] that the  $G_\pi^{A/n}$  increase with  $N = A - Z$  and the  $G_\pi^{A/P}$  increase with  $Z$  are practically the same.

(d) In refs. [12, 20] production of fast leading protons in the collisions of relativistic D,  $^4\text{He}$  ions with different nuclei B was investigated. It was found that for  $p_\perp \sim 0$  and large  $\alpha$  (the FB nucleons in D,  $^4\text{He}$  lab. frame)  $B$  dependence of the inclusive cross sections is similar (fig. 8.9a). This is in agreement with the universality relation (7.7). The  $B$  dependence of  $G_B^{A/P}$  (fig. 8.9b) is also consistent with the expectations of the Glauber approach of section 7.6 (eq. (7.26) the solid curve in fig. 8.9b<sup>†</sup>) but it contradicts (as in the case of  $\gamma$ , pA reactions) the expectations of the empirical nuclear scaling hypothesis [14] based on the assumption of factorization of  $G_B^{A/P}/\sigma_{in}^{AB}$  (the dashed curve in fig. 8.9b), (see also note added in proof).

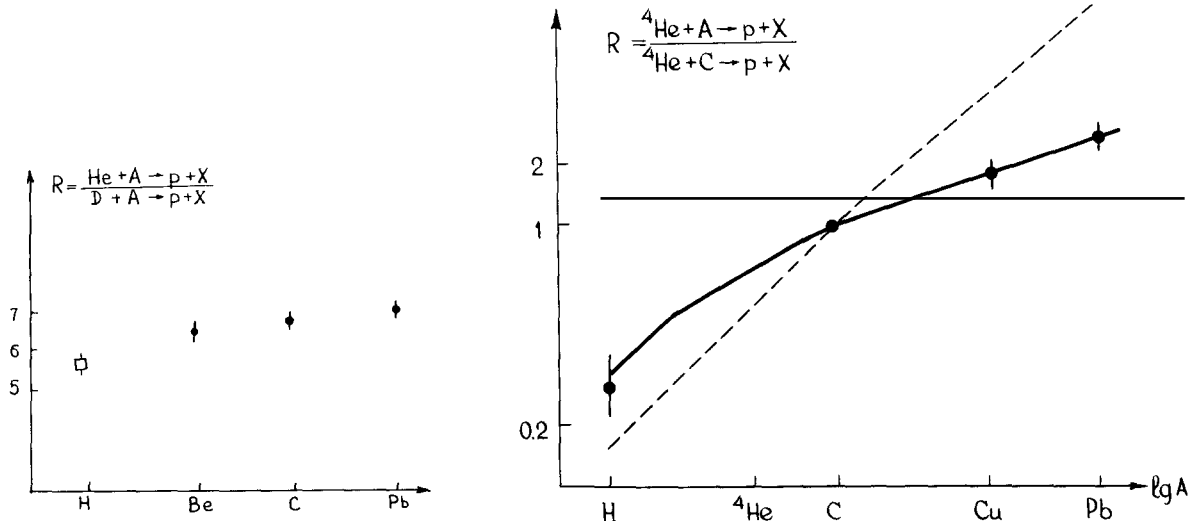


Fig. 8.9a. The ratio of the FB proton yields in the  $^4\text{He} + \text{B}$  and  $\text{D} + \text{B}$  reactions measured in [12] ( $\bullet$ ) and in the  $^4\text{He} + \text{p}$ ,  $\text{D} + \text{p}$  reactions [13] ( $\square$ ).

Fig. 8.9b. The  $B$ -dependence of the FB nucleon yields in  $^4\text{He} + \text{B} \rightarrow \text{p} + \text{X}$  reaction [20]. Solid curve is the result of the calculation using eq. (7.26). The dashed curve is the prediction of the empirical nuclear scaling hypothesis [14]. Both calculations are normalized for  $B = 12$ .

<sup>†</sup> In the calculation we use the expression for  $T(b)$  in the optic limit. For a more accurate comparison of eq. (7.26) with the data the radius of NN scattering amplitude should be accounted in the calculation of  $T(b)$ .

**Theoretical discussion.** In the framework of the geometrical (Glauber type) picture discussed in section 7 the universal  $A$  dependence of  $G_h^{A/N}$  follows from the local nature of the FNC mechanism of the FB nucleon production (see eq. (7.6)). It clearly demonstrates qualitative difference between  $A$ -dependence of inclusive cross sections and the total (inelastic)  $hA$  cross section inherent in the Glauber picture. The  $A$ -dependence of  $(1/A)G_h^{A/N}$  arises from the  $A$ -dependence of  $(1/A)\rho_A^N$  and the cascade factor  $\lambda$  (see eq. (7.25)). First let us consider the lightest nuclei where cascade effects are small ( $\lambda_A \sim 1$ ). What are manifestations of the cluster structure of the lightest nuclei?

It was shown above that the ratio  $G_p^{He/P}/G_p^{D/P}$  is quantitatively described by the FNC model.

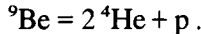
A non-monotonous behaviour of  $G_h^{A/N}$  for  ${}^{6,7}\text{Li}$  observed in [13, 17] can be understood in the framework of the cluster model (see, e.g. [164]). In the case of  ${}^6\text{Li}$  we expect [71] that

$$G_h^{6\text{Li}/N} = G_h^{4\text{He}/N} + 1.5 G_h^{D/N} \quad (8.5)$$

(cf. eq. (8.3)). The ratio of the left- and right-hand sides of eq. (8.5) measured in [13, 17] at  $\alpha = 1.67$ ,  $p_\perp = 0$ , is equal  $1.05 \pm 0.09$ . Similarly, in the framework of the cluster model  ${}^7\text{Li} \approx {}^4\text{He} + {}^3\text{H}$ . Thus using estimate (5.6) for  $\rho_H^P$  and  $\rho_{He}^N$  we obtain:

$$G_p^{7\text{Li}/P}(p_N) \approx G_p^{4\text{He}/P}(p_N) + G_p^{3\text{H}/P}(p_N) \approx \frac{13}{9} G_p^{4\text{He}/P}(p_N). \quad (8.6)$$

Experimentally  $G_p^{7\text{Li}/P}(p_N)/G_p^{4\text{He}/P}(p_N)|_{\alpha=1.66, p_\perp=0} = 1.33 \pm 0.13$ . We can also use the cluster model to estimate the yield of FB protons from  ${}^9\text{Be}$ , since



Thus roughly  $G_p^{9\text{Be}/P}(p_N)/G_p^{4\text{He}/P}(p_N) \approx 2$ . Experimentally [13, 17] this ratio is equal  $2.55 \pm 0.25$ . Similarly using the above analysis of  ${}^6\text{Li}$  we obtain

$$G_p^{9\text{Be}/P}(p_N)/G_p^{6\text{Li}/P}(p_N) \approx 1.75$$

though experimentally it is equal  $2.42 \pm 0.05$  [17],  $2.5 \pm 0.1$  [18].

Thus the data [17, 18] are consistent with the expectations based on the cluster model. It is necessary to study this effect in detail and in particular in the range of the three-nucleon correlation. The measurements of reactions using  ${}^3\text{He}$ ,  ${}^3\text{H}$  targets are evidently necessary.

To estimate the  $A$  dependence of  $G_h^{A/N}$  at  $A > 12$  we need a specific model of  $hA$  collisions to calculate  $\nu_{\text{eff}}(A)$ , the number of struck nucleons. For certainty we adopt the quark-parton model of Nikolaev [188, 179] based on the additive quark model [189] supplemented by the formation length concept [178], which reasonably describes production of the forward particles in the high energy  $hA$  collisions. According to this model  $\lambda_{Ta} \approx 2$ ,  $\lambda_C \sim 1$  at high energies [179]. Using eq. (2.40) to estimate the  $A$ -dependence of  $\rho_A^N$  we obtain†:

$$\frac{A_C}{A_{Ta}} \frac{G_p^{Ta/P}}{G_p^{C/P}} = \frac{\lambda_{Ta}}{\lambda_C} \frac{A_C}{A_{Ta}} \frac{\rho_{Ta}^N}{\rho_C^N} \sim 2 \times 1.5 = 3$$

† We shall demonstrate below that such value of  $\lambda_A$  enables to explain also the  $A$ -dependence of pion and light ion production. However, these values of  $\lambda_A$  are subject to considerable uncertainty. In particular in [179] secondary interactions of pions with  $p_\pi \lesssim 1 \text{ GeV}/c$  were neglected. In the future FB production would provide one of the best ways of studying  $\lambda_A$ .

which is in a reasonable agreement with experimental value of the ratio  $\sim 3.5$  at  $E_p = 400$  GeV [18].

The value of the screening factor  $\kappa_h$  as determined from the 400 GeV data for  $^6\text{Li}$  using parameters of the  $^6\text{Li}$  WF given above is equal to  $\kappa_p = 1.0 \pm 0.2$ . The Dubna data at  $E_p = 8.9$  GeV [17] renormalized by a factor 1.5–2 suggested above (see footnote ¶ on p. 313) lead to  $\kappa_p \approx 0.65$ –0.85. These numbers are consistent with our estimate of  $\kappa_p \approx 0.8 \pm 0.15$  (eq. (3.41)). (Note however that some small increase of the average energy transfer in the inelastic interactions with  $E_{\text{inc}}$  would lead to a certain increase of  $\kappa_h$ .)

For carbon  $a_2 = 7$  if we use the 400 GeV data [18] with  $\kappa_h = 1$  as for  $^6\text{Li}$  and take  $\lambda_C = 1$ . (Remind that  $a_2$  characterizes the probability of two-nucleon correlation in nucleus per nucleon as compared to that in the deuteron (cf. eq. (2.38)).) Such value of  $a_2(C)$  is surprisingly close (especially in view of uncertainties in  $\lambda_C$ ) to the estimate [71a] of  $a_2$  via the number of quasideuteron pn pairs in nuclei  $L \cdot N \cdot Z/A$ . (Here  $L$  is the Levinger factor for photonuclear reactions [112]. Experimentally  $L(C) = 8$ –10 (see e.g. [84] and references therein).) Using the Wigner model [162] to account for singlet pp and pn pairs we obtain:  $a_2(C) = 5L/6 \sim 7$ –8.

To describe isotopic dependence of  $G_n^{A/p}$  and different  $A$ -dependence of  $G_h^{A/p}$ ,  $G_h^{A/n}$  a rather detailed theory would be necessary. In particular an isotopic effect could be due to different variation of the proton and neutron densities with increase of the number of the neutrons which was observed in the other experiments (see, e.g. [116]).

## 8.2. Intermediate energies: $T_N^{\text{Inc}} \leq 1$ GeV

In recent years there has been considerable interest in the study of inclusive production of the FB protons in the proton–nucleus collisions at  $T_p = 600$ –800 MeV. In the experiments performed recently by S. Frankel and collaborators [23–25] it was discovered that the FB nucleons are produced with a rather large cross section in the kinematical region forbidden for the scattering from three-, four- and even five-nucleon systems. (First observation of this effect in the reaction  $p + C \rightarrow p + X$  at  $T_p = 1.15$  GeV,  $\theta = 137^\circ$  was made by Leksin and collaborators in 1966 [2].) Similar experiment was then performed by Komarov and collaborators, who observed also correlations between the FB nucleon and forward nucleon [26, 27, 28].

### 8.2.1. Inclusive data

A comparison of high energy data discussed above with the  $T_N \leq 0.8$  GeV data [23–26] reveals several important distinctions:

(a) In the discussed energy range  $G_N^{A/N}$  strongly decreases with  $T_N$  and it is much smaller than at high energies. For example [23–25]

$$G^{^6\text{Li}/p}(T_p = 400 \text{ GeV})/G^{^6\text{Li}/p}(T_p = 0.8 \text{ GeV})|_{p_N=0.6 \text{ GeV}/c, \theta=180^\circ} \approx 20$$

$$G^{^6\text{Li}/p}(T_p = 0.8 \text{ GeV})/G^{^6\text{Li}/p}(T_p = 0.6 \text{ GeV})|_{p_N=0.6 \text{ GeV}/c, \theta=180^\circ} \approx 6.$$

(b) For  $A > 12$   $G_N^{A/N}$  is roughly proportional to  $A$  though at high energies  $G_N^{A/N} \sim A^{1.4-1.5}$ .

(c) The  $p_N$ -dependence of  $G_p^{A/N}$  is much more sharp: e.g. for  $\text{Ta} \sim \exp\{-15p_N^2\}$  at  $\theta = 160^\circ$  for  $T_p = 0.8$  GeV as compared to  $\sim \exp\{-10p_N^2\}$  for  $T_p \geq 5$  GeV.

(d) The angular dependence of the spectra is much stronger than at high energies and it exists even for small nucleon momenta  $\sim 400$  MeV/c (compare fig. 8.10 and figs. 8.4, 8.5).

(e) In difference from high energies the shape of momentum distribution is not universal: for lightest

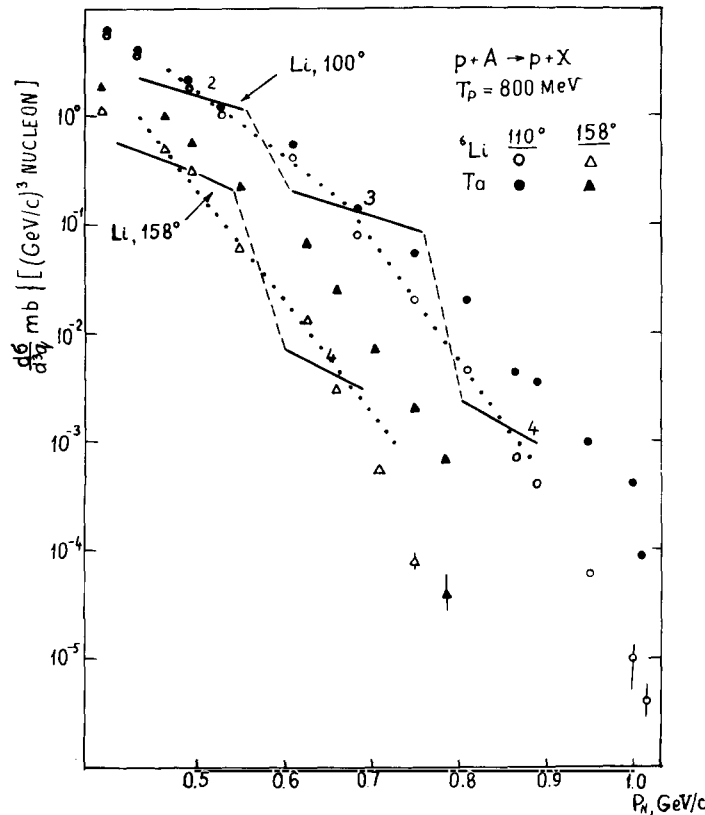


Fig. 8.10. The differential cross sections per nucleon for  ${}^6\text{Li}$  and  ${}^{181}\text{Ta}$  targets [25]. The solid curve is the prediction of the FNC model based on eq. (7.16). The dotted curve indicates the smearing effects.

nuclei  $A = 6, 9$  the decrease is considerably faster than for heavier nuclei. The spectra become roughly proportional for  $A \geq 12$  only.

### 8.2.2. Correlation data

In an important experiment Komarov and colleagues at Dubna [27, 28] have observed the correlation between fast backward protons of energies from 50 up to 90 MeV emitted with  $\theta = 122^\circ$  and fast forward proton emitted with  $\theta = -12^\circ$  from 640 MeV proton scattering on  ${}^{12}\text{C}$ . The kinematics was chosen in accordance with the quasi-free scattering of the incident proton on the correlated nucleon pairs



It was estimated that two-proton coincidence events contribute at least 20% into the inclusive FB proton emission in the investigated kinematics. Evidently, this number provides a lower bound only; (i) in reaction (8.7) the forward emitted protons are produced also with the energies lower than measured in refs. [27, 28] owing to the limited experimental acceptance, etc. (see discussion in [28]), (ii) the FB proton could be accompanied also by the emission of neutron of the same energies or other light nuclei fragments. Thus the total contribution of reaction (8.7) into  $G_p^{\text{A}/\text{p}}$  could be much larger (see discussion below).

In refs. [30, 31] correlation between direction of the projectile proton spin and the value of  $G_N^{A/N}(p_N)$ , i.e. the analysing power  $-A_y$  was investigated for the inclusive reaction  $p + A \rightarrow p + X$ . No correlation was observed in ref. [30], though in a more precise experiment [31] small correlation was found at backward angles:  $|A_y^{^6\text{Li}}| \leq 5\%$ ,  $A_y^{^3\text{Li}} \approx A_y^{^8\text{Be}}, |A_y^{^{\text{Ta}}}| < 1\%$ .

### 8.2.3. Theoretical discussion

Since large energy and momentum are transferred to the nucleus in the reactions with FB protons it is natural to expect that only few closely located nucleons participate in its absorption [60, 62, 71, 72]. (Actually this reasoning reminds the original argumentation of Bethe and Levinger [112], independently developed also by Tamm and Khokhlov [113], for the nuclear photo-disintegration and of Bruckner, Serber and Watson [114] for slow pion absorption.) Here we shall demonstrate that the FNC model (with the same parameters  $a$ , as those used to explain the high-energy data) seems to be able to describe also the basic features of the intermediate-energy data.

Qualitatively in the framework of the FNC model the observed sharpening of the spectrum and its lower absolute value are due to decrease of the kinematical region permitted for production of FB nucleons from two-, three-nucleon correlations. Since the kinematical boundaries for  $j$ -nucleon correlations depend strongly on the emission angle (see fig. 7.8), the suppression of 2-, 3-nucleon correlations is more strong at large angles  $\theta \sim 180^\circ$ . This leads to an increase of the angular anisotropy. A change of  $A$ -dependence occurs because in the discussed energy range the incident proton penetrates the nucleus (without loosing considerable fraction of its energy) by only one mean free path  $\sim 2$  fm. Thus correlations near the backward surface can be destroyed only, whereas in the high energy processes correlations in the whole nuclear volume can be destroyed.

As a result

$$G_N^{A/N} \sim G_{\text{in}}^{NA} a_j(A)|_{j=3,4} \sim A^{0.7} A^{0.20-0.25} \sim A^{0.9-0.95}$$

for  $a \geq 12$  which is in a reasonable agreement with the experimental observation that  $(1/A)G_N^{A/N}$  is approximately  $A$  independent for  $A > 12$ .

The important feature of the FNC mechanism is that scattering from the different correlations contribute incoherently into the proton yield. This property is not specific for the spectator or the direct production mechanism because it follows mainly from the inclusive nature of the projectile–nucleus interaction (the quasi classical picture is reasonable for the nucleon and  $K^+$  projectiles since the NN and  $K^+N$  cross section only weakly depends on  $E_{\text{inc}}$ . For pion projectiles this approximation should be poorer both due to the strong energy variation of the  $\pi N$  cross section and the presence of the pion absorption channels).

Since the probability of a  $j$ -nucleon correlation rapidly decreases with  $j$  it is natural to expect that the correlations with minimal  $j$  allowed at given  $p_N$  and  $E_{\text{inc}}$  will dominate in the yield. If so in the ratio

$$R = \frac{1}{A_1} G_N^{A_1/N}(p_N) / \frac{1}{A_2} G_N^{A_2/N}(p_N) \quad (8.8)$$

the dependence on the inclusive scattering cross section from the  $j$ -nucleon correlation and consequently the effects of the final state interaction should cancel out. Therefore the ratio  $R$  should depend mainly on the minimal number  $j$  of  $j$ -nucleon correlation permitted at a given  $p_N$  and  $E_{\text{inc}}$ , but not on the

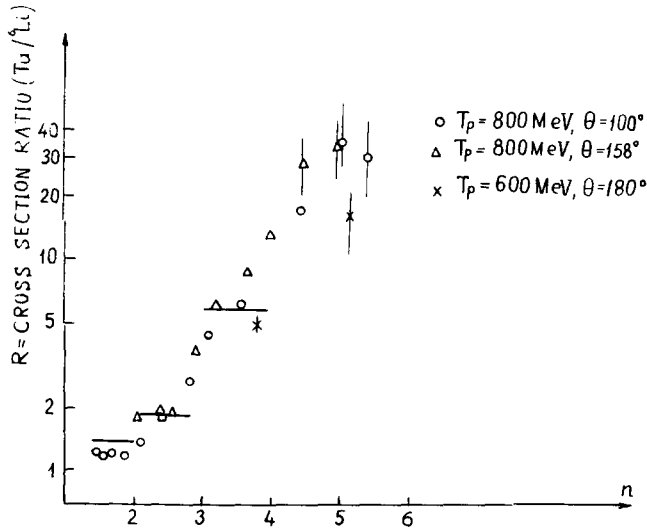


Fig. 8.11. The test of  $n$ -scaling for the ratio of the FB nucleon yields per nucleon from  $^{181}\text{Ta}$  and  $^6\text{Li}$  using the data [24, 25]. The solid curves are the FNC model predictions calculated using the above analysis of high energy data.

emission angle or  $E_{\text{inc}}$ .† The kinematical boundary of  $n$ -nucleon correlation is determined from the condition that the invariant mass of the recoiling system should be larger than  $nm_N$

$$(E_{\text{inc}} - \sqrt{m^2 + p_N^2} + nm_N)^2 - (p_{\text{inc}} - p_N)^2 = (nm_N)^2. \quad (8.9)$$

To account for the kinematical boundaries of the FNC contributions it is convenient to solve eq. (8.9) for arbitrary real  $n$

$$n(T_{\text{inc}}, p_N) = \frac{(p_{\text{inc}}^2 - 2p_{\text{inc}}p_{N\text{Z}} + p_N^2 - (T_{\text{inc}} - T_N)^2)}{2m_N(T_{\text{inc}} - T_N)}. \quad (8.10)$$

Evidently the variable  $n$  varies from  $j-1$  to  $j$  in the  $j$ -nucleon correlation region (i.e. the region permitted for the scattering from correlations with  $k \geq j$  only).‡

To check that the ratio  $R$  depends mainly on  $n$  ( $n$ -scaling) we compare in fig. 8.11 the 800 MeV data [25] and the data [24] obtained at  $T_p = 600$  MeV and find that  $n$ -scaling is reasonably fulfilled, though there is no scaling if one plots the ratio  $R$  as a function of e.g. nucleon momentum  $p_N$ .

$R$  can be roughly calculated neglecting contributions of all but minimal kinematically allowed correlation  $j$ . In this approximation the value of the inclusive cross section  $p + (j\text{-nucleon correlation}) \rightarrow p + X$  cancels in the ratio. Thus  $R$  is equal to the relative probability of  $j$ -nucleon correlations in nuclei  $A_1$  and  $A_2$  times the ratio of the inelastic total cross sections (cf. derivation of eq. (7.16)):

$$\frac{G_p^{A_1/N}(p_N)}{G_p^{A_2/N}(p_N)} = \frac{a_j(A_1)}{a_j(A_2)} \frac{\sigma_{\text{in}}^{NA_1}}{\sigma_{\text{in}}^{NA_2}}. \quad (8.11)$$

† This universality is expected to work at  $T_{\text{inc}} \lesssim 1$  GeV only, where the contribution of correlations near the nuclear surface dominates. For comparison with higher energies it is necessary to introduce the factor  $\nu_{\text{eff}}(A_2)/\nu_{\text{eff}}(A_1)$  into the right-hand side of eq. (8.8).

‡ This variable is similar to the cumulative variable introduced by Stavinsky [185].

We neglect here some difference between the relative number of correlations close to the nuclear surface and in the centre since the surface region is rather small compared to the mean free path of the projectile nucleon ( $\lesssim 2$  fm). Note also that in the intermediate-energy reaction with a heavy nuclear target the FB nucleon traverses a considerably smaller distance inside the nuclei ( $\lesssim 2$  fm) than at high energies, hence the final state rescatterings are much smaller in this case.

Contribution of  $k > j$  correlations to the ratio can be estimated in line with discussion of eq. (7.15) as

$$R(\alpha, p_\perp) = \frac{\sigma_{in}^{NA_1}}{\sigma_{in}^{NA_2}} \frac{\sum a_k(A_1) \rho_k(\alpha, p_\perp)}{\sum_{k \leq j} a_k(A_2) \rho_k(\alpha, p_\perp)}. \quad (8.12)$$

Taking the parameters  $a_j$  and the WFs  $\rho_j$  from the fits to the 400 GeV reactions  $p + {}^6\text{Li}$ ,  $\text{Ta} \rightarrow p + X$  (figs. 8.4, 8.5) with  $\lambda_{\text{Ta}} = 2$  we obtain the solid curves in fig. 8.11. (Several enthusiastic observers have found indications of steps in this figure.)

In the case of the 800 MeV data [25] at  $\theta = 100^\circ$  it is possible to make the comparison with the Saturn 800 MeV data [29] on the reaction  $D + p \rightarrow p + X$ .†

$$R({}^6\text{Li}, D, p_N = 0.4 \text{ GeV}/c, \theta = 100^\circ) = 4 \pm 1,$$

though use of eq. (8.10) leads to  $R = 3.6$ .

A similar check of  $n$ -scaling can be made using  ${}^9\text{Be}:{ }^6\text{Li}$  ratio at  $T_p = 600, 800$  MeV [24, 25]. The comparison reveals that  $n$ -scaling is well satisfied and that the value of the ratio is close to the value  $a_j$  extracted from the 400 GeV data using eq. (8.11). We want to emphasize that in the case of these and other light nuclei the comparison of the high-energy and the intermediate-energy data is not sensitive to the interaction of the secondary particles ( $\lambda_A \approx 1$ ).

To calculate the magnitude of  $G_N^{A/N}$  within the FNC model we can use eq. (7.16) with parameters  $a_j$  of the few-nucleon correlation determined from the fits to the 400 GeV data [18] (figs. 8.4, 8.5). Evidently, eq. (7.16) could give only a rough description of the FNC contribution since in the discussed energy range the final state interaction between the forward moving particles originating from the destroyed correlation and the FB nucleon could be essential.‡ However this effect is not large as compared to the large variation of the cross section due to change of kinematical boundaries of FNC which is taken into account in eq. (7.16). Results of calculation for  ${}^6\text{Li}$  are given by solid curves in fig. 8.10. Dashed curves denote transitional regions between  $j$ - and  $j + 1$ -nucleon correlations where eq. (7.16) cannot be used (see discussion after eq. (7.15)).

Note however that for medium and heavy nuclei one could expect that the Fermi motion of correlated nucleus in the nuclear average field would smear the behaviour of the spectrum near the kinematical boundaries of correlations, modifying prediction of eq. (7.16) in a way close to the dotted curve in fig. 8.10.

Similar description works also for heavier nuclei like C, Ta in the range  $T_N = 600\text{--}800$  MeV up to  $n \sim 5$ . (Note that in the case of Ta we could estimate  $a_{5,6}$  from the 400 GeV data.)

Thus the FNC model enables to describe reasonably the main characteristics of inclusive data such as the absolute value of the cross section, its momentum and angular dependence without introducing any new parameters into the model, just by accounting for the difference in the number of destroyed

† The large error for the ratio is due to the quoted uncertainties in the absolute normalization of the experimental data [25, 29].

‡ In the case of intermediate-energy scattering due to large cross section for production of slow  $\Delta$ -isobars contribution of  $\Delta + N \rightarrow N + N$  reaction into the FB nucleon yield is enhanced (cf. [205]). Another source of FB nucleons is absorption of slow secondary pions by pairs of nucleons [200].

correlations at high and intermediate energies and for presence of the kinematical boundaries. It seems necessary to extend the measurements to the lightest nuclei  $A = 3, 4$  and to check the accuracy of the  $R(n)$  scaling in a wider range of targets. It would be also interesting to find out down to which projectile energies such scaling works. This would help to determine the region where the scattering from FNC dominates. At present it seems justified to conclude that the scattering off FNCs explains a considerable part of the observed cross section.<sup>†</sup>

Let us discuss now the correlation data [27, 28]. In the framework of the FNC model contribution of scattering from (p, n) pairs is expected to be larger than from (pp) pairs due to larger number of pn pairs. The (pn) pair contribution could be further enhanced due to the  $\Delta$ -isobar production in the intermediate state (see, e.g. [190]). Therefore correlations with a fast forward neutron should be as large as for the case of the fast forward proton. In the kinematics of refs. [27, 28] the two-nucleon correlations are expected to contribute about 70% of the inclusive yield if we use our fit to the high energy data for a rough estimate. Hence the pp correlations should contribute about 35% into the inclusive proton yield. This number seems to be consistent with the experimental number  $\sim 20\%$  in view of the experimental uncertainties discussed above. (In particular, the estimate of the contribution of pp coincidences into the inclusive yield with account of absorption of the forward emitted nucleon [27] give the number  $28 \pm 4\%$ .)

A small value of the analysing power  $A_y$  observed in [30, 31] seems also to agree qualitatively with the FNC model. Indeed  $A_y$  should be small for the spectator mechanism since in this case it arises from the Glauber screening effects only, though in the direct mechanism which constitutes small fraction of cross section  $A_y$  would be rather large [191]. Using the estimate of [191] for the value of  $A_y$  in the direct mechanism and assuming that it constitutes about 1/5 of the total FB nucleon yield we obtain reasonable agreement with the observed value of  $A_y$  for light nuclei. To summarize, we have demonstrated that the intermediate energy data are consistent with the FNC model expectations. If more detailed experiments would confirm this conclusion it would be possible to use these reactions to study superdense matter configurations in nuclei. For example one can study the reaction  $p + {}^6\text{Li} \rightarrow p + X$  using the FB nucleon in the region e.g.  $n \sim 5$  as a trigger and investigate the invariant mass spectra of several forward emitted nucleons. If multiquark resonances exist, they would be enhanced in the same spectrum of the recoiling system.

### 8.3. Onset of scaling in $\gamma, h + A \rightarrow p + X$ reactions

No systematic experimental data exist now in the transition region where a change of the momentum and  $A$ -dependence of  $G_h^{AN}(p_N)$  occurs. Hence to simplify the presentation, we shall combine here the discussions of the theory and of the available experimental data.

(a) For light nuclei in an average process one nucleon of the target participates in the interaction both at intermediate and high energies ( $\nu_{\text{eff}} \sim 1$ ). Thus the change of the shape of  $G_h^{AN}$  should be determined mainly by the change of the kinematical regions available for scattering from two-, three-nucleon correlations (cf. eq. (7.16)). As a result  $G_h^{AN}(p_N)$  should first become energy independent at small momenta when  $p_N$  is within the two-nucleon correlation-region  $n(E_h, p_N) \leq 2$  (cf. the discussion of the Feynman scaling onset for the deuteron case, section 3), i.e. a break is expected in the space of

<sup>†</sup> We want to emphasize once more that at low energies the mechanism of interaction with the FNC could qualitatively differ from the high energy spectator mechanism. Presence of  $n$ -scaling at low energies would indicate only that the energy and momentum are transferred to the nucleus in a local way. As to the absolute value of the cross section, real danger was to predict it to be much larger than the experimental one if WF is normalized according to high energy data. This is just the case for the average field models [37, 44, 46, 59, 61, 63] (see section 8.6).

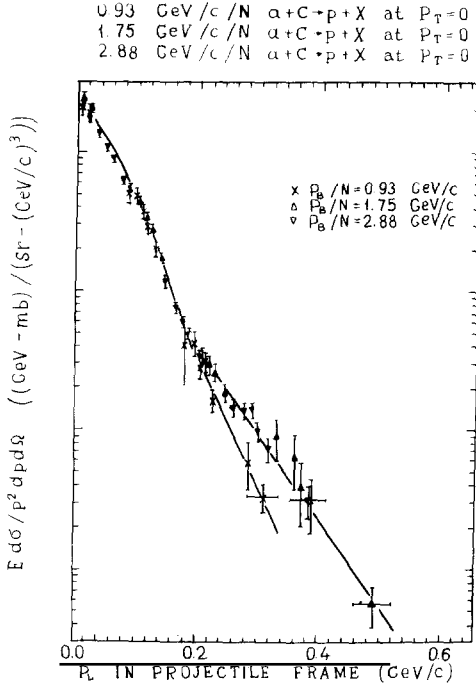


Fig. 8.12. Onset of scaling in  ${}^4\text{He} + \text{C} \rightarrow \text{p} + \text{X}$  reaction [20].

$G_h^{A/N}$  near the kinematical boundary of the two-nucleon correlation region. Inspection of few available data for helium and carbon fragmentation ( ${}^4\text{He} + \text{C} \rightarrow \text{p} + \text{X}$ ,  $p_{\text{inc}} = 0.64$  (GeV/c)/nucleon,  $p_\perp = 0$ , [20];  $\text{p} + \text{C} \rightarrow \text{p} + \text{X}$ ,  $p_{\text{inc}} = 1.15$  GeV/c,  $\theta = 137^\circ$ , [2];  $\text{p} + \text{C} \rightarrow \text{p} + \text{X}$ ,  $p_{\text{inc}} = 2.2$  GeV/c,  $\theta = 162^\circ$ , [16]) indicate that in all three cases there is indeed a break just near  $n = 2$  (see, e.g. fig. 8.12). Evidently this effect should be checked in special experiments with the emphasize on the lightest nuclei.

(b) For heavy nuclei the shape of the momentum distribution is expected to become approximately energy independent at the same energies as for light nuclei, since the energy which could be transferred to FNCs in the first projectile interaction is the same in both cases (though a more smooth behaviour is expected near the kinematical boundaries of FNCs due to the contribution of interactions with  $\nu > 2$ ).

However due to increase of essential longitudinal distance the absolute value of  $G_h^{A/N}$  should increase up to the energies [71]

$$E_{\text{critical}}^h \approx \nu_A E_0 \quad (8.13)$$

where  $E_0$  is the energy where the limiting fragmentation for the reaction  $\text{h} + \text{D} \rightarrow \text{p} + \text{X}$  occurs (cf. eq. (7.19)). (Actually the situation is more complicated: (a) there is a distribution in  $\nu$  (eq. (7.3)); (b) the three-nucleon correlations are rather important; (c) the secondary interactions of the produced hadrons also increase with  $E_{\text{inc}}$ . Thus some increase of  $C_A$  is expected at  $E^h > E_{\text{critical}}^h$ . These effects can be easily taken into account in line with eqs. (7.14–16) provided one uses some specific model of the hadron-nucleus interaction.) On the contrary, in the case of photonuclear reaction  $\nu \approx 1$  since  $\sigma_{\gamma A} \sim A \sigma_{\gamma N}$ . Thus we expect here the onset of scaling for light and heavy nuclei at approximately the same energy (some differences could arise from the secondary hadron interactions) [71]

$$E_{\text{critical}}^{\gamma} \approx E_0. \quad (8.14)$$

The energy dependence of  $G_{\pi}^{A/P}$  was investigated [15] at  $E_{\pi^-} > 1.5$  GeV where the momentum dependence of  $G_{\pi}^{A/P}$  does not change with  $E_{\pi}$ . The integral of inclusive cross section

$$\sigma_p = \int \frac{d^2\sigma}{dp d\Omega} dp d\Omega|_{0.4 < p < 1.0 \text{ GeV}/c, 159.6 < \theta < 164.4}$$

was measured. The ratio  $\sigma_p/\sigma_{\text{in}}^{hA}$  is presented in fig. 8.13 together with the fit using eq. (8.13) with  $E_0 = 1.4$  GeV. For  $\nu$  we use the fit from [176]:  $\nu = 0.7A^{0.3}$ . It can be seen from the figure that eq. (8.13) reasonably describes the change of  $A$ -dependence of  $G_{\pi}^{A/P}$ .

There is no direct measurements of the energy dependence of  $G_{\gamma}^{A/\pi}$  since a bremsstrahlung photon spectrum was used in [21]. However we could apply the standard differential method to estimate the energy dependence of the ratio  $R = G_{\gamma}^{\text{Pb}/P}(p_N)/G_{\gamma}^{\text{C}/P}(p_N)$  using measurements [21] with different  $E_{\gamma \text{ max}}$ . We found [71] that  $R$  becomes practically energy independent at considerably lower energies than in the pion case (see fig. 8.14). This is in line with eq. (8.14).

(c) The role of increase of the essential longitudinal distances can be illustrated also [71] by the example of the semi-inclusive reactions like  $\pi^- + A \rightarrow p + h^+ + X$  reaction studied in [181] at  $E_{\pi} = 3.4$  GeV. Correlation between emission of a FB proton and a fast forward  $h^+$  ( $p_{h^+} \sim 3$  GeV/c) was investigated for  $A = \text{Al, Cu, Pb}$ . For light nuclei a small negative correlation  $R = \sigma_{\text{in}}^{hA} G_{\pi}^{A/P+h^+}/(G_{\pi}^{A/h^+} - 1)$  is expected since in such process the energy transfer to the FNC is smaller than in the average process. With increasing  $A$  the negative correlation should increase approximately as

$$R + 1 \sim 1/\nu_{\text{eff}}(A) \quad (8.15)$$

because selection of events with the fast forward  $h^+$  corresponds to selection of collisions with  $\nu = 1$ . The estimate (8.15) (with  $\nu_{\text{eff}}(A)$  calculated using  $E_{\pi} = 3.4$  GeV data shown in fig. 8.13 and eq. (2.40)) reasonably describes both the  $A$ -dependence of  $R$  and its absolute value.

It would be of interest to study correlations in the similar reactions at much higher projectile energies. If  $h$  has large  $x$  in the projectile fragmentation region

$$R = \frac{\nu_{\text{eff}}(x)}{\nu} - 1.$$

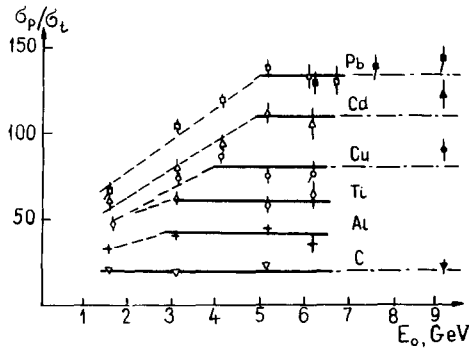


Fig. 8.13. Energy dependence of  $C/\sigma_{\text{in}}^{hA}$  for  $\theta = 160^\circ$  in  $\pi(p)A$  scattering [15]. Full points correspond to proton scattering. The straight lines represent the fit using eq. (8.13).

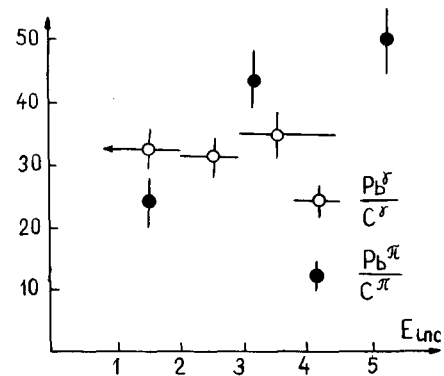


Fig. 8.14. The comparison of the energy dependence of the FB proton yield in pion and photon scattering.

Therefore it is possible to study in such a reaction the space-time picture of the interaction of fast hadrons (leptons) with nuclei. One can study here the relative importance of low and high energy secondary hadron interactions simply by varying the type and momentum of the FB particle ( $N, \pi, K^\pm$ ). Measurements of correlations with the number of FB particles could provide also a sensitive test of the models for Drell-Yan and high  $p_T$  processes on nuclei (for an encouraging attempt of explaining correlations between slow and fast particles observed in the CERN experiment of Faessler et al. [168] in the framework of the quark-parton model [188] combined with the FNC model see [179]).

#### Unresolved questions:

(1) There exists one experimental indication that the onset of scaling could be more complicated than described above. In ref. [187] the reaction  $\pi^- + C \rightarrow n + X$  was investigated at  $E_{\pi^-} = 3$  GeV,  $\theta = 162^\circ$ . Due to isotopic invariance  $G_{\pi^-}^{12C/n} = G_{\pi^-}^{12C/P}$ .<sup>†</sup> At high energies  $G_{\pi^-}^{C/P} = G_{\pi^-}^{C/P}$  due to dominance of the Pomeron exchange. Thus at high energies  $G_{\pi^-}^{12C/n} = G_{\pi^-}^{12C/P}$ . However according to [187]  $G_{\pi^-}^{12C/n}/G_{\pi^-}^{12C/P} \sim 1.5$  at  $E_{\pi^-} = 3$  GeV, though  $G_{\pi^-}^{12C/P}$  is practically energy independent at  $E_{\pi^-} > 1.5$  GeV [15]. In other words the data [15, 187] indicate that  $G_{\pi^-}^{12C/P}$  depends on the projectile energy quite differently than  $G_{\pi^-}^{12C/P}$  (see note added in proof).

(2) In ref. [32] a surprisingly large nucleon polarization was observed in  $\pi^- + ^{12}C \rightarrow p + X$  reaction at the average  $E_{\pi^-} = 3$  GeV,  $\theta = 162^\circ$ :  $P = 0.55 \pm 0.18$  at  $p_N > 0.5$  GeV/c, though for heavy nucleus (Pb) polarization is consistent with zero. Under the same conditions polarization was investigated for the proton as a projectile ( $E_p = 6$  GeV). The data indicate that polarization has a negative sign and is much smaller than in the pion case. For heavy nuclei (Pb) the observed polarization is consistent with zero.

To interpret the first effect an accurate account of the differences in  $\pi^\pm N$  interaction at  $E_\pi \leq 1$  GeV is necessary, since the effective energies essential in the interaction of pion with forward nucleons of the correlation are rather small even at  $E_\pi^{\text{inc}} = 3$  GeV. This has not been done so far.

Polarization of the FB nucleons could arise (a) due to polarization in hN elastic amplitude via Glauber screening diagrams (this mechanism is effective for  $j > 2$  correlations. In the case of two-nucleon correlation expected polarization is rather small); (b) due to the final state rescatterings of the FB nucleons. Though it is rather difficult now to calculate quantitatively the value of polarization expected in these mechanisms it is clear that in the case (a) the increase of polarization with  $E_{\text{inc}}$  considerably depends on the projectile as in elastic hN scattering. It is small in the two-nucleon correlation region. On the contrary in the case (b) polarization would be finite at high  $E_{\text{inc}}$  and would not significantly depend on the projectile. The data [32] seem to favour the first possibility since polarizations are quite different in  $\pi$ , p cases and they are correlated with the magnitude of polarization in the elementary amplitude. Note also that large polarization is observed only in the region where  $j \geq 3$  correlations dominate.<sup>‡</sup>

In conclusion, we have demonstrated in sections 8.1–8.3 that the FNC model reasonably explains the basic features of existing experimental data in the 0.6–400 GeV range. In the region of the two-nucleon correlation the description actually has no free parameters in the case of light nuclei. Measurements with the lightest nuclei are necessary to obtain the definite tests of the FNC model in the 3,4-nucleon correlation region.

The study of correlations between the FB nucleons and forward nucleons for high energy projectiles is of interest also. For example for light nuclei ( $\nu_{\text{eff}} \sim 1$ ) in the two-nucleon correlation (neglecting the  $j > 2$  correlation and direct mechanism contributions) we obtain for the spectator mechanism:

<sup>†</sup> The reactions  $\pi^\pm + C(D, ^6Li) \rightarrow p(n) + X$  provide the high counting rate method of calibrating the neutron spectrometers.

<sup>‡</sup> Recent measurement of polarization at 640 MeV in the reaction  $p + ^{12}C \rightarrow p + X$  [33] are in accordance with this observation.

$$G_h^{A/(P_1+P_2)}(\alpha_1, k_{1\perp}, \alpha_2, k_{2\perp}) = G_h^{A/P_1}(\alpha_1, k_{1\perp}) \frac{1}{\sigma_{in}^{hN}} G_n^{N/P_2} \left( \frac{\alpha_2}{2-\alpha_1}, k_{2\perp} + \frac{\alpha_2 k_{1\perp}}{2-\alpha_1} \right) \quad (8.16)$$

where  $2 > \alpha_1 > 1$ ,  $\alpha_2 < 2 - \alpha_1$ .

For heavy nuclei the correlation would be much smaller due to emission of  $\nu$  forward nucleons in an average hA collision and due to the final state rescatterings of the emitted nucleons. It can be seen from eq. (8.16) that expected correlation is small and smeared over a rather wide  $\alpha, k_\perp$  region. Thus it would be much harder to find such a correlation at high energies than at intermediate energies [27, 28], where it is small (section 8.2). (Actually understanding this point has been the motivation of searching for  $x, \alpha$  correlations in the neutrino experiments several years ago [45] (section 6).) See however Appendix D.

#### 8.4. Backward production of fast light ions

Production of FB deuteron, tritons, helium 3 has several features rather similar to the case of FB nucleon production considered above [16–18]: (a) the shape of the momentum distributions is practically universal for  $A \geq 12$  and has strong angular dependence, (b) cross section increase with  $E_h$  up to  $E_h(A) \sim A^{1/3} E_0(E_h^D(A)) \approx E_h^P(A)$ . The main differences are a more slow decrease of  $G_h^{A/D,T}$  with the ion momentum than for  $G_h^{A/P}$  and a more fast increase of cross section with the atomic mass number (see fig. 8.7). The  $A$ -dependence is strongest for the heaviest ions. The ratio  $G_p^{Ta/3He}(p)/G_p^{Ta/3H}(p)$  is approximately constant reflecting the  $N/Z$  ratio in the Ta target [18].

*Theoretical discussion.* Natural source of the FB light ions is the coalescence of the nucleons originating from the destruction of nearby FNCs and/or one FNC by the projectile. This mechanism leads to a universal momentum dependence of the FB ion spectra due to universality of the FB nucleon spectra and to the similar incident energy dependence of the nucleon and ion spectra:  $E_{crit}^D(A) \sim E_{crit}^N(A)$ , which is consistent with the data. For small  $p_\perp$  we can calculate the shape of  $G_h^{A/D,T}(p)$  in non-relativistic approximation with the overlap integral using eq. (7.24) and assuming that  $(N/Z)G_h^{A/n}(p_N) \sim G_h^{A/P}(p_N)$ . We also take into account that the average number of collisions in high energy scattering is larger than in the Glauber model used in section 7.4 by a factor  $\lambda_A$ . As a result eq. (7.24) for production of light ions B at  $p_B > B p_F$ ,  $P_{B\perp} \approx 0$  can be rewritten as follows

$$G_h^{A/B}(p) = \zeta_B \lambda_A \left( \frac{N_B}{Z_B} \right)^{N_B} \left[ \frac{G_h^{A/P}(p/B)}{\lambda_A} \right]^B \left[ \sigma_{in}^{hN} \frac{Ap^2}{(Bp_F)^2} \right]^{1-B}. \quad (8.17)$$

Eq. (8.17) reasonably describes the momentum dependence  $p + A \rightarrow D, T + X$  reactions at  $p_\perp = 0$  [17] in the range where e.g. cross section of the deuteron emission changes by the factor  $5 \times 10^4$  (see fig. 8.15 a,b). In ref. [18] production of light ions was investigated for  $E_p = 400$  GeV at laboratory angles of  $70^\circ$ – $160^\circ$ . In this case the angular dependence of  $G_p^{A/P}$  neglected in the derivation of eq. (7.26) makes the comparison semiquantitative only. However eq. (8.17) describes  $1:10^4$  ( $1:10^3$ ) variation of  $G_p^{A/D}(G_p^{A/T})$  cross sections with accuracy 1.5–2 at  $160^\circ$ . For smaller angles eq. (8.17) underestimates the deuteron yield by a factor 2–4 at maximum momentum  $p_D \approx 1.45$  GeV/c. Since the discrepancy is largest at small angles where the input nucleon spectra strongly increase with decreasing  $\theta$  it could be due to neglect of the angular dependence of  $G_p^{A/N}$  in the derivation of eq. (7.26) and a more complicated form of the overlapping integral at  $p_\perp \approx 0$ .

To calculate the  $A$ -dependence of  $G_N^{A/B}$  we can apply eq. (8.17) using (as in the case of the FB

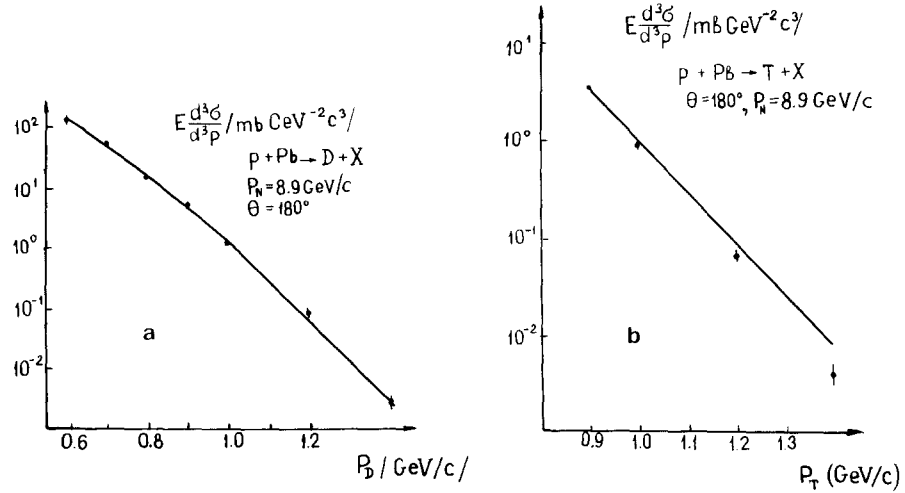


Fig. 8.15. The comparison of eq. (8.17) with the data [17]. The curves are normalized at  $p_D = 0.6$  GeV/c,  $p_T = 0.9$  GeV/c.

nucleon production)  $\lambda_A$  from [188]. This procedure should work at  $\theta < 180^\circ$  also since the overlapping integral for the light ion formation seems to be a weak function of  $A$ . Comparison with the 400 GeV data [18] demonstrates that eq. (8.17) reasonably describes  $A$ -dependence of the FB ion spectra for  $A \geq 12$  at large angles (the solid curves in fig. 8.7) and its variation with decrease of  $\theta$ .† Note that the cross section of the ion emission is actually proportional to  $\lambda_A$  provided the  $A$ -dependence of FNCs is correctly taken into account since only nucleons from the nearby points can coalesce into the ion. (Thus the double inclusive cross section  $h + A \rightarrow N + N + X$  should increase with  $A$  faster than the deuteron yield approximately by the factor  $\nu_{\text{eff}}$  (cf. eq. (7.4)). No measurements of the  $A$ -dependence of  $G_h^{A/N_1, N_2}$  are available yet.) The cascade factor  $\lambda_A$  and the  $A$ -dependence of FNC quite differently influence the nucleon and light ion production at different emission angles (due to a slower  $A$ -dependence of  $G_N^{A/N}$  at  $90^\circ$ ). Thus the description of the  $A$  dependence of  $G_p^{A/D, T}$  can be considered as an independent test of the assumed model of secondary particles interactions and of the  $A$  dependence of the FNCs.

The values of the numerical fit factors  $\zeta_{D,T}$  are rather small:  $\zeta_D \sim 7 \times 10^{-2}$ ,  $\zeta_T \sim 2 \times 10^{-3}$ . However to confirm the discussed interpretation and to understand the possible role of emission of FB ions from destruction of a single FNC it seems necessary to estimate these factors quantitatively. In principle this could be done in line with [173] accounting for the Glauber type geometry of high energy collisions. Comparisons with reactions like  $h + A \rightarrow kN + X$  for  $A < 12$  and especially with similar deep inelastic reactions  $\ell + A \rightarrow \ell' + D$ ,  $kN + X$  for  $A \leq 12$  would help.

### 8.5. The fast backward pion production

In the previous subsections we have considered production of FB light nuclear fragments. The history of studying production of other hadrons in the kinematical region forbidden for the scattering from a free stationary nucleon starts from the well-known experiment by Lederman and colleagues [1]. In this experiment the below threshold  $\bar{p}$ -production was investigated with the aim to measure the high

† We want to point out that the  $A$  dependence calculated on the basis of eq. (8.17) is much faster than original Batler and Pearson estimate [173], where it was assumed that nucleons are emitted from the whole nuclear volume but not from a tube as in the Glauber approach of section 7.4.

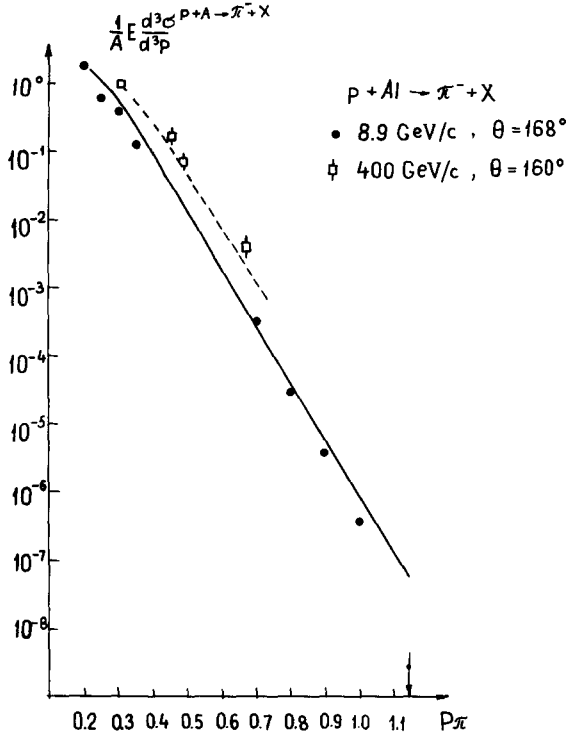


Fig. 8.16. Comparison of the FNC model predictions with the FB pion yields at  $E_p = 9$  GeV [17] and  $E_p = 400$  GeV [18].

momentum component of nuclear WF.<sup>†</sup> Recently the FB pion production with similar kinematics was rather extensively studied mostly for proton projectiles in the range  $T_p = 0.6\text{--}400$  GeV [11–13, 17–20, 22, 34, 35, 192]. Since only few limited data samples are available for production of other FB particles: K,  $\Lambda$ ,  $\bar{p}$  [193, 183],<sup>‡</sup> we shall restrict our analysis to the pion case.

### 8.5.1. Main features of the data

Though the FB pion yield is much smaller than the nucleon yield (for example at  $E_p = 400$  GeV [18]  $G_p^{C/\pi^-}(\alpha, p_\perp)/G_p^{C/p}(\alpha, p_\perp)|_{\alpha=1.5, p_\perp=0} \approx 5 \times 10^{-4}$ ) there are several common features in p,  $\pi$  production: (a) the invariant cross section  $G_p^{A/\pi}(p_\pi)$  decreases roughly exponentially with the pion kinetical energy  $T_\pi$  (see, e.g. fig. 8.16); (b)  $\alpha$  dependence of  $G_p^{A/\pi}$  at small  $p_\perp$  is rather close to that of  $G_p^{A/p}$ ; (c) the momentum shape of  $G_p^{A/\pi}$  of the spectra weakly depends on  $A$  (for  $A \geq 4$ ) in the kinematical region forbidden for the scattering from a free nucleon and for  $\alpha < 1.5$  the spectra are proportional to  $G_p^{D/\pi}$  (fig. 3.22); (d) at high energies and  $\alpha_\pi > 1$   $G_p^{A/\pi}(\alpha)$  increases with  $A$  roughly as  $G_p^{A/p}(\alpha)$  for  $A \leq 12$ , though for  $A > 12$  the increase of  $G_p^{A/\pi}$  with  $A$  is much more slow (fig. 8.7).<sup>§</sup> A similar trend is

<sup>†</sup> It was assumed in the analysis that  $\bar{p}$ 's produced in the collision of the projectile with a high momentum nucleon of the target nucleus. This natural assumption was then used in many analyses of FB pion production. However in the theoretical analysis [1] the recoil effect (cf. eq. (7.20)) was neglected. As a result it was not taken into account that the scattering off two-nucleon correlations was forbidden in the studied kinematics. Thus [71] the extracted WF considerably underestimated the high momentum nucleon component of the nuclear WF.

<sup>‡</sup> No peculiarities were observed in these measurements as compared to pion production. One possible exception is a rather large polarization of  $\Lambda$ -particles emitted with  $\theta \sim 90^\circ$  [192, 183] which is difficult to interpret now since the  $\Lambda$  polarization in the projectile–nucleon collisions is poorly known in the energy range involved ( $< 10$  GeV).

<sup>§</sup> Similarity of  $\alpha$ -distributions and  $A$ -dependence (for  $A < 12$ ) of FB proton and pion yields seems to be an important phenomenological indication of the common origin of these particles, at least for light nuclei.

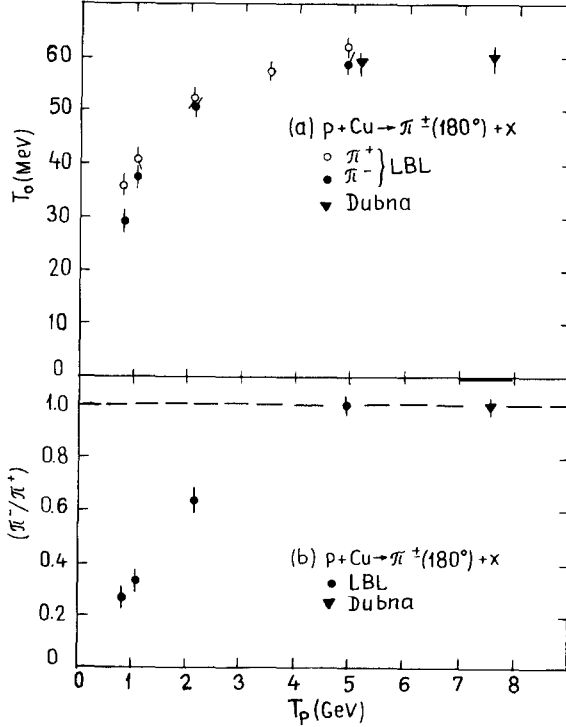


Fig. 8.17. Energy dependence of (a)  $T_0$  parameter for pions, and (b) the  $(\pi^-/\pi^+)$  ratio at  $180^\circ$  obtained by integrating each spectrum up to 100 MeV for  $p$ -Cu collisions from 0.8–4.89 GeV [22].

observed at the intermediate energies ( $T_p \leq 0.8$ ) [34, 35] where  $A$ -dependence of both  $p$  and  $\pi$  spectra is considerably more slow.

The onset of limiting fragmentation was studied quite recently [22] for  $\theta_{lab} = 180^\circ$  and  $T_\pi \leq 0.5$  GeV. The data indicate that the limiting value is reached first at small  $T_\pi$  (small  $\alpha_\pi$ ) and that the region where the limiting fragmentation is reached increases with the projectile energy. (This is similar to the pattern of scaling onset discussed in section 8.3 for nucleon production.) Thus in the region  $T_\pi < 0.5$  GeV the slope of the energy spectra  $T_0(G_p^{A/\pi}(T_\pi) \sim \exp(-T_\pi/T_0))$  increases rapidly with primary energy up to  $\sim 3$ –4 GeV, where a limiting value  $\approx 60$  MeV appears to be reached (fig. 8.17a).

The  $\pi^-/\pi^+$  ratio is small at  $T_p \leq 1$  GeV then rises sharply and reaches a limiting value  $\sim 1$  again around 3–4 GeV (fig. 18.17b). Really, the approximate equality of  $\pi^-$ ,  $\pi^+$  yields at high energies is a consequence of the general properties of strong interaction – dominance of vacuum exchange and approximate equality of the number of protons and neutrons in nuclei.‡

**Theoretical discussion.** We shall demonstrate below that the FNC model enables to describe the basic features of the FB pion production without introducing any new parameters into the model.

† It was observed in [22] that there is apparently no scaling in  $x = p_\pi^{\text{cm}} / (p_\pi^{\text{cm}})_{\text{max}}$ , expected in the model of Schmidt and Blankenbecler (e.g. at  $x = 0.2$  cross section varies by a factor  $10^3$  in the studied energy range). This is in line with the observation [71] that  $x$ -scaling is strongly violated for the case of nucleon production.

‡ Thus, we shall ignore preliminary indications [18] from 400 GeV,  $p + Ta \rightarrow \pi^\pm + X$  reaction at  $\theta_{lab} = 160^\circ$  that  $\pi^+/\pi^-$  ratio increases from about 1 at  $p_\pi \sim 0.5$  GeV/c to about 4 at  $p_\pi \sim 0.9$  GeV. Actually, calculations of the absolute value of  $G_p^{A/\pi}$  have led us to conclusion that it is  $\pi^+$  data that should be lowered.

### 8.5.2. High energies

The observed universality of the momentum shape of the pion spectra follows from universality of the shapes of (section 2.4) manifested in the universality of the FB nucleon spectra (section 8.1). The  $A$ -dependence of  $G_h^{A/\pi}$  is determined by the  $A$  dependence of  $\rho_A^N$  because production of FB pions in the interactions of secondary hadrons is strongly suppressed,  $\lambda_A^\pi \sim 1$  (see the discussion in section 7.4). Thus, for light  $A$  the  $A$ -dependences of  $G_p^{A/\pi}$ ,  $G_p^{A/p}$  should be approximately the same (cf. eqs. (7.18) and (7.25)). This is in good agreement with data [17, 18]. In particular in [17] a cluster structure of  ${}^6\text{Li}$  was observed not only for FB nucleons (section 8.1) but also for FB pions. The difference of  $A$  dependences of  $p$ ,  $\pi$  yields for  $A > 12$  is reasonably explained by the cascade enhancement factor  $\lambda_A^p$  for nucleon production (eq. (7.25)).

Indeed  $G_p^{A/p}/\lambda_A$  should be proportional to  $G_p^{A/\pi}$ . This agrees well with the 400 GeV data [18], provided we use the same  $\lambda_A$  as in sections 8.1–8.3 (broken curve in fig. 8.7).

A caution. The  $\pi N$  cross section in the discussed energy range of FB pions is larger than in the case of NN scattering. This could lead to some absorption of pions especially at the resonance energies via multi-step reactions like  $\pi + N \rightarrow N^*$ ,  $N^* + N \rightarrow N + N$  or  $\pi + d \rightarrow N + N$ . Probably, this effect was observed [17, 18] in the  $\Delta(1240)$  region. To suppress the final state interaction of FB particles one should measure  $K^+$  production. Note that  $G_p^{A/K^+}(\alpha)$  and  $G_p^{A/\pi}(\alpha)$  are expected to be rather close at large  $\alpha$  at high energies because

$$G_p^{N/K^+}(\alpha)/G_p^{N/\pi}(\alpha) \sim \frac{1}{3} - \frac{1}{5}$$

at large  $\alpha$  [140].

The similarity of  $\alpha$ -dependence of the  $p$ ,  $\pi$  spectra follows from the steep exponential decrease of  $\rho_A^N$  with  $\alpha$  because according to eq. (7.17)  $G_p^{A/\pi}$  is equal to the convolution of  $\rho_A^N(x) \sim \exp(-Bx)$  with  $B \sim 7$  and  $\rho_h^{N/\pi}(a/x) \sim (1 - a/x)^n$  with  $n \sim 2$ . Thus,  $G_p^{A/\pi}$  has the same exponential slope rather weakly modified by pre-exponential factor (cf. eq. (5.15)). As a result since at large  $p_\pi$

$$\alpha|_{p_{\pi\perp}=0} = (E_\pi + p_\pi)/m_N \approx 2T_\pi/m_N + m_\pi/m_N + O(m_\pi^2/m_N p_\pi)$$

we obtain  $T_0 \approx m_N/2B \approx 65$  MeV. The pre-exponential factor leads to small decrease of  $T_0$ . This value of  $T_0$  is in good agreement with the value of  $T_0$  at large energies [17, 18, 22] (see fig. 8.17a).

*Let us now consider the absolute value of  $G_p^{A/\pi}$ .* In the  ${}^4\text{He}$  case we use the data on  $G_p^{D/\pi}$  obtained in the same experiment (which were analysed in section 3.5) to calculate the contribution of the two-nucleon correlations and apply eq. (7.18) to determine the three-nucleon correlation contribution, which is a small correction at small  $\alpha$  but dominates at  $p_\pi \geq 0.6$  GeV/c. The result of calculation shown by the shaded region in fig. 3.22 is in good agreement with the data [13].

For heavier nuclei we use the model WF introduced in section 5 (eq. (5.11)) and calculate  $G_p^{A/\pi}$  on the basis of eq. (7.18).

In the case of Dubna data [17] we can use  $G_p^{p/\pi^\pm}$  measured in the same experiment, thus avoiding uncertainties in the absolute normalization of the data. This procedure (which is similar to the calculation of section 3.5 for  $G_p^{D/\pi}$ ) leads to the solid curve in fig. 8.16. In the case of 400 GeV data [18] there is no measurement of the  $p + p \rightarrow \pi^\pm + X$  reaction in the region of large  $\alpha$  and  $p_\perp \sim 0$  necessary for the calculation. This introduces a considerable uncertainty in the calculation.

Experimentally [18]  $G_p^{A/\pi}$  is proportional  $A$  in the region of small  $p_\perp$  at  $\theta = 160^\circ$  permitted for

scattering from a free stationary nucleon. However an experimental fit [140] to the data of reaction  $p + p \rightarrow \pi + X$  obtained at rather large  $p_\perp$  extrapolated to this region leads to cross section which is smaller than the observed one by a factor 2. This could be due to inadequacy of these fits at low  $p_\perp$ .

Thus, we renormalize the fits by the factor 2. The result of calculation is given by the dashed curve in fig. 8.16. Similar fits were obtained for other emission angles. However in this case there is an additional uncertainty since  $\rho_A^N(\alpha, k_\perp)$  is not known well at large  $k_\perp$ . Thus, we conclude that the FNC model gives reasonable description of the data. However to increase the accuracy of predictions the measurements of the elementary cross section for large  $x$  and  $p_\perp \sim 0$  are necessary.

### 8.5.3. Intermediate energies

Change of  $A$ -dependence and of the energy slope  $T_0$  in the transition from high to intermediate energies is determined basically by the same two factors as in the case of FB nucleon production: decrease of essential longitudinal distances, and suppression of the two-nucleon correlation contribution. In the case of intermediate energies these effects can be taken into account using eq. (7.20). This has not been done so far. (The same equation is valid for light nuclei in the transition region, though for  $A > 12$  a specific model of  $hA$  interaction at the medium energies is necessary.)

Note that the spectral function  $\tilde{\rho}(\alpha, k_\perp, M_{\text{Rec}}^2)$  in eq. (7.20) can be approximated by the effective (reduced) single nucleon density matrix which describes the proton production at the same projectile energies (see eq. (7.16) and section 8.2). It is easy to check that the momentum dependence of this effective single nucleon density matrix is close to that extracted from the same data by Frankel [59] in the framework of model [44]. Thus, since the pion yields observed at  $T_p = 0.6 \text{ GeV}$  [35],  $T_p = 0.73 \text{ GeV}$  [34] were found [35] to be in agreement with the effective WF of Frankel they should be reasonably described also by the FNC model.

Another qualitative consequence of eq. (7.20) is the decrease of  $\pi^-/\pi^+$  ratio with decrease of  $T_p^{\text{inc}}$ . This ratio can be roughly estimated assuming that leading pions are produced via reaction  $p + N \rightarrow \Delta + N$ . If  $N = Z = A/2$  we have

$$\frac{G_p^{A/\pi^-}}{G_p^{A/\pi^+}} \approx \frac{G_p^{p/\pi^-} + G_p^{n/\pi^-}}{G_p^{p/\pi^+} + G_p^{n/\pi^+}} \approx \frac{1}{11}.$$

This value qualitatively agrees with the data [22] where at  $T_p = 0.8 \text{ GeV}$  this ratio is equal 0.25 (fig. 8.17b).

On the basis of eq. (7.20) we could expect the same kind of  $n$ -scaling for the ratios of pion yields as for the ratios of proton yields which was observed in section 8.2,<sup>†</sup> i.e. the ratios of pion yields and nucleon yields in the  $j$ -nucleon correlation region should be approximately the same. Though this relation agrees with the data [34] for  $A < 27$ , for larger  $A$  the pion yield slower increases with  $A$  than the proton yield. As a result  $R = (G_p^{\text{Pb}/\pi^-}/G_p^{\text{Be}/\pi^+})/(G_p^{\text{Pb}/p}/G_p^{\text{Be}/p}) \approx 1/2$  instead of 1 expected on the basis of eqs. (7.16), (7.20). Probably this violation is due to pion absorption, because the data were obtained in the  $p_\pi$  region corresponding to  $\Delta$ -isobar where high energy data [17, 18] indicate presence of the minimum in the  $A$ -dependence of the pion yield. To clear up this point the measurements are necessary for  $p_\pi > 0.4 \text{ GeV}$ .

In summary, the FNC model provides reasonable description of the pion yield. More detailed calculations are necessary to describe quantitatively the energy dependence of the shape of distribution.

<sup>†</sup> It is easy to define variable  $n$  for pion production so that it would vary from  $j - 1$  to  $j$  in the  $j$ -nucleon correlation region (see [185]).

The problem of the final state pion interaction should be also cleared up. The study of  $K^+$  production would be of much help in this point.

### 8.6. Discussion of other models of the fast backward particle production

During recent years a large number of models have been suggested for the explanation of certain features of the data. Evidently the experimental investigation of FB particle production is by no means completed.<sup>†</sup> Nevertheless we shall explain below that the existing data put strong constraints on the production mechanism.

First let us consider approaches which relate the FB particle production to the presence of a high momentum nucleon component in the nuclear WF.

(a) Average field models [37, 44, 46, 59, 61, 63]. It is assumed in these models that the fast nucleon momentum is balanced by the rest of the nucleus, but not by one or two nucleons as in the FNC model. As a result only the direct mechanism (section 7.3) contributes to the FB particle yield, i.e. the fast backward particle is produced in the projectile-fast backward nucleon collision. An additional assumption is made in these works that the impulse approximation can be used. (It is hard to justify the last assumption at the intermediate energies since the projectile does not penetrate the interior of the nucleus (cf. discussion in sections 7.2, 8.2). However this is not essential for the model predictions of the shape of momentum distributions. At high energies the application of the impulse approximation can be understood in a Pickwickian sense due to the AGK cancellation of the Glauber screening correction for the inclusive spectrum<sup>‡</sup>: the hadron projectile interacts with several nucleons, producing  $\nu \sim A^{1/3}$  forward nucleons in association with the FB particle. The average field model was introduced independently by Amado and Woloshyn [44] in response to the backward proton experiments of Frankel et al. [23] at  $T_N = 0.6\text{--}0.8\text{ GeV}$  and by Schmidt and Blankenbeckler [46, 47] who analysed the LBL data [11, 12] in the range  $T_N = 1\text{--}2\text{ GeV}$ .<sup>§</sup> It was then developed and compared with the data in a number of works [59, 61, 63].<sup>¶</sup> The basic difference between the approaches is in the choice of  $\rho_A^N(\alpha, k_\perp)$ . In [46] it was assumed on the basis of the quark counting rules that

$$\rho_A^N(\alpha, k_\perp) \sim (1 - \alpha/A)^{6A-7} \quad (8.18)$$

while in [44, 59] the mass of the recoiling  $A - 1$  nucleon system was considered independent of the momentum of the interacting nucleon (coherent recoil). Then in the limit of large  $A$

$$\begin{aligned} \rho_A^N(\alpha, k_\perp) &= m_N A n_N(k) \\ k &= \sqrt{m_N^2(1 - \alpha)^2 + k_\perp^2} \end{aligned} \quad (8.19)$$

<sup>†</sup> For extensive list of necessary experiments see [71b,d].

<sup>‡</sup> It is worth noting that the impulse approximation picture of the FB nucleon production, motivated by hard collision models [194] cannot explain the observed large cross section of the simultaneous emission of several FB nucleons [181, 182]. The interpretation of FB nucleon production as hard process is hardly compatible with the large multiplicity of FB nucleons (e.g.  $\langle n_p \rangle_{pN>0.3\text{ GeV}/c, \theta>90} \approx 0.8$  in pTa collisions at  $E_p = 400\text{ GeV}$ ) since in NN collisions hard processes constitute a small fraction ( $\sim 10^{-2}$ ) of the total cross section.

<sup>§</sup> Note that LBL data for nuclear fragmentation cover the range  $p_N < 0.2\text{ GeV}/c$  which is traditionally interpreted as evaporation.

<sup>¶</sup> The predictions of the average field model and the FNC model differ most apparently in the case of the FB nucleon production where according to the FNC model the spectator mechanism dominates. Thus, we shall restrict this discussion to the case of nucleon production.

where  $n(k)$  is the single nucleon density matrix which was taken in the form

$$n(k) \sim \exp(-k/k_0). \quad (8.20)$$

As seen from eqs. (8.18), (8.19), (8.20) both models predict a quite similar form of  $\rho_A^N(\alpha, 0)$  at  $A \gg 1$ ,  $1 < \alpha < A$ , namely

$$\rho_A^N(\alpha, 0) \sim \exp(-D\alpha)$$

where  $D \approx 6$  [44],  $D = m/k_0$  [59].

At high energies the form eq. (8.18) reasonably fits the shape of FB nucleon spectra for  $A \geq 4$  at  $p_\perp = 0$  (see fig. 8.1) while for  $A = 2$  it does not reproduce the shape of the spectra (fig. 3.18). At the same time the value of  $k_0$  extracted from the data [23–26] at  $T_p = 0.6\text{--}0.8 \text{ GeV}$ , which corresponds to  $D \sim 13$  does not fit the high energy data (fig. 8.1). Thus, the average field model does not provide a consistent description of the energy dependence of the shape of the spectra. In particular if from  $D = 7$  the high energy fit is used to describe the intermediate-energy data [23–26] the predicted yield is much larger and smoother than the experimentally observed one.

It is also difficult to explain in this model the absolute value of high energy proton yield. This problem is present not only in the case of neutrino scattering [9] (see [87] section 6 and in particular fig. 6.4) but also in the case of hadronic reactions. For example, to explain the data [13] on the  $p + {}^4\text{He}$  reaction the value  $\int n(k) d^3k \theta(k - 0.35 \text{ GeV}/c) \geq 0.5$  is necessary, which is hard to adjust in the conventional theory of  ${}^4\text{He}$ .<sup>†</sup> For heavier nuclei the necessary integral would exceed unity.

In the case of intermediate energies the correlation measurements of Komarov et al. [27, 28] present additional difficulty for this model. Note also that the analysing power of the inclusive reaction  $p + A \rightarrow p + X$  was found [30, 31] to be much smaller than the prediction of Frankel and Woloshyn [191].

(b) In the Weber–Miller model [49] the spectator mechanism for the average field configurations was considered i.e. it was assumed that the projectile scatters from the  $(A - 1)$  nucleon recoiling system. This mechanism can give a considerable contribution for  $p_N \sim 0.3 \text{ GeV}/c$ , i.e. for momenta close to the average one. However at larger momenta it is strongly suppressed due to final state interaction (see section 7.4 and [53, 71]). In the model certain basic experimental data can hardly be explained such as universality of nucleon spectra from light and heavy nuclei and from lepton and hadron projectiles, angular anisotropy of the FB nucleon emission  $\langle x \rangle_\alpha - \alpha$  correlation in  $\bar{\nu}\text{Ne}$  scattering.

The mechanisms of FB particle production discussed below are based on the specific hypotheses on the strong interaction and/or nuclear structure.

(c) It was suggested in [50, 52] that FB particles are produced in the projectile interaction with a compact group of nucleons-cluster, termed fluctuons after the mechanism proposed by Blokhintsev [195] and recast in the parton language by Baldin [36]. It was assumed [50, 52] that collision is hard and that FB particles originate from parton decays. It is not clear how to explain in the model (i) the universality of nucleon spectra in  $\nu$ ,  $\bar{\nu}$  and hadron scattering; (ii) the large value of  $p/\pi \geq 10^2$  (at the same  $\alpha$ ) for FB particle production (this ratio does not exceed 1/3 in high  $p_T$  processes [196]); (iii) different energy dependence of  $C(E)$  for light and heavy nuclei (experimentally there is no screening in hard collision processes); (iv) hard collision processes constitute a very small fraction of the NN total cross

<sup>†</sup> Here  $n(k)$  is normalized according to  $\int n(k) d^3k = 1$ .

section. Therefore large absolute rate of the FB nucleon production can hardly be explained. A reduction factor giving the probability that the nucleons are at small relative distances is also present in this approach; (v) the origin of  $\langle x_\alpha \rangle - \alpha$  correlation in  $\bar{\nu}$  Ne scattering is not clear.

An attempt to combine the cluster decomposition with the model of Schmidt and Blankenbecler [46] which is quite similar to the flucton model was undertaken in [63]. However only the shapes of pion momentum distributions were considered in this model.

(d) In several papers [197] it was assumed that the incident hadron coherently interacts with  $\nu$  nucleons at its impact parameter as with a single hadron of mass  $\nu m_N$  (this model is often referred to as a coherent tube or effective target model). Analysis of the Bethe–Heitler process in section 2.1 (see also section 4.2) demonstrates that no such coherency arises in the perturbation theory of QED or QCD. Generally this is due to the fundamental property of the strong interaction that the Lorentz contraction of longitudinal distances, the main motivation of the models [197], is combined with a slowing down of the interaction (time dilatation). Note also that only pion production, which constitutes a small fraction of FB nucleon production is considered in the model [197]. (For a recent critical comparison of the coherent tube model with the correlation data in hA scattering see [168].)

(e) Several cascade mechanisms were suggested in the literature for FB particle production (i) elastic rescatterings of secondary protons at fixed nucleons [198], (ii) rescattering of secondary heavy resonances [38, 64, 199]. For this mechanism rather small internucleon distances are essential, (iii) absorption of secondary slow pions by quasideuteron pairs [200] (these calculations overestimate the effect due to neglect of wave properties of slow particles [174] (see section 7.4)). To calculate this effect reliably one should properly account for the time of hadron formation. This has not been done so far. In [201] an ad hoc assumption was made that some heavy clusters are produced. It was further assumed that such cluster can accumulate mass from several nucleons and decay with emission of FB particles. It is difficult to explain in these cascade approaches (even qualitatively) various regularities of the experimental data: the universality of nucleon spectra from light and heavy nuclei, similarity of  $\alpha$ -dependences of  $p, \pi$  spectra, large ratio of  $p, \pi$  yield, correlations in deep inelastic scattering, different magnitude and sign of the polarization of FB nucleons for  $\pi$  and  $p$  projectile, etc.

Let us summarize this section. We have demonstrated that the FNC model gives a quantitative description of a large number of regularities observed in the fast backward nucleon and pion production for different projectiles and in a wide energy range. It seems to us that any successive competing model should provide a consistent description of the regularities of the data reviewed in this section and in sections 3, 5 and 6. The above consideration indicates that this program is not simple and has not been attempted yet in other models.

## 9. Summary and outlook

The theoretical analysis of available experimental data performed in this review shows that special high energy processes present an effective method for studying short-range correlations in nuclei especially in the case of lightest nuclei. If this conclusion is confirmed for nuclei of average size and for heavy nuclei by direct experiments it would have strong impact on the future development of nuclear physics, the theory of strong interaction and astrophysics. Hopefully, the processes discussed in this review will provide a possibility to study the properties of superdense matter in the laboratory. They may help to

transform the nucleus into a well-understood instrument for the investigation of the space-time evolution of strong interactions. Since the necessary experiments can be performed at existing high-energy facilities (used now for the purposes of elementary particle physics) one can achieve fast progress in this field. Throughout the review we have enumerated some experiments, which are necessary to confirm or to reject the existence of relativistic nuclear physics as an independent subject which deserves special study. Below we shall briefly summarize some of the experiments which we believe to be of top priority. All these experiments are devoted to incoherent processes which are much more efficient for our purposes than coherent experiments like high  $Q^2$  elastic lepton, hadron scattering. These proposed experiments are:

(A) ( $e, e'$ ) deep inelastic reactions at  $x \geq 1$  and for large invariant mass of the hadron final state are a direct method to establish the absolute size of the high momentum nucleon component in the nuclear wavefunction. The expected effect is large  $(1/A)F_{2A}(x, q^2)|_{x \sim 1.2} \approx (6-8) \frac{1}{2}F_{2D}(x, q^2)$  (see section 5) and it can be studied e.g. at the SLAC 20 GeV linac. For small  $A$  ( $2 < A \leq 7$ ) the cluster structure of nuclei can be investigated. Similar though not so easily interpretable information can be obtained from high  $Q^2(e, e')$  processes near the elastic threshold.

(B) A systematic study of ( $e, e'p$ ) deep inelastic reactions with fast backward proton in the nucleus rest frame gives the practical possibility to measure the value of high momentum nucleon components and to separate short-range pn, pp, three nucleon correlations etc. (section 6).

(C) The investigation of high energy reactions  $(e, \gamma, h) + D \rightarrow p + \dots$  with a polarized deuteron target is necessary to check directly the nuclear core hypothesis. For backward proton momentum  $> 0.2-0.3$  GeV/c in the deuteron rest frame the cross section of these processes should strongly depend on the deuteron polarization (see fig. 3.9).

(D) systematic study of sufficiently high energy (ISR?) fragmentation processes  $h + A \rightarrow p(\pi) + \dots$  from the lightest nuclei at  $x_F > 1.5$  is important for investigation of few nucleon correlations and for a comparison of the QCD-prediction concerning few nucleon correlations with experiment (see section 4).

## Acknowledgements

We are grateful to V.N. Gribov for his stimulating discussions of the problems of a relativistic description of the bound state during last seven years. We are indebted to V.N. Gribov and A.B. Migdal for an illuminating explanation of the L.D. Landau attitude to the relationship between microscopic and Fermi liquid approaches to the theory of many-body system with strong interaction. We would like to thank the staff of LNPI and ITEP theoretical departments especially Y.I. Azimov, D.I. Dyakonov, L.N. Lipatov and M.G. Ryskin for fruitful discussions of problems of quantum field theory and QCD. We thank also A.M. Baldin, J.D. Bjorken, K.A. Ter-Martirosyan for stimulating questions and encouragement. We are indebted to V.A. Khodel, V.N. Efimov and L.A. Sliv for valuable discussion of nuclear structure. It is a great pleasure to acknowledge numerous enlightening discussions and stimulating correspondences with the members of experimental groups involved in the study of short-range nuclear structure in ITEP, IHEP, JINR, EPI, SLAC, FNAL and especially R. Arnold, B. Chertok, K. Egyan, V.B. Gavrilov, V.S. Kaftanov, V.D. Khovansky, V.V. Komarov, E. Kuznetsov, V. Makeev, G.A. Leksin, F. Nezrick, M.M. Savitsky, V.S. Stavinsky, B. Roy, L. Schröder. We are also grateful to G. Brown for thorough reading of the manuscript and valuable comments.

## Appendix A. QCD constraints for relativistic description of the nucleus

The aim of this appendix is to demonstrate that exact sum rules valid in any renormalizable quantum field model (QCD) put certain constraints on the approximation schemes of the nucleus.<sup>†</sup>

The first group of sum rules are the Adler, Dashen, Gell-Mann, Fubini sum rules for the amplitude of the process  $J^\alpha + A \rightarrow J^\beta + A$  valid at any  $q^2$  [109]. Here  $J^\alpha$  is a vector current and  $\alpha$  is its SU(3) index.  $A$  denotes the target. For the structure function  $F_{2A}(\nu, q^2)$  defined by eq. (3.10) for any target these sum rules have the form:

$$\frac{1}{\pi} \int F_{2A}^{\alpha\beta}(\nu, q^2) \frac{d\nu}{\nu} = i f^{\alpha\beta\gamma} \left. \frac{\langle A | J_0^\gamma | A \rangle}{2E_A} \right|_{E_A \rightarrow \infty}. \quad (\text{A.1})$$

Here  $f^{\alpha\beta\gamma}$  are structure constants for SU(3). In quantum field theory (QCD) this sum rule accounts for probability conservation.

For  $q^2 \rightarrow -\infty$  an additional sum rule is valid in quantum field theory

$$\sum_j \int_0^1 D_A^j(x, q^2) dx = \left. \frac{\langle A | T_{00} | A \rangle}{P_A^2} \right|_{P_A \rightarrow \infty}. \quad (\text{A.2})$$

Here  $D^j(x, q^2)$  is the density of the partons of the sort  $j$  [110], a conventional generalization of  $F_2(x, q^2)$  to account for different types of partons (quarks, gluons). The sum in eq. (A.2) goes over all sorts of partons  $j$ . The sum rule (A.2) follows directly from the condition that all momentum of the target  $A$  is carried by partons.  $T_{\mu\lambda}$  is the energy-momentum tensor. The right hand side of eq. (A.2) is independent of the target due to the condition  $q_\mu T_{\mu\lambda} = 0$  (universality of graviton interaction).

Since eqs. (A.1), (A.2) are valid for any target they can be used to put constraints on the approximate description of the nuclear structure. For illustration we consider here models, which assume that the nucleus is a many nucleon system. In these models  $F_{2A}(\nu, q^2)$  is expressed through the nucleon structure functions and nucleon density matrix  $\rho_A^N(\alpha, k_\perp)$  (see eqs. (5.1)). Substituting  $F_{2A}$  into sum rules (A.1), (A.2) applying eqs. (5.1) and using the sum rules (A.1, 2) for nucleon structure function we deduce sum rules for  $\rho_A^N(\alpha, k_\perp)$ :

$$\int_0^A \frac{d\alpha}{\alpha} \int d^2 k_\perp \rho_A^N(\alpha, k_\perp) = A \quad (\text{A.3})$$

$$\int_0^A \frac{d\alpha}{\alpha} \alpha \int d^2 k_\perp \rho_A^N(\alpha, k_\perp) = A. \quad (\text{A.4})$$

Our approach used in this review uses infinite momentum frame WFs for the nucleus. Then eqs. (A.3), (A.4) are naturally fulfilled due to the normalization of the nuclear WF (see section 2.4).

<sup>†</sup> Such constraints are of special importance for the models used in the analysis of data on the deep inelastic scattering off nuclei, since these data are often used to check the validity of the sum rules discussed in the Appendix. So if a model does not satisfy the discussed constraints this would lead to an artificial violation of the sum rules.

On the contrary in the Bethe-Salpeter (BS) formalism with virtual nucleons both eqs. (A.3), (A.4) are not fulfilled. In this approach the region of integration is  $-\infty < \alpha < A$  (cf. eq. (3.14)). As a result this method leads to the so called West correction of the total cross section, which is comparable to the Glauber correction in the case of scattering from the deuteron [128]. It is easy to check however by analysing how singularities in the energy plane pinch the contour of integration in the Feynman diagrams that contribution of the region  $\alpha < 0$  is exactly cancelled. It was demonstrated in [43, 58] by exact calculation of the simplest triangle Feynman diagram. A transition to IMF diagrams is another way to obtain this result.

In the approach with IMF BS WF [43, 46–48, 57, 61, 69] the condition  $0 < \alpha < A$  and the sum rule (A.3) are valid. However due to lack of symmetry between interacting nucleon and nucleon-spectator sum rule (A.4) is violated.

Note that the approach with scattering amplitudes from virtual particles with large spin  $\geq 2$  (clusters of nucleons within nucleus) leads to another puzzle. Analyticity and unitarity state that in impulse approximation the cross section for the scattering from a virtual boson or fermion with spin  $j$  increase with incident energy more rapidly than  $S^{4j-5}$  or  $S^{4j-7}$  respectively [202], i.e. they violate the Froissart bound.<sup>†</sup>

## Appendix B. Properties of $\ell + N \rightarrow \ell' + N' + X$ deep inelastic reactions

To estimate the proton spectrum in reaction  $\ell + N \rightarrow \ell' + N' + X$  at high  $Q^2$  we assume in line with quark-parton model and QCD calculations in the leading logarithmic approximation that each spectator configuration, i.e. each nucleon without a knocked-out parton, fragments independently:

$$\frac{d\sigma^{\ell+N \rightarrow \ell'+N'+X}}{dx dy (dz/z) d^2 p_\perp} = \sum_{q,\bar{q}} q^N(x, q^2) \cdot \frac{d\sigma^{\ell+q \rightarrow \ell'+q}}{dy} (xE_\nu) G_q^{N/p}(z, p_\perp, x, q^2).$$

The sum is taken over all sorts of partons;  $q^N(x, q^2)$  are the conventional parton distributions,  $G_q(z, p_\perp, x, q^2)$  are the fragmentation functions of the rest of the nucleon (nucleon without quark  $q(x, q^2)$ ),  $z = \alpha/(1-x)$ .

The main properties of  $G$  are the following ones (see e.g. the discussion in [45b]): (i)  $G = 0$  for  $z > 1$ , (ii) for small  $x$  (scattering off sea partons)  $G \sim \text{const.}$  at  $z \rightarrow 1$ , (iii) for large  $x$  (scattering off valence quarks)  $G \sim (1-z)$  at  $z \rightarrow 1$ , (iv)

$$\sum_{N=p,n} \int_0^1 (G_{q(\bar{q})}^{N/N_1}(z, k_\perp) - G_{q(\bar{q})}^{N/\bar{N}_1}(z, k_\perp)) \frac{dz d^2 k_\perp}{z} = \frac{2}{3} \binom{4}{3}$$

(here  $G_{q(\bar{q})}^{N/N_1}$  includes decays of baryonic resonances).

Using rather limited data on the reactions  $e + p \rightarrow e + p + X$  [132],  $e + p \rightarrow e + \Lambda + X$  [203] and above constraints we choose  $G_{q,\bar{q}}$  in the form:

$$G_{\text{val}} = (1/2.1)(B/\pi)\sqrt{z}[(1-z)\theta(z-0.6) + 0.4\theta(0.6-z)] \exp(-Bp^2)$$

$$G_{\text{sea}} = \frac{1}{4}(B/\pi)\sqrt{z} \exp(-Bp^2), \quad B = 4(\text{GeV}/c)^{-2}.$$

<sup>†</sup> Evidently the enumerated drawbacks of using the off-mass-shell amplitudes are a consequence of the approximations made and one should not extend them to the general notion of virtual particle.

### Appendix C. The behaviour of the QCD vertices in the limit $x \rightarrow 1$

We present here the rules necessary for the asymptotic calculation of light-cone diagrams in QCD perturbation theory at  $x \rightarrow 1$ . It is convenient to use the infinite momentum gauge  $A_0 = A_z$ . The diagram technique, which is similar to that in QED [144], is given in [65b]. It is easy to demonstrate (see e.g. [65]) that in leading order in  $\alpha_s$  and  $(1-x)$  diagrams with 3, 4 gluon vertices and with instantaneous quark exchanges do not contribute. Therefore only diagrams with emission (absorption) of transverse gluons and instantaneous Coulomb exchange are essential. Exchange by transverse gluons gives large contribution if the gluon carries large fraction of quark longitudinal momentum. In this case

$$p_i = x_i P, p_{i\perp}$$

$$\bar{u}(p_1) \gamma_\mu u(p_2) \epsilon_\mu^{(g^\pm)}|_{x_2/x_1 \rightarrow 0} \Rightarrow m \sqrt{\frac{x_1}{x_2}} \lambda_g \delta_{\lambda_g \lambda_1} \equiv G_{q\bar{q}g_T}. \quad (\text{C.1})$$

Here  $\lambda_1/2(\lambda_g)$  is the helicity of the fast quark (gluon). On the contrary, contribution of the Coulomb exchange is large if  $x_1 \sim x_2$ . In the case of  $x_2/x_1 \rightarrow 0$  the Coulomb exchange contribution is suppressed:

$$\frac{\bar{u}(p_2) \gamma_0 u(p_1) \bar{u}(p_3) \gamma_0 u(p_4)}{q^2} \Rightarrow \frac{\sqrt{x_1 x_2 x_3 x_4}}{(x_1 - x_2)^2}. \quad (\text{C.2})$$

The expressions for the energy denominators are the same as in  $\lambda\varphi^3$  theory.

If the diagram can be constructed using only maximal vertices ( $G_{q\bar{q}g_C}$  with  $x_1 \sim x_2$  and  $G_{q\bar{q}g_T}$  with  $x_1/x_2$  or  $x_2/x_1 \rightarrow 0$ ) the behaviour of the structure function is the same as according to quark counting rules. Otherwise the cross sections are smaller than according to the quark counting rules.

Let us give some examples: (a) Pion structure function. It is described by the diagram of fig. C1 (the  $g_T$  exchange gives a similar contribution)

$$\begin{aligned} F_{2\pi}(x) &\sim \int \frac{G_{q\bar{q}g_C}^2}{[(m^2 + k_\perp^2)/x + (m^2 + k_\perp^2)/x_2 - m_\pi^2]^2} \frac{dx_2}{x x_2} \delta(x + x_2 - 1) d^2 k_\perp \\ &\sim (1-x)^2 (1-x) \frac{1}{(1-x)} \sim (1-x)^2. \end{aligned} \quad (\text{C.3})$$

This is the well known result of Farrar and Jackson [145]. In the nucleon case only diagram of fig. C2

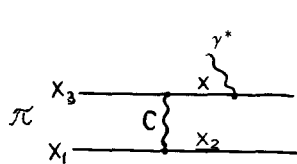


Fig. C1.

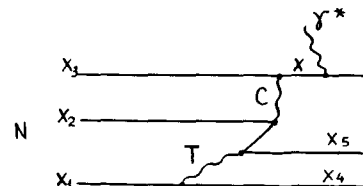


Fig. C2.

contributes:

$$F_{2N}(x) \sim \int \frac{dx_4 dx_5 d^2 k_{\perp 4} d^2 k_{\perp 5}}{x_4 x_5 x} \delta(1 - x - x_4 - x_5) \\ \times \frac{1}{((m^2 + k_{\perp 4}^2)/x_4 + \text{const})^2 \cdot ((m^2 + k_{\perp 4}^2)/x_4 + (m^2 + k_{\perp 5}^2)/x_5 + \text{const})^4} \left(\frac{1}{\sqrt{x_4 x_5}}\right)^2 \sim (1-x)^3. \quad (\text{C.4})$$

Contribution of other diagrams is suppressed by a small factor  $\sim (1-x)^2$ . For example calculation of the diagram of fig. C3 where the C gluon is changed to the transverse gluon leads to:

$$\int \frac{dx_4 dx_5}{x_4 x_5} d^2 k_{\perp 4} d^2 k_{\perp 5} \delta(1 - x - x_4 - x_5) \\ \times \frac{(\sqrt{x_4 x_5})^2}{[(m^2 + k_{\perp 4}^2)/x_4 + \text{const}]^4 \cdot [(m^2 + k_{\perp 4}^2)/x_4 + (m^2 + k_{\perp 5}^2)/x_5 + \text{const}]^4} \sim (1-x)^5. \quad (\text{C.5})$$

The additional suppression factor  $\sim (1-x)^2$  is due to the presence of two additional energy denominators which are not compensated by maximal vertices.

Although the  $x$  dependence of  $F_{2N}(x)$  as given by eq. (C.4) is in reasonable agreement with experimental data one can not use perturbative QCD to calculate the absolute value of  $F_{2N}(x)$ . The simplest way to discover this problem is to check that in eq. (C.4) the integration region  $k_{\perp}^2 \sim m^2$  is essential. Since  $m$  (the bare quark mass) is small ( $\sim$  several MeV) this integration region corresponds to large impact parameters ( $\sim 1/m$ ) much larger than nucleon radius. This inconsistency shows that effects of confinement are essential in the calculation of the absolute value of  $F_{2N}(x)$ ,  $F_{2\gamma}(x)$ , etc. at  $x \rightarrow 1$ . Therefore at present perturbative QCD could be used only for dimensional estimates of  $F_{2h}(x)$ . For opposite attitude see e.g. [208].

In the attempts considered in section 4 to estimate the high momentum component of the two-nucleon WF we were faced with the same problems. There were several attempts to calculate this WF within the MIT bag model [209]. However the recent theoretical analysis [210] indicates that it is difficult to explain internucleon short-range repulsion in this model. This is not surprising since the bag model could be used to describe only the static properties of hadrons but not the scattering processes because the causality is violated in the model [209]. The simplest example is calculation of the pion decay within the bag model (I. Kobzarev, private communication). Indeed according to the bag model the decay arises due to annihilation of free  $q$  and  $\bar{q}$  within the bag cavity. After annihilation the gluonic cavity remains intact though only leptons should be present in the final state.

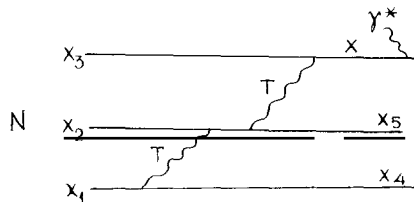


Fig. C3.

## Appendix D. On the correlations between the fast backward nucleons and the forward emitted particles

Selection of events with the FB nucleons should effect the spectra of the particles in the region permitted for the scattering from a free stationary nucleon. Study of such correlation could be of use for the experimental determination of the number of the target nucleons participating in the production of the FB nucleon.

The simplest case is the high energy lepton scattering from the light nucleus where secondary hadron interactions and rescatterings off the emitted nucleons ( $\pi, K$ ) off the residual nucleus can be neglected. In the two nucleon correlation approximation the inclusive cross section of the emission of the particle “a” with momentum  $\beta, p_\perp$  associated with the FB nucleon trigger with momentum  $\alpha, k_\perp$  ( $G_1^{A/a, N}$ ) is as follows (cf. eq. (3.17))

$$G_1^{A/a, N}(\alpha, k_\perp, \beta, p_\perp) = (\sigma_{in}^{1N})^{-1} G_1^{A/N}(\alpha, k_\perp) G_1^{N/a}(\beta/\alpha_1, +\beta/\alpha_1 \cdot (k_\perp + p_\perp)), \quad (D.1)$$

where  $\alpha_1 = 2 - \alpha$  is the light cone fraction of the struck nucleon momentum. We want to emphasize that the form of eq. (D.1) follows just from the Lorentz transformation law.\* Thus, it is convenient to introduce the correlation function  $B_1^{A/a}(\alpha, k_\perp, \beta, p_\perp)$ :

$$B_1^{A/a}(\alpha, k_\perp, \beta, p_\perp) = G_1^{A/a, N}(\alpha, k_\perp, \beta, p_\perp) / \{\sigma_{in}^{1N} G_1^{A/N}(\alpha, k_\perp)\}.$$

$B_1$  is equal to 0 for  $\beta > \alpha_1$ . This is just a consequence of the kinematics of the scattering off the two nucleon correlation.

It is convenient to consider the average  $\langle p_\perp \rangle_\beta$  for triggered events

$$\langle p_\perp \rangle_\beta = \frac{\int p_\perp B_1^{A/a}(\alpha, k_\perp, \beta, p_\perp) d^2 p_\perp}{\int B_1^{A/a}(\alpha, k_\perp, \beta, p_\perp) d^2 p_\perp} = -(\beta/\alpha_1) k_\perp. \quad (D.2)$$

This equation is valid for any particle “a” and it is insensitive to the relative amount of pp and pn correlations. Thus, it is feasible for experimental search of pair correlations. Eq. (D.2) should be compared with eq. (6.2) for the  $x - \alpha$  correlation in deep inelastic scattering.

Another quantity convenient for the experimental study is  $B_1$  averaged over  $p_\perp$ :

$$\int B_1^{A/a}(\alpha, k_\perp, \beta, p_\perp) d^2 p_\perp = \int G_1^{N/a}(\beta/\alpha_1, q_\perp) d^2 q_\perp \equiv \tilde{G}_1^{N/a}(\beta/\alpha_1). \quad (D.3)$$

Thus, this distribution in  $\beta$  differs from the one for the scattering off a free nucleon by the rescaling of the light cone fraction only. It follows from eq. (D.3) that the  $\beta$ -distribution for events with FB nucleon trigger is strongly shifted in the case of  $\pi, K$  production. In the case of nucleon production the change should be noticeable only in the region  $\beta > \alpha_1$ , where  $B = 0$  and for  $\beta \sim \alpha_1$  because for  $x = \beta/\alpha_1 \lesssim 0.5-0.7$  in the elementary  $\ell(h) + N \rightarrow N + X$  reaction  $\tilde{G}_{\ell(h)}^{N/N}$  weakly depends on  $x$ .

In the case of hadron projectiles the account of the Glauber screening in the interaction with the correlated pair (section 2.5) leads to the violation of eq. (D.1). However, one can prove using the approach developed in section 2.5, that eqs. (D.2), (D.3) are not changed.

\* At the intermediate energies eq. (D.1) is modified since in this case the Lorentz transformation has a more complicated form.

In the case of  $j \geq 3$  nucleon correlations the hadron projectile can inelastically interact with several nucleons of the correlation, leading to increase of the associated hadron multiplicity as compared to the average case. The correlation in the transverse momentum plane becomes weaker as  $\alpha_1 \simeq (3 - \alpha)/2$  in eq. (D.2). Similarly eq. (D.3) with  $\alpha_1 \simeq (3 - \alpha)/2$  should describe the shape of the distribution over  $\beta$  though not the normalization because several forward moving nucleons of the correlation could be struck.

For heavy nuclei the hadron projectile interacts with several nucleons ( $\sim \nu$ ). Thus, the correlations decrease approximately as  $1/\nu$ . However using the reggeon diagram technique one can prove that the average  $\langle p_\perp \rangle_\beta$  is determined by the interaction with the correlated pair only (contributions of other interactions is cancelled due to the symmetry of integration over  $p_\perp$ ). Thus,

$$\int p_\perp B_h^{A/a}(\alpha, k_\perp, \beta, p_\perp) d^2 p_\perp = -\frac{\beta}{\alpha_1} k_\perp \tilde{G}_h^{N/a}\left(\frac{\beta}{\alpha_1}\right). \quad (\text{D.4})$$

One can estimate also the longitudinal spectrum:

$$\int B_h^{A/a}(\alpha, k_\perp, \beta, p_\perp) d^2 p_\perp \simeq \tilde{G}_h^{N/a}(\beta/\alpha_1) + (\nu - 1) \tilde{G}_h^{N/a}(\beta). \quad (\text{D.5})$$

We want to emphasize that the secondary interactions of N and “a” with the residual nucleus would effectively lead to decrease of the correlation as compared to eqs. (D.4), (D.5).

## Appendix E. Position of the nuclear core and the non-relativistic quark model

We would like to note that there exists a natural mechanism for an effective core in the nucleon–nucleon potential [45] within the quark model.

Indeed, it is known from deep inelastic lepton scattering that the average transverse momenta of quarks  $\langle k_\perp^2 \rangle$  are strongly limited. In configuration space this corresponds to a suppression of small interquark distances  $\leq 1/\langle k_\perp^2 \rangle$  in the nucleon. Therefore the core could result just from suppression of configurations with 6 quarks concentrated in the volume, which is normal for 3 quarks. Thus, we can estimate the radius of the core, requiring that the density of the overlapping nucleons should be of order of the maximal quark density in the nucleon. We obtain

$$2\rho_N^q(r_c/2) = \rho_N^q(0). \quad (\text{E.1})$$

Here  $r_c$  is the core radius (by definition  $r_c$  is the distance between nucleon centres). In the non-relativistic quark model quark density is proportional to the charge density  $\rho_N^{ch}$ .  $\rho_N^{ch}$  is the Fourier transform of the electric form factor of the nucleon:  $\rho_N^{ch}(r) = A \exp(-\mu r)$ . Here for an estimate we use a dipole fit to the nucleon form factor:  $F_N(q) = (1 + q^2/\mu^2)^{-2}$ .

From eq. (E.1) we have

$$r_c = 2 \ln(2)/\mu \simeq 0.35 \text{ fm} \quad (\text{E.2})$$

in agreement with nuclear physics estimates. (See e.g. [107, 108].) The above derivation revives in some sense an original argumentation by R. Jastrow [204], who considered the nuclear core as a result of collision of two hard spheres.

The existence of nuclear core shows that there is no considerable diquark configurations in the nucleon. Otherwise a compact three diquark configuration in the deuteron would be expected and therefore short-range nucleon–nucleon interaction would be attractive.

### Note added in proof

Recently a number of experimental and theoretical papers related to the problems discussed in the review have appeared.

First we shall discuss the experimental data:

1. Quite recently the analysis of the data on the deep inelastic structure functions of  $\mu$ -C scattering was performed by NA-4 collaboration in CERN (NA-4, private communication).  $F_{2^{12}\text{C}}(x, Q^2)$  was studied in the region  $1 \leq x \leq 1.4$  and  $Q^2 = 50\text{--}200 \text{ GeV}^2$ . Though preliminary, the data indicate a rather large tail of  $F_2(x, Q^2)$  at  $x \geq 1$ , consistent within the experimental uncertainties with the estimate of section 5 based on the analysis of the fast backward (FB) proton and pion production in high-energy reactions.

If confirmed in the further analysis, these data would establish the absolute value of the high-momentum component in the nuclear WF and confirm interpretation of FB particle production as due to the scattering off few-nucleon correlations.

It is worth noting that a combined analysis of FB nucleon production and deep inelastic scattering will put strong restrictions on the presence of configurations with hidden colour in nuclei. Indeed, contribution of such configurations is not suppressed in deep inelastic scattering though it is difficult to produce FB nucleon in the scattering from such configurations. Let us consider for example 6 quark (6q) configuration with mixed colour symmetry in the deuteron [56]. The probability of emission of a FB proton is proportional to  $\frac{1}{10}P \cdot f$ . Here the factor  $\frac{1}{10}$  is due to color combinatorics: only 10% of the configurations in such 6q bag correspond to the NN component [56]. The factor  $P$  is the probability of 6q admixture in the deuteron WF. According to [211]  $P \sim 2\%$ . The factor  $f$  is the probability to obtain high momentum nucleon in the 6q bag. It is less than 1 and decreases with increasing the bag radius (cf. calculation of the overlap between 6q and two nucleon WF in [211]). As a result such an approach will have serious difficulties in the explanation of large FB proton yield in high energy processes.

2. Preliminary data on  $e + {}^{3,4}\text{He} \rightarrow e + X$  reactions in the threshold region at high-momentum transfer and  $x > 1$  will be presented to the Versal conference (July, 1981) [212]. In the region of two-nucleon correlation:  $1 < x < 2$  covered for  ${}^3\text{He}$  only these data confirm the prediction [45] (section 5) that the shapes of electron spectra from  ${}^3\text{He}$  and D are rather close and that the ratio of cross sections weakly depends on  $Q^2$  up to  $Q^2 \leq 4 \text{ GeV}^2$ . The comparison of  ${}^3\text{He}$  and  ${}^4\text{He}$  data seem to confirm the expectation of the FNC model (eq. (5.16)) that in the region of 3-nucleon correlation the ratio  $\nu W_2^{{}^4\text{He}}(x, Q^2)/\nu W_2^{{}^3\text{He}}(x, Q^2)$  is approximately constant. It is important now to study  $\nu W_2^{{}^4\text{He}}$  in the two-nucleon correlation region and to investigate the structure of the recoil system (sections 5, 6).

3. In [213] the  $\nu + \text{Ne} \rightarrow \mu^- + p + X$  reaction with FB proton was investigated, for larger  $Q^2$ ,  $W^2$  than in the  $\bar{\nu} + \text{Ne} \rightarrow \mu^+ + p + X$  experiment [9] discussed in section 6. In difference from [9] their analysis (see also [214]) indicates a rather large value of the secondary hadron interaction. They observe  $x - \alpha$  correlation (cf. section 6) at  $\alpha > 1.4$  which is however smaller than the one observed in [9]. It appears that both these observations are interrelated since cascades lead to decrease of this correlation (see eq. (6.12)).

4. In recent work [215] the correlation between two FB protons with small relative momenta produced in the  $h + A \rightarrow p + p + X$  reaction has been studied. The data analysed within the model [216] indicate  $R_e$  – longitudinal (along the projectile) radius of the FB nucleon emission region increases with  $A$  approximately as  $A^{1/3}$  though  $R_t$  – transverse radius is approximately  $A$  independent. For example for

the lead target  $R_\ell = (5.5 \pm 1.1)f$  and  $R_t = (1 \pm 1)f$ . Evidently this observation is in line with the prediction of the Glauber model of FB nucleon production described in section 7 where  $R_\ell \sim R_A$ ,  $R_t \sim 2r_N$ . Here  $R_A(r_N)$  is the radius of nucleus (nucleon).

5. A detailed study of the FB proton production in the nucleus–nucleus collisions was performed in [217]. The data generally confirm universality of the FB proton spectra and the pattern of the scaling onset discussed in section 8. The dependence of  $G_B^{A/p}(p_N)$  of the projectile B atomic number is rather close to the estimate eq. (7.26) for light B ( ${}^4\text{He}$ ). For heavy projectiles the FB proton yield increases faster than according to eq. (7.26). This could be due to destruction of many-body correlations in the central collisions (neglected in eq. (7.26)) and difference in the final state interaction.

6. The deuteron fragmentation in the  $D + C \rightarrow p + X$  reaction at  $p_D = 9 \text{ GeV}/c$  and  $p_\perp = 0$  was studied in [218]. The shape of proton spectrum is consistent with  $\alpha$ -scaling except the region  $p_N \sim 0.35 \text{ GeV}/c$  (in the deuteron rest frame) where a bump was observed. The position of the bump is close to the kinematics of  $N\Delta$  rescattering mechanism (fig. 2.21). Comparison of these data (corrected on the dependence of the atomic number of the projectile) and the data [217] with the previous data [16–18] indicate that their normalisation is closer to the data [16, 18]. This is in line with our theoretical analysis of section 8.

7. The energy dependence of reactions  $\pi^- + C \rightarrow p, n + X$  at  $90^\circ$  was investigated in [219]. The data confirm the previous observation [187] that at small incident energies the proton and neutron yields are rather different. The authors suggest that this difference is due to large cross section of the  $\pi^- + N \rightarrow \rho N'$  reaction at small energies. This leads to enhancement of the direct mechanism and enables to explain both the energy dependence of the scaling violation terms and their relative contribution to the proton and neutron yields.

8. In [220] the spectra of protons produced by  $1 \text{ GeV}$  protons at  $156^\circ$  from a wide range of nuclei ( $A = 2–207$ ) have been measured. It was shown that for  $A < 12$  in the slope of the spectra changes at proton momenta  $350–450 \text{ MeV}/c$ . In the case of deuterium data violation of  $\alpha$ -scaling of the order of 2 is observed. Both effects could be caused by rescattering of the  $\Delta$ -isobar in the intermediate state [190, 205], since production of slow  $\Delta$ -isobars is enhanced at  $E_N \sim 1 \text{ GeV}$ .

Now let us discuss the theoretical works:

1. Several papers have analysed the data [9] on the  $e + {}^3\text{He} \rightarrow e + X$  reaction. In [221] the data were analysed actually in the FNC model assuming quark counting rules and precocious scaling in the Nachtmann variable to describe the structure functions of 2,3-nucleon clusters. In [222, 223] the data were interpreted as an indication of a large high momentum component in the  ${}^3\text{He}$  WF. It was found in [222] that variational calculations of  ${}^3\text{He}$  WF indicate a larger high momentum component than the previous estimates, thus diminishing the discrepancy both with inelastic and elastic  ${}^3\text{He}$  form factors. In [223] it was observed that the data are roughly consistent with so called  $y$ -scaling introduced by West [39] on the basis of the average field model where the mass of recoiling  $A - 1$  nucleon system is minimal. Note that this assumption is quite different from the FNC model where this mass is expected to be rather large especially if  $W^2$  is not small (cf. eq. (5.4)).

2. In new paper of Wong and Blankenbecler [224] the authors came to the conclusion (cf. [71]) that the hard collision mechanism suggested by Schmidt and Blankenbecler [46] gives negligible contribution to the FB proton yield at  $p_\perp = 0$ . They also agree with conclusion of [71] that  $\alpha$  is the best scaling variable for analysis of FB nucleon production. For the explanation of the observed yield the authors develop relativistic generalization of the Weber–Miller model [49] (remind that for this mechanism there is no simple relationship between the observed nucleon yield and the WF of the ground state [53, 71b], cf. section 7.4). The contribution of FNC's is still neglected in this approach.

3. Another attempt to introduce the IMF many-nucleon WF of the nucleus was made in [225] within the

coherent tube model [197]. The data on the FB pion production were fitted. The authors emphasize that the introduced IMF WF has no relation to the rest frame theory of the nuclei. This assumption is not valid in the quantum field theory where such relationship can be strictly proven (in the region where non-relativistic quantum mechanical theory of nuclei is valid) by direct calculation of Feynman diagrams (cf. section 2). The prove is based on the observation that at small nucleon momenta  $k$  taking residue over  $k_0$  and over  $k_+ = k_0 + k_z$  leads to the same result for WF but not for the scattering amplitude.

## References

- [1] L. Lederman, in: Proc. V. Erevan School on Elementary particles, p. 251 (1966);  
D.E. Dorfan et al., Phys. Rev. Lett. 14 (1965) 995;  
P.A. Piroué et al., Phys. Rev. 148 (1966) 1315.
- [2] Yu.D. Baukov et al., Izvestia Akad. Nauk SSSR, Fizika 30 (1966) 521.
- [3] A.M. Baldin et al., in: Proc. Rochester Meeting, ADS/OPF, N.Y., 1971, p. 131; Yad. Fiz. 18 (1973) 79; 20 (1974) 1201.
- [4] R.G. Arnold et al., Phys. Rev. Lett. 35 (1975) 776.
- [5] W.P. Schütz et al., Phys. Rev. Lett. 38 (1977) 259;  
R.G. Arnold, Contributed paper to Madison Conf. 1980.
- [6] F. Martin et al., Phys. Rev. Lett. 38 (1977) 1320.
- [7] R.G. Arnold et al., Phys. Rev. Lett. 40 (1978) 1429.
- [8] D. Day et al., Phys. Rev. Lett. 43 (1979) 1143.
- [9] J.P. Berge et al., Phys. Rev. D18 (1978) 1367; D22 (1980) and private communication.
- [10] A.A. Ivanilov et al., Pis'ma v Zh. ETF 30 (1979) 330.
- [11] J. Papp et al., Phys. Rev. Lett. 34 (1975) 601.
- [12] J. Papp, preprint LBL-3633, Berkeley 1975.
- [13] A.M. Baldin et al., preprint JINR, P1-11168, Dubna 1977.
- [14] Yu.D. Baukov et al., Yad. Fiz. 18 (1973) 1246; 19 (1974) 1266;  
G.A. Leksin, in: Proc. XVIII Int. Conf. on High Energy Physics 1, A6-3, Dubna (1977).
- [15] N.A. Burgov et al., Yad. Fiz. 24 (1976) 1183.
- [16] N.A. Burgov et al., Yad. Fiz. 30 (1979) 720.
- [17] A.M. Baldin et al., preprint JINR P1-11302, Dubna (1978); P1-12396, Dubna (1979).
- [18] Yu.D. Baukov et al., Phys. Rev. C20 (1979) 764, 2257; 21 (1980).
- [19] H. Steiner, in: VII Int. Conf. on High energy physics and nuclear structure (Zurich, 1977) p. 261.
- [20] L.M. Anderson Jr., preprint LBL-6769, Berkeley, 1978;  
L.M. Anderson Jr. et al., preprint LBL-9493, Berkeley, 1979.
- [21] K.V. Alanakyan et al., Yad. Fiz. 25 (1977) 545; 26 (1977) 1018.
- [22] L.S. Schroeder et al., Phys. Rev. Lett. 43 (1979) 1787.
- [23] S. Frankel et al., Phys. Rev. Lett. 36 (1976) 642.
- [24] H. Brody et al., Phys. Lett. 71B (1978) 79.
- [25] S. Frankel et al., Phys. Rev. C18 (1978) 1375.
- [26] V.I. Komarov et al., Phys. Lett. 69B (1977) 37.
- [27] V.I. Komarov et al., Phys. Lett. 80B (1978) 30.
- [28] V.I. Komarov et al., Nucl. Phys. A326 (1979) 297.
- [29] F.L. Fabbri et al., Lett. Nuovo Cim. 17 (1976) 21.
- [30] T.A. Kallne, A.W. Stetz and R.M. Woloshyn, Phys. Lett. 74B (1978) 140.
- [31] S. Frankel et al., Phys. Rev. Lett. 41 (1978) 148.
- [32] N.A. Burgov et al., Pis'ma v Zh. ETF 31 (1980) 700.
- [33] P. Zulkarneev et al., preprint JINR P1-80-83, Dubna (1980).
- [34] D.R.F. Cochran et al., Phys. Rev. D6 (1972) 3085.
- [35] C.F. Perdrisat, S. Frankel and W. Frati, Phys. Rev. C18 (1978) 1764.
- [36] A.M. Baldin, preprint JINR P7-5769, Dubna (1971).
- [37] S. Brodsky, SLAC-PUB-1497 (1974);  
S. Brodsky and B. Chertok, Phys. Rev. D11 (1976) 3003.
- [38] L.L. Frankfurt and M.I. Strikman, in: Materials of the X Winter School of the Leningrad Nuclear Physics Institute, vol. 2, Leningrad (1975)  
pp. 449–480.

- [39] G.B. West, Phys. Reports 18C (1975) 264.
- [40] L.L. Frankfurt and M.I. Strikman, Phys. Lett. 65B (1976) 51; Pis'ma v Zh. ETF 24 (1976) 311; in: Proc. XVIII Int. Conf. on High Energy Physics 1, A6–16, Dubna (1977).
- [41] E. Lehman, Phys. Lett. 62B (1976) 296.
- [42] L. Bertocchi and D. Treliani, Nuovo Cim. 36A (1976) 1.
- [43] L.L. Frankfurt and M.I. Strikman, Phys. Lett. 64B (1976) 435; preprint LNPI N 238 (1976).
- [44] R.D. Amado and R.M. Woloshyn, Phys. Rev. Lett. 36 (1976) 1435.
- [45] L.L. Frankfurt and M.I. Strikman, Phys. Lett. 69B (1977) 93; Yad. Fiz. 25 (1977) 1177.
- [46] I.A. Schmidt and R. Blankenbecler, Phys. Rev. D15 (1977) 3321.
- [47] I.A. Schmidt and R. Blankenbecler, Phys. Rev. D16 (1977) 1318.
- [48] I.A. Schmidt, SLAC report no. 203 (1977).
- [49] H.J. Weber and L.P. Miller, Phys. Rev. 16C (1977) 726.
- [50] A.V. Efremov, Yad. Fiz. 24 (1976) 1208.
- [51] S.B. Gerasimov and N. Giordanesky, preprint JINR P2-7687, Dubna (1974);  
G.A. Lobov et al., Pisma v Zh. ETF 23 (1976) 118;  
V.A. Karmanov and I.S. Shapiro, E. Ch. A. Ya. 9 (1978) 237.
- [52] V.V. Burov, V.K. Lukyanov and A.I. Titov, Phys. Lett. 67B (1977) 46; E. Ch. A. Ya. 10 (1979) 815.
- [53] R.D. Amado and R.M. Woloshyn, Phys. Lett. 69B (1977) 400; Phys. Rev. C16 (1977) 1255.
- [54] A. Krzywicki, Phys. Rev. D14 (1976) 152.
- [55] C.E. De Tar, Phys. Rev. D17 (1978) 323; 19 (1979) 1928(E); 19 (1979) 1451.
- [56] V.A. Matveev and P. Sorba, Nuovo Cim. Lett. 20 (1977) 443.
- [57] G.E. Brown M. Rho and V. Vento, Phys. Lett. 84B (1979) 383;  
C. Carlson, F. Myhrer and G.E. Brown, preprint Nordita 79/15 (1979).
- [58] P.V. Landshoff and J.C. Polkinghorne, Phys. Rev. D18 (1978) 158;  
D. Kusno and M.J. Moravcsik, Phys. Rev. D20 (1979) 2734.
- [59] S. Frankel, Phys. Rev. Lett. 38 (1977) 1338; Phys. Rev. C17 (1978) 694.
- [60] T. Fujita and J. Hüfner, Nucl. Phys. A314 (1979) 317;  
T. Fujita, Nucl. Phys. A324 (1979) 409.
- [61] M. Chemtob, Nucl. Phys. A314 (1979) 387.
- [62] R.M. Woloshyn, Nucl. Phys. A306 (1978) 333.
- [63] R.H. Landau and M. Gyulassy, Phys. Rev. C19 (1979) 149.
- [64] L.L. Frankfurt and M.I. Strikman, Nucl. Phys. B148 (1979) 107; Yad. Fiz. 27 (1978) 1361; in: Materials of the XII Winter School of LNPI, vol. 2, Leningrad (1977) pp. 132–208.
- [65] A.I. Vainstein and V.I. Zakharov, Phys. Lett. 72B (1978) 368;  
S.G. Grigoryan, S.V. Esaybegyan and N.L. Ter-Isaakyan, Yad. Fiz. 27 (1978) 1321.
- [66] S. Brodsky, SLAC-PUB – 2395 (1979).
- [67] B.L. Bakker, L.A. Kondratuk and M.V. Terent'ev, Nucl. Phys. B158 (1979) 497.
- [68] L.A. Kondratuk and L.V. Schevchenko, Yad. Fiz. 29 (1979) 792.
- [69] M. Chemtob, Nucl. Phys. A336 (1980) 299.
- [70] S.A. Nissen-Meyer, Nucl. Phys. A306 (1978) 449;  
J.H. Kuhn and S.A. Nissen-Meyer, Nucl. Phys. A312 (1978) 409.
- [71] L.C. Frankfurt and M.I. Strikman, Phys. Lett. 83B (1979) 407; in: Materials of the XIII Winter School of LNPI, vol. 1, Leningrad (1978) pp. 139–191; Yad. Fiz. 29 (1979) 490; E. Ch. A. Ya. 11 (1980) 571.
- [72] L.L. Frankfurt and M.I. Strikman, Pis'ma v Zh. TEF 30 (1979) 373.
- [73] R.D. Amado, Phys. Rev. C19 (1979) 1473.
- [74] T. Yukawa and S. Furui, Phys. Rev. C20 (1979) 2316.
- [75] L.L. Frankfurt and M.I. Strikman, Pis'ma v Zh. ETF 31 (1980) 416; Phys. Lett. 94B (1980) 216; Nucl. Phys. B181 (1981) 22.
- [76] A. Fernandes-Pacheco, J.A. Grifols and I.A. Schmidt, Nucl. Phys. B151 (1979) 518.
- [77] R.G. Arnold, C.E. Carlsson and F. Gross, Phys. Rev. C21 (1980) 1426.
- [78] V.N. Gribov, in: Materials of the VIII Winter School of LNPI, vol. 2, Leningrad (1973) pp. 64–94.
- [79] V.N. Gribov, B.L. Ioffe and I.Ya. Pomeranchuk, Yad. Fiz. 2 (1965) 768.
- [80] T.H. Bauer, R.D. Spital, D.R. Yennie and F.M. Pipkin, Reviews of Modern Physics 50 (1978) 261.
- [81] L.L. Frankfurt and M.I. Strikman, Phys. Lett. 75B (1978) 257.
- [82] J.G. Zabolitsky and W. Ey, Phys. Lett. 76B (1977) 1527.
- [83] G.E. Brown, Unified theory of nuclear models and forces (North-Holland, Amsterdam 1967).
- [84] G. Ricco, in: Lecture Notes in Physics 61 (1977) 223.
- [85] R. Hartmann et al., Nucl. Phys. A308 (1978) 345.
- [86] A.N. Gorbunov, Proc. Lebedev Physics Institute 71 (1974) 3.

- [87] L.L. Frankfurt, M.M. Savitsky and M.I. Strikman, preprint ITEP N 57, Moscow (1980), Phys. Lett. 97B (1980) 294.
- [88] A. Kaidalov, Phys. Reports 50 (1979) 157.
- [89] V.N. Gribov, Zh. TEF 30 (1970) 709.
- [90] R.P. Feynman, Photon-hadron Interactions (Benjamin, 1972).
- [91] H. Lehnmann, K. Symanzik and W. Zimmermann, Nuovo Cim. 1 (1950) 205.
- [92] W. Zimmermann, Nuovo Cim. 10 (1958) 567.
- [93] S. Mandelstam, Nuovo Cim. 30 (1963) 1113.
- [94] N. Hoshisaki, Journal Phys. Soc. Japan 44 (1978) 173 and references therein.
- [95] G. Alexander et al., Phys. Rev. 154 (1966) 1284.
- [96] Y. De Alfaro, S. Fubini, G. Furlan and C. Kostetti, Currents in Hadron Physics (North-Holland, Amsterdam-London 1973).
- [97] M.A. Shifman, A.I. Vainstein and V.I. Zakharov, Nucl. Phys. B147 (1979) 385, 448 and 519.
- [98] M. Baker and K.A. Ter-Martirosyan, Phys. Reports 28 (1976) 1.
- [99] G.E. Brown and A.D. Jackson, The nucleon interaction (North-Holland, Amsterdam-Oxford 1976).
- [100] S. Weinberg, Phys. Rev. 150 (1966) 1313.
- [101] J. Kogut and L. Susskind, Phys. Reports 8 (1973) 75.
- [102] See, for example J.M. Namyslowski, Phys. Rev. C20 (1979) 2356 and references therein.
- [103] V.A. Matveev, in: Proc. XVIII Int. Conf. on High Energy Physics 1, A5-34, Dubna (1977).
- [104] L. Foldy, Phys. Rev. 122 (1961) 275.
- [105] M.V. Terent'ev, Yad. Fiz. 24 (1976) 207.
- [106] L.L. Frankfurt and M.I. Strikman, Yad. Fiz. 32 (1980) 220.
- [107] T. Hamada and I.D. Johnston, Nucl. Phys. 34 (1962) 382;  
J. Humberstone and J.B.G. Wallace, Nucl. Phys. A141 (1970) 362.
- [108] R.V. Reid Jr., Ann. of Phys. 50 (1968) 411.
- [109] S.L. Adler, Phys. Rev. 139B (1965) 1638;  
R. Dashen and M. Gell-Mann, in: Proc. 3d Coral Cables Conf. on Symmetry principles at High Energy 1966.
- [110] A.M. Polyakov, Zh. ETF 60 (1971) 1572.
- [111] V.N. Gribov and L.N. Lipatov, Yad. Fiz. 15 (1972) 781;  
L.L. Frankfurt, Yad. Fiz. 16 (1972) 1250.
- [112] J.S. Levinger, Phys. Rev. 84 (1951) 43.
- [113] Yu.K. Khokhlov, Zh. ETF 23 (1952) 241.
- [114] K.A. Bruekner, S. Serber and K.M. Watson, Phys. Rev. 84 (1951) 258.
- [115] H. Uberall, Electron Scattering from Complex Nuclei, part A (New York-London 1971).
- [116] G.D. Alkhazov, S.L. Belostotsky and A.A. Vorobyov, Phys. Reports 42 (1978) 91.
- [117] M. Erikson and T.E.O. Erikson, Ann. of Phys. 36 (1966) 323.
- [118] S.J. Brodsky and G.K. Farrar, Phys. Rev. Lett. 31 (1973) 1153.
- [119] L.D. Faddeev, Zh. ETF 39 (1960) 1059.
- [120] V.N. Gribov, Zh. ETF 88 (1968) 392.
- [121] A. Capella and A.B. Kaidalov, Nucl. Phys. B111 (1976) 477;  
A. Capella and A. Kryzwicki, Phys. Lett. 67 (1977) 84.
- [122] V.A. Abramovsky, V.N. Gribov and O.V. Kancheli, Yad. Fiz. 18 (1974) 308.
- [123] E.M. Levin and M.I. Strikman, Yad. Fiz. 23 (1976) 412.
- [124] S. Stein et al., Phys. Rev. D12 (1975) 1884.
- [125] W. Fabian and H. Arenhövel, Nucl. Phys. A314 (1979) 253.
- [126] K.M. Hanson et al., Phys. Rev. D8 (1973) 753.
- [127] D. Bloom et al., Phys. Rev. D5 (1972) 528.
- [128] G. West, Phys. Lett. 37B (1971) 509;  
W.B. Atwood and G. West, Phys. Rev. D7 (1973) 773.
- [129] K. Gottfried, Phys. Rev. Lett. 18 (1967) 1174.
- [130] J.S. Levinger, in: Springer Tracts in Modern Physics 77 (1973) 88.
- [131] L.J. Allen and H. Fiedeley, in: Lecture Notes in Physics 82 (1978) 57.
- [132] L.S. Osborne et al., Phys. Rev. Lett. 41 (1978) 76.
- [133] J.F. Gunion, S.J. Brodsky and R. Blankenbecler, Phys. Rev. D8 (1973) 287.
- [134] M. Gourdin, Nuovo Cim. 28 (1963) 533.
- [135] S.N. Bilenkaya et al., Zh. ETF 61 (1971) 2225.
- [136] V.A. Matveev, R.M. Muradyan and A.N. Tavkhelidze, Lett. Nuovo Cim. 7 (1973) 719.
- [137] G.C. Mantovani et al., Phys. Lett. 65B (1976) 401.
- [138] Y. Benecke et al., Phys. Rev. 188 (1969) 2159.
- [139] A. Abdivaliev et al., Yad. Fiz. 27 (1978) 1356.

- [140] J.R. Johnson et al., Fermilab-Pub-77/98 EXP, 7100.284 (1977);  
F.E. Taylor et al., Phys. Rev. D11 (1976) 1217.
- [141] R.L. Jaffe and F.E. Low, Phys. Rev. 19 (1979) 2105.
- [142] R.L. Jaffe, Phys. Rev. 15 (1977) 267, 281.
- [143] B.T. Chertok, Phys. Rev. Lett. 41 (1978) 1155.
- [144] J.B. Kogut and J.E. Soper, Phys. Rev. D1 (1970) 2901.
- [145] G. Farrar and D.R. Jackson, Phys. Rev. Lett. 35 (1975) 1416.
- [146] L.L. Frankfurt and M.I. Strikman, Yad. Fiz. 32 (1980) 220.
- [147] A.M. Green, Reports on Prog. in Physics 39 (1976) 1109.
- [148] V. Bakken et al., Physica Scripta 19 (1979) 491.
- [149] See for example K. Erkelenz, Phys. Reports 13 (1974) 191.
- [150] M.B. Kisslinger, Phys. Lett. 79B (1978) 474;  
H.J. Pirner, Phys. Lett. 85B (1979) 190.
- [151] R.L. Anderson et al., Phys. Rev. Lett. 38 (1977) 880;  
R.G. Kennet, CALT-68-742 (1979).
- [152] D. Cutts et al., Phys. Rev. Lett. 43 (1979) 319.
- [153] J.F. Gunion, Phys. Lett. 88B (1979) 150.
- [154] H.A. Bethe and R.E. Peierls, Proc. Roy. Soc. A148 (1935) 146.
- [155] K. Henley, in: Proc. of Workshop on Intermediate-Energy Physics 1 (1979) 1.
- [156] R. Amado, Phys. Rev. C19 (1979) 1473.
- [157] See for example J.D. Bjorken, Acta Phys. Polonica B5 (1974) 893.
- [158] I. Sick, Nucl. Phys. A335 (1980) 555.
- [159] J.S. McCarthy, Nucl. Phys. A335 (1980) 27.
- [160] L.L. Frankfurt and M.I. Strikman, Phys. Lett. 76B (1978) 333.
- [161] A.E.L. Dieperink and T. de Forest, Ann. Rev. Nucl. Sci. 25 (1975) 1.
- [162] E. Wigner, Phys. Rev. 51 (1937) 106.
- [163] Yu.A. Dokshitzer, D.I. Dyakonov and S.I. Troyan, Phys. Reports 58 (1980) 269.
- [164] R.L. Herndon and Y.C. Tung, Methods Comp. Phys. 6 (1966) 153.
- [165] T. De Forest, Ann. of Phys. 45 (1967) 365.
- [166] L.S. Osborne et al., Phys. Rev. Lett. 40 (1978) 1624.
- [167] L. Hand et al., Z. Phys. C1 (1979) 139.
- [168] M.A. Faessler et al., Nucl. Phys. B157 (1979) 1.
- [169] K. Gottfried, preprint CERN, TH-1735 (1973).
- [170] R. Glauber, in: High Energy Physics and Nuclear Structure (Plenum Press 1970) p. 311.
- [171] L. Bertocchi and D. Treleany, J. Phys. G3 (1977) 147.
- [172] E.A. Remler, preprint Weizmann Institute (1978).
- [173] S.T. Butler and C.A. Pearson, Phys. Rev. 129 (1963) 836.
- [174] L.L. Frankfurt and M.I. Strikman, Yad. Fiz. 32 (1980) 968.
- [175] J.P. Schiffer, Nucl. Phys. A335 (1980) 339.
- [176] W. Busha, Acta Phys. Polonica B8 (1977) 333.
- [177] A. Bialas, Fermilab-Pub-78/75-THY (1978).
- [178] O.V. Kancheli and S.G. Matinyan, Yad. Fiz. 11 (1972) 1305;  
O.V. Kancheli, Pis'ma v Zh. ETF 18 (1973) 274.
- [179] N.N. Nikolaev, Landau Inst. Preprint N5 (1980).
- [180] L.L. Frankfurt and M.I. Strikman, Yad. Fiz. 32 (1980) 1403.
- [181] L.S. Vorobyev et al., Pis'ma Zh. ETF 26 (1977) 113.
- [182] M.G. Gornov et al., Yad. Fiz. 25 (1977) 606.
- [183] B.A. Shahbazian et al., Preprint JINR EI-11519, Dubna (1978).
- [184] B.S. Aladashvili et al., Yad. Fiz. 27 (1978) 704.
- [185] V.S. Stavinsky, E. Ch. A. Ya. 10 (1979) 949.
- [186] A.M. Baldin et al., preprint JINR 1-8858 (1975).
- [187] Yu.B. Baukov et al., Yad. Fiz. 30 (1979) 1283.
- [188] N.N. Nikolaev, Phys. Lett. 70B (1977) 95;  
N.N. Nikolaev and A.Ya. Ostapchuk, preprint CERN TH.2575 (1978).
- [189] L.L. Frankfurt and E.M. Levin, Pis'ma v Zh. ETF 2 (1965) 105;  
H.J. Lipkin and F. Scheck, Phys. Rev. Lett. 16 (1966) 71.
- [190] G. Alberi et al., preprint CERN TH-2113 (1975).
- [191] S. Frankel and R.W. Woloshyn, Phys. Rev. C16 (1977) 168.

- [192] T. Hayashiro et al., *Nuovo Cim. Lett.* 16 (1976) 71.
- [193] I.I. Vorobiev et al., *Pis'ma v. Zh. ETF* 22 (1975) 390;  
G.A. Leksin and A.V. Smirnitsky, *Pis'ma v. Zh. ETF* 28 (1978) 97, 179; preprint ITEP-87 (1977).
- [194] D. Sivers, S.J. Brodsky and R. Blankenbecler, *Phys. Reports* 23 (1976) 1.
- [195] D.I. Blōkhintsev, *Zh. ETF* 33 (1957) 1295.
- [196] J.W. Cronin et al., *Phys. Rev. D* 11 (1975) 3105.
- [197] E.V. Shuryak, *Yad. Fiz.* 24 (1976) 630;  
G. Berlad, A. Dar and G. Eilam, *Phys. Rev. D* 13 (1976) 161; preprint Technion-Ph-79-71;  
T. Fujita, *Phys. Rev. Lett.* 39 (1977) 174.
- [198] V.B. Kopeliovich, *Yad. Fiz.* 26 (1977) 168.
- [199] M.A. Brown and V.V. Vecherin, *Yad. Fiz.* 25 (1977) 1276.
- [200] K.K. Gudima et al., preprint JINR E2-11107, Dubna (1977);  
O.A. Abdinov et al., *Yad. Fiz.* 30 (1979) 396.
- [201] B.N. Kalinkin et al., *Acta Phys. Polonica B* 9 (1978) 375.
- [202] L.L. Frankfurt, *Pis'ma Zh. ETP* 13 (1971) 650.
- [203] I. Cohen et al., *Phys. Rev. Lett.* 40 (1978) 1614.
- [204] R. Jastrow, *Phys. Rev.* 79 (1950) 389.
- [205] V.B. Kopeliovich and V.B. Radomanov, preprint JINR P2-11938, Dubna (1978).
- [206] A.M. Baldin, in: *Proc. Conf. on Extreme States in Nuclear Systems, Dresden* (1980) vol. 2, p.1.
- [207] P.A.M. Dirac, *Rev. Mod. Phys.* 21 (1949) 1392.
- [208] S.J. Brodsky and G.P. Lepage, SLAC-PUB-2447 (1979); SLAC-PUB-2605 (1980).
- [209] A. Chodes et al., *Phys. Rev. D* 9 (1974) 3471; D10 (1974) 2599;  
T. De Grand et al., *Phys. Rev. D* 12 (1975) 2060.
- [210] See, for example, M. Rho, *Nucl. Phys.* A354 (1981) 3 and references therein.
- [211] V.K. Lukyanov and A.I. Titov, in: *Proc. Conf. on Extreme States in Nuclear Systems, Dresden* (1980) vol. 2, p. 60.
- [212] S. Rock et al., Contribution to 9-ICOHEPANS, Versal (July 1981).
- [213] E. Wolin and B.S. Yuldashev, Internal Report, HEP-Phy-78 (1981) Univ. of Washington, Seattle.
- [214] T.H. Barnett et al., *Phys. Lett.* 77B (1978) 443.
- [215] A.V. Vlasov et al., preprint ITEP-53 (1981).
- [216] S.E. Koonin, *Phys. Lett.* 70B (1977) 43.
- [217] J.V. Geaga et al., *Phys. Rev. Lett.* 45 (1980) 1993.
- [218] V.G. Ableev et al., Contribution to 9-ICOHEPANS, Versal (July 1981).
- [219] Yu.D. Baukov et al., *Yad. Fiz.* 34 (1981).
- [220] M.N. Andronenko et al., Preprint LNPI 671 (1981).
- [221] H.J. Pirner and J.P. Vary, *Nucl. Phys.* A358 (1981) 413.
- [222] C. Ciofi degli Atti, E. Pace and G. Salme, *Nucl. Phys.* A358 (1981) 183.
- [223] I. Sick, D. Day and J.S. McCarty, *Phys. Rev. Lett.* 45 (1980) 871.
- [224] C. Wong and R. Blankenbecler, *Phys. Rev. D* 22C (1980) 2433.
- [225] G. Berlad, A. Dar and G. Eilam, *Phys. Rev. D* 22 (1980) 1547.